RESPONSE OF HORIZONTALLY CURVED THIN-WALLED BOX-GIRDER BRIDGE TO VEHICULAR LOADS

A Thesis Submitted
in Partial Fulfilment of the Requirements
for the Degree of

DOCTOR OF PHILOSOPHY

By

K. Nallasivam

DEPARTMENT OF CIVIL ENGINEERING

INDIAN INSTITUTE OF TECHNOLOGY GUWAHATI

DECEMBER, 2006

Dedicated to

My Nation and My Grand Mother Nallammal

CERTIFICATE

It is certified that the work contained in the thesis entitled "**Response of Horizontally Curved Thin-Walled Box-Girder Bridge to Vehicular Loads**", by K. Nallasivam, a student of the Department of Civil Engineering, Indian Institute of Technology, Guwahati, submitted for the award of the degree of Doctor of Philosophy, has been carried out under our supervision and that this work has not been submitted elsewhere for a degree.

Dr. S. Talukdar
Associate Professor
Department of Civil Engineering
Indian Institute of Technology
Guwahati, Assam, India

Dr. Anjan Dutta
Associate Professor
Department of Civil Engineering
Indian Institute of Technology
Guwahati, Assam, India

December, 2006

ACKNOWLEDGEMENT

I would like to place on record my deep sense of gratitude and sincere thanks to my thesis supervisors Dr. Anjan Dutta and Dr. S. Talukdar for their invaluable guidance and full hand cooperation throughout all the aspects of this research work. I am grateful for their endless patience, constant encouragement, willingness to discuss and readiness to help me. Without their help, motivation and commitment, this research would not have been possible.

My special thanks to many past and current B. Tech students of Indian Institute of Technology Guwahati for their help and support. I am also thankful to all my innumerable friends. They have always been a constant source of inspiration and support, not to mention their valuable suggestions and help, during my entire stay at IIT Guwahati.

I thank all the Faculty members of the Civil Engineering Department, Indian Institute of Technology Guwahati, who played a vital role in bringing me up to this level. The assistance of technical and non-technical staff of the Civil Engineering Department in my thesis work is also gratefully acknowledged.

I am grateful to my father M. Kanagaraj and mother K. Saraswathi for their constant inspiration and help. I express my sincere gratitude to my aunty M. Shanbagavalli and my uncle S. Subramaniam for their endless love and encouragement.

Above all, the person to whom I will always remain indebted is my wife Er. M. Kodeeswari for making the possibility of this research a reality. During the difficult times of finishing this dissertation, her support and patience was unfailing.

My heartfelt thanks to my daughter N. Sri Navya for all the sacrifices and compromises she made during my research work.

(K. Nallasivam)

IIT Guwahati
December, 2006

ABSTRACT

The curved girder bridges have become popular due to the increased demand for curved roadway alignment for the smooth dissemination of congested traffic along with advancement in fabrication and erection technology. However, due to geometric complexities, in addition to experiencing conventional structural actions, which are extension, flexure and torsion, cross-section of curved box-girders may warp out of the sectional plane and distort in the cross-section. The bridges are traversed by heavy and high speed vehicles and the problem of vehicle-bridge interaction becomes an important subject for the bridge engineers, since the vibrations might affect the durability of the bridge structure and to the safety and comfort of passengers. In a bridge, the fluctuating wheel load goes on repeating with the passage of time and degradation of the bridge may start with increased number of load repetition leading to fatigue damage.

In the present work, a thin-walled box-beam finite element has been used to model the horizontally thin-walled curved box-girder. In addition to the usual six degrees of freedom at each node, represented by the three displacements and the three rotations, three more degrees of freedom have been incorporated in the formulation to account for the warping and distortion effects, which occur in box-beams. Single cell and multi-cell box-girder bridges have been analyzed under static loading. The effect of shear lag has been incorporated using effective width concept. Emphasis has been given to evaluate the stress parameters which are specifically important for thin-walled section. Effect of radius of curvature has been studied.

An experiment on free vibration has been conducted in the laboratory with a perspex sheet model of a curved bridge. The natural frequencies obtained from the theoretical analysis have been compared with experimental results. Modal displacements have been obtained through frequency response functions at different sensor locations to obtain the displacement configuration at principal mode of vibration.

For dynamic analysis of the bridge, an appropriate vehicle model has been chosen incorporating principal components of motion, which includes heave, pitch and roll degrees of freedom of vehicle sprung mass in addition to bounce motion of the unsprung masses. The effect of centrifugal forces due to the motion of vehicle along the curved bridge has also been considered. The roughness of the bridge deck has been considered as the realization of homogeneous random process in space. A generalized power spectral density of the road roughness has been considered to model the random input to the vehicle. The response of the bridge has been obtained using suitable numerical schemes with simulation of deck roughness input from assumed power spectral density. A detailed parametric study has been conducted to examine the influence of various bridge vehicle parameters on the impact factors for the different stress resultants.

Having obtained the stresses induced by moving vehicle at critical location of the bridge, a systematic approach has been outlined based on linear damage accumulation rule and appropriate fatigue constants of the bridge detail. Fatigue analysis has been performed using time domain cycle counting method and compared with the results obtained by spectral methods in frequency domain approach. In time domain approach, rain flow counting method has been used to identify cycle range and thereafter to develop the stress range frequency histogram taking into consideration the

annual traffic volume. The linear damage accumulation theory is applied to calculate fatigue life by finding number of cycles/year corresponding to specific stress range and number of cycles sustainable at that stress range to cause fatigue failure.

The fatigue damage accumulation from simulated time history has been verified by recasting the problem in frequency domain. The power spectral density of the stress of the critical member has been found and based on the assumption of Raleigh's peak stress distribution, the expected fatigue damage has been calculated. In order to reduce the computational time in Rayleigh's method, another approach based only single spectral moment was considered. Both the spectral methods are numerically tested with the curved box-girder single span bridge with vehicle moving at constant speed over undulating bridge surface. Various bridge-vehicle parameters have been considered to study their effects on the fatigue life of the bridge. The fatigue life obtained by spectral method has also been compared with that obtained in the time

CONTENTS

LIST OF TABLES

LIST OF FIGURES

NOMENCLATURE

A	Cross-sectional area
A_{sy} , A_{sz}	Effective shear cross-sectional areas in the y direction and the z direction
$b_{e,i}$	Effective breadth between mid-line of webs
$\left[\bar{B}\right]$	Strain displacement matrix
B_I	Torsional warping bi-moment
B_{II}	Distortional warping bi-moment
$\left[c_b\right]$	Bridge damping matrices
cs_{ip}	Suspension damping of the vehicle
cu_{ip}	Vehicle tyre damping
$[D]$	Elasticity matrix
$\left[\bar{D}\right]$	Generalized Elasticity matrix
$\left[\bar{D}_b\right]$	Generalized Elasticity matrix for bending
$\left[\bar{D}_d\right]$	Generalized Elasticity matrix for distortion
$\left[\bar{D}_t\right]$	Generalized torsional elasticity matrix
$D(t)$	Cumulative damage accumulation
E	Young's modulus of elasticity
E_1	Conversion modulus of elasticity
$\{F(\omega)\}$	Finite Fourier transform of the force matrix
g	Acceleration due to gravity
G	Shear modulus of elasticity
h	Depth between mid-line of top and bottom slabs
$h_r(x)$	Random road surface roughness of the bridge
$\left[H(\omega)\right]$	Complex frequency response function matrix of the system

$\left\|H(\omega)\right\|$	Compliance magnitude
I	Moment of inertia for roll of the vehicle
I_y	Moment of inertia of the entire cross-section about the *y* axis
I_z	Moment of inertia of the entire cross-section about the *z* axis
J	Moment of inertia for pitch of the vehicle
$J_1, J_2\ , J_3$	Jacobian factors at the 1st, 2nd and 3rd nodes of the element
J_I	Torsional warping moment of inertia
J_{II}	Distortional warping moment of inertia
J_d	Distortional second moment of area
J_B	Bredt torsional moment of inertia
J_C	Central second moment of area
J_T	Total torsional moment of inertia
J_V	St. Venant torsional moment of inertia
k_d	Distortional frame stiffness of the box section per unit length
$[k_b]$	Bridge stiffness matrices
$[K^e]$	Element stiffness matrix
ks_{ip}	Vehicle suspension stiffness
ku_{ip}	Vehicle tyre stiffness
$K,\ m$	Fatigue strength parameters
$[M]$, $[K]$, $[C]$	Global mass, stiffness and damping matrix
$[m_b]$	Bridge mass matrices
m_{dR}	Additional distortional moment per unit length
$[M^e]$	Element mass matrix
m_{ip}	Unsprung mass
m_s	Sprung mass
M_d	Distortional moment

M_x	Torsional moment about x axes
M_y, M_z	Primary bending moments about y and z axes
M_T	Pure torsional moment
$M_{T,B}$	Pure torsional moment for closed section
$M_{T,I}$	Secondary or flexural torsional moment resulting from warping shear stresses
$M_{T,P}$	Total pure torsional moment
$M_{T,V}$	St.Venant torsional moment component
n_b	Number of stress range blocks in the histogram
n_j	Number of stress cycles at stress range level Sr_j
N_j	Number of cycles at constant stress range level Sr_j from (S-N curve) to cause failure
N_f	Number of cycles to failure
N_x	Axial force
$q_{B,i}$	Bredt shear flow around the i^{th} cell
$\overline{q}_{B,i}$	Bredt's unit shear flow distribution function around the i^{th} cell
Q_y, Q_z	Internal shear forces in the y and z directions
S_r	Stress range
$S_\sigma(x_1, \omega)$	Power spectral density of the stress at location x_1 as function of circular frequency
$\left[S_{FF}(\omega)\right]$	Cross spectral density matrix of excitation
$\left[S_{XX}(\omega)\right]$	Cross spectral density matrix of the response
v	Vertical deflection
v_{ip}	Bridge displacements under front / rear wheels at any arbitrary time (t)
$V_s(S)$	Distribution function of the tangential displacement
$V_t(S)$	Distribution function of the normal displacement in distortion
w_t	Tangential displacement
x	Global coordinate measured left end of the bridge

$\{X\}$	Vector of nodal amplitude of vibration
$\{X(\omega)\}$	Finite Fourier transform of the response matrix
$\{\chi\}$	Response vector
z	Sprung masses vertical displacement (heave motion along vertical axis)
z_{ip}	Unsprung masses vertical displacement(heave motion along vertical axis)
α_k	Amplitude of the cosine wave
α_s	Spectral roughness coefficient
$\alpha(\omega)$	Receptance matrix
β_r	Roughness exponent
γ_d	Distortional angle
γ_d'	Rate of distortion angle
λ_k	k^{th} moment of the spectral density function
Λ_c	Modal damping matrix
Λ_k	Modal stiffness matrix
$[\delta]$	Displacements in the global co-ordinate system
$[\delta],[\ddot{\delta}]$	Global displacements and accelerations
$\{\bar{\delta}^e\}$	Nodal values of the global displacements
$[\bar{\delta}]$	Generalized displacements in the local co-ordinate system
ΔD_j	Incremental damage for each cycle
ϕ_x, ϕ_y, ϕ_z	Rotations about the global X, Y and Z axes
ψ	Rotation about the transverse axis (roll)
$\psi_{e,i}$	Effective breadth ratio
$\psi_{\theta x}$	Torsional strain
ψ_{yx}	Flexural strain about *y* axis
ψ_{zx}	Flexural strain about *z* axis
ψ_{wtx}	Torsional warping strain

ψ_{dx}	Distortional strain
ψ_{wdx}	Distortional warping strain
$\{\bar{\varepsilon}\}$	Generalized strain vector
$\{\boldsymbol{\varepsilon}_{\mathbf{b}}\}$	Strains in the case of bending
$[\bar{\varepsilon}_{\mathrm{d}}]$	Generalized distortional strain vector
$\{\bar{\varepsilon}_{\mathrm{t}}\}$	Generalized strain vector due to torsion
ε_x	Axial strain in the x direction
ε_{yx}	Shear strain in *y* direction
ε_{zx}	Shear strain in *z* direction
ζ	Damping ratio
ζ_d	Distortional distribution factor
ζ_i	Model damping ratio
θ	Rotation about the longitudinal axis (pitch)
θ_x	Twisting angle due to St. Venant torsion
θ'_x	Rate of twist
θ_y, θ_z	Rotations about the y and z axis
Ω_k	Spatial frequency
Ω_i	Twice the enclosed area of the i^{th} cell
$\Gamma(.)$	Gamma function
ν	Poisson's ratio
μ_t	Torsional warping shear parameter
$\{\bar{\sigma}\}$	Generalized stress vector
$[\bar{\sigma}_{\mathrm{b}}]$	Generalized stress vector for bending
$\{\bar{\sigma}_{\mathrm{d}}\}$	Generalized stress vector represents the distortional stress resultants
$\{\bar{\sigma}_{\mathrm{t}}\}$	Generalized stress vector represents the torsional stress resultants
$\sigma_{x,b}$	Longitudinal bending stress

σ_I	Torsional warping stress
σ_{II}	Distortional warping stress
ρ	Mass density of the material
ω	Measured circular eigen frequency
ω_I	Unit torsional warping function
ω_{II}	Unit distortional warping function
$\hat{\omega}_I$	Unit torsional warping function or reduced sectorial coordinate for a closed section
$\hat{\omega}_{IB}$	Unit torsional warping of a closed section with respect to pole B

CHAPTER 1

INTRODUCTION AND LITERATURE REVIEW

1.1 INTRODUCTION

The numbers of vehicles in cities all over the country have risen by a substantial margin and inevitably the traffic flows have increased dramatically. In consequence, traffic congestion and slow driving vehicles speed have become very serious problems. The primary reasons for increased popularity of curved girder bridges were the increased demand for curved roadway alignment for the smooth dissemination of congested traffic along with advancement in fabrication and erection technology. The construction of curved box girder bridges in interchanges of modern highway systems has become popular for economic, aesthetic, and environmental factors. The actual curving of girders has allowed greater span lengths, fewer piers, and more aesthetically pleasing structures than straight girders used as chords in forming a curved alignment. The curved box girder bridges, in fact created new design challenges for engineers.

Curved box girders have found wide application for modern highway bridges and interchanges in large urban areas mainly for their high torsional rigidity and high stiffness-to-mass ratio. Due to geometric complexities, in addition to experiencing conventional structural action, that is, extension, flexure and torsion, cross-section of curved box girders may warp out of the sectional plane and distort in the cross-section. The shear lag effect may also be significant in wide flange cross-sections and should be considered in the design.

A three-dimensional finite element analysis can, of course, offer the most comprehensive treatment for such structures. It can readily take into account a variety of structural geometries, supports and loading conditions, and has made possible the accurate assessment of structural effects. However, such an analysis involves very extensive computations leading to expensive computing costs and in some cases to voluminous computing output. However, at the preliminary analysis and design stage, it is likely to be impractical to conduct a full three-dimensional analysis, since the bridge geometries and loading conditions, etc. could be modified for instance. It is, therefore, desirable at this stage to use a realistic but simplified method of analysis, which is both reasonably accurate and economic. The adoption of such an element for analysis is one of the primary objectives of this thesis.

The bridges are traversed by heavy and high speed vehicles and the problem of vehicle-bridge interaction becomes an important subject for the bridge analysis. The interaction of vehicles and the structures, which they traverse have been studied by many investigators. In particular, attention is paid to vibrations that might affect the durability of the bridge structure and to safety and comfort of passengers. It is therefore necessary to adopt a mathematical model to be able to describe the dynamic behavior of the supporting structure and vehicles in terms of interaction systems. A moving vehicle on a bridge generates deflection and stresses that are generally greater than those caused by the same vehicular loads applied statically. Vehicles are complex structural systems with combinations of wheels and body connected by suspension elements. The shock and vibration caused by surface unevenness are transmitted from wheels to the super structure of vehicle through the suspension system. The vertical irregularities of surface in longitudinal and transverse directions induce heave, pitch, roll, yaw and axial motions in the vehicle.

Bridge vehicle vibration is a complex phenomenon governed by a large number of different parameters such as characteristics of vehicle (number of axles, axle spacing, axle loads, damping provided by the shock absorbers and the internal friction in springs), characteristics of bridge structure, such as bridge geometry support conditions, mass and stiffness distribution, vehicle speed, profile of the bridge deck, the number of vehicles and their path.

In design practice of bridges, the dynamic effect caused by the fluctuating component induced by the moving vehicle is taken into consideration by increasing the live load by a factor termed as impact factor. Although it simplifies the procedure of design, the true behavior of bridge subjected to moving loads with various characteristics is not reflected at all. As such, coupled vehicle-bridge dynamic problem needs to be considered to obtain the design coefficients for various stress resultants in a curved box-girder bridge.

Bridges are susceptible to repetitive vehicular loads. The structural components within a bridge system are subject to fatigue. Structural fatigue can be defined as the process of accumulation of damage due to application of time varying stresses. It can be expected to occur whenever a structure is subjected to time varying loads and in many situations may govern the design. Fatigue behavior is also an important consideration in the determining the condition of bridge structures subjected to cyclic loads. Specifically, the expected life of the highway bridge subjected to random, variable-amplitude traffic cycles are highly dependent upon damage accumulation caused by various fatigue mechanisms. Each time a load cycle is applied, an incremental amount of damage occurs. This damage is cumulative in nature and accumulation continues till the failure occurs. A vital need thus exists in rapidly and

accurately determining the amount of fatigue damage sustained by bridge superstructures by direct or analytical method.

The fatigue provisions in the codes of practice for the design of bridges do not explicitly consider the stresses induced in the bridge components due to dynamic interaction with the moving vehicles. Specifically, the expected life of the highway bridge subjected to random, variable-amplitude traffic cycles are highly dependent upon damage accumulation caused by various fatigue mechanisms. The fatigue of the bridge components is usually a result of high cycle fatigue where stress level is much lower than that is required to cause failure under static condition. The present study has been undertaken to evaluate the fatigue damage of horizontally curved bridges from vehicle induced stress history.

1.2 LITERATURE REVIEW

Literature review has been presented in five sections. First section discusses the works done by various researchers to gain understanding of structural action of thin-walled members. Second section provides reviews of the published works on the analysis of thin-walled box-girder bridges using finite element method of analysis. Third section reviews the works of past investigators on the free vibration analysis of thin-walled box-girder bridge. Fourth section provides a survey of the works done on vehicle-bridge interaction problems, modelling of vehicle and categorization of pavement roughness. Fifth section furnishes the review of the previous works on the assessment of fatigue life by using different approaches and their applications in different fields of engineering.

1.2.1 Structural Action of Thin-Walled Members

Thin-walled beams have been widely used in engineering applications because of their high stiffness-to-mass ratio. In particular, thin-walled beams with closed cross-sections are very important structural elements when high torsional and bending rigidities are required. For instance, most load carrying members in automobiles and airplanes are made of thin-walled closed beams. The most popular use of thin-walled structures in civil engineering is found in medium and large span bridges in which box-girders are frequently used to support the load. The primary advantage of box-girder construction lies in its high torsional stiffness. It is a necessary quality of a large span bridge where heavily loaded traffic lane produces eccentric live load effect on the bridge. Further, in case of curved box-girder, warping and distortion of the cross-section occurs besides conventional structural action such as extension, flexure and torsion.

Vlasov (1961) has presented a rigorous theory for thin-walled beams. In order to explain torsional warping, Vlasov divided torsional moment into pure and warping components, which correspond to the St. Venant shear stresses and torsional warping shear stresses respectively. Vlasov introduced a new type of force termed ‘bimoment’ and defined additional functions of the properties of a section termed as the sectorial coordinate and the torsional warping moment of inertia.

Based on Vlasov’s thin-walled beam theory, Waldron (1985) presented a method for the analysis of circular curved single cell beams. Member curvature and secondary shear deformation effects were fully taken into account. Suitable geometrical and sectorial functions were derived to describe the transverse distribution of stress in curved, thin-walled box girders subject to generalized loading. A strain

energy approach was adopted to obtain member flexibility matrix, and included the effects of torsional warping.

Waldron (1987) presented again an equivalent beam method of analysis for thin-walled beam structures. He incorporated the effect of torsional warping by the addition of an extra degree of freedom representing the action of warping restraint.

The issues related to both torsion and distortional were addressed by Heins and Oleinik (1976) where they analyzed single and continuous curved box-girder bridge subjected to varying loads. The bending and torsional distortions as well as cross-sectional distortions were determined throughout the box-girder. The forces that were determined included bending moment and shear, pure torsion, warping torsion, and bi-moment. The stresses related to all the forces were also determined.

Turkstra and Fam (1978) carried out numerical investigation of single-cell curved box-girders to show the effect of curvature, number of diaphragms and web spacing under eccentric and uniform loads. It was shown that the importances of warping and distortional stresses were important in relation to the longitudinal normal bending stresses as obtained from curved beam theory.

The problem of distortion in thin-walled box-spine beams was elaborately discussed by Boswell and Zhang (1984). The distortion of a cross-section was characterized by a single representative parameter termed the ‘distortional angle’, and appropriate functions of this parameter were used as the degrees of freedom in a finite element representation. The basic differential equation for distortion was also derived. Derivations of expressions to obtain the distortional normal and shear stresses in a thin-walled section were also presented. The interaction between bending, torsion and distortion was discussed.

Kermani and Waldron (1993) developed an equivalent beam method of analysis for the thin-walled beams to include the effects of warping torsion and distortion in addition to the more familiar actions of bending moment and torsion. However, the method was applicable to only straight single cell box girders with at least one axis of symmetry.

Boswell and Li (1995) considered the relationships between torsional warping, distortional warping for the analysis of thin-walled beams. Numerical problems were solved for a thin-walled beam with both open and closed cross-section profiles.

In the elementary theory of bending, it is assumed that the cross sections of a girder, which is plane before bending remains plane after bending. However, for a girder with wide flange such as box girders, this assumption is not always justifiable. The longitudinal stresses in flanges of wide-flange beams are distributed non-uniformly throughout the flange width. The stresses are maximum at the edge and decrease towards the centre and therefore can not be obtained accurately from the elementary bending theory. To account for this effect (often termed as shear lag), the evaluation of stresses for the design of such wide-flange beams, the effective width concept is generally used. Extensive investigations on the shear lag effect were carried out by researchers over the years.

Jonsson (1999) also presented a rigorous treatment for the distortion of thin-walled beams. A general differential equation was derived for the determination of axial warping displacements of thin-walled beams from in-plane distortional displacements. The methods for calculation of torsional shear flows, flexural and torsional warping shears were generalized to include distortion. However, the distortional warping functions were determined neglecting the effect of shear lag.

Moffat and Dowling (1975) studied the shear lag phenomenon in steel box-girder bridge by means of the finite element analysis. From the result so obtained, design rules based on the effective width concept were formulated. Thus, in designs, the shear lag effect was indirectly considered utilizing the concept of effective flange width.

Hasebe *et al*. (1985) presented the problem of effective width and the shear lag phenomenon of the curved girder bridges. The investigation showed the effect of curvature, load distribution, ratio of width of the flange to span length, and cross-sectional dimensions on the effective width of curved girders.

Maisel (1985) extended the generalized coordinate method developed by Vlasov to account for torsional, distortional and shear lag effects in straight, thin-walled, box beams of uniform section. Single-cell or multi-cell sections with side cantilevers could be analyzed by the method. The method could also be applied to both single span and continuous box girder bridges. However, the suitability of the method was limited to straight box girders only.

Burgan and Dowelling (1990) presented a comprehensive guide to designers for dealing with shear lag problem in structural design. The effect of shear lag on the elastic behavior of box girders was addressed and simple design rules for estimating its influence were described. The method was based on parametric studies using finite element analysis, which was further validated against experimental results.

Tesar (1996) studied the shear lag influence on flexural and torsional behavior of thin-walled box beam bridges using refined technical theory of torsion-bending behavior. Numerical verification of these theoretical approaches was presented.

Luo and Li (2000) investigated the influences of shear lag for thin-walled curved box girders, including longitudinal warping. The longitudinal warping

displacement functions of the flange slabs were approximated by a cubic parabolic curve instead of a quadratic curve of Reissner's method. On the basis of the thin-walled curved bar theory and the potential variational principle, the equation of equilibrium considering the shear lag, bending and torsion (St.Ventant and warping) for a thin-walled curved box-girder were established. The closed-form solutions of equation were derived and Vlasov's equation was further developed. Numerical examples were presented to verify the accuracy and applicability of the method.

Luo *et al.* (2002) conducted two experimental studies on shear lag effect for box-girders with varying depth of cross section and the other for box-girders under simultaneous axial and lateral loads. Three perspex glass models built specifically for research work were used to perform the experiments with the purpose of investigating the shear lag phenomenon of box girders and providing a benchmark for further analytical and numerical studies of shear lag effect. Finite element analysis was also conducted to check the accuracy of the numerical methods in predicating shear lag effect in these two situations. In general, the experimental results matched reasonably well with the numerical predictions.

Wu *et al.* (2003) presented an initial value solution of the static equilibrium differential equations of thin-walled box beams considering both shear lag and shear deformation. This solution was used to establish the related finite element stiffness matrix and equivalent nodal force vector.

In general many researchers developed closed form theory for thin-walled open as well as closed box-beam section. However, it is appreciated that the thin-walled beams with closed cross-sections are very important structural elements when high torsional and bending rigidities are required. While a few researchers have not included all the complex structural actions of thin-walled beams with closed cross-

sections in their analysis, the procedures developed based on closed-form solutions of Vlasov's (1961) theory considered adequately all such important components like torsion, torsional warping, distortional and distortional warping.

1.2.2 Finite Element Method of Analysis of Thin-Walled Box-Girder Bridges

Different numerical methods of analyses of thin-walled box bridge include analysis of box beams using Finite strip method and Finite element method. The finite strip method may be thought of as a special form of the finite element method. It approximates the behavior of each plate in a box bridge by an assemblage of narrower longitudinal finite strips.

The analysis of slab bridges by the finite strip method was first attempted by Cheung (1971). In addition, a curved strip was applied by Cheung (1969) to the solution of curved bridges decks. The spline finite strip was also used to analyze various type of bridges. Initially, Fan (1982) analyzed straight slab and box-girder bridges. Li *et al.* (1988) carried out analysis based on the curvilinear coordinates system. The spline finite strip method was extended to the elasto-static analysis of circular and non-circular box-girder bridges. Abdullah and Abul-Razzak (1990) applied finite strip method to the analysis of a pre-stressed concrete box-girder bridge using higher order bending and in-plane strips. The higher order finite strip gave good results for the analysis of both simply supported and continuous pre-stressed box-girder bridges.

The analysis of thin-walled box-girder bridges has been a focus of attention for many investigators in recent years. Various theories and analytical methods have been developed. The finite element method of analysis is generally recognized as the most versatile technique for the analysis of box bridge deck structures. During the past two decades, the finite-element method of analysis has rapidly become a very popular

technique for the computer solution of complex problems in engineering. Nowadays a logical alternative for modeling curved box girder bridges is to combine finite element technique with thin-walled beam theory to develop one dimensional thin-walled box beam elements. Several investigators have combined thin-walled beam theory of Vlasov (1961) and finite element technique to develop a thin-walled box beam element for elastic analysis of straight and curved box bridges.

Fam and Turkstra (1975) introduced finite element scheme analysis of box bridge with orthogonal boundaries and arbitrary combinations of straight and horizontally curved sections. A variety of special purpose elements were developed to suit the behavioral characteristics of thin box sections.

Mikkolo and Paavola (1980) conducted a finite element analysis for rectangular single-cell box-girder with side cantilevers. Shape functions are represented by cubic polynomials in each element as in the finite element solution of beam problems. It was observed that the known displacement functions describing the deformation modes of the cross-section must be chosen in advance for each type of cross-section. Thus, difficulties exist in extending the method for more complicated or more general types of cross section. It was observed that the method presented by them was applicable only in the case of single box cell.

Gunnlaugsson and Pedersen (1982) developed a finite element formulation considering seven degrees of freedom at each node for beam with thin-walled cross-sections. They presented calculation of stresses and deformation of beam with different types thin-walled cross-sections.

Zhang and Lyons (1984) developed a thin-walled box beam finite element, applicable for the analysis of box girder bridges. They considered only one distortional mode and the effective width concept was used to include shear lag effects. In

contrast to conventional beam formulation, warping and distortional effects which were essential for the analysis of box beam formulation were included in the thin-walled beam element formulation. They included three extra additional degrees of freedom for thin-walled box beam finite element of curved bridge. These additional degrees of freedom were the rate of change of twisting angle, distortional angle of the cross-section and the rate of change of distortional angle. The thin-walled box beam element could be used effectively for static analysis of single or multi-cell box beams curved in space and subjected to general loading conditions.

Boswell and Zhang (1985) presented the results of experimental investigation of the behavior of four types of thin-walled box beam and compared the results with those obtained from the specially developed thin-walled box-beam finite element theoretical analysis. The behaviors of the individual models were studied, with particular attention being given to the torsion and distortion of the box-section, the cross-sectional distributions of the longitudinal and transverse bending stresses and the deflection.

Hsu *et al.* (1990) developed a more exact horizontally curved beam finite element in which the true warping degree of freedom conforms to the bi-moment (warping). The variational method was used to formulate the stiffness matrix in an explicit form.

Shanmugam and Balendra (1991) described an experimental and theoretical study of the behavior of multi-cell structures curved in plan. They made perspex models of multi-cell box-girders that were curved in plan. The results of eight tests on two perspex models of different span/radius ratios subjected to different loading conditions were presented. The experimental results were compared with theoretical

values obtained by employing the finite element method and good agreements between the results were demonstrated.

Razaqpur and Li (1994) used Vlasov's thin-walled beam theory combined with special shear lag warping function to derive a box beam finite element for curved thin-walled box-girder bridge with exact shape functions that could be used to analyze single and multi-cell box girders.

Paavola (1992) developed a numerical model for analyzing thin-walled girders. The theory was based on the conventional idea of Vlasov developed originally for torsional problems of thin-walled girders with closed cross-sections. This idea was combined with the finite element method. The effect of torsion, distortion, torsional and distortional warping were included in the analysis.

Kim and Kim (1999) proposed a new C_0 –continuous displacement-based box beam finite element for straight box bridges. Direct kinematic variables representing torsion, warping and distortion were used for both static and dynamic analysis.

Kim and Kim (2002) formulated a one-dimensional beam theory for the analysis of thin-walled curved box beams under torsion and out-of-plane bending. In addition to the conventional three kinematic variables, two additional variables representing warping and distortional deformations of a beam cross section were included in the present theory

Yaping *et al.* (2002) presented a finite curved beam element method of analyzing of curved thin-walled box-beam bridge based on the energy principle. The analysis considered both shear lag and warping torsion effects.

Park *et al.* (2005) proposed the expanded method for exact distortional behavior of multi-cell box-girder subjected to eccentric loadings. This method decomposes the eccentric loading into flexural, torsional and distortional forces by

using the force equilibrium. Based on the method, a thin-walled box beam finite element, which could be applied to practical distortional analysis of straight multi-cell box girder bridges, was also developed. The box beam element possessed nine degree of freedom per node to consider each separate behavior of multi-cell box girder. The validation of the box beam element was demonstrated through a series of comparative studies using a conventional shell element proposed by other researchers.

Desantiago and Mohammadi (2005) presented a simple three dimensional finite-element analysis for a series of single span horizontally curved bridges. The analyses were carried out using a typical truck load and also the dead load of the bridge as the primary force on bridges. In each analysis, the behavior of bridges was investigated, and the major internal forces developed in members were determined. Specifically, an increase in the bending moment and the existence of a torsional moment were observed for the cases, where the horizontal angle of curvature was large.

Thus, it has been observed that a large number of finite elements were developed by different researchers for the analysis of box girder bridges. While a few of them were not completely robust in the representation of all the complex actions of a curved box girder bridge, the three noded 1D beam element by Zhang and Lyons (1984) with nine degrees of freedom at each node was observed to be very well representative of the structural actions and computationally efficient. While, shell elements were considered for the accurate analysis of such curved box-girder bridge, the total number of degrees of freedom with shell elements would be much higher in comparison to the 1D idealization considered by Zhang and Lyons (1984). The main advantage of such idealization in the analysis would be to reduce unnecessary computational cost such as during preliminary design stages, where a full three-

dimensional analysis would be unnecessary, the effect on computational time requirement will be more pronounced when forced vibration studies (e.g. vehicle induced vibration) are carried out. Thus it is observed that while accurate estimation of responses are obtained using the 1D beam element, the idealization leads to a computationally less expensive procedure in comparison to the analysis using standard finite elements (e.g. shell). In view of this, it has been proposed to introduce 1D beam element by Zhang and Lyons (1984) in the present study.

1.2.3 Free Vibration of Thin-Walled Box-Girder Bridges

The studies of free vibrational characteristics of thin walled box girder bridges have been carried out by many researchers since modal characteristics are important for understanding the dynamic response behaviour of a structure.

Culver (1967) obtained the exact solution for the equations governing the free vibrations of simply supported horizontally curved beams leading to the evaluation of natural frequencies of the horizontally curved beams.

Petyt and Fleischer (1971) investigated three finite element models for determining the radial vibrations of curved beams. One of these was then used to investigate the variation of the six lowest natural frequencies of beams with subtended angle. Simply supported, hinged and clamped end conditions of the curved beam were considered.

Yoo and Fehrebach (1981) derived a general matrix formulation to determine the natural frequencies of curved beam. The warping contribution and rotary inertia effect with respect to flexure and torsion were included.

Mukhopadhyay and Sheikh (1995) investigated the large amplitude free flexural vibrations of horizontally curved beams using finite element approach.

Yoon *et al.* (2005) presented the finite element formulation for free vibration analysis of horizontally curved steel I- girder bridges. Stiffness as well as mass matrices of both the curved and straight beam elements were formulated. Each node of both of them possessed seven degrees of freedom including the warping degree of freedom.

Fam and Turkstra (1975) dealt finite element scheme for static and free vibration analysis of box bridge with orthogonal boundaries and arbitrary combinations of straight and horizontally curved sections.

Lees *et al.* (1976) calculated the natural frequencies and mode shapes of a number of box beams using the finite element displacement methods. Both the in-plane and transverse motion in the vibrations of box beam were presented.

Tabba and Turkstra (1977) examined the problem of free vibrations of curved thin-walled girders of non-deformable asymmetric cross-section. The general governing differential equations were derived for quadruple coupling between the two flexural, tangential and torsional vibrations. A parametric study was conducted to investigate the effect of relevant parameter on natural frequencies. Eigen functions satisfying the orthogonality condition were given. The solution derived herein for the general case was also shown to cover a variety of special cases of straight and curved girders with doubly symmetric or singly symmetric cross-sections.

Shanmugam and Balendra (1986) described dynamic analysis for free vibration characteristics of multi-cell structures by using the simplified grillage technique. Comparisons of the results were obtained for structure with different boundary

conditions with those obtained by the finite element method. The effect of the natural frequencies was also investigated.

Noor *et al.* (1989) developed the simple mixed finite element models for free vibration of thin-walled beams with arbitrary open cross section. The analytical formulation was based on Vlasov's type thin-walled beam theory, which included the effect of flexural-torsional coupling, the additional effects of transverse shear deformation and rotary inertia. The high accuracy and effectiveness of the mixed models developed were demonstrated by means of numerical examples of thin walled beams with symmetrical and unsymmetrical cross-section.

Snyder and Wilson (1992) presented a closed form solution for the out-of-plan free vibration frequencies of horizontally curved thin-walled beam which was continuous over multiple supports. The bending and twisting of this beam was coupled in the mathematical model used. This coupled bending/twisting behavior caused two free vibration frequencies to be associated with each vibration mode shape.

Kou *et al.* (1992) presented the free vibration analysis of continuously curved girder bridges, based on the direct stiffness method, which included warping and adopting lumped mass matrices. The results obtained were compared with results based on other theories.

Stavridis and Michaltsos (1999) proposed for the evaluation of the eigen frequencies of a thin-walled beam curved in plan for transverse bending and torsion mode with various boundary conditions. The static differential equations for curved thin-walled beams using established Vlasov theory were appropriately extended and treated through the introduction of four dimensionless geometric quantities.

Yoon *et al.* (2006) investigated new equation of motion governing dynamic behavior of thin-walled curved beams. Explicit numerical expressions were derived to

predict the complex dynamic behavior of the thin-walled curved beams. Stiffness as well as mass matrices of the curved beam elements for finite element analysis was formulated to allow explicit evaluation of the dynamic behavior. Each node possessed seven degree of freedom including the warping degree of freedom. They included comparisons of the natural frequencies of the thin-walled curved beams from the finite element formulations with those reported by other investigators.

. The literature survey showed that a good deal of effort had been put forward by past researchers on the evaluation of modal parameters of box-girder bridges using different techniques. While some researcher carried out free vibration analysis based on closed form solution, a few conducted finite element analysis without considering torsion and torsional warping, distortional and distortional warping effect in the analysis. Since natural frequencies are important parameters to be considered in design, especially for checking the safety of bridge under dynamic excitation, use of appropriate finite element formulation is necessary to accurately predict the same. It is also desired to use a computationally efficient model which can represent all complex structural actions in a horizontally curved thin walled box girder bridge. In the present study, the thin-walled box beam finite element developed by Zhang and Lyons (1984), which is computationally efficient as well as reasonably representative of thin-walled box girder behaviour have been considered for the free vibration analysis of thin walled box girder bridges. However, as per the records available, this element has not been used for the dynamic analysis. Laboratory vibration testing of thin walled curved box girder bridge model is one of the ways to validate the theoretical model and to accept its applicability for further use. Thus, in the present work, experimental free vibration analysis has also been conducted on a Perspex sheet model of the curved

bridge to validate the natural frequencies and mode shapes of the theoretical bridge model.

1.2.4 Vehicle-Bridge Interaction

The determination of dynamic response of bridges due to the passage of moving vehicles is a problem of considerable interest. In particular, the interaction problem between vehicles and bridge structures makes the dynamic analysis very complex and accurate estimation of dynamic loads acting on a structure is very important for structural design and control. To understand the phenomenon and to develop rational design procedure, a number of different approaches can be found throughout the literature, most of them attempting to improve the analytical model of the physical interaction between the bridge and vehicles moving over it. The moving vehicle loads are space and time-dependent, because the position of wheel loads change with time and the suspension of vehicle oscillates, due to irregularities of the bridge deck and vertical displacement of bridge deck under tires. In design practice, usually the static load is increased by an impact factor to account for the dynamic effect of load. The impact factor is usually specified by formula based on the length of the bridge in most of the bridge codes. However, this method of design does not include the effects of various factors such as the type of bridge, speed, bounce, mass distribution, suspension characteristics of the vehicle and the profile of the bridge surface.

Fybra (1972) outlined a detail procedure for calculating the response of structure subjected to moving mass. Analytical solutions for the single span and continuous span beam and simply supported isotropic plate were obtained by time domain and frequency domain method. Transformation techniques were used to

convert differential equations to algebraic equations in most of the problems discussed.

Fleming and Romualdi (1961) analyzed the dynamic response of single span and three span continuous highway bridges to transient loads. An analogous mathematical model was considered and the appropriate equations of motion were solved on a digital computer. Several specifics cases were analyzed to evaluate the effect of load characteristics and bridge geometry on highway bridge impact.

Tan and shore (1968) presented a method of analysis for investigating the dynamic response of an identical horizontally curved bridge under the passage of a force system consisting of masses that simulate a vehicle.

Gupta and Rupert (1980) studied the highway bridges that were subjected to time-dependent forces when traversed by moving load. These time dependent forces were affected by several parameters of the bridge and vehicle. They made a systematic and more comprehensive study to determine the effects of vehicle braking on the bridge response. In cases, where the vehicle motion was not uniform but subjected to acceleration or braking, a redistribution of axle loads took place. This results from horizontal internal forces exerted on the system in addition to the other loading components.

Green *et al.* (1995) studied the effects of heavy vehicles with leaf spring and air spring suspension on the dynamic response of short-span highway bridges. The dynamic responses of bridges were calculated by modeling the bridge and the vehicle separately and combining the modes with an iterative procedure. The bridge model was obtained by combining mode shapes with dynamic wheel loads in a convolution integral. This bridge calculation procedure was validated by experiments on two highway bridges. The validated, nonlinear models consist of a leaf-sprung, four axle

articulated vehicle, and a similar vehicle fitted with air suspension and hydraulic dampers. These two vehicle models were combined with three different bridge models to predict dynamic responses.

Jagmohan Humar and Ahmed (1995) studied the bridge vehicle response considering a single sprung mass moving along the deck, which was idealized as rectangular isotropic plate. The plate was discretized as finite elements and the nonlinear equations were solved by numerical integration. The objectives of their study were to identify the parameters governing the response of isotropic plate models and to examine the nature of the dynamic response of the models to central and off-central vehicles.

Michaltsos *et al.* (1996) carried out linear dynamic response of a simply supported uniform beam under a moving load of constant magnitude and velocity by including the effect of its mass. They used a series solution for the dynamic deflection in terms of normal modes. The individual and coupling effect of the mass of moving load, its velocity and other parameters were studied. It was observed that the bridge deflection increased at higher velocity with increase in the ratio of vehicle mass to bridge mass.

Henchi *et al.* (1998) proposed a general and efficient method for the solution of the dynamic interaction problem between a bridge, discretized by a three-dimensional finite element model, and a dynamic system of vehicles running at a prescribed speed, using the central difference scheme to solve the coupled equation system. They suggested that fully coupled method takes less computational time than the uncoupled iteration method and it showed close agreement with the result of published literature on uncoupled method.

Munirudrappa and Dhruvaraja (1999) studied the dynamic analysis of highway bridges. They idealized the bridge as a continuous beam with discrete masses being lumped at the nodal points. The road surface irregularities were assumed to be in sinusoidal form. The variation of bending moment, shear force and deflection with time were investigated for some typical bridges. The influence of shallow area of settlement in bridge approach was also examined for impact factors.

Sasidhar and Talukdar (2003) studied the response of a girder bridge induced by vehicle traveling at variable speed. The deck unevenness was considered as the realization of homogeneous random process described by power spectral density (PSD) function. The response of the bridge and vehicle was obtained using Monte Carlo simulation technique. A detailed parameter study was conducted to examine the effect of variable speed, deck unevenness and suspension characteristics on the dynamic amplification factor of the bridge response.

Kwasniewski *et al.* (2006) presented results of the finite element analysis of dynamic interaction between a heavy truck and a selected highway bridge on US 90 in Florida. Several static and dynamic field tests were performed on the same bridge. The experimental data was used for validation of the FM models of the bridge and the truck.

Green and Cebon (1994) developed a procedure to predict the dynamic response of bridge to a given set of vehicle loads. The method involved in convolution of the vehicle loads with modal responses of the bridge. The convolution integral was solved by transforming to the frequency domain using Fast Fourier transform (FFT). The method was then extended by an iterative procedure to include dynamic interaction between the bridge and an arbitrary model of vehicle

Henchi *et al.* (1997) studied the dynamic response of multi-span structure under convoy of moving loads. They developed a dynamic model coupled with a FFT algorithm. The model was highly efficient for calculation of the response of bridges under multi-axle moving forces. They presented dynamic amplification factor as a function of the speed of moving loads.

Vibrational behavior of simple-span highway girder bridges induced by heavy truckload was studied by Chang (1994). The surface unevenness was considered as the main source of bridge vibration under moving load. The dynamic characteristics of bridge response were investigated in the time and frequency domains. The studies concluded that the impact factor used in current design codes was underestimated with rough deck profiles. They suggested an impact factor based on span length, surface roughness and vehicle speed.

Chatterjee *et al.* (1994) investigated the dynamic behavior of multi-span continuous bridges under a moving vehicle load, by considering the effect of interaction between the vehicle and the bridge pavement, the torsion in the bridge due to eccentrically placed vehicle and the randomness of the surface irregularity of the pavement. The responses of the bridge was obtained in the time domain by using an iterative procedure employed at each time step to take into account the nonlinearity of the pavement vehicle interactive force. The solution procedure was made efficient by utilizing a continuum approach for determining the eigen functions of the bridge deck and by obtaining the deck response at each iteration.

Yang (1995) developed a set of formulae for simple supported and continuous beams subjected to moving loads. They adopted a non-dimensional speed parameter, involving driving frequency of the vehicle, length of bridge and vehicle speed. They concluded that the impact factors for the deflections, bending moments, and shear

forces at mid span were linearly proportional to the speed parameter and were multiplied by certain modification factors to yield results for continuous beams and supports.

Mermertas (1998) presented vehicle-bridge interaction for a vehicle on simply supported curved bridge deck considering the effect of vehicle speed and guide way parameters. In the dynamic model, the vehicle was considered to have four-degree of freedom, with lumped masses, linear springs and dampers. The finite element method was used for solving the governing differential equation of the vehicle-bridge system.

Senthilvasan *et al.* (2002) compared experimental investigation results for dynamic response of curved bridge under moving truckloads with the design code predictions as well as with those obtained from computer simulated model.

Inbanathan and Wieland (1987) presented dynamic response of a simply supported box girder bridge due to a vehicle moving across the span. The effect of the randomly varying dynamic force generated by the vehicle moving over a rough bridge deck was considered in the analysis.

Galdos *et al.* (1993) presented the dynamic impact factors of horizontally curved steel box girder bridges. Static and dynamic bridge behavior was studied under several truck loading. A rational methodology for determining the impact factor was developed and alternate impact factor criteria were proposed to replace the current AASHTO specification and the Ontario highway bridge design code.

The dynamic characteristics of box girder bridges were mostly carried out by Huang *et al*. (1995, 2001). Initially they carried out the bridge model as I-girder bridge and later improved to box-girder bridges. They developed a procedure for obtaining the dynamic response of thin-walled box girder bridges due to truck loading. The box

girder bridge was divided into a number of thin-walled beam elements. Both warping torsion and distortion were considered in their study. The model of vehicle used was the AASHTO HS20-44 truck simulated as a nonlinear vehicle model with 11 independent degrees of freedom.

Sennah *et al.* (2004) presented a method for determining the dynamic impact factors for horizontally curved composite single or multi-cell box-bridges under AASHTO truckloads. The bridges were modeled as a 3-D structures using commercial available software.

Lee and Yhim (2005) conducted three-dimensional dynamic analysis of long–span box-girder bridges subjected to moving loads, using four node Lagrangian and Hermite finite elements. The numerical results have shown good agreement with the experimental data from an existing two-span prestressed concrete box-girder bridge under moving vehicles.

A bridge is subjected to a variety of vehicular loading. The vehicle has been modeled with different degree of complexities. Choices concerning vehicle type and characteristics are quite important for accurately predicting bridge loads and deflections. For the purpose of dynamic analysis, a vehicle is assumed to be composed of a body, wheel with tires and suspension system. There are a variety of configurations, including a truck with or without trailer and different axle loads and spacing.

Hino *et al.* (1984), Green and Cebon (1997) and Lu Sun (2001) considered single/double degree of freedom vehicle model crossing a simply supported bridge. The vehicle model included wheel-hop and pitch modes of vibration. The study was useful to understand the behavior of simple bridge under dynamic moving load.

Mermertas (1998), Yang and Wu (2001) and Zhu and Law (2003) studied vehicle induced vibration of bridges. The vehicle model was considered to have four-degree of freedom consisting of heave motion in vehicle body, two-wheel tyre and pitch rotation in vehicle body. The studies were focused on simply supported curved bridge decks or continuous beam. The heave-pitch and heave-roll models incorporate the interaction between two modes at a time and are more complete in comparison to the previous study.

Huang and Wang (1992), Yadav and Upadhyay (1993), Henchi *et al.* (1998), Tan *et al*. (1998), Marchesiello *et al.* (1999), Piombo *et al.* (2004) and Zhu and Law (2005) studied the dynamic response of bridges or railway track with three-dimensional vehicle model. The vehicle model was represented by a rigid body motions, including pitching and rolling rotations. At each of the axle locations, there were vertical degrees of freedom, which relate the forces and displacements between vehicle body, suspension systems and tires. In total, there was seven degree of freedom in the vehicle model: vertical displacement of the chassis centre (bounce), pitching and rolling rotations about the two axes of the chassis and four vertical displacement of wheel tyres at each of its axle locations.

Huang *et al*. (1995, 2001) used vehicle model that were AASHTO HS20-44 truck tractor and trailer type with eleven independent degrees of freedom. The model consists of five sprung masses which were tractor, semi trailer, and three wheel/axle sets. The tractor and trailer were individually assigned three degree of freedom corresponding to the vertical displacement, rotation about the longitudinal axis (roll), and rotation about traverse axis (pitch). Each wheel set was provided with the one vertical displacement and one rotation angle.

The bridge deck unevenness causes moving vehicles to pick up dynamic excitation, which in turn imposes oscillatory loads on the deck. The analyst needs to choose an appropriate model for the deck roughness. Attempts have been made to model the roughness in terms of statistical parameters form profile measurements of a large number of road or bridge surfaces.

Shinozuka (1971) presented an efficient and practical method of simulating multivariate and multidimensional process with specific cross-spectral density. When the cross-spectral density matrix of an n-variant process was specified, its component process could be simulated as the sum of cosine function with random frequencies and random phase angle. A homogeneous multidimensional process could also be simulated in terms of the sum of the cosine functions with random frequencies and random phase angle.

Dodds and Robson (1973) showed that typical road surfaces could be considered as realization of homogeneous and isotropic two-dimensional Gaussian random processes. The complete description of the roughness was provided by single auto correlation function evaluated from longitudinal profile.

Honda *et al.* (1982) showed that power Spectral Density (PSD) of pavement profile was related to parameters called roughness and waviness index. These parameters could shift the roughness level up and down and thus guidelines for classification of roads in terms of roughness were framed.

The effect of time dependent forces on bridges was studied by Coussy *et al.* (1988).The authors analyzed the influence of surface irregularities on the dynamic response of bridges by modeling the surface irregularities using PSD function. The analysis was carried out in frequency domain.

Marcondes *et al.* (1991) proposed a model of relationship between pavement PSD and parameter called International Roughness Index (IRI). In order to establish the relationship, spectral analyses of different measured profiles were carried out whereas IRI was computed using mathematical model of quarter car simulation.

The surface irregularity of the bridge pavement was considered by Chatterjee *et al.* (1994) as a random process characterized by a power spectral density function (PSD) of the irregularity. The irregularity profile of the bridge pavement was synthetically generated from PSD using Monte Carlo simulation technique.

The effect of random road surface roughness and long-term deflection of the prestressed concrete bridge on the impact effect due to moving vehicles were investigated by Au *et al.* (2000). The generated random road surface roughness was described by zero-mean stationary Gaussian process, which was employed in their study.

The passage of vehicles over the bridge induces its self weight in addition to dynamic tyre force resulted from the vibration of vehicles due to unevenness of the deck. The horizontally curved thin walled section bridge girders present more complicated structural action, where bending and torsion due to moving loads are coupled resulting in transverse and lateral deformation accompanied by warping as well as distortion of girder cross section. Unlike straight bridges, the horizontally curved bridges are additionally loaded due to centrifugal thrust, which are liable to affect the dynamic characteristics of the bridge. Initially many researchers calculated the response of structure subjected to moving mass only without coupling of vehicle motion with the bridge. Although, this assumption is appropriate for the case where ratio of bridge/vehicle mass is very high. In modern long span slender bridges, the bridge-vehicle motion has significant role.

Literature survey shows that bridge-vehicle interaction is an important area that attracted various researchers towards analytical and numerical studies. While the literatures on straight girder bridges are abundant, very limited reports on curved box-girder bridges are available, especially on the dynamic behavior of such bridges subjected to random moving loads. It may be noted that the roughness of the bridge deck was considered as the realization of homogeneous Gaussian process in space. This fact was established by experimental observations. However, with the variation of vehicle speed, the dynamic input no longer remains stationary in time although, the source of excitation is homogeneous in spatial domain. Many of the earlier studies on bridge vehicle interaction did not consider the variation of vehicle forward velocity. In other words, the formulation was not general to include the effect of non-stationarity.

1.2.5 Fatigue due to Vehicle Induced Loads

Bridges are subjected to the repeated action of moving load, which may develop fatigue crack and sometimes lead to the failure of a component of a bridge. Fatigue behavior is also an important consideration for the design of bridges subjected to repeated action of moving loads. A vehicle passage over a bridge induces loads, which vary with the time leading to the development of fatigue in the structural member.

The fatigue behaviour of structures were studied by several authors theoretically and experimentally. Bennantine *et. al*. (1990) described the theory of fatigue damage in metallic specimens, where it was customary to study the fatigue strength of the structural member based on constant amplitude fatigue test and the results were represented in the form of S-N curve.

Miner (1945) used S-N curve approach to formulate a linear damage accumulation rule, which enabled one to predict fatigue damage at each incremental stress range. Later on, Miner's linear damage hypothesis has found several applications in studies related to fatigue damage assessment.

Fatigue design criteria based on the S-N curve approach in conjunction with linear damage hypothesis were incorporated in American Association of State Highway and Transportation Official's (AASHTO) guide specification for fatigue of steel bridges (1989), in British Standard Institution's code of practice for fatigue design of steel, concrete and composite bridges (1980), in Indian Railway's bridge rules (1964) and in Indian Road Congress (IRC) specification for road bridges of composite construction(1986) . The drawback of these methods lies on the fact that the charts used are based on constant amplitude fatigue test data, which does not reflect the stress developed in the members due to the dynamic interaction of vehicles with the bridge.

When structures or components are subjected to repeated applications of random forces, as with traffic loadings on the bridge, the number of cycles at which failure occurs are random variables. Dowling (1972) developed statistical cycle counting method for handling the complicated stress cycles induced by the variable amplitude load.

Wirsching and Light (1980) presented a model for predicting high cycle fatigue under wide band random stress processes based on the cycle counting method and a linear fatigue damage accumulation. They also developed a closed form expression for fatigue damage directly from knowledge of the moments of the stress power spectral density. The fatigue damage of wide band model could be obtained from an equivalent narrow band process using a correction factor.

Wirsching *et al.* (1982) conducted a study to develop an engineering model which was used for design purposes to predict metal fatigue under wide band random process. They described Palmgren-Miner's rule and gave a statistical summaries, which provided a description of the performance of the Miners rule.

Lutes *et al.* (1984) presented a stochastic fatigue damage theory to model uncertainty about stress time history. Numerical simulations were performed based on the existence of S-N curves for constant amplitude fatigue.

Lutes and Larsen (1990) conducted study on the variable amplitude fatigue prediction characterizing the stress by power spectral density (PSD) function. Such an approach was found useful when one would need to predict fatigue life without knowing all the details of loading and stress time history. The accuracy of spectral approximation method was tested with rain-flow analysis of simulated time histories of stress for both unimodal and bimodal power spectral density functions. A new spectral method that involved one spectral moment was found to be substantially more accurate than the commonly used Rayleigh approximation method for some situations. The single moment method was significantly simpler than other spectral methods that involved three or four spectral moments. The studies emphasized on the determination of expected rate of fatigue damage using a hypothetical stress spectra of unimodal and bimodal characteristics. This method was not applied in case of real stress spectra obtained in a bridge from the interaction of moving loads.

Repetto and Solari (2001) proposed a mathematical model to derive a histogram of stress cycles, the accumulated damage and the fatigue life of slender vertical structures in along-wind vibrations. The formulation was in closed form based on a probabilistic counting cycle method for narrow band process. The method was suitable to the engineering applications in the structural field.

Gu *et al.* (1999) suggested a method in the mixed frequency-time domain for estimating the fatigue life of steel girders of the Yangpu cable-stayed bridge due to buffeting taking into consideration the effects of wind direction and the background component of the buffeting response on the critical stress. The results showed that the effects of wind direction on the fatigue life of the Yangpu Bridge were significant.

Li *et al.* (2002) examined typhoon induced fatigue damage in steel decks of long span bridge. The strain-time histories at critical locations of deck sections of long span bridges during typhoon passing the bridge area have been investigated by using on-line strain data acquired from the structural health monitoring system permanently installed on the bridge. Continuum damage mechanics model as well as traditional Miner's rule has been employed in the analysis. The results showed that fatigue damage induced by hourly typhoon loading is significantly greater than that for normal daily traffic.

Fu and Cebon (2000) investigated fatigue failure of component subject to random stress histories with bi-model spectral densities. Such spectral densities were often experienced by chassis and suspension component of road vehicles. Some of the methods for predicting fatigue damage using frequency-domain statistics of random stress processes were reviewed.

Bennantine and Tovo (2006) discussed the fatigue analysis of broad-band Gaussian random processes, with attention focused on the distribution of rain flow cycles and the fatigue damage under the linear rule. Several spectral methods were reviewed.

Holmes (2002) has derived closed-form expressions for estimating the upper and lower limits of fatigue life of structures subjected to along wind loading assuming that mean wind speed follows a Weibull probability distribution. The results could be

used for initial calculations to determine whether fatigue under wind loading was a problem that needs to be considered for particular structures avoiding extensive numerical calculations. The theory developed could also be applied to the accumulated fatigue damage from many storms of the temperate synoptic type and to fatigue damage generated in a tropical cyclone event.

Repetto (2005) emphasized the need to establish the bounds of fatigue life as an essential condition in design of structures and illustrated the approach for the case of a wind induced fatigue. This study was devoted to cycle counting methods, starting from the spectral properties of the loading process. Focusing attention on bi-model processes, which were usual in dynamic response of structures, the cycle histograms obtained by the peak and peak-valley counting methods were expressed in closed form.

An alternative way for the fatigue assessment study of the structural members is based on the principles of fracture mechanics, which assumes an initial crack of a certain length and envisages its propagation until it has attained a critical length.

Paris and Erdogen (1963) developed a crack growth model which formed the basis of such study. From practice, it is generally known that a bridge with a fatigue crack can serve for a long time in normal conditions.

Zhao *et al.* (1994) and Ranganathan and Ravi (1994) conducted studies on fatigue reliability of bridge components taking account of the phase of crack propagation.

Illinois Department of Transportation (1992) conducted a study on several steel bridges of various design. The stress range frequency histogram was analyzed to calculate damage incurred by the traffic passing over the bridge. The fraction of life

consumed after 25 years traffic exposure in the cover-plated girder was found to be 6% to 10% of the service life of the bridge. With 10% increase of truck weight and 5% traffic growth, the fraction of life consumed in the same cover plated steel girder increased to as high as 30%. However, the stress magnitude in an element depends on its cross section and the distribution of load, as such the conclusions derived from these studies may not hold good for other steel railway bridges having different structural arrangement and traffic history.

Erzurumlu and Toprac (1972) reported experimental investigation on the fatigue behavior of orthotropic steel bridge decks. Results of fatigue tests on steel orthotropic decks with both conventional and biserrated trapezoidal ribs were presented. In their first phase, test on two types of deck to rib plate welded connections unflanged and flanged ribs, and on two types of rib splices butt joint and diaphragm splices reveal that the unflanged rib to deck plate connection and the butt joint rib splice exhibit satisfactory fatigue strength.

Fatigue behaviour of steel and metal structures is more precisely known to date compared to plain, reinforced and prestressed concrete. The fatigue damage evaluations of steel railway bridges were discussed by Fryba (1996). The observation from the field study conducted on steel railway bridges showed principal bridge elements like main girders endure a higher number stress cycles per year and also include stress cycles in higher stress range classes. The secondary bridge elements and orthotropic bridge deck endure lower number of stress cycles and stress ranges were also lower.

Mohammadi *et al.* (1998) presented the application of field data for condition assessment and prediction of service life of highway bridges composed of steel girders

with reinforced concrete deck slabs. The field stress range data compiled for each bridge was used along with a probabilistic method to estimate fatigue life.

Fisher and Yuceoglu (1981) compiled qualitative data concerning the cracking of 142 steel bridges in the United States and Canada. They identified out-of-plane distortion and large initial defects as the two most common specific causes of fatigue crack development

Hahin *et al*. (1993) conducted studies on fatigue damage of steel bridges in the state of Illinois from the collected field data. The bridges were instrumented with foil strain gauges to determine their frequencies of loading and magnitudes of stresses induced by traffic over a 3-to-8 hour period. They instrumented the fatigue prone section, such as the cover plated wide flanges, for each stress range increment gathered by the data-acquisition system and published the cumulative damage sustained over an extended number of years. They proposed a new equation for factor of safety for welded structures subjected to fatigue

Dicleli and Bruneau (1995) developed fatigue based methodology to assess the reduction in service life of steel bridge due to heavy-permit trucks. It was found that a reasonably large number of special permits can be issued at small reductions in fatigue life, but because stress ranges in excess of the constant-amplitude fatigue limit significantly alter the shape of the S-N curve, it was essential to appreciate that the concept of infinite fatigue life cannot be relied upon anymore.

Agerskov and Nielsen (1999) studied fatigue damage accumulation in steel highway bridge under random loading and compared with experimental results, results of analysis based on fracture mechanics, and results obtained using current codes of practice and specifications.

Li *et al.* (2001) developed fatigue damage model to account for the damage accumulation process in bridge subjected to in-field traffic loading. Fatigue life prediction analyses were made. Good agreements were obtained between the analytical and experimental results.

Dougall *et al.* (2006) focused on the fatigue damage caused in steel bridge girders by the dynamic tire forces that occurred during the crossing of heavy transport vehicles. This work quantified the difference in the fatigue life of a short-span and a medium-span bridge due to successive passages of either a steel-sprung or an air-sprung vehicle.

Huang *et al.* (1993) calculated the fatigue lives of highway steel bridges using a reliability-based methodology. The fatigue life of both non-composite and composite steel beam bridges for different vehicle speeds and classes of road surface roughness were calculated from the generated stress time-histories.

Wang *et al.* (2000) performed truck loading and fatigue damage analysis for girder bridges based on the weight-in-motion data. Fatigue damage analysis was performed according to the Miner's linear damage rule. The studies were conducted based on the hypothesis of fatigue damage accumulation and was well suited for structures, which were in design phase.

Chotickai and Bowman (2006) developed new fatigue load model based on weight-in-motion data collected from three different sites in Indiana. The bridge models included single and continuous spans. Based on Miner's hypothesis, fatigue damage accumulations were computed for details at various locations on the bridge models and compared with the damage predicted for the 240-KN AASHTO fatigue truck, a modified AASHTO fatigue truck with an equivalent effective gross weight, and other fatigue truck models.

The fatigue behavior of metallic specimens has been investigated widely. The field studies conducted on some of the bridges was used to predict fatigue damage and remaining service life of the bridges. Since fatigue damage assessment of bridge components by conducting full scale fatigue testing is often prohibitive, a need therefore exists to apply fatigue damage analysis to different bridges at design stage.

Fatigue behaviour of steel and metal structures is more precisely known compared to plain, reinforced and prestressed concrete. Fatigue behaviour of concrete and reinforced concrete structures are mainly explained from the experimental observations. Due to non-linearity of stress strain behaviour, linear damage accumulation rule for concrete structures has restricted applications. A probabilistic approach to predict the flexural strength of plain concrete was introduced by Oh (1986) which utilized constant amplitude fatigue testing of concrete specimen. The distribution of fatigue life of concrete under a given stress level is found from experimental results and presented as Weibull probability law. Concrete subjected to stress reversal deteriorates faster which is explained by the interaction of the differently oriented micro-cracks in compression and tension loading.

Perdikaris *et al.* (1989) conducted model tests under static, fixed pulsating and moving wheel-load to study the effect of deck continuity and reinforcing pattern on ultimate and fatigue strength of concrete bridge deck slab supported on steel girders. It was found that fatigue loading causes progressive deterioration of the bond between reinforcement and concrete. Failure might occur normally due to re-bar fatigue fracture or spalling of concrete in compression zone.

Scalafli and Bruhwiler (1998) showed that for slender flexural elements like slabs fatigue failure of concrete under normal compression forces was unlikely to occur and recommended that additional bending stresses for reinforcement should be

considered. The conclusion followed from the fatigue test results in the reinforced concrete slab specimen.

The fatigue loading has different effects on prestressed concrete bridges. Due to fatigue of prestressing steels and auxiliary reinforcement, durability of bridge may be effected. Particularly in partial prestressing, there is a high stress increment in reinforcing and prestressing steel in comparison to fully prestressed or undamaged bridge. In post tensioned bridges at the zone where cracks appear, the tensile axial force in the prestressing steel acts combined with high lateral pressure and relative slips occur between the wires and duct. This phenomenon known as “fretting fatigue” reduces significantly fatigue resistance of steel.

Wollman (1988) reported an experimental research works where “fretting fatigue” and its progression on failure was observed. The expression to evaluate fatigue strength of post tensioned steel was developed in the form of S-N curve. However, model of researchers take the stress increment greater than 100 MPa. Therefore, there is a lack of data regarding low stress increments on S-N curve.

Minguillon and Cases (1998) developed a model for the fatigue analysis of prestressed concrete bridges. The model included nonlinear behaviour under the action of external loads. The S-N curve and Palgren-Miner hypothesis were chosen for the definition of fatigue strength of reinforcing and prestressing steels. In the development of methodology, emphasis was given to find the position of plane of strains that balanced the internal load induced axial force and bending moment.

In prestressed concrete, there may be closure of cracks after removal of overloading. Seible *et al.* (1992) explained how the loss of bond and drop in tensile stress in the tendons were not recovered after crack closure. This is very important result for fatigue. However, authors also commented that since fatigue depended on

stress fluctuation and final stress increments were not very sensitive to the loss of bond, full bond behaviour could be assumed.

Literature survey shows that Fatigue behaviour of structures has been studied by several authors theoretically as well as experimentally. Several researchers determined the fatigue strength of the structural member based on constant amplitude fatigue test and the results were represented in the form of S-N curve. In actual field loading conditions, it is not justified to consider the bridge under constant amplitude cyclic loading. The codal previsions mainly based on constant amplitude test data are having shortfall for dynamic interaction between bridge and vehicle not being considered. These load time histories are much more complicated compared to periodic loadings used in laboratory fatigue testing and as such a realistic approach was necessary to apply for bridges subject to random moving load. Many researchers carried out studies mainly using two approaches, one in the time domain analysis using simulated response time history and other in the frequency domain analysis using power spectral density of stress and spectral moments of different orders. While time domain cycle counting method has been applied to many bridge structures, the application of spectral moments was limited to simple structural element for illustrative purpose. It was found that time domain analysis by simulation of stress histories consumes more computational time compared to spectral methods which is based on closed form expression of expected fatigue damage. However, it is found that fatigue calculation for curved box-girder bridges has been attempted so far neither by cycle counting method nor by spectral analysis. Since curved box-girder bridges present complicated structural response under moving vehicles, it is felt necessary to estimate fatigue life of such bridges by suitable methods.

1.3 SCOPE AND OBJECTIVES OF THE PRESENT INVESTIGATION

Considering the detailed literature survey, it is realized that computationally efficient, well representative of the behavior of the thin-walled box-girder procedure for analysis of curved box-girder bridges is highly desired particularly for preliminary analysis and conceptual design stage. Further, such an effective methodology is also an important requirement for dynamic analysis.

The studies on free vibrational characteristics of a structure are important for understanding the dynamic response behavior of the same structure subjected to any excitation. Thus, it is realized that experimental evaluation of modal parameters are needed for the validation of theoretical model adopted in the present investigation. The agreement between the theoretical and experimental model is necessary to proceed for the detail dynamic analysis of the curved thin walled box girder bridge when subject to moving load of complex configuration at constant and variable velocity.

The bridge vehicle interaction study is also regarded as very important since accurate evaluations of impact factors are highly significant for safe and economic design of a bridge structures. However, efficient vehicle model along with an appropriate bridge model are primary requirements for the solution of such coupled bridge-vehicle dynamic system.

Further, since the bridge structures are subjected to fluctuating stresses due to vehicle induced vibration, assessment of fatigue life is also considered essential for the design of bridge. The prediction of fatigue life of a bridge is very much involved as the stress history of a bridge component due to moving vehicle differs widely from that found in constant amplitude fatigue test of the specimen. The fatigue provisions in the codes of practice for the design of steel bridges do not faithfully utilize the stresses induced in the bridge components due to dynamic interaction with the moving

vehicles. This is particularly significant in case of curved thin walled box girder configurations because of coupling of flexural and torsional stresses accompanied by warping and distortion of the cross section.

Keeping in view the increasing use of the curved thin-walled box-girder bridge in modern highways, a study has been undertaken to carry out static and dynamic analysis by adopting a computationally efficient model. Since limited number of studies has been carried out by past researchers on the curved thin-walled box-girder bridge, especially on the dynamic behavior of bridges, the present study is aimed to fulfil the following objectives.

1. To model the horizontally curved thin-walled box-girder bridge for static and dynamic analysis.
2. To study free vibrational characteristics of the curved bridge.
3. To conduct a laboratory experiment with a fabricated model of curved box-girder bridge to find out the modal parameters and to validate the theoretical model.
4. To conduct elaborate study on the bridge vehicle interaction problem of curved box-girder bridges with emphasis on the evaluation of impact factors corresponding to various stress resultants and with varying parameters that may affect the dynamic response of the bridge due to moving vehicles. A generalized design guideline for curved thin walled box girder bridges of single span has been established in terms of impact factor which includes effect of bridge span, radius of curvature and speed of vehicle.
5. To outline a systematic approach for the evaluation of fatigue life of a curved thin-walled box-girder bridge from the vehicle induced stress

history by using both time domain and frequency domain method and to compare the efficiency and applicability of both the methods.

1.4 ORGANIZATION OF THESIS

In the present thesis, six chapters has been included. Chapter-1 gives introduction, literature review and scope of the present work. Chapter-2 presents theory of thin walled box girder bridge and finite element formulation. Numerical examples for static loading including IRC standard loadings have been presented for single cell and multi-cell cross sections. Comparison with the results obtained by ANSYS is also given. Free Vibration analysis of thin walled section curved girder has been incorporated in Chapter-3. Experimental validation of the theoretical results is also given in this Chapter. Chapter-4 focuses the vehicle-bridge interaction study by choosing an heave-pitch-roll vehicle model and random roughness profile of the bridge deck. Impact factors for various stress resultants for variation of vehicle-bridge parameters have been presented. Finally, a design guideline in terms of impact factor has been outlined for various stress resultants taking into consideration of the span, radius of curvature and vehicle speed. Fatigue analysis of the curved thin walled section box girder bridge has been given in Chapter-5. Time domain methods and Spectral methods for fatigue analysis is discussed and results have been shown for steel box girder bridge obtained by Time domain method and two different spectral methods. Chapter-6 provides general conclusions arrived at the study. It also points out scope of the further study. Appendices A-F follows the Chapter-6. References and list of publication from the present work are given at the end.

CHAPTER 2

FINITE ELEMENT FORMULATION OF THIN-WALLED CURVED BOX-GIRDER BRIDGE

2.1 INTRODUCTION

The box-girder bridge consists of a top and bottom flange connected by vertical or inclined webs to form a cellular or box-like section. A curved box-girder bridge is basically a rigid curved deck beam structure that is resting on piers at each end. Typical cross-sections of box-girder bridges are shown in Fig.2.1. The advantage of the hollow section is that the material is efficiently used in bending, torsion and shear. In long spans, the dead load is the controlling load, and thus economy in dead load becomes important. Thin-walled beams have been widely used in engineering applications because of the high stiffness-to-mass ratio. In particular, thin-walled beams with closed cross-sections are very important structural elements when high torsional and bending rigidities are required.

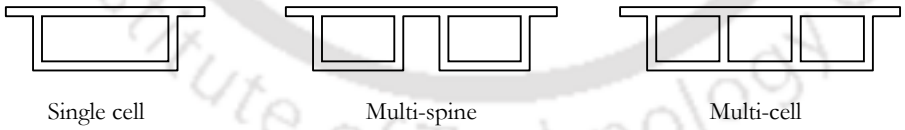

Fig .2.1 Types of box girder bridges

The task of the development of appropriate strategy for the analysis of thin-walled box - girder bridges were going on for last three decades. Maisel (1985), Kermani and Waldron (1993) developed a very much generalized method for the analysis of straight box-girder under static loading, which accounts for warping torsion and distortion in addition to the

more familiar beam actions. However, during the past two decades, the finite-element method of analysis has rapidly become a very popular technique for the solution of complex problems in engineering. A logical alternative for modeling of curved box-girder bridges is to combine finite element technique with thin-walled beam theory. In the present study, one-dimensional beam element developed by Zhang and Lyons (1984) has been used to model the thin-walled curved box-girder bridge. It incorporates the effects of extension, flexure, torsion, torsional warping, distortion and distortional warping.

It is understood that although a continuous bridge structure is three-dimensional in reality, an idealized one-dimensional form has certain simplifying advantages in many circumstances. However, the commonly used truss or beam type elements are viewed as over simplified to represent curved box-girder bridges. The one-dimensional beam element, which is being considered for the present study, may be regarded as a general beam element representing thin-walled box-girder section. In order to appreciate the finite element formulation representing thin-walled box-girder, different structural actions of thin-walled box-girder have been elaborated in the subsequent sections.

2.2 BASIC ASSUMPTIONS FOR THIN-WALLED BOX-GIRDER

The conventional assumptions associated with linear elastic small displacement theory have been adopted. These assumptions are material is homogeneous, isotropic, linearly elastic, and that the actual deformations are small compared to the structural dimensions. Additional assumptions, which have been considered are mainly related to thin-walled structural behaviour and are as follows:

1. Plane sections remain plane; but not necessarily normal to the beam axis, when subjected to flexure. This will allow the consideration of shear deformation.

2. For warping torsion analysis, cross-sections are assumed to remain un-deformed in their own plane, but may rotate about the flexure axis (locus of the shear centers) and be subject to longitudinal warping.

3. The bending action of an individual component plate normal to its plane is represented by the flexural behaviour of an equivalent transverse frame.

2.3 STRUCTURAL ACTIONS IN BOX-GIRDERS

The structural design of box-girder bridges presents many difficulties because of the complex interaction of the individual structural effects. In addition to biaxial bending and torsion, a box-girder undergoes torsional warping, distortional warping and shear lag effects. Distortion or deformation of the cross-section due to torsional loading leads to a change in the shape of the section, which arises from transverse bending of the walls of the box-girder. Warping of the cross-section corresponds to out-of-plane displacements of points on the cross-sections, causing plane sections not to remain plane. The longitudinal displacements caused by torsion and distortions are termed as torsional warping and distortional warping respectively. Shear lag leads to a decrease in the longitudinal bending stresses calculated by simple bending theory away from the webs. Torsional warping is treated by the original Vlasov's theory (1961), distortional warping is considered using an extended version of Vlasov's theory (1961), while shear lag is taken into account using the effective breadth concept.

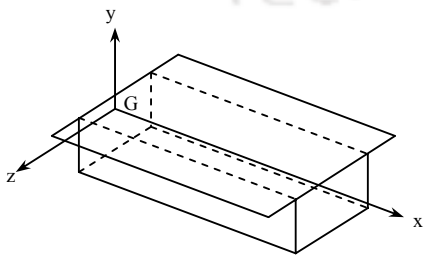

Fig. 2.2 Co-ordinate axes x,y and z

2.3.1 **Bending Action of Thin-Walled Members**

Assuming that the origin of the *x, y* and *z* axes coincide with the centroid of the cross-section (Fig. 2.2) and the neutral axis passes through the centroid of the cross-section, the normal stress at any point in the cross-section can be expressed as,

$$\sigma_{x,b} = \frac{\hat{M}_z}{I_{zz}} y - \frac{\hat{M}_y}{I_{yy}} z \tag{2.1}$$

where, $$\hat{M}_z = \frac{M_z + M_y \frac{I_{zy}}{I_{yy}}}{1 - \frac{I_{zy}^2}{I_{zz} I_{yy}}} \quad \text{and} \quad \hat{M}_y = \frac{M_y + M_z \frac{I_{zy}}{I_{zz}}}{1 - \frac{I_{zy}^2}{I_{zz} I_{yy}}} \tag{2.2}$$

Since the *y* axis is fixed as an axis of symmetry in the present approach, then I_{zy} is zero. Eq. 2.2 reduces to

$$\hat{M}_z = M_z \quad \text{and} \quad \hat{M}_y = M_y \tag{2.3}$$

and Eq. 2.1 becomes

$$\sigma_{x,b} = \frac{M_z}{I_{zz}} y - \frac{M_y}{I_{yy}} z \tag{2.4}$$

where M_z and M_y are the internal bending moment about x and y axes respectively, I_{zz} and I_{yy} are the moment of inertia about the x and y axes and I_{zy} is the product of inertia respectively.

2.3.2 Shear Lag Effect

Shear lag is the non-uniform distribution of longitudinal normal (bending) stresses in a thin-walled flanged member caused by a lag of shear strain in the flange plates. Simple bending theory assumes the longitudinal strain to be proportional to the distance from the neutral axis, but this no longer holds if shearing deformations are considered.

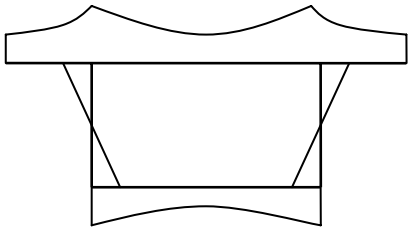

Fig. 2.3 Positive shear lag

In a box-girder with wide, thin flanges, shearing strains may be sufficient to cause the central longitudinal displacement to lag behind that at the edge of the flange causing a distribution of bending stress similar to that shown in Fig. 2.3 and Fig. 2.4. This phenomenon is termed as shear lag or stress diffusion.

Shear lag is an important consideration in the design of thin-walled structures. The "shear lag" phenomenon reduces the effectiveness of the webs and flanges and can result in the deflections and stresses at the web-flange intersections of a girder being significantly underestimated in calculations based on the elementary theory of bending.

A shear lag anomaly, known as 'Negative Shear Lag' was also observed along with the usual (positive) shear lag phenomenon as can be seen in Fig. 2.4. However, this is of mere academic importance rather than that of practical significance, as the stresses induced as a result of positive shear lag far exceeds that of the negative one (Lee *et al.* 2002).

For design purpose, it is often convenient when calculating the deflections or stresses of a wide-flanged girder to replace the actual breadth b_i of each flange by a certain reduced breadth $b_{e,i}$, such that the application of the elementary theory of bending to the transformed girder cross-section gives the correct value of maximum deflection or longitudinal stress. The reduced breadth, $b_{e,i}$ is termed the effective breadth.

A term, the effective breadth ratio, $\psi_{e,i}$ which is the ratio of the effective breadth of each flange to its actual breadth, is given by

$$\psi_{e,i} = \frac{b_{e,i}}{b_i} \tag{2.5}$$

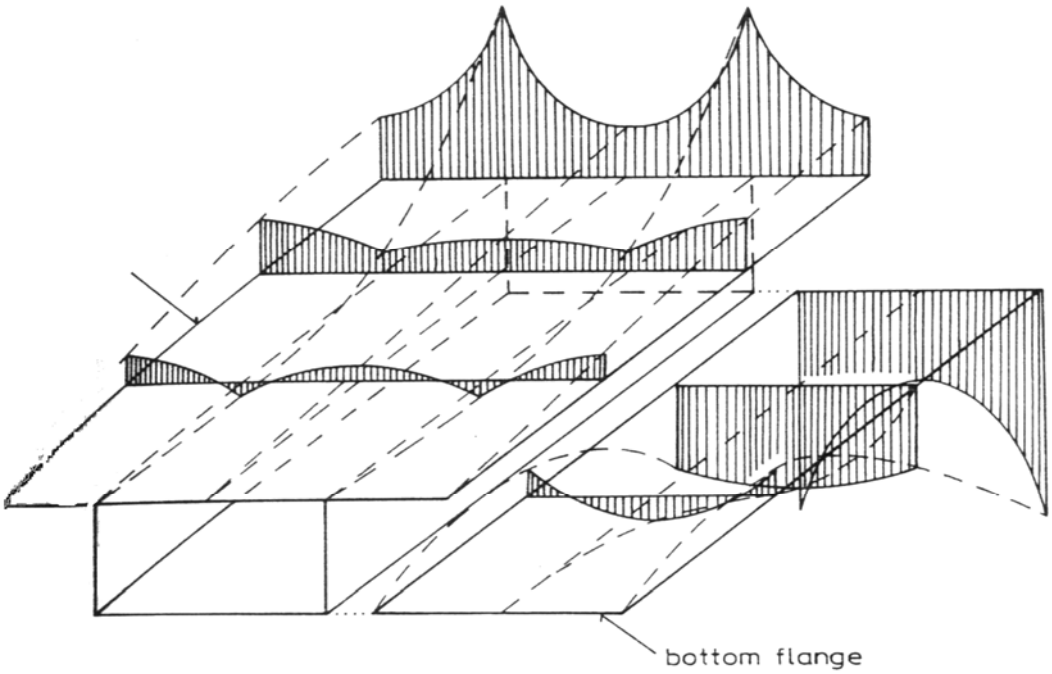

Fig .2.4 Longitudinal stresses in flanges of a cantilever box-girder depicting positive and negative shear lag

Moffat and Dowling (1975) used finite element method for carrying out a parametric study of the effective breadth ratio. The total effective breadth of a flange associated with each web is taken as the sum of the effective breadths of the portions of flange considered separately on each side of that web. Thus, the effective breadth of each position shall be taken as $\psi_{e,i}\, b_i$ or $0.5\psi_{e,c}\, b_c$ for parts projecting beyond an outer web respectively.

They gave effective breadth ratios at the mid-span, quarter-span, and support sections for different support conditions, loading conditions and different breadth of flange to length ratios ($b_i/2L$ or b_c/L).

Thus, the availability of effective breadth ratios enables the peak stress at a web-flange junction ($\sigma_{x,m}$) to be calculated accurately. However, in order to have an estimate of the longitudinal stresses ($\sigma_{x,b}$) in parts of the flange remote from the web-flange junction, the formula suggested by Moffat and Dowling (1975) may be used.

$$\sigma_{x,b} = \sigma_{x,m}\xi \tag{2.6}$$

where

$$\xi = \left[4\left(\frac{x}{b_i}\right)^2 - \frac{(3\psi_e - 1)}{2}\left\{1 - 4\left(\frac{x}{b_i}\right)^2\right\}\right] \quad \text{for parts between webs,} \tag{2.7}$$

$$\xi = \left[\left(\frac{x}{b_c}\right)^2 - \frac{(3\psi_e - 1)}{2}\left\{1 - \left(\frac{x}{b_c}\right)^2\right\}\right] \quad \text{for projections,} \tag{2.8}$$

$\sigma_{x,m}$ is the maximum stress at the web-flange junction, x is the distance measured from the mid-point of individual flange plates or the extreme edge of side cantilevers to the point considered, b_i is the width of between neighboring webs, b_c is the width of the side cantilevers. Distribution of longitudinal flange stresses with allowance for shear lag has been shown in Fig. 2.5.

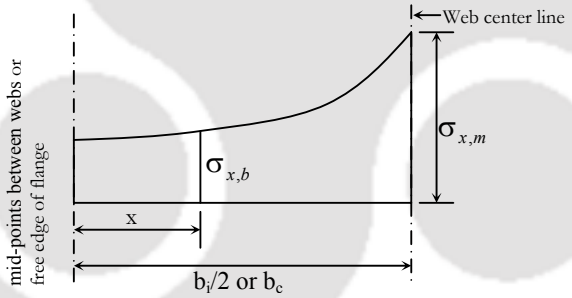

Fig 2.5 Distribution of longitudinal flange stresses with allowance for shear lag

2.3.3 Torsion of Thin-walled Girder

2.3.3.1 Pure Torsion of Open and Closed Section Members

The pure torsional moment for an open section is given by the well-known formula

$$M_{T,V} = GJ_V \frac{\partial \theta_x}{\partial x} \tag{2.9}$$

where, G is the shear modulus, θ_x is the twisting angle due to St. Venant torsion, and J_V is the St. Venant torsional moment of inertia and is given by

$$J_V = \sum_{i=1}^{m} \frac{l_i t_i^3}{3} \tag{2.10}$$

for a composite member, where l_i is the length of each composite member, t_i its thickness and m is the total number of such composite members.

For a closed section, the pure torsional moment (Fig 2.6) is given by

$$M_{T,B} = GJ_B \frac{\partial \theta_x}{\partial x} \tag{2.11}$$

$$\text{where } J_B = \oint \bar{q}_B R_t ds = \sum_{i=1}^{n} \bar{q}_{B,i} \Omega_i \tag{2.12}$$

J_B is referred to as the Bredt torsional moment of inertia (length^4).

$$\text{and} \quad \bar{q}_{B,i} = \frac{q_{B,i}}{G \frac{\partial \theta_x}{\partial x}} \tag{2.13}$$

is defined as the unit shear flow distribution function relating to pure torsion.

Ω_i is twice the enclosed area of the i^{th} cell, R_t is the perpendicular distance from the shear center E_s and $q_{B,i}$ is the Bredt shear flow around the i^{th} cell.

The total pure torsional moment is now given by

$$M_{T,P} = M_{T,V} + M_{T,B} = G(J_V + J_B) \frac{\partial \theta_x}{\partial x}$$

$$= GJ_T \frac{\partial \theta_x}{\partial x} \tag{2.14}$$

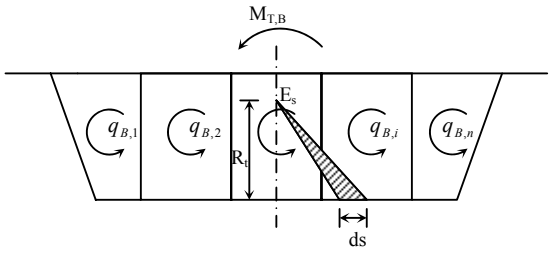

Fig.2.6 Multi-cell box girder subjected to Bredt torsional moment $M_{T,B}$

2.3.3.2 Torsional Warping

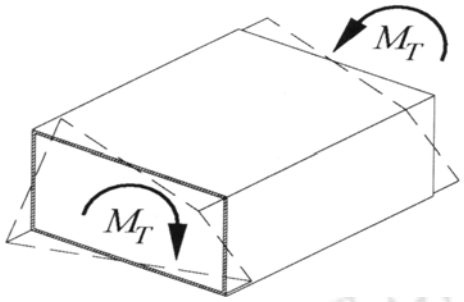

Fig .2.7.Torsional warping

With the exception of bars with solid and hollow circular cross sections, bars subjected to torsion tend to warp. The fundamental assumption in St. Venant's pure torsion analysis is that cross sections are free to warp without restraint. This assumption is not satisfied if the beam has external supports, or if the beam is not prismatic, or when the torsional moment varies along the length of the beam. Even in these cases, St. Venant's hypothesis of free warping gives good approximate results for beams with solid cross-sections. For thin-walled cross sections (Fig2.7), however, this is no longer true. The twisting resistance of such sections is so small and the axial displacements are so large that the axial stresses caused by restrained warping cannot be neglected.

The general differential equation for warping torsion is given by

$$-\frac{1}{\mu_t} E_1 J_I \frac{\partial^4 \theta_x}{\partial x^4} + G J_T \frac{\partial^2 \theta_x}{\partial x^2} = m_{x,ext} \tag{2.15}$$

where, $m_{x,ext}$ is a continuously distributed twisting moment,

$$\mu_t = 1 - \frac{J_B}{J_C} \tag{2.16}$$

is called the warping shear parameter,

$$J_C = \int_A R_t^2 \, dA \tag{2.17}$$

is called the central second moment of area and R_t is the perpendicular distance from the shear center to the tangent to the mid-line of wall at the point considered. Considering the

deformation of the cross-section in the case of pure torsion, the tangential displacement of a point on the cross-section is given by

$$w_t = R_t \theta_x \tag{2.18}$$

where θ_x is the twisting angle of the section in its plane in pure torsion.

For an open section, the shear strain at the mid-line of the section is assumed to vanish. Thus,

$$\gamma_{xs} = \frac{\partial u_x}{\partial s} + \frac{\partial w_t}{\partial x} = 0 \tag{2.19}$$

where u_x denotes the warping displacement.

Substituting Eq. 2.18 in Eq. 2.19 and integrating once we obtain

$$u_x = u_{x,0} - \int_0^s R_t ds . \frac{\partial \theta_x}{\partial x} = -\omega_I \frac{\partial \theta_x}{\partial x} \tag{2.20}$$

in which the unit torsional warping function for an open section

$$\omega_I = \omega_{I,0} + \int_0^s R_t ds \tag{2.21}$$

is equal to twice the value of the area shaded in Fig. 2.8 and is also called the sectorial coordinate (in length^2).

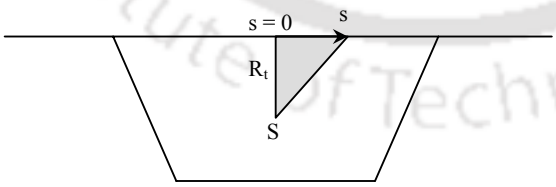

Fig. 2.8 Method of determination of sectorial coordinate

For a closed section, the unit warping function is still defined as the negative warping per unit rate of the angle of twist.

$$u_x = -\hat{\omega}_I \frac{\partial \theta_x}{\partial x} \tag{2.22}$$

The shear strain at the mid-line of the section in the case of closed section is assumed to be equal to that obtained from the Bredt formula,

$$\gamma_{xs} = \frac{\partial u_x}{\partial s} + \frac{\partial w_t}{\partial x} = \frac{q_B}{Gt} \tag{2.23}$$

Substituting Eq. 2.13, 2.18 and 2.22 in Eq. 2.23, we get

$$-\frac{\partial \hat{\omega}_I}{\partial s} + R_t = \frac{\overline{q}_B}{t} \tag{2.24}$$

Integrating Eq. 2.24 once, we obtain

$$\hat{\omega}_I = \hat{\omega}_{I,0} + \int_0^s \left(R_t - \frac{\overline{q}_B}{t} \right) ds \tag{2.25}$$

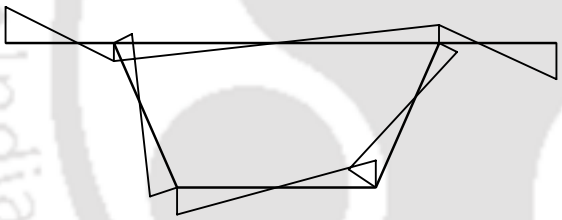

Fig. 2.9 Distribution of torsional warping sectorial co-ordinate around a single cell trapezoidal box girder

where $\hat{\omega}_I$ is the unit torsional warping function for a closed section and is also called the reduced sectorial coordinate.

In particular, for an open section, in which $\overline{q}_B = 0$, we obtain

$$\hat{\omega}_I = \omega_I = \omega_{I,0} + \int_0^s R_t ds \tag{2.26}$$

The sign of the first integral in Eq. 2.25 is determined on the basis of the sense of rotation of R_t as it sweeps through the area in the direction of increasing s (Fig. 2.9). For a

right hand co-ordinate system, if this rotation is clockwise, the contribution to the integral is negative, and if it is counterclockwise, the contribution is positive. It is vice versa if the co-ordinate system is left handed.

The torsional warping stresses are given by the following expression

$$\sigma_I = E_I \frac{\partial u_x}{\partial x} = -E_1 \hat{\omega}_I \frac{\partial^2 \theta_x}{\partial x^2} \tag{2.27}$$

where $E_1 = \frac{1}{1-\nu^2}$ is the conversion modulus of elasticity.

The stresses arising due to torsional warping are self-equilibrating and have a zero longitudinal force resultant and a zero moment resultant. This type of force introduced has been termed as 'torsional warping bimoment' (Vlasov 1961) (Fig2.10).

$$B_I = \int_A \sigma_I \hat{\omega}_I dA \tag{2.28}$$

By defining a new type of geometric property of the cross-section,

$$J_I = \int_A \hat{\omega}_I^2 \, dA \tag{2.29}$$

which is known as the torsional warping moment of inertia, we obtain from Eq.2.27, 2.28 and 2.29.

$$B_I = -E_I J_I \frac{\partial^2 \theta_x}{\partial x^2} \tag{2.30}$$

Substituting Eq. 2.30 in Eq. 2.27, we obtain

$$\sigma_I = \frac{B_I \hat{\omega}_I}{J_I} \tag{2.31}$$

The total torsional moment with respect to the shear center including the torsional moment resulting from warping shear stresses is given by

$$M_T = M_{T,P} + M_{T,I}$$

$$= M_{T,V} + M_{T,B} + M_{T,I} \tag{2.32}$$

where

$M_{T,P}$ is the primary torsional moment referred to the St.Venant shear stresses and/or the Bredt shear stresses,

$M_{T,V}$ is the St.Venant torsional moment component,

$M_{T,B}$ is the Bredt torsional moment component,

$M_{T,I}$ is the secondary or flexural torsional moment resulting from warping shear stresses.

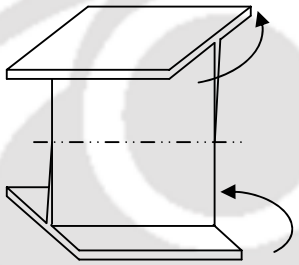

Fig. 2.10 Bi-moment action

The shear centre of a cross-section may be defined as the point in the cross-section through which shear loads must act to produce no twisting. The coordinates for the shear centre *A* at a section with respect to any arbitrary chosen pole *B* is given by (Fig. 2.11)

$$e_z = \frac{I_{z\hat{\omega}_B} I_y - I_{y\hat{\omega}_B} I_{yz}}{I_y I_z - I_{yz}^2} \tag{2.33}$$

$$e_y = \frac{I_{z\hat{\omega}_B} I_{yz} - I_{y\hat{\omega}_B} I_z}{I_y I_z - I_{yz}^2} \tag{2.34}$$

For a uni-symmetrical section with *y* as the axis of symmetry, and because of the anti-symmetry of the $\hat{\omega}_I$ diagram (Fig. 2.9), Eq. 2.33 and 2.34 can be written as

$$e_z = 0 \tag{2.35}$$

$$e_y = -\frac{I_{y\hat{\omega}_B}}{I_y} \tag{2.36}$$

where

$$I_{y\hat{\omega}_B} = \int \hat{\omega}_{IB}.z\, dA \quad \text{and} \quad I_{z\hat{\omega}_B} = \int \hat{\omega}_{IB}.y\, dA \quad (2.37)$$

are the sectorial products of inertia about the centroidal z and y axes respectively.

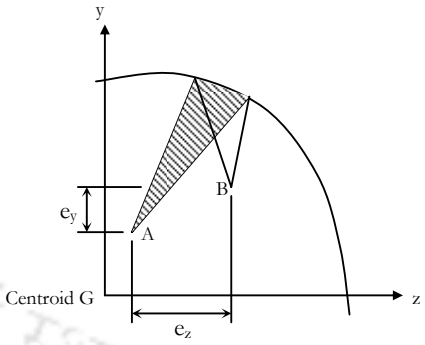

Fig. 2.11 Shear center determination

2.3.4 Distortion of Thin-walled Girder

Thin-walled box-girder subjected to torsional loading, tend to distort in the plane of the cross-section due to their low cross-sectional rigidity. This in-plane deformation of the cross-section is termed 'distortion', and if it is not constant along the beam, causes additional out-of-plane displacements called 'distortional warping', which when restrained, longitudinal normal stresses will be developed.

A sufficient number of stiff diaphragms or cross bracings can avoid distortion of a thin-walled box-girder bridge. However, a limited number of these diaphragms are generally provided as a large number of diaphragms or cross bracings may not be desirable as they increase the weight of the structure and complicate construction.

The distortion of the cross-section of box-girder thin-walled bridge is the main source of warping stresses and hence may provide a significant contribution to the bending stresses. Further, the additional transverse bending stresses due to distortion of the cross-section may be of the same order of magnitude as the longitudinal bending stresses. It is, therefore, very important that the distortional behaviour of thin-walled box-girder bridges are properly accounted for in the analysis in addition to bending and torsional effects.

2.3.4.1 Cross-Sectional Deformation

A single-cell box-girder is shown in Fig. 2.12, where the cross-section distorts under eccentric load. The corner points of the box are displaced vertically by an amount $\pm\bar{v}_t$ and by $\bar{w}_t$, $\bar{w}_b$ in the horizontal direction at the top and bottom, respectively. A characteristic distortional angle γ_d may be defined representing the change in angle between the top flange of the cross-section and the inclined side web as described by the box corners.

This may be written as

$$\gamma_d = \gamma_F + \gamma_W \tag{2.38}$$

where γ_F and γ_W are the rotations of the top flange and side web of the cross-section, respectively, obtained from the following equations.

$$\gamma_F = 2\bar{v}_t / b_t \tag{2.39}$$

$$\gamma_w = (\bar{w}_t + \bar{w}_b) / h \tag{2.40}$$

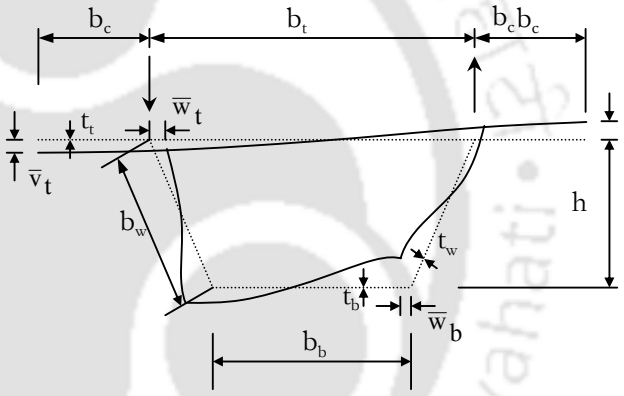

Fig. 2.12 Deformed shape of a single cell box girder subjected to torsional load

By analogy with warping torsion, the tangential displacement w_t, along the midline of the wall can be expressed as the product of a distribution function $V_s(S)$ of the tangential displacement and the distortion angle γ_d.

$$w_t = V_s(S)\gamma_d \tag{2.41}$$

To develop an approximate theory for distortion neglecting shear deformation, it may be assumed that the in-plane displacement is accompanied by sufficient warping to neutralize the average shear strains in the plate that form the cross-section. This can be expressed as

$$\frac{\partial w_t}{\partial x} + \frac{\partial u_x}{\partial s} = 0 \tag{2.42}$$

After substitution of Eq. 2.41 in Eq. 2.42 and subsequent integration gives

$$u_x = -\omega_{II} \frac{\partial \gamma_d}{\partial x} \tag{2.43}$$

$$\text{where, } \omega_{II} = \int_0^s V_s(S) ds \tag{2.44}$$

indicates the distribution of the longitudinal displacement and is defined as the unit distortional warping function (Fig.2.13) and has dimensions of L^2.

Differentiating Eq. 2.43 once, we obtain

$$\varepsilon_x = \frac{\partial u_x}{\partial x} = -\omega_{II} \frac{\partial^2 \gamma_d}{\partial x^2} \tag{2.45}$$

and the corresponding warping stresses are given by

$$\sigma_{II} = -E_1 \omega_{II} \frac{\partial^2 \gamma_d}{\partial x^2} \tag{2.46}$$

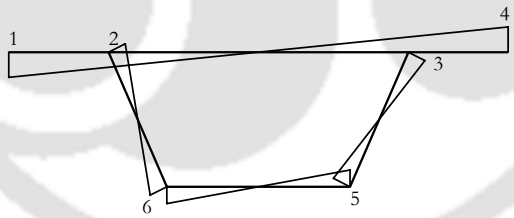

Fig.2.13. Distribution of distortional warping function

The distortional forces are self-equilibrating as in warping torsion. To represent the resultant of the distortional warping stresses, a distortional bi-moment is defined as

$$B_{II} = \int_A \sigma_{II} \omega_{II} dA = -E_1 J_{II} \frac{\partial^2 \gamma_d}{\partial x^2} \tag{2.47}$$

where,

$$J_{II} = \int_A \omega_{II}^2 dA \tag{2.48}$$

which is called the distortional warping moment of inertia.

From Eq. 2.46 and 2.48, one finally obtains

$$\sigma_{II} = \frac{B_{II}}{J_{II}} \omega_{II} \tag{2.49}$$

which is analogous to the warping stresses obtained earlier for warping torsion.

2.3.4.2 Generalized Distortional Force (Distortional Moment)

For a characteristic distortional angle γ_d, there exists a generalized distortional force, which is represented by the distortional moment M_d (Fig.2.14), (Boswell and Zhang 1984),

$$M_d = \frac{1}{2}\left(\frac{b_t}{b_b} m_{xV} - m_{xH}\right) \tag{2.50}$$

where, $m_{xH} = -p_z e_y$ and $m_{xV} = p_y e_z$ (2.51)

are the external twisting moments.

For loads applied at the cantilever portion of the cross-section, the distortional moment is given by (Zhang 1983).

$$M_d = \frac{p_y}{2}\left[\alpha_d e_z - (1+\alpha_d)(1-\zeta_d) b_z\right] \tag{2.52}$$

where $\alpha_d = b_b / b_t$ is the ratio of the width of the bottom flange to the top flange and

$$b_z = e_z - \frac{b_t}{2} \qquad (2.53)$$

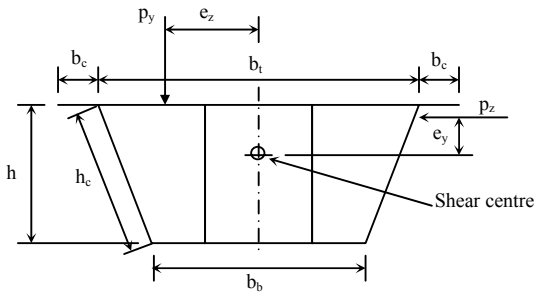

Fig.2.14. Eccentric loads applied to a box section

The distribution factor ζ_d is the ratio of the distributed moment in the top flange to the applied fixed moment and can be obtained from the frame analysis of a frame formed from a unit slice of the box-girder due to a unit fixed moment.

2.3.4.3 Transverse Flexural Resistance of the Cross-Section to Distortion

Transverse flexural stiffness of the individual plates of a box section provides resistance to distortion in addition to that contributed by the constraint of warping.

If the effective frame stiffness of the section k_d per unit length is defined as the resisting component corresponding to a unit distortional angle, then by equating the internal energy per unit length $\left(\frac{1}{2} k_d \gamma_d^2\right)$, and the external energy $\left(\frac{1}{2} M_d \gamma_d\right)$, we get

$$M_d = k_d \gamma_d = E_1 J_d \gamma_d \qquad (2.54)$$

where, J_d is defined as the distortional second moment of area.

The distortional frame stiffness can be evaluated by the analysis of a frame of unit length of the box-girder, constrained horizontally and vertically at the lower corner points as shown in Fig.2.15. It is loaded by diagonal forces with unit horizontal components. This frame has been analyzed using SAP 2000 in the present case.

$$S_H = 1 \qquad (2.55)$$

$$S_V = \frac{2h}{b_t + b_b} \tag{2.56}$$

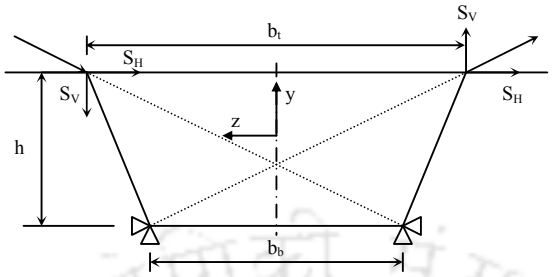

Fig.2.15. Plane frame of unit length for assessing frame stiffness

The influence distortional angle $\tilde{\gamma}_d$, the frame stiffness k_d and the distortional second moment of area J_d are given by the formulae (Zhang 1983)

$$\tilde{\gamma}_d = \frac{b_t(w_1 + w_2) + 2h(v_1 - v_2)}{2hb_t} \tag{2.57}$$

$$k_d = \frac{4h^2 b_t}{b_t(w_1 + w_2) + 2h(v_1 - v_2)} \tag{2.58}$$

$$J_d = \frac{4h^2 b_t}{E_1[b_t(w_1 + w_2) + 2h(v_1 - v_2)]} \tag{2.59}$$

where w_1, w_2 and v_1, v_2 are the horizontal and vertical displacements respectively at the upper corner points of the section as shown in Fig.2.16.

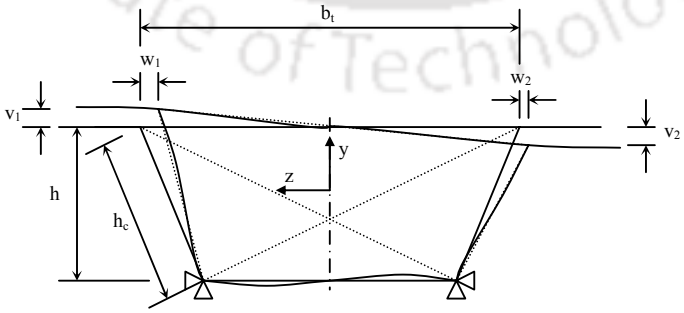

Fig.2.16. Deformation of the plane frame

2.3.4.4 Transverse Bending Stresses

The frame corresponding to a particular section as shown in Fig 2.15 is analyzed and the distribution of associated transverse distortional bending moments $\tilde{m}_{db}$, distortional shear forces $\tilde{q}_{db}$ at the junction of the individual plates are evaluated. These become influence values of moment and stress and are associated with the influence distortional angle $\tilde{\gamma}_d$. If γ_d is the actual distortion angle at a particular section, then the transverse distortional moments and distortional shear forces per unit length are given by (Boswell and Zhang 1984).

$$m_{db} = \frac{\tilde{m}_{db}}{\tilde{\gamma}_d}\gamma_d \tag{2.60}$$

$$q_{db} = \frac{\tilde{q}_{db}}{\tilde{\gamma}_d}\gamma_d \tag{2.61}$$

For a single cell box-girder, only one distortional mode is considered to obtain the transverse distortional bending stress σ_{db} associated with Eq. 2.60 and 2.61. However, for multi-cell box-girders, the final influence value is obtained by the superposition of the influence values of the various distortional modes.

$$\tilde{\sigma}_{db} = \sum_{i=1}^{n} \tilde{\sigma}_{db,i} \tag{2.62}$$

where *n* is the total number of distortional modes (Fig.2.17) which is also equal to the number of cells of the box section too.

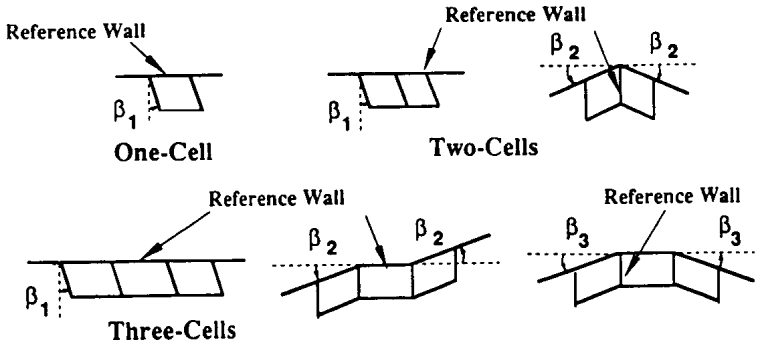

Fig. 2.17. Modes of distortion

The transverse distortional bending stresses in deformable box-girders may be of the same order as the longitudinal bending stresses under the same loading. Consequently, traverse distortional bending can generate significant longitudinal stresses due to the Poisson's ratio effect and are by no means negligible in comparison with the longitudinal bending stresses. The longitudinal bending moments of the plates arising due to the Poisson's ratio effect may be approximately estimated by multiplying the transverse bending moments by Poisson's ratio (Zhang 1983).

$$m_{lb} = \nu\, m_{db} \tag{2.63}$$

2.3.4.5 ***Curvature Effect on Single-Spine Horizontally Curved Box-Girder***

For a single-spined box-girder bridge curved in plan, it is assumed that the cross-sectional dimensions are small in relation to the radius of curvature. A modified transverse frame analysis (Fig.2.18) is employed for the distortional analysis of single-spined horizontally curved box girder, where the plate elements having curved web plates are replaced by equivalent flat rectangular members Fig.2.19. The individual plates are then considered to have a width equal to the average of the outer and inner edge dimensions of the

plate. The width of the equivalent web plates, for instance, in a multi-cell box-girder as shown in Fig. 2.20 is determined by Zhang (1983).

$$b_{n+i+2} = 1 - \frac{z_i + z_{n+i+2}}{2R} \qquad (i = 1,2,\ldots,n+1) \qquad (2.64)$$

where n is the total number of cells,

z_i and z_{n+i+1} are the local z co-ordinates of the end nodes of the web plate elements respectively.

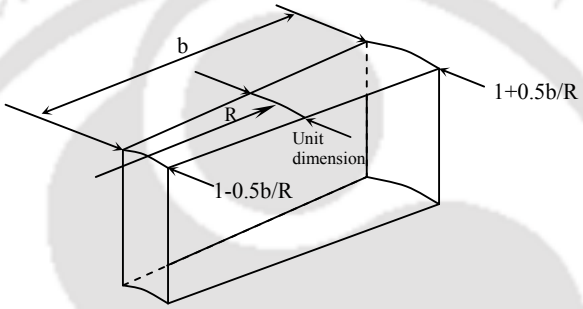

Fig. 2.18. Typical frame considered at a nodal section in the transverse frame analysis

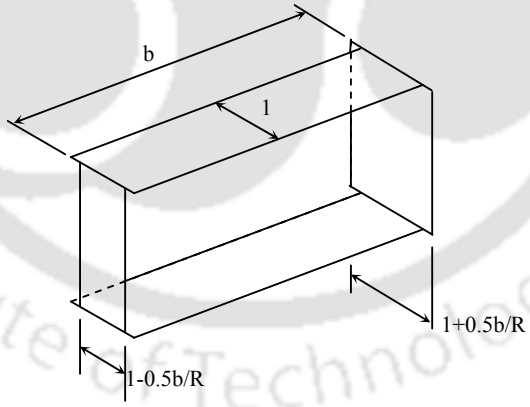

Fig. 2.19.Equivalent transverse frame

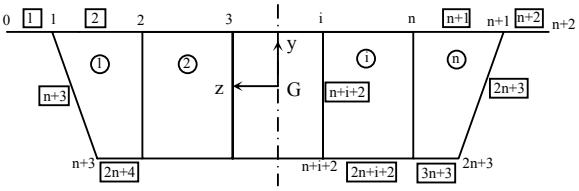

Fig. 2.20. Multi-cell cross-section

Additional distortional forces occur in box-girders curved in plan due to the radial component of the longitudinal bending stresses. The additional distortional moment per unit length is expressed as (Zhang 1983)

$$m_{dR} = 0.5\int_A \frac{M_z y}{I_z R}\left[y - (y_S - y_G)\right]\, dA \tag{2.65}$$

where, M_z is the longitudinal bending moment about the z axis,

I_z is the moment of inertia of the entire cross-section about the z axis,

y is the coordinate of a point on the centroid of the walls, referred to the neutral axis of bending of the cross-section,

y_S is the vertical coordinate of the shear center from the mid-line of the top flange,

y_G is the vertical coordinate of the centroid from the top flange,

R is the radius of curvature.

The bending moments M_z are not known at the outset and the equivalent distortional loading is not known in advance. The distribution of bending moments in curved box-girders is first evaluated assuming non-deformable cross-sections. The distortional loading is then treated as the sum of the distortional component of the loading and the additional distortional component given by Eq.2.65.

The basic differential equation for distortion is given by

$$\frac{\partial^4 \gamma_d}{\partial x^4} + 4\lambda_{II}^4 \gamma_d = \frac{1}{E_1 J_{II}}\left(\mu_d \frac{M_z}{R} + M_d\right) \tag{2.66}$$

where, μ_d is the initial curvature multiplication factor and from Eq.2.65 is given by

$$\mu_d = \frac{0.5}{I_z}\int_A y[y - (y_S - y_G)]\, dA \tag{2.67}$$

and

$$\lambda_{II} = \sqrt[4]{\frac{k_d}{4E_1 J_{II}}} \tag{2.68}$$

is called the distortional decay coefficient.

2.4 FINITE ELEMENT FORMULATION OF CURVED BOX-GIRDER BRIDGE

Considering the principle of minimum potential energy as the basis for constructing a finite element approximation involving a displacement field u, the increment of the total potential energy due to any such admissible displacements requires

$$\Delta \Pi = 0.$$

The total potential energy increment $\Delta\Pi$ can be expressed as

$$\Delta \Pi = \int_V \{\Delta\varepsilon\}^T [D] \{\varepsilon\} dV - \int_V [\Delta\varepsilon]^T [D] \{\varepsilon_0\} dV + \int_V \{\Delta\varepsilon\}^T \{\sigma_0\} dV - \int_V \{\Delta u\}^T \{b\} dV - \int_A \{\Delta u\}^T \{S\} dA - \Sigma \{\Delta u\}^T [P] \tag{2.69}$$

where $\{\varepsilon\}$ is the strain tensor, $\{\varepsilon_0\}$ is the initial strain tensor, $\{\sigma_0\}$ is the vector of initial residual stresses, $[D]$ is the elasticity matrix, b is the vector of body forces, $\{S\}$ is the vector of surface tractions, $[P]$ is the vector of external concentrated forces, V is the volume and A is the surface area.

We finally obtain the general form of the stiffness equation from Eq. (2.69)

$$[K] \{\delta\} = \{f\} \tag{2.70}$$

where $[K]$ is defined as the stiffness matrix, $\{\delta\}$ is the generalized nodal displacement vector and $\{f\}$ is the vector of nodal forces. The subsequent section on finite element implementation of thin-walled box-girder has been carried out based on the formulation of Zhang (1983).

2.4.1 Definition of Element Geometry

The thin-walled box-girder element as shown in Fig. 2.21 is considered as curved in space. However, the cross-sections are generated by straight lines having a vertical axis of

symmetry. The element axis is defined as the locus of the centroids, which may be eccentric from but parallel to the flexural axis. The element has two end nodes and a midpoint node situated on the axis.

A local rectangular coordinates system (x, y, z) along the curve axis is used in the element formulation. The origin of the Cartesian coordinate system is located at the centroid of the cross-section, and the orientation of the local axes yz is assumed to coincide with the principal axes of the cross-section. The local x axis is tangential to the element axis in the direction of the node 1 toward node 3. The local y axis usually represents the vertical axis of symmetry; the local z axis being defined by a right handed orthogonal system Fig. 2.21.

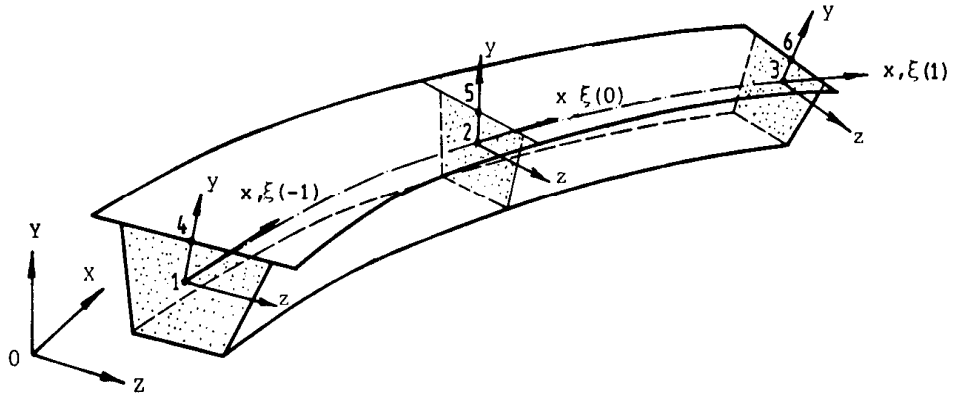

Fig. 2.21. Thin-walled box beam element with three nodes

The global cartesian coordinates are in terms of a natural co-ordinate ξ, which varies between -1 and +1 on the respective face of the element.

Let $r = X.\mathbf{i} + Y.\mathbf{j} + Z.\mathbf{k}$ be the position vector of a point P on the element axis, then a unit tangent vector along the x direction becomes

$$\mathbf{e}_x = J^{-1}\left[\left(\frac{\partial X}{\partial \xi}\right)\mathbf{i} + \left(\frac{\partial Y}{\partial \xi}\right)\mathbf{j} + \left(\frac{\partial Z}{\partial \xi}\right)\mathbf{k}\right] \tag{2.71}$$

where **i, j** and **k** are unit vectors in the global *x*, *y*, *z* directions respectively, and the Jacobian factor referring to the Jacobian matrix is

$$J = \left[\left(\frac{\partial X}{\partial \xi} \right)^2 + \left(\frac{\partial Y}{\partial \xi} \right)^2 + \left(\frac{\partial Z}{\partial \xi} \right)^2 \right]^{1/2} \tag{2.72}$$

To fix the orientation of the local *y* axis, the coordinates of the reference node 4-6, which in most case can be the mid-points of the top flanges are required. The local *z* axis can then be determined by vector multiplication

$$\mathbf{e}_z = \mathbf{e}_x \times \mathbf{e}_y \tag{2.73}$$

2.4.2 Displacement Field and Degrees of Freedom

2.4.2.1 Displacement Field due to Axial Loading and Bending

As the strains in the direction normal to the beam axis are assumed to be negligible, the displacement throughout the element can be uniquely defined by the three translations *u*, *v* and *w* on the beam axis and the two rotations θ_z, θ_y about the *z* and *y* axes respectively. This can be written in matrix form as

$$\{u_t\} = \begin{Bmatrix} u \\ v \\ w \end{Bmatrix} = \begin{Bmatrix} u - y\theta_z + z\theta_y \\ v \\ w \end{Bmatrix} \tag{2.74}$$

2.4.2.2. Displacement Field due to Warping Torsion and Distortion

The three displacement components of a point on the wall are the tangential displacement w_t, the normal displacement v_t and the axial displacement u_x. The displacements w_t and v_t are in the plane of the cross-section under consideration, and u_x is normal to the section. The positive direction of the tangential displacement component w_t is identical to the positive direction of the curvilinear coordinate *S*. The positive direction of the axial

displacement component follows the positive direction of the x axis. The three displacement components w_t, v_t and u_x comprise a right-handed orthogonal system which is shown in Fig.2.22.

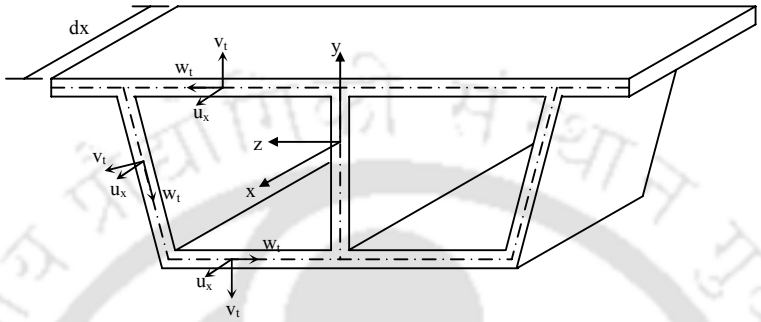

Fig. 2.22 Elementary frame showing displacement components

The three displacement components can be related to the twisting angle and the distortional angle of the cross-section as

$$w_t = R_t\theta_x + V_s(S)\gamma_d$$

$$v_t = V_t(S)\gamma_d \tag{2.75}$$

$$u_x = -\hat{\omega}_I \frac{\partial\theta_x}{\partial x} - \omega_{II}\frac{\partial\gamma_d}{\partial x}$$

or in matrix notation

$$\{u_b\} = \begin{Bmatrix} w_t \\ v_t \\ u_x \end{Bmatrix} = \begin{Bmatrix} R_t & 0 & V_s & 0 \\ 0 & 0 & V_t & 0 \\ 0 & -\hat{\omega}_I & 0 & -\omega_{II} \end{Bmatrix} \begin{Bmatrix} \theta_x \\ \theta_x' \\ \gamma_d \\ \gamma_d' \end{Bmatrix} \tag{2.76}$$

where θ_x is the angle of twist, θ_x' is the rate of twist, γ_d is the distortional angle, γ_d' is the rate of distortion, R_t is the perpendicular distance from the shear centre to the tangent to the mid-line of the wall, $V_s(S)$ is the distribution function of the tangential displacement in distortion,

$V_t(S)$ is the distribution function of the normal displacement in distortion, $\hat{\omega}_I$ is the unit torsional warping function, and ω_{II} is the unit distortional warping function.

2.4.3 Strain Components and Stress Resultants

2.4.3.1 Strains and Stress Resultants due to Axial Loading and Bending

The strains in the case of bending at a point in the element domain can be expressed as

$$\{\varepsilon_b\} = \begin{Bmatrix} \varepsilon_x^b \\ \gamma_{yx}^b \\ \gamma_{zx}^b \end{Bmatrix} = \begin{Bmatrix} \dfrac{\partial u}{\partial x} \\ \dfrac{\partial v}{\partial x} + \dfrac{\partial u}{\partial y} \\ \dfrac{\partial w}{\partial x} + \dfrac{\partial u}{\partial z} \end{Bmatrix} \tag{2.77}$$

where $\gamma_{zx}^b, \gamma_{yx}^b$ and $\varepsilon_x^{\ b}$ are the shear strains and axial strains respectively.

Substituting Eq. (2.74) in (2.77),

$$\{\varepsilon_b\} = \begin{Bmatrix} \varepsilon_x^{\ b} \\ \gamma_{yx}^b \\ \gamma_{zx}^b \end{Bmatrix} = \begin{Bmatrix} \dfrac{\partial u}{\partial x} - y\dfrac{\partial \theta_z}{\partial x} + z\dfrac{\partial \theta_y}{\partial x} \\ \dfrac{\partial v}{\partial x} - \theta_z \\ \dfrac{\partial w}{\partial x} + \theta_y \end{Bmatrix} \tag{2.78}$$

$$\{\varepsilon_b\} = \begin{bmatrix} 1 & 0 & 0 & z & y \\ 0 & 1 & 0 & 0 & 0 \\ 0 & 0 & 1 & 0 & 0 \end{bmatrix} \{\bar{\varepsilon}_b\} \tag{2.79}$$

where $$\{\bar{\varepsilon}_b\} = \begin{Bmatrix} \dfrac{\partial u}{\partial x} \\ \dfrac{\partial v}{\partial x} - \theta_z \\ \dfrac{\partial w}{\partial x} + \theta_y \\ \dfrac{\partial \theta_y}{\partial x} \\ -\dfrac{\partial \theta_z}{\partial x} \end{Bmatrix} \tag{2.80}$$

The corresponding stress components at a point in the element domain can be obtained in the linear-elastic case as

$$\begin{Bmatrix} \sigma_x^b \\ \tau_{yx}^b \\ \tau_{zx}^b \end{Bmatrix} = [D_b] \begin{Bmatrix} \varepsilon_x^b \\ \gamma_{yx}^b \\ \gamma_{zx}^b \end{Bmatrix} \tag{2.81}$$

where the elasticity matrix is given by

$$[D_b] = \begin{bmatrix} E_1 & 0 & 0 \\ 0 & G & 0 \\ 0 & 0 & G \end{bmatrix} \tag{2.82}$$

Substituting Eq.2.79 and 2.82 into the integral expression of Eq.2.69, we obtain

$$\int_V \{\Delta\varepsilon_b\}^T [D_b] \{\varepsilon_b\} dV = \int_{-1/2}^{1/2} \{\Delta\bar{\varepsilon}_b\}^T \{\bar{\sigma}_b\} dx \tag{2.83}$$

where

$$\{\bar{\sigma}_b\} = [\bar{D}_b] \{\bar{\varepsilon}_b\} \tag{2.84}$$

$$[\bar{D}_b] = \int_A \begin{bmatrix} 1 & 0 & 0 \\ 0 & 1 & 0 \\ 0 & 0 & 1 \\ z & 0 & 0 \\ y & 0 & 0 \end{bmatrix} \begin{bmatrix} E_1 & 0 & 0 \\ 0 & G & 0 \\ 0 & 0 & G \end{bmatrix} \begin{bmatrix} 1 & 0 & 0 & z & y \\ 0 & 1 & 0 & 0 & 0 \\ 0 & 0 & 1 & 0 & 0 \end{bmatrix} dA \tag{2.85}$$

$$\left[\bar{D}_b\right]=\int_A\begin{bmatrix} E_1 & 0 & 0 & E_1 z & E_1 y \\ 0 & G & 0 & 0 & 0 \\ 0 & 0 & G & 0 & 0 \\ E_1 z & 0 & 0 & E_1 z^2 & E_1 zy \\ E_1 y & 0 & 0 & E_1 zy & E_1 y^2 \end{bmatrix} dA \tag{2.86}$$

Integrating over the region A and since the z and y axes are the principal axes of the cross-section, this gives

$$\int_A E_1 z dA = 0\,, \qquad \int_A E_1 y dA = 0\,, \qquad \int_A E_1 zy dA = 0$$

$$I_y = \int_A z^2 dA \qquad \text{and} \qquad I_z = \int_A y^2 dA$$

Hence, we obtain

$$\left[\bar{D}_b\right]=\begin{bmatrix} E_1 A & 0 & 0 & 0 & 0 \\ 0 & GA & 0 & 0 & 0 \\ 0 & 0 & GA & 0 & 0 \\ 0 & 0 & 0 & E_1 I_y & 0 \\ 0 & 0 & 0 & 0 & E_1 I_z \end{bmatrix} \tag{2.87}$$

where A is the cross-sectional area and I_y, I_z are the moments of inertia with respect to y and z axes respectively.

To account for non-uniform shear strain distribution, and effective shear cross-sectional area is introduced, Eq.2.87 becomes

$$\left[\bar{D}_b\right]=\begin{bmatrix} E_1 A & 0 & 0 & 0 & 0 \\ 0 & GA_{sy} & 0 & 0 & 0 \\ 0 & 0 & GA_{sz} & 0 & 0 \\ 0 & 0 & 0 & E_1 I_y & 0 \\ 0 & 0 & 0 & 0 & E_1 I_z \end{bmatrix} \tag{2.88}$$

where A_{sy} and A_{sz} represent the beam effective shear cross-sectional areas in the y and z-direction respectively.

The effective shear areas can be expressed as

$$A_{Sz} = \frac{1}{\mathrm{F_{Sz}}}.\mathrm{A} \quad \text{and} \quad A_{Sy} = \frac{1}{\mathrm{F_{Sy}}}.\mathrm{A} \tag{2.89}$$

where F_s is defined as the shear-deformation factor, which depends on the form of the cross-section. For a Rectangular section, $F_s = \frac{6}{5}$, For a Solid circular section $F_s = \frac{10}{9}$, for a thin-walled hollow circular section, $F_s = 2$. For an I or box-section having flanges and webs of uniform thickness F_s is given by

$$F_s = \left[1 + \frac{3\left(D_2^2 - D_1^2\right)D_1}{2D_2^3}\left(\frac{t_2}{t_1} - 1\right)\right]\frac{4D_2^2}{10r^2} \tag{2.90}$$

where D_1 =Distance from neutral axis to the nearest surface of the flange,

D_2 = Distance from neutral axis to extreme fiber,

t_1 = Thickness of web (or web in box-girder)

t_2 = Width of flange

r = Radius of gyration of section with respect to the neutral axis.

The stress vector $[\bar{\sigma}_b]$ represents the conventional stress resultants for a beam, i.e., axial force, shear force and bending moments.

$$[\bar{\sigma}_b] = \begin{bmatrix} N_x & Q_y & Q_z & M_y & M_z \end{bmatrix}^T \tag{2.91}$$

The generalized shear strain vector $\{\bar{\varepsilon}_b\}$ represents the axial strain, the shear strain and the curvatures.

2.4.3.2 Strains and Stress Resultants due to Warping Torsion

The strains due to torsion at a point in the element domain can be expressed as

$$\{\varepsilon_t\} = \begin{Bmatrix} \gamma_{xs}^t \\ \varepsilon_x^t \end{Bmatrix} = \begin{Bmatrix} \phi_I \dfrac{\partial \theta_x}{\partial x} \\ -\hat{\omega}_I \dfrac{\partial^2 \theta_x}{\partial x^2} \end{Bmatrix} \tag{2.92}$$

Eq.2.92 can be written as

$$\{\varepsilon_t\} = \begin{bmatrix} \phi_I & 0 \\ 0 & \hat{\omega}_I \end{bmatrix} \{\bar{\varepsilon}_t\} \tag{2.93}$$

where the generalized strain vector due to torsion is

$$\{\bar{\varepsilon}_t\} = \begin{Bmatrix} \dfrac{\partial \theta_x}{\partial x} \\ -\dfrac{\partial^2 \theta_x}{\partial x^2} \end{Bmatrix} \tag{2.94}$$

Considering the primary torsional shear strain and neglecting the secondary shear stresses associated with the normal warping stresses, the function $\{\phi_I\}$ may be given as

$$\{\phi_I\} = \begin{Bmatrix} 2y_n \\ \dfrac{\bar{q}_B}{t} \end{Bmatrix} \tag{2.95}$$

where y_n is the normal coordinate to the mid-line of the wall, $\bar{q}_B$ is the unit Bredt shear flow function, t is the thickness of the wall.

The corresponding stress components are given by

$$\{\sigma_t\} = \begin{Bmatrix} \tau_{xs}^t \\ \sigma_x^t \end{Bmatrix} = [D_t] \begin{Bmatrix} \gamma_{xs}^t \\ \varepsilon_x^t \end{Bmatrix} \tag{2.96}$$

where the elasticity matrix

$$[D_t] = \begin{bmatrix} G & 0 \\ 0 & E_1 \end{bmatrix} \tag{2.97}$$

Substituting Eq. 2.93 and 2.97 into the strain energy expression gives

$$\int_V \{\Delta\varepsilon_t\}\ [D_t]\ \{\varepsilon_t\}\ dV = \int_{-l/2}^{l/2} \{\Delta\bar{\varepsilon}_t\}\{\bar{\sigma}_t\}\,dx \tag{2.98}$$

where the generalized stress vector is

$$\{\bar{\sigma}_t\} = \left[\bar{D}_t\right]\ \{\bar{\varepsilon}_t\} \tag{2.99}$$

The generalized torsional elasticity matrix can be expressed as

$$\left[\bar{D}_t\right] = \int_A \begin{bmatrix} \phi_I & 0 \\ 0 & \hat{\omega}_I \end{bmatrix} \begin{bmatrix} G & 0 \\ 0 & E_1 \end{bmatrix} \begin{bmatrix} \phi_I & 0 \\ 0 & \hat{\omega}_I \end{bmatrix} dA$$

$$= \int_A \begin{bmatrix} G\phi_I^2 & 0 \\ 0 & E_1\hat{\omega}_I^2 \end{bmatrix} dA \tag{2.100}$$

where, $\int_A E_1\hat{\omega}_I^2 dA = E_1 J_1$ (2.101)

and $\int_A G\phi_I^2 dA = GJ_T$ (2.102)

Hence, we can write the generalized torsional elasticity matrix as

$$\left[\bar{D}_t\right] = \begin{bmatrix} GJ_T & 0 \\ 0 & E_1 J_1 \end{bmatrix} \tag{2.103}$$

where, J_T is the torsional moment of inertia

J_I is the torsional warping moment in inertia

The generalized elasticity matrix is modified to include the deformational influence due to the warping shear stresses as

$$\left[\bar{D}_t\right] = \begin{bmatrix} GJ_T & 0 \\ 0 & \dfrac{1}{\mu_t} E_1 J_1 \end{bmatrix} \tag{2.104}$$

in which μ_t is the warping shear parameter.

The generalized stress vector represents the torsional stress resultants, which are the torsional moment and the torsional bimoment

$$[\bar{\sigma}_t] = \begin{bmatrix} M_T & \frac{1}{\mu_t} B_I \end{bmatrix}^T \tag{2.105}$$

2.4.3.3 Strains and Stress Resultants due to Distortion

The strain energy increment due to internal work done by distortion includes two parts:

1) The strain energy increments due to the internal work done by the distortional warping stresses

$$\int_V \Delta\varepsilon_{x,d} E_1 \varepsilon_{x,d} dV = \int_{-½}^{½} \Delta\left(-\frac{\partial^2 \gamma_d}{\partial x^2}\right) \int_A E_1 \omega_{II}^2 dA \left(-\frac{\partial^2 \gamma_d}{\partial x^2}\right) dx \tag{2.106}$$

$$= \int_{-½}^{½} \Delta\left(-\frac{\partial^2 \gamma_d}{\partial x^2}\right) B_{II} dx \tag{2.107}$$

2) The strain energy increment associated with the transverse frame action of the box, *i.e.*, due to the internal work done by the transverse bending

$$\int_V \Delta\varepsilon_{db} E_1 \varepsilon_{db} dV = \int_{-½}^{½} \Delta\gamma_d E_1 J_d \gamma_d dx$$

$$= \int_{-½}^{½} \Delta\gamma_d M_d dx \tag{2.108}$$

where γ_d is the distortional angle, M_d is the generalized distortional moment, and B_{II} is the distortional moment.

Rewriting the above expressions in matrix form

$$\int_V \{\Delta\varepsilon_d\} [D_d] \{\varepsilon_d\} dV = \int_{-½}^{½} \{\Delta\bar{\varepsilon}_d\}^T \{\bar{\sigma}_d\} dx \tag{2.109}$$

where the generalized distortional strain vector is

$$[\bar{\varepsilon}_d] = \begin{bmatrix} \gamma_d & -\frac{\partial^2 \gamma_d}{\partial x^2} \end{bmatrix} \tag{2.110}$$

and the generalized elasticity matrix is

$$\left[\bar{D}_d\right]=\begin{bmatrix} E_1 J_d & 0 \\ 0 & E_1 J_{II} \end{bmatrix} \tag{2.111}$$

in which J_d is the distortional second moment of area, and J_{II} is the distortional warping moment of inertia.

The generalized stress vector $\{\bar{\sigma}_d\}$ represents the distortional stress resultants, i.e., the distortional moment and the distortional bimoment

$$\left[\bar{\sigma}_d\right]=\left[M_d \quad B_{II}\right]^T \tag{2.112}$$

2.4.4 Stress - Strain Relationship

The generalized displacements in the local co-ordinate system are given by

$$\left[\bar{\delta}\right]=\left[u,v,w,\theta_x,\theta_y,\theta_z,\theta'_x,\gamma_d,\gamma'_d\right]^T \tag{2.113}$$

where u,v,w are the translations along the local *x, y, z* axes respectively, θ_x is the angle of twist, θ'_x is the rate of twist, θ_y and θ_z are bending rotations about *y* and *z* axes respectively, γ_d is the distortion angle, γ'_d is the rate of distortion.

The corresponding displacements in the global co-ordinate system are given by

$$\left[\delta\right]=\left[U,V,W,\phi_x,\phi_y,\phi_z,\theta'_x,\gamma_d,\gamma'_d\right] \tag{2.114}$$

where U,V,W are the translations along the *X, Y, Z* global axes respectively, ϕ_x, ϕ_y,ϕ_z are rotations about the same axes respectively, while the rate of twist θ'_x and distortional variables γ_d, γ'_d remain in locals. The thin-walled box element has, therefore, nine degrees of freedom at each node.

With reference to the principal local system defined, the relation between the generalized stress resultants and the generalized strain components can be expressed from the Timoshenko beam theory and the thin-walled beam theory as Fig.2.23.

$$\{\bar{\sigma}\} = \left[\bar{D}\right] \{\bar{\varepsilon}\} \tag{2.115}$$

where the generalized stress vector is

$$\left[\bar{\sigma}\right] = \left[N_x, Q_y, Q_z, M_T, M_y, M_z, \frac{1}{\mu_t} B_1, M_d, B_{11} \right]^T \tag{2.116}$$

in which N_x is the axial force, Q_y, Q_Z are the shear forces, M_T is the pure torsional moment, M_y, M_z are the primary bending moments, B_1 is the torsional warping bimoment, M_d is the distortional moment, B_{11} is the distortional warping bimoment and μ_t is the warping shear parameter.

Displ.	*Forces*
U	N_x
V	Q_y
W	Q_z
θ_x	M_T
θ_y	M_y
θ_z	M_z
θ_x'	B_I
γ_d	M_d
γ_d'	B_{II}

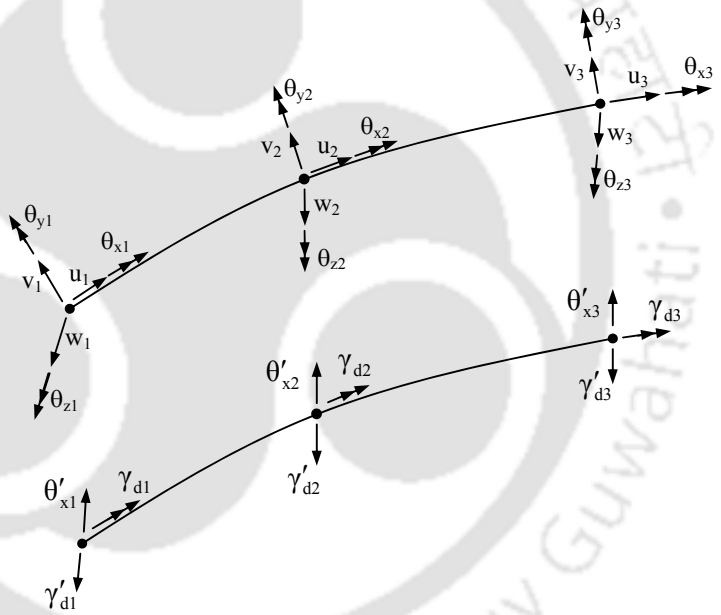

Fig. 2.23. Generalized forces and displacements

The generalized strain vector is

$$\left[\bar{\varepsilon}\right] = \left[\varepsilon_x, \varepsilon_{yx}, \varepsilon_{zx}, \psi_{\theta x}, \psi_{yx}, \psi_{zx}, \psi_{wtx}, \psi_{dx}, \psi_{wdx} \right]^T \tag{2.117}$$

where

axial strain

$$\varepsilon_x = \frac{\partial u}{\partial x} \tag{2.118}$$

shear strain in y – direction

$$\varepsilon_{yx} = \frac{\partial v}{\partial x} + \frac{\partial u}{\partial y} = \frac{\partial v}{\partial x} - \theta_z \tag{2.119}$$

shear strain in z – direction

$$\varepsilon_{zx} = \frac{\partial w}{\partial x} + \frac{\partial u}{\partial z} = \frac{\partial w}{\partial x} + \theta_y \tag{2.120}$$

torsional strain

$$\psi_{\theta x} = \frac{\partial \theta_x}{\partial x} \tag{2.121}$$

flexural strain about y – axis

$$\psi_{yx} = \frac{\partial^2 u}{\partial x \partial z} = \frac{\partial \theta_y}{\partial x} \tag{2.122}$$

flexural strain about z – axis

$$\psi_{zx} = \frac{\partial^2 u}{\partial x \partial y} = -\frac{\partial \theta_z}{\partial x} \tag{2.123}$$

torsional warping strain

$$\psi_{wtx} = -\frac{\partial^2 \theta_x}{\partial x^2} - \frac{1}{R}\frac{\partial \theta_z}{\partial x} \tag{2.124}$$

distortional strain

$$\psi_{dx} = \gamma_d \tag{2.125}$$

distortional warping strain

$$\psi_{wdx} = -\frac{\partial^2 \gamma_d}{\partial x^2} \tag{2.126}$$

The radius of curvature R introduced in the torsional warping strain component can be expressed as

$$R = \left[\left(\frac{\partial^2 X}{\partial \xi^2} \right)^2 + \left(\frac{\partial^2 Y}{\partial \xi^2} \right)^2 + \left(\frac{\partial^2 Z}{\partial \xi^2} \right)^2 \right]^{-1/2} \tag{2.127}$$

where X, Y, Z are the global co-ordinates of the points on the beam axis curve.

A modification has been made to the torsional warping strain to take into account the effect caused by the initial curvature.

Finally, as a result of orthogonalisation the rigidity matrix can be shown to be

$$\left[\bar{D}\right] = \begin{bmatrix} E\,A & & & & & & & & \\ & GA_{sy} & & & & & & 0 & \\ & & GA_{sz} & & & & & & \\ & & & GJ_T & & & & & \\ & & & & E\,I_y & & & & \\ & & & & & E\,I_z & & & \\ & & & & & & \frac{1}{\mu_t}E_1 J_I & & \\ & & 0 & & & & & E_1 J_d & \\ & & & & & & & & E_1 J_{II} \end{bmatrix} \tag{2.128}$$

where A is cross-sectional area: A_{sy}, A_{sz}, are effective shear areas in the y and the z directions respectively; J_T is torsional moment of inertia; I_y , I_z are bending moments of inertia about the y and z axes respectively; J_I is torsional warping moment of inertia; J_d is distortional second moment of area; and J_{II} is distortional warping moment of inertia. It should be noted that the bending moments of inertia should be calculated on the basis of an effective flange breath replacing the actual width to account for the effect of shear lag. The material properties are characterized by the Young's modulus of elasticity E and the shear modulus G which is expressed as

$$G = \frac{E}{2(1+v)} \tag{2.129}$$

where v is the Poisson's ratio.

The conversion modulus of elasticity is

$$E_1 = \frac{E}{\left(1-\nu^2\right)} \tag{2.130}$$

2.4.5 Shape Functions to Define the Displacement Field

Only C_0 continuity is required for the extensional and flexural effects, and the following quadratic shape functions are used

$$N_i = \frac{1}{2}\left(\xi^2 + \xi_0\right) \quad \text{for } i = 1 \text{ and } 3$$

$$N_i = \left(1-\xi^2\right) \qquad \text{for } i = 2 \tag{2.131}$$

where $\xi_0 = \xi\xi_i$.

Since the governing equations for torsion and distortion are fourth order (Eq.2.15 and 2.66) and the beam being three-noded, fifth order C_1 continuity is required for torsion and distortion.

$$N_{11} = \left(\frac{\xi^2}{4}\right)\left(4 - 5\xi - 2\xi^2 + 3\xi^3\right)$$

$$N_{12} = \left(\frac{J_1}{4}\right)\xi^2\left(1-\xi\right)\left(1-\xi^2\right)$$

$$N_{21} = \left(\frac{\xi^2}{4}\right)\left(4 + 5\xi - 2\xi^2 - 3\xi^3\right) \tag{2.132}$$

$$N_{22} = \left(\frac{J_2}{4}\right)\xi^2\left(1+\xi\right)\left(\xi^2 - 1\right)$$

$$N_{31} = \left(1-\xi^2\right)^2$$

$$N_{32} = J_3\xi\left(1-\xi^2\right)^2$$

where $\xi_0 = \xi\xi_i$ and J_1, J_2 and J_3 are the Jacobian factors at the three nodes of the element.

A special form of transformation, referred to as hierarchical mapping is adopted for mapping the geometry. The hierarchical shape functions are defined in terms of the natural coordinate ξ as

$$M_i = \tfrac{1}{2}(1+\xi_0) \qquad \text{for } i\text{=1 and 2} \tag{2.133}$$

$$M_i = (1-\xi^2) \qquad \text{for } i\text{=3}$$

where $\xi_0 = \xi_i\ \xi$

2.4.6 Formulation of Displacements and Strains

The generalized displacements in the local coordinate system are

$$\left[\bar{\delta}\right] = \left[\bar{N}\right]\ \left\{\bar{\delta}^e\right\} = \left[\bar{N}_1 \bar{N}_2 \bar{N}_3\right]\left\{\bar{\delta}^e\right\} \tag{2.134}$$

where $\left\{\bar{\delta}^e\right\}$ are the nodal values of the global displacements and

$$\left[\bar{N}_i\right] = \begin{bmatrix}
N_i\,\mathrm{i.e_x} & N_i\,\mathrm{j.e_x} & N_i\,\mathrm{k.e_x} & 0 & 0 & 0 & 0 & 0 & 0 \\
N_i\,\mathrm{i.e_y} & N_i\,\mathrm{j.e_y} & N_i\,\mathrm{k.e_y} & 0 & 0 & 0 & 0 & 0 & 0 \\
N_i\,\mathrm{i.e_z} & N_i\,\mathrm{j.e_z} & N_i\,\mathrm{k.e_z} & 0 & 0 & 0 & 0 & 0 & 0 \\
0 & 0 & 0 & N_{i1}\,\mathrm{i.e_x} & N_{i1}\,\mathrm{j.e_x} & N_{i1}\,\mathrm{k.e_x} & N_{i2} & 0 & 0 \\
0 & 0 & 0 & N_i\,\mathrm{i.e_y} & N_i\,\mathrm{j.e_y} & N_i\,\mathrm{k.e_y} & 0 & 0 & 0 \\
0 & 0 & 0 & N_i\,\mathrm{i.e_z} & N_i\,\mathrm{j.e_z} & N_i\,\mathrm{k.e_z} & 0 & 0 & 0 \\
0 & 0 & 0 & \frac{\partial N_{i1}}{\partial x}\mathrm{i.e_x} & \frac{\partial N_{i1}}{\partial x}\mathrm{j.e_x} & \frac{\partial N_{i1}}{\partial x}\mathrm{k.e_x} & \frac{\partial N_{i2}}{\partial x} & 0 & 0 \\
0 & 0 & 0 & 0 & 0 & 0 & 0 & N_{i1} & N_{i2} \\
0 & 0 & 0 & 0 & 0 & 0 & 0 & \frac{\partial N_{i1}}{\partial x} & \frac{\partial N_{i2}}{\partial x}
\end{bmatrix} \tag{2.135}$$

where $\mathbf{i.e_x}$, $\mathbf{i.e_y}$ ….., $\mathbf{k.e_z}$ are the direction cosines.

The strains are obtained from

$$\left\{\bar{\varepsilon}\right\} = \left[L\right]\ \left\{\bar{\delta}\right\} \tag{2.136}$$

where $[L]$ is a linear operator and can be written directly from the definition of the generalized strain vector.

$$[L]=\begin{bmatrix} \frac{\partial}{\partial x} & 0 & 0 & 0 & 0 & 0 & 0 & 0 & 0 \\ 0 & \frac{\partial}{\partial x} & 0 & 0 & 0 & -1 & 0 & 0 & 0 \\ 0 & 0 & \frac{\partial}{\partial x} & 0 & 1 & 0 & 0 & 0 & 0 \\ 0 & 0 & 0 & \frac{\partial}{\partial x} & 0 & 0 & 0 & 0 & 0 \\ 0 & 0 & 0 & 0 & \frac{\partial}{\partial x} & 0 & 0 & 0 & 0 \\ 0 & 0 & 0 & 0 & 0 & -\frac{\partial}{\partial x} & 0 & 0 & 0 \\ 0 & 0 & 0 & 0 & 0 & -\frac{1}{R}\frac{\partial}{\partial x} & -\frac{\partial}{\partial x} & 0 & 0 \\ 0 & 0 & 0 & 0 & 0 & 0 & 0 & 1 & 0 \\ 0 & 0 & 0 & 0 & 0 & 0 & 0 & 0 & -\frac{\partial}{\partial x} \end{bmatrix} \tag{2.137}$$

The strain displacement matrix $\left[\bar{B}\right]$ is

$$\left[\bar{B}\right]=\left[L\right]\left[\bar{N}\right]=\left[\bar{B}_1 \quad \bar{B}_2 \quad \bar{B}_3\right] \tag{2.138}$$

$$\left[\bar{B}_i\right]=\begin{bmatrix} \frac{\partial N_i}{\partial x}\mathrm{i.e_x} & \frac{\partial N_i}{\partial x}\mathrm{j.e_x} & \frac{\partial N_i}{\partial x}\mathrm{k.e_x} & 0 & 0 & 0 & 0 & 0 & 0 \\ \frac{\partial N_i}{\partial x}\mathrm{i.e_y} & \frac{\partial N_i}{\partial x}\mathrm{j.e_y} & \frac{\partial N_i}{\partial x}\mathrm{k.e_y} & -N_i\mathrm{i.e_z} & -N_i\mathrm{j.e_z} & -N_i\mathrm{k.e_z} & 0 & 0 & 0 \\ \frac{\partial N_i}{\partial x}\mathrm{i.e_z} & \frac{\partial N_i}{\partial x}\mathrm{j.e_z} & \frac{\partial N_i}{\partial x}\mathrm{k.e_z} & N_i\mathrm{i.e_y} & N_i\mathrm{j.e_y} & N_i\mathrm{k.e_y} & 0 & 0 & 0 \\ 0 & 0 & 0 & \frac{\partial N_{i1}}{\partial x}\mathrm{i.e_x} & \frac{\partial N_{i1}}{\partial x}\mathrm{j.e_x} & \frac{\partial N_{i1}}{\partial x}\mathrm{k.e_x} & \frac{\partial N_{i2}}{\partial x} & 0 & 0 \\ 0 & 0 & 0 & \frac{\partial N_i}{\partial x}\mathrm{i.e_y} & \frac{\partial N_i}{\partial x}\mathrm{j.e_y} & \frac{\partial N_i}{\partial x}\mathrm{k.e_y} & 0 & 0 & 0 \\ 0 & 0 & 0 & -\frac{\partial N_i}{\partial x}\mathrm{i.e_z} & -\frac{\partial N_i}{\partial x}\mathrm{j.e_z} & -\frac{\partial N_i}{\partial x}\mathrm{k.e_z} & 0 & 0 & 0 \\ 0 & 0 & 0 & -\frac{\partial^2 N_{i1}}{\partial x^2}\mathrm{i.e_x} & -\frac{\partial^2 N_{i1}}{\partial x^2}\mathrm{j.e_x} & -\frac{\partial^2 N_{i1}}{\partial x^2}\mathrm{k.e_x} & -\frac{\partial^2 N_{i2}}{\partial x^2} & 0 & 0 \\ & & & -\frac{1}{R}\frac{\partial N_i}{\partial x}\mathrm{i.e_z} & -\frac{1}{R}\frac{\partial N_i}{\partial x}\mathrm{j.e_z} & -\frac{1}{R}\frac{\partial N_i}{\partial x}\mathrm{k.e_z} & & & \\ 0 & 0 & 0 & 0 & 0 & 0 & 0 & N_{i1} & N_{i2} \\ 0 & 0 & 0 & 0 & 0 & 0 & 0 & -\frac{\partial^2 N_{i1}}{\partial x^2} & -\frac{\partial^2 N_{i2}}{\partial x^2} \end{bmatrix} \tag{2.139}$$

$$\{\bar{\varepsilon}\} = \left[\bar{B}\right]\{\bar{\delta}^e\} \tag{2.140}$$

The derivatives of the shape functions with respect to Cartesian coordinates x are related by

$$\frac{\partial N_i}{\partial x} = J^{-1}\frac{\partial N_i}{\partial \xi} \tag{2.141}$$

$$\frac{\partial^2 N_i}{\partial x^2} = J^{-1}\frac{\partial J^{-1}}{\partial \xi}\frac{\partial N_i}{\partial \xi} + (J^{-1})^2\frac{\partial^2 N_i}{\partial \xi^2} \tag{2.142}$$

where $$J^{-1} = \left[\left(\frac{\partial X}{\partial \xi}\right)^2 + \left(\frac{\partial Y}{\partial \xi}\right)^2 + \left(\frac{\partial Z}{\partial \xi}\right)^2\right]^{-\frac{1}{2}} \tag{2.143}$$

$$\frac{\partial J^{-1}}{\partial \xi} = -\left[\frac{\partial X}{\partial \xi}\frac{\partial^2 X}{\partial \xi^2} + \frac{\partial Y}{\partial \xi}\frac{\partial^2 Y}{\partial \xi^2} + \frac{\partial Z}{\partial \xi}\frac{\partial^2 Z}{\partial \xi^2}\right] \times \left[\left(\frac{\partial X}{\partial \xi}\right)^2 + \left(\frac{\partial Y}{\partial \xi}\right)^2 + \left(\frac{\partial Z}{\partial \xi}\right)^2\right]^{-\frac{3}{2}} \tag{2.144}$$

2.4.7 The Element Stiffness, Mass Matrix and the Equivalent Nodal Force Vector

The element stiffness matrix may be written as

$$\left[K^e\right] = \int_{-1/2}^{1/2}\left[\bar{B}\right]^{\mathrm{T}}\left[\bar{D}\right]\left[\bar{B}\right]dx = \int_{-1}^{+1} J\left[\bar{B}\right]^{\mathrm{T}}\left[\bar{D}\right]\left[\bar{B}\right]d\xi \tag{2.145}$$

where $\left[\bar{B}\right]$ is the strain displacement matrix.

The element mass matrix may be written as

$$\left[M^e\right] = A\int_{-1/2}^{1/2}\left[\bar{N}\right]^{\mathrm{T}}\rho\left[\bar{N}\right]dx = A\int_{-1}^{+1}\mathrm{J}\left[\bar{N}\right]^{\mathrm{T}}\rho\left[\bar{N}\right]d\xi \tag{2.146}$$

The nodal force vector equivalent to internal and external forces is written as

$$\left\{f^e\right\} = \int_1\left[\bar{N}\right]^{\mathrm{T}}\{b\}dx + \int_1\left[\bar{N}\right]^{\mathrm{T}}\{q\}dx + \sum\left[\bar{N}\right]^{\mathrm{T}}\{P\} + \int_1\left[\bar{B}\right]^{\mathrm{T}}\left[\bar{D}\right]\{\varepsilon_0\} - \int_1\left[\bar{B}\right]^{T}\{\sigma_0\}dx \tag{2.147}$$

where $\{b\}$ is body force vector, $\{q\}$ is distributed force vector, $\{P\}$ is concentrated force vector, $\{\varepsilon_0\}$ is initial strain vector including temperature effects, and $\{\sigma_0\}$ is initial stress vector.

The distributed force vector is given by

$$[q] = \begin{bmatrix} p_x & p_y & p_z & m_{x,ext} & m_{y,ext} & m_{z,ext} & b_I & m_d & b_{II} \end{bmatrix} \tag{2.148}$$

The concentrated force vector is given by

$$[P] = \begin{bmatrix} \bar{P}_x & \bar{P}_y & \bar{P}_z & \bar{M}_x & \bar{M}_y & \bar{M}_z & 0 & \bar{M}_d & 0 \end{bmatrix} \tag{2.149}$$

Exact integration of Eq. (2.145) and Eq. (2.146) is achieved by using a three-point Gauss quadrature for the axial and bending contributions and a six-point Gauss quadrature for the torsional and distortional contributions.

The normal stresses at the points on the mid-line of the flanges can be obtained by following expression,

$$\sigma_x = \frac{N_x}{A} + \frac{M_y}{I_y} z - \xi \frac{M_z}{I_z} y + \frac{B_I}{J_I} \omega_I + \frac{B_{II}}{J_{II}} \omega_{II} \tag{2.150}$$

where ω_I and ω_{II} are the torsional and distortional warping functions respectively. The factor ξ is expressed in Eq. (2.7) and Eq. (2.8).

A computer program has been developed for the determination of cross-sectional properties of thin-walled box-girder and the complete procedure of evaluation of stresses for a curved thin-walled box-girder bridge is shown in a flow chart for in Appendix A, Appendix B and Appendix G respectively.

2.4.8 Boundary Conditions

For some conventional support conditions used in bridge construction the following holds true:

(a) If the bridge is fixed at the support, no deformation arises in the support cross-section, and therefore the following may be written

$$\left.\begin{array}{l} u = v = w = 0 \\ \theta_x = \theta_y = \theta_z = 0 \end{array}\right\} \qquad \begin{array}{l} U = V = W = 0 \\ \phi_x = \phi_y = \phi_z = 0 \end{array}$$
$$\theta_x' = \gamma_d = \gamma_d' = 0 \tag{2.151}$$

(b) If the support cross-section is connected by a pinned support and is braced by a rigid diaphragm, and yet is free to warp, then the independent boundary conditions are

$$u = v = w = 0 \qquad U = V = W = 0$$
$$\theta_x = \gamma_d = 0 \tag{2.152}$$

(c) If the cross-section is supported by a linear roller which is oriented perpendicularly to the longitudinal axis, and also is braced by a rigid diaphragm, but is free to warp, the boundary conditions may be adjusted to

$$v = w = 0$$
$$\theta_x = \gamma_d = 0 \tag{2.153}$$

(d) If the free end cross-section of a cantilever is braced by a diaphragm to resist its transverse deformation only, yet is free to warp, only one boundary condition applies and that is $\gamma_d = 0$ (2.154)

2.5 NUMERICAL EXAMPLES

Different types of box-girder bridge problems have been investigated to check the validity and generality of the adopted finite element formulation in this numerical study.

2.5.1 A Straight Box-Girder Subjected to an Eccentric Load

A simply-supported straight box-girder problem (Fig 2.24) given by Kermani and Waldron (1993) has been considered. The span is 30 m and the diaphragms are located only at the ends. Two cases are considered for the diaphragm action: i) the diaphragms are

infinitely rigid in their own plane and prevent distortion of the two ends while they offer no resistance to warping, ii) the diaphragms offer both distortional and warping restraint. At mid-span there is a point load of 1000 kN acting eccentrically over one web. Thin-walled box -girder elements have been used with an 8 element mesh to analyze the beam. Plots for deflection, rotations about *x* and *z* axis, rate of rotation about *x* axis, distortional angle, rate of distortional angle, bending moment, shear force, pure torsion (Figs. 2.25 (a), (b), (c), (d), (e), (f), and Figs. 2.26. (a), (b), (c)) for case(i) and torsional bimoment, distortional moment and distortional bimoment (Figs. 2.27. (a), (b), (c) and Figs.2.28 (a), (b), (c)) for cases (i) and (ii) are presented.

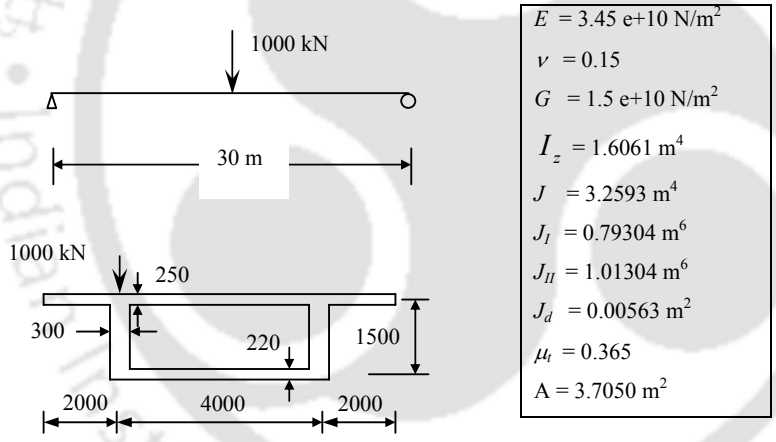

Fig. 2.24. Loading and geometry (mm) of the straight beam model

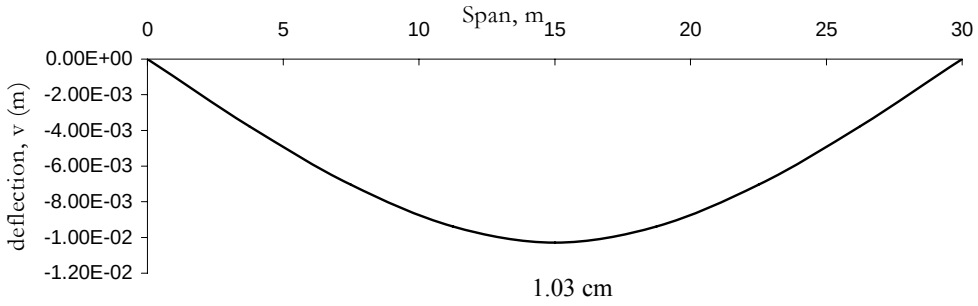

(a)

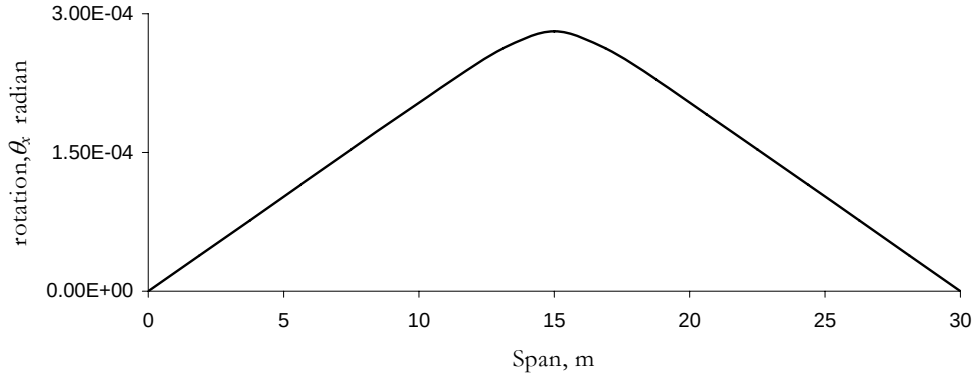

(b)

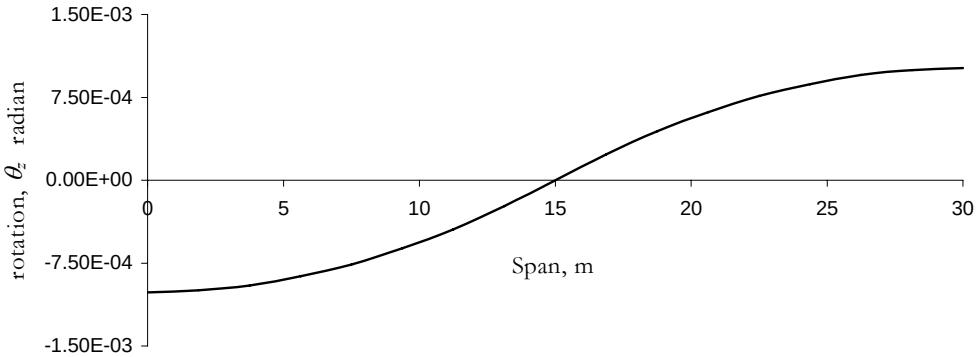

(c)

Fig. 2.25. (a) Deflection, v (b) Rotation, θ_x (c) Rotation, θ_z with distortional restraint and no warping restraint [case (i)]

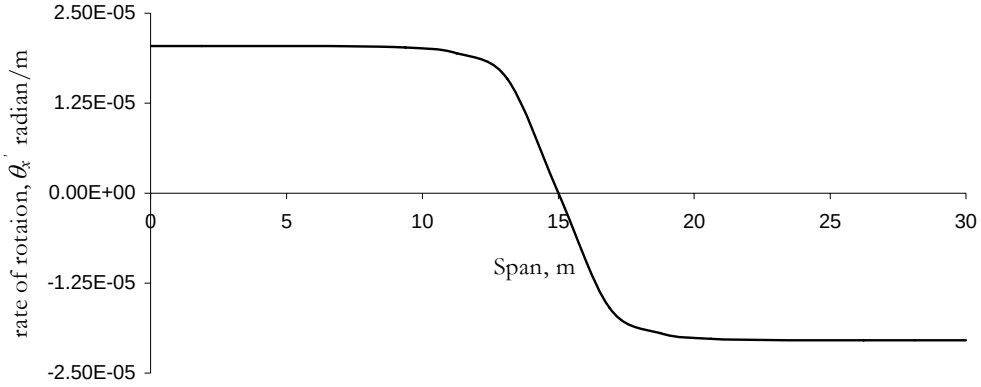

(d)

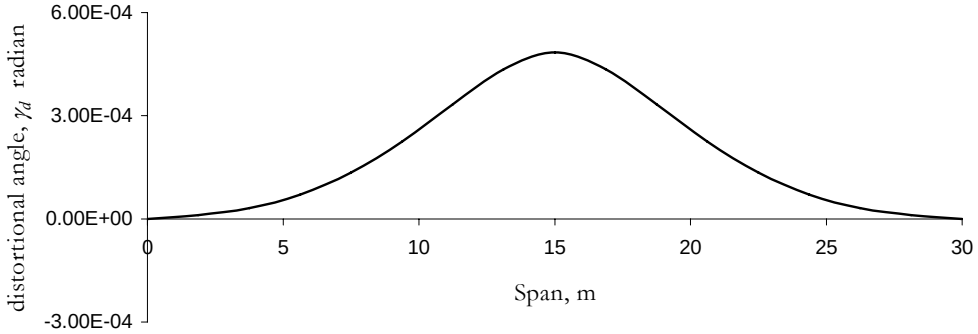

(e)

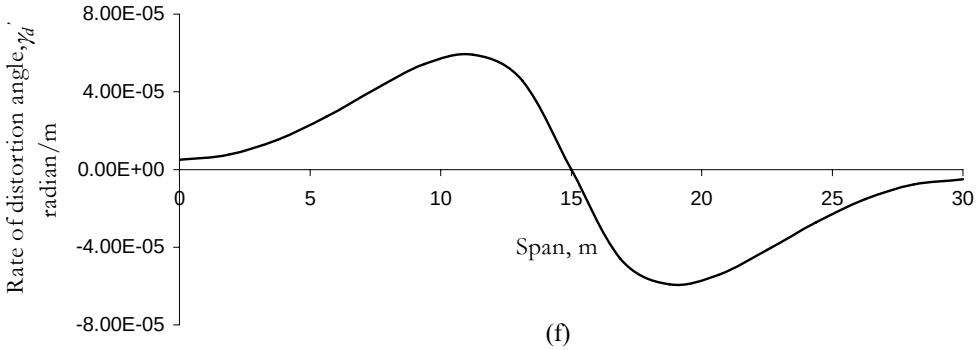

(f)

Fig. 2.25. (d) Rate of rotation (e) Distortion angle (f) Rate of distortional angle with distortional restraint and no warping restraint [case(i)]

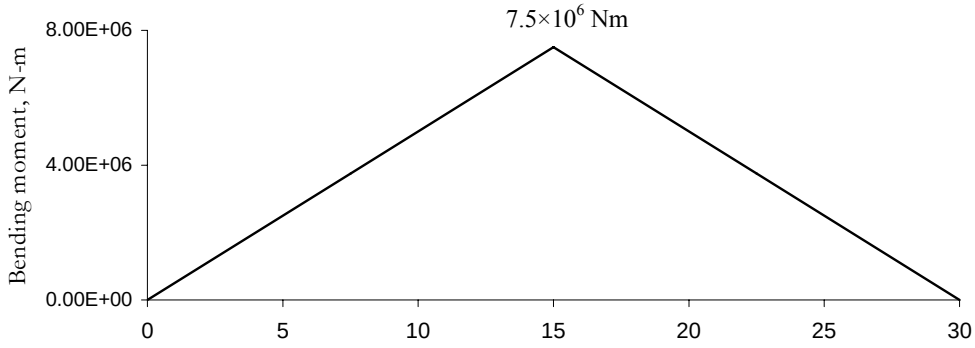

(a)

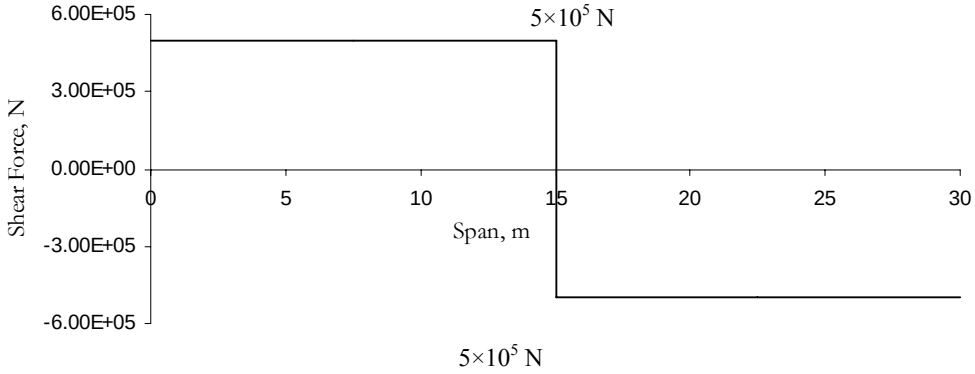

(b)

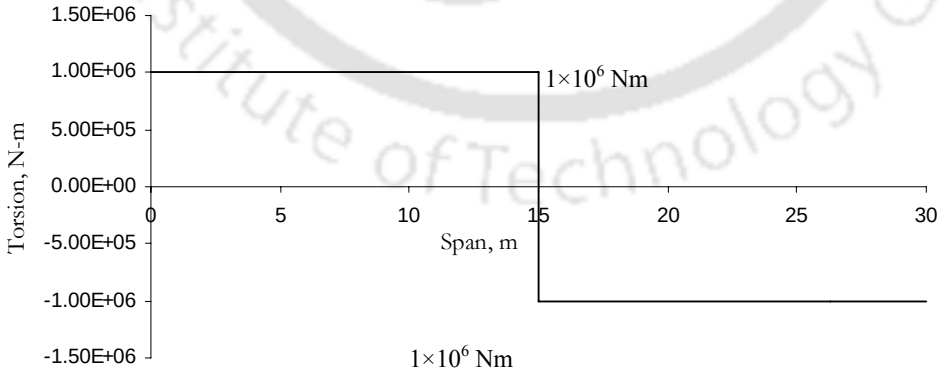

(c)

Fig. 2.26 (a) Bending moment (b) Shear Force (c) Torsional moment with distortional restraint and no warping restraint [case (i)]

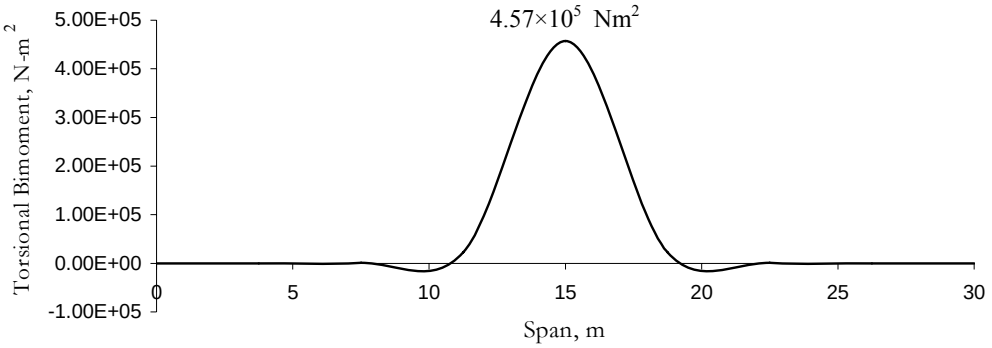

(a)

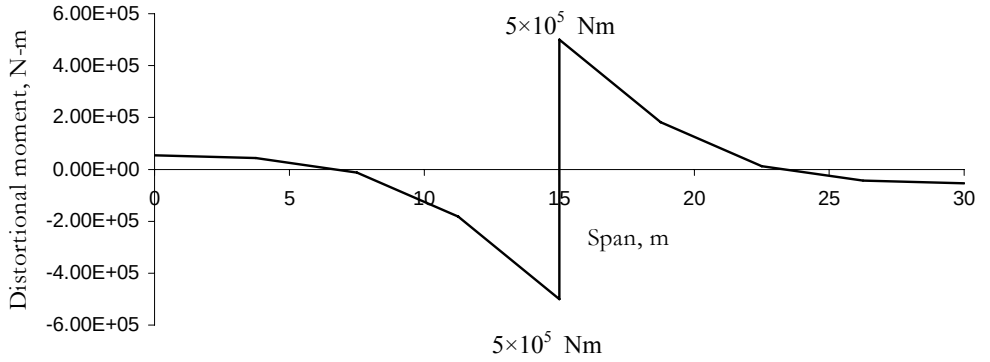

(b)

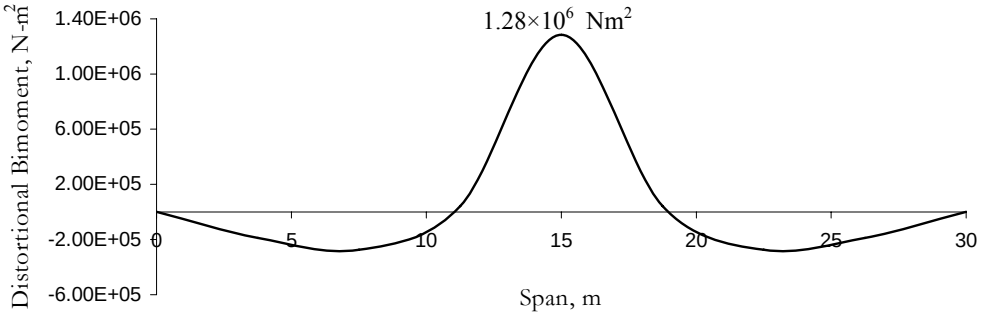

(c)

Fig. 2.27. (a) Torsional bimoment (b) Distortional moment, (c) Distortional Bimoment with distortional restraint and no warping restraint [case (i)]

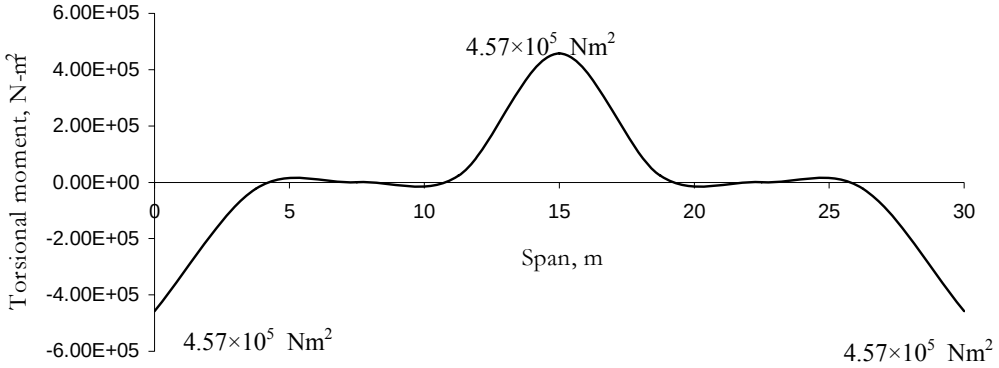

(a)

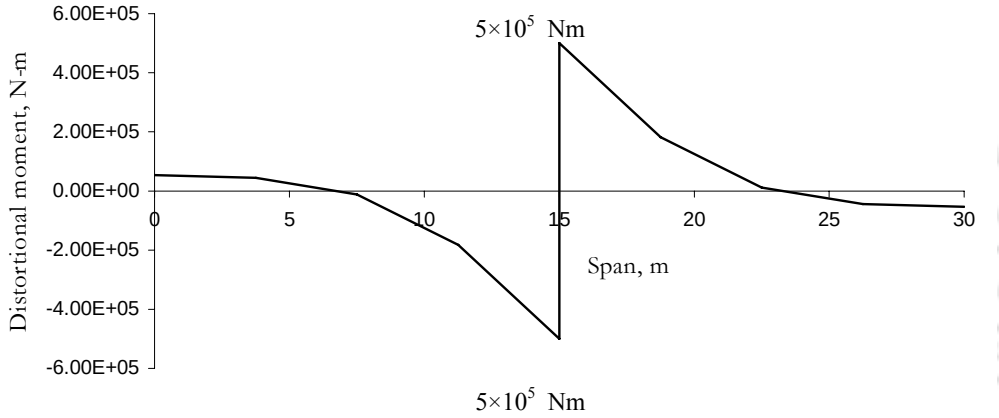

(b)

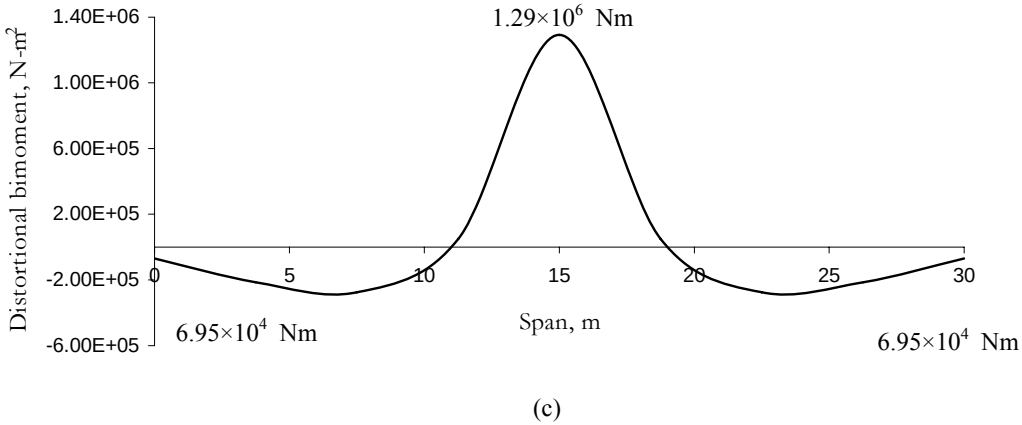

(c)

Fig. 2.28. (a) Torsional Bimoment, (b) Distortional moment, (c) Distortional Bimoment With full distortional and warping restraint [case(ii)]

2.5.2 A Simply-Supported Curved Box-Girder Bridge

A simply supported curved box-girder bridge with cantilever slabs has been considered**.** The support cross-section is connected by a pinned support at one end and by a linear roller at the other ends. The end section are braced by a rigid diaphragm at both ends and yet is free to warp. The span of the bridge is 30.10 m and the radius of curvature is 76.2m. The cross-section is as shown in Fig.2.29. An asymmetrical point load of 4.45 x10^3 N producing torsional effects has been applied at mid-span just above the web (Fig2.29). The bridge has been discretized using thirty thin-walled box-girder elements in order to evaluate different response parameters. Major responses such as deflection, rotations about *x* and *z* axes, rate of rotation about *x* axis, distortional angle, rate of distortional angle along the span length have been plotted in Fig. 2.30(a)-(f). Further, important stress resultants such as shear force, bending moment, torsional moment, torsional bi-moment, distortional moment and distortional bi-moment are also plotted in Fig. 2.30(g)-(l). Fig 2.31(a) displays the longitudinal normal stresses at mid-span. The longitudinal normal stresses have been calculated for both nine degrees of freedom thin-walled box-girder as well as conventional six degrees of freedom beam element. The longitudinal stress distribution with and without effective width have also been observed for the six degrees of freedom beam element. It is observed that the longitudinal normal stresses are substantially effected due to the contribution of B_I, B_{II} and shear lag, which are not accounted for in the conventional beam formulation with six degrees of freedom. Fig. 2.31(b) shows the transverse distortional bending stresses at mid-span. It is observed that a reasonably large amount of transverse stresses may be developed due to distortion. The example problem has been considered from Zhang (1983) and results have been validated. Further, in order to demonstrate the effect of curvature on the static analysis, Table 2.1 and 2.2 show the variation of various displacement / rotation and force / moment corresponding to various degree of freedom of the bridge with

varying radius (38.10 m – ∞). It is observed that the response parameters corresponding to torsion have increased appreciably with the reduction in radius of curvature. This will thus necessitate increased torsional stiffness requirement as the radius of curvature of the bridge is decreased. While the flexural components have been observed to be almost unchanged, the distortion components reduce slightly with the reduction in the radius of curvature. Thus, the design of bridge remains unaffected except the torsional rigidity, which needs to be augmented as the radius of curvature of the bridge, is decreased.

In order to compare the evaluated values of different response parameters, the thin-walled box-girder bridge has been analyzed using shell elements in the general purpose finite element software ANSYS. The finite element model of the straight box-girder bridge is shown in Fig.2.32. Table 2.3 shows the maximum magnitude of different response parameters as obtained from the analysis using shell elements and have been found to match very well with the results of the straight bridge as shown in the last column of Table 2.1 and 2.2.

Further, all the response parameters have been evaluated for IRC loading (IRC:6,2000) of Class 70R and of Class A loading (Appendix C) and the values of response parameters corresponding to the maximum magnitude for a particular location of the vehicle have been shown in Table 2.4 and 2.5. One lane of Class 70 R loading has been considered, while two lanes of Class A loading is considered for the analysis as the width of the carriageway is more than 5.3 m for the example under consideration. The vehicle loads have been placed symmetrically as well as asymmetrically maintaining a minimum distance from the kerb and also a minimum distance between two rows of vehicle for Class A loading (Table.C.1.2).It is observed that the maximum magnitude of vertical deflection, rotation about z direction and corresponding stress resultant (viz. shear force and bending moment) are high in IRC Class A train of vehicles compared to IRC 70R Tracked as well as Wheeled Vehicle loading class.

The torsional and distortional displacement components and their corresponding stress resultants vary differently for different loading cases as the distance between wheels and their locations significantly influence the values of those response parameters.

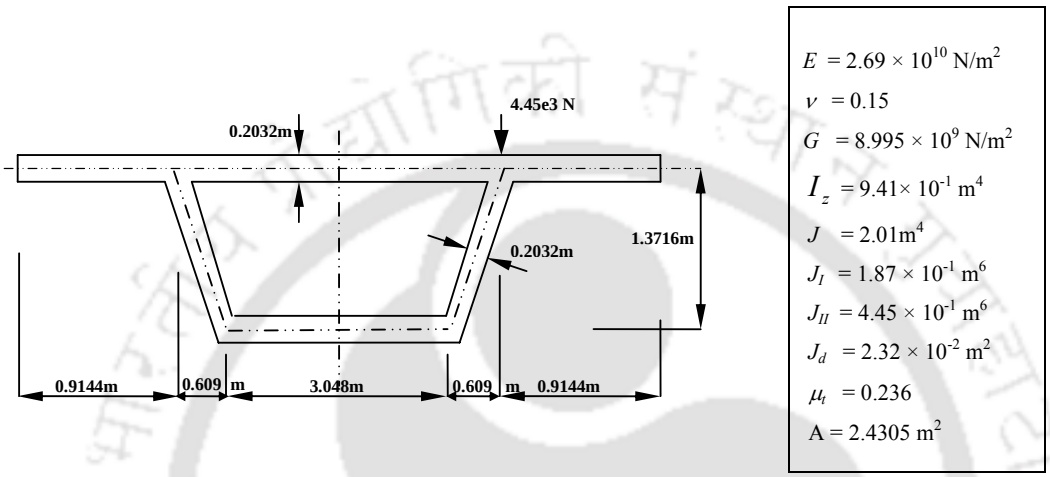

Fig.2.29. Cross-section and loading

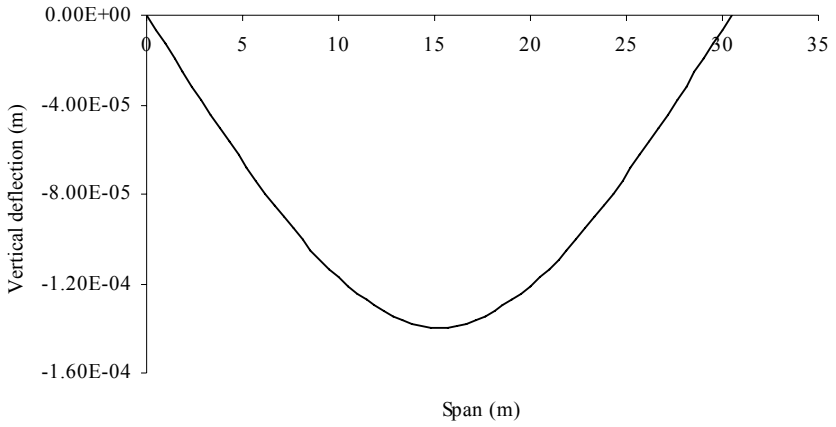

Fig 2.30 (a) Vertical deflection (v)

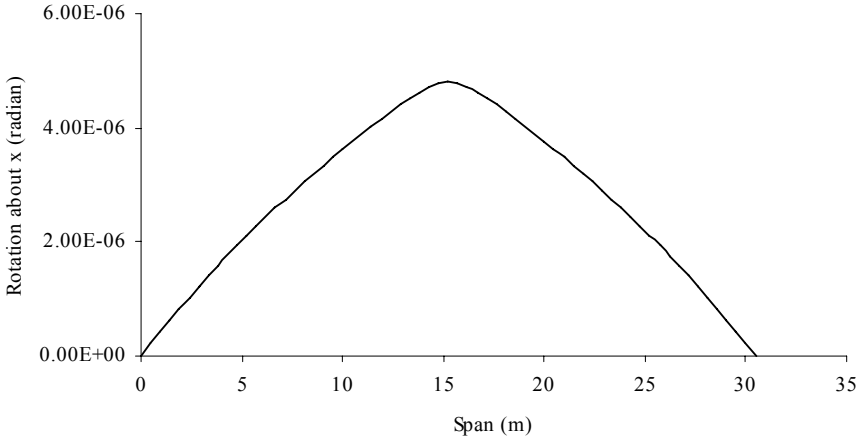

Fig 2.30 (b) Rotation about x (θ_x)

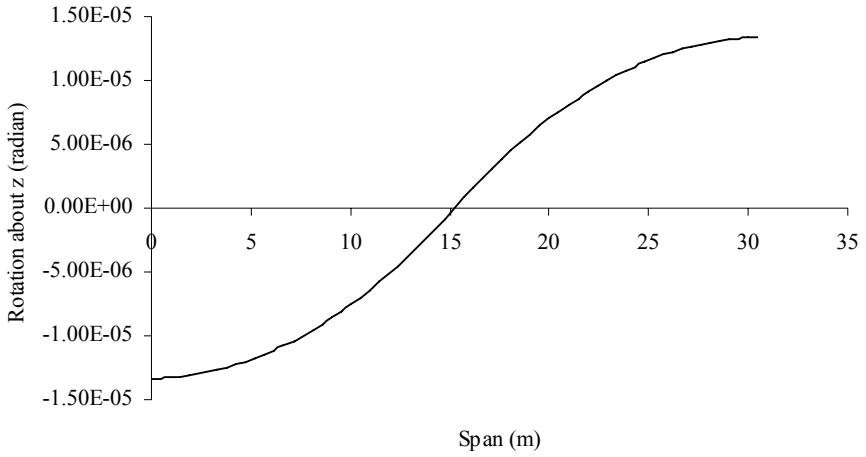

Fig 2.30 (c) Rotation about z (θ_z)

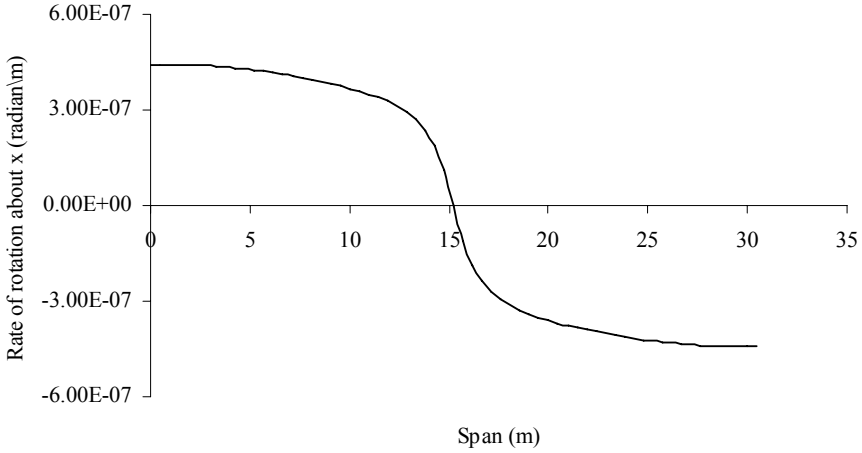

Fig 2.30 (d) Rate of rotation about x (θ'_x)

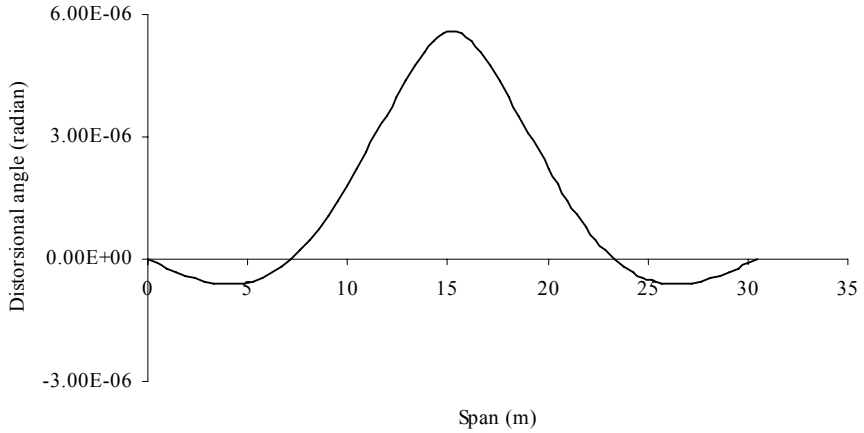

Fig 2.30 (e) Distortional angle (γ_d)

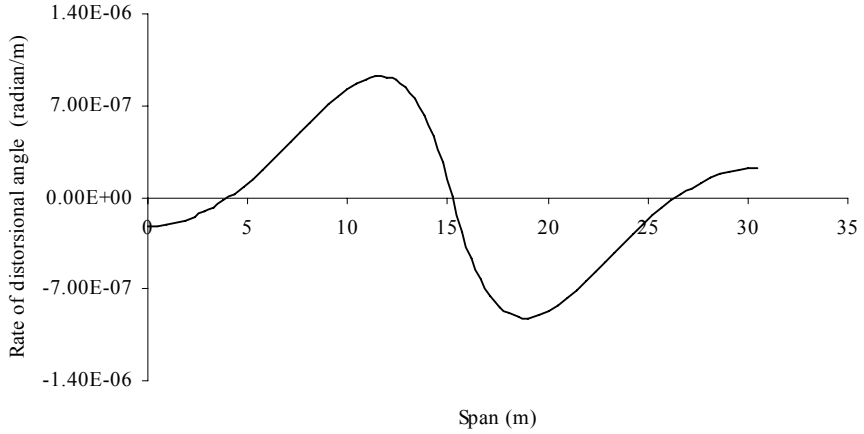

Fig 2.30 (f) Rate of distortional angle (γ'_d)

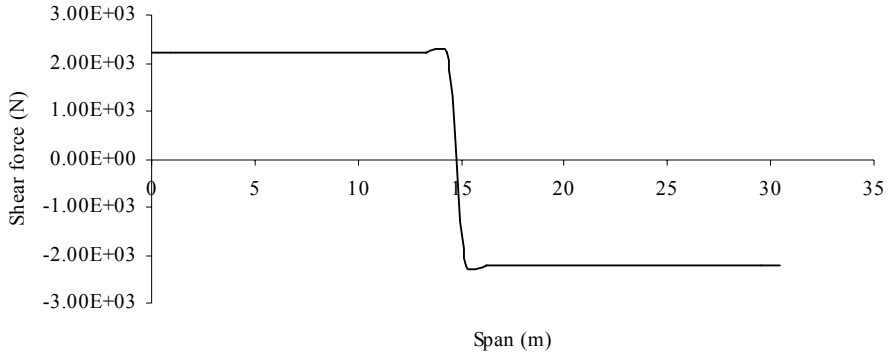

Fig 2.30 (g) Shear force (Q_Y)

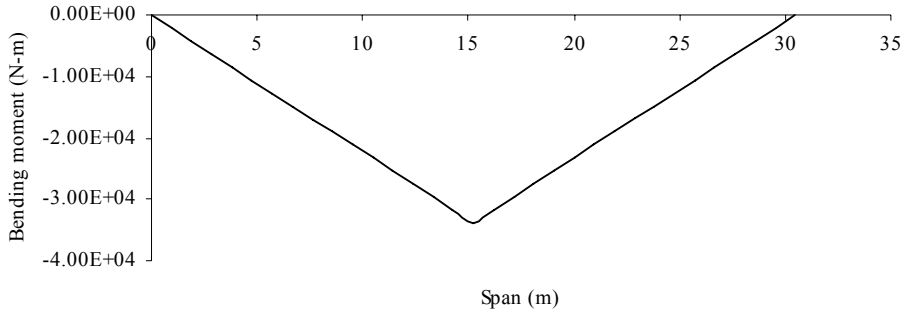

Fig 2.30 (h) Bending moment (M_z)

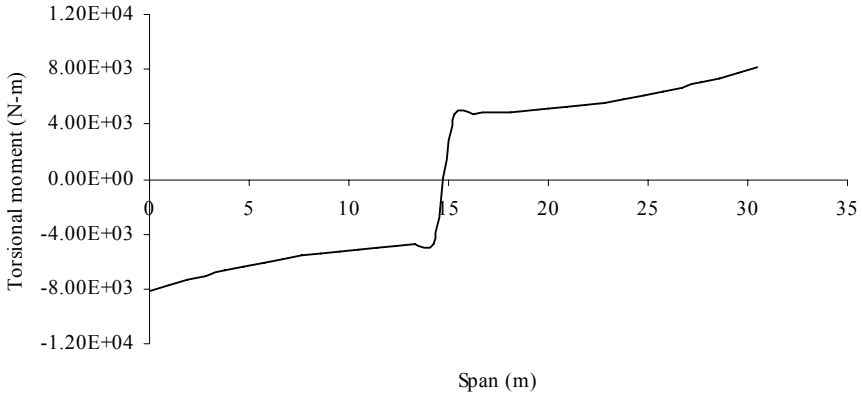

Fig 2.30 (i) Torsional moment (M_x)

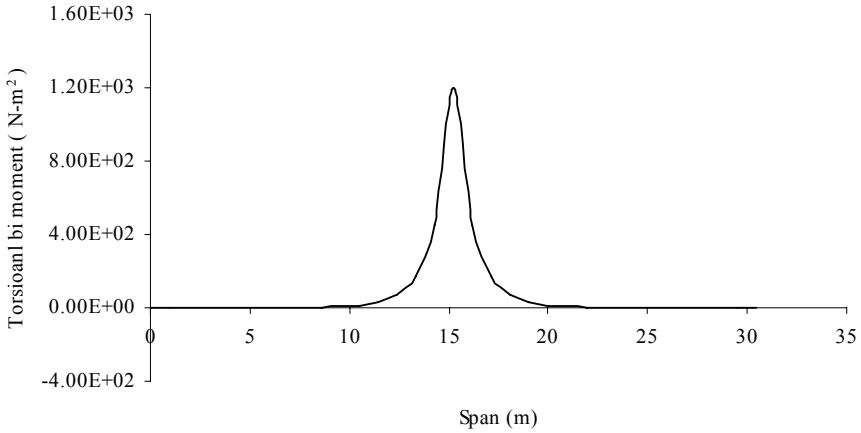

Fig 2.30 (j) Torsional bi moment (B_I)

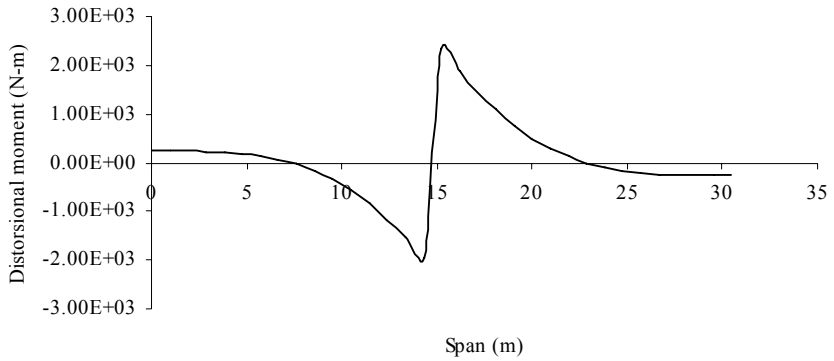

Fig 2.30 (k) Distortional moment (M_D)

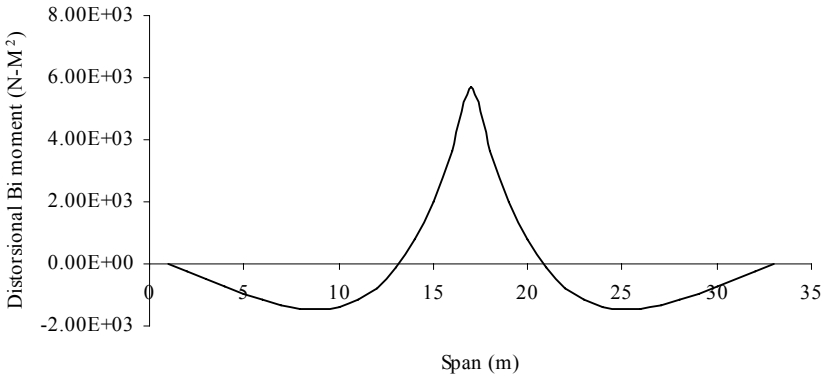

Fig 2.30 (l) Distortional bi moment (B_{II})

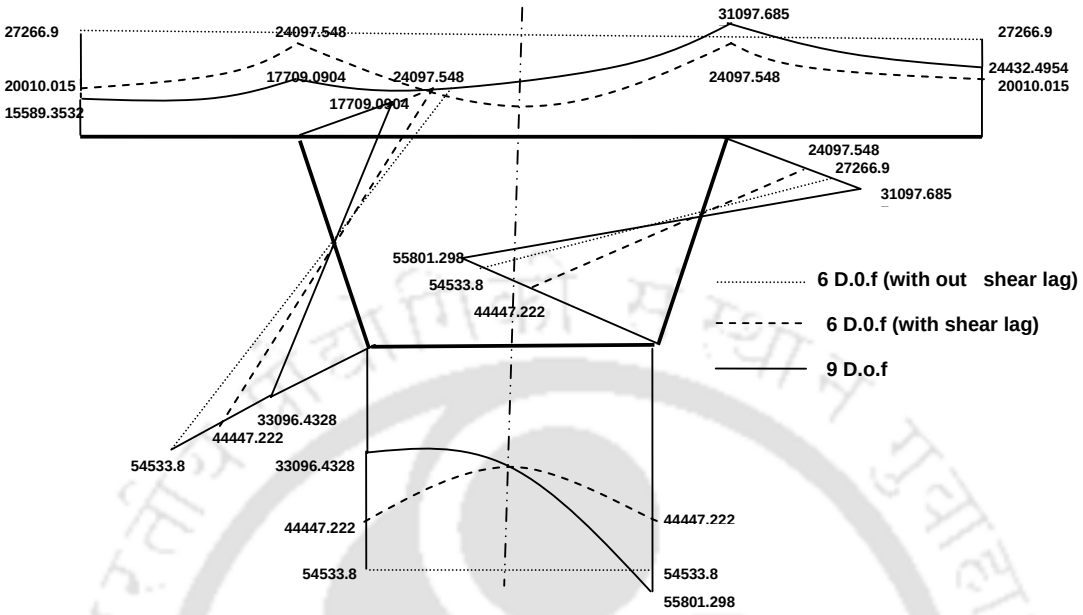

Fig 2.31 (a) Longitudinal normal stresses at mid-span (N/m^2)

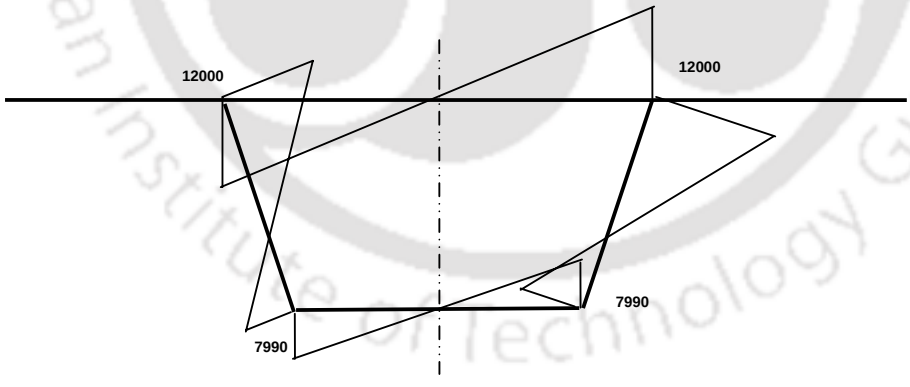

Fig 2.31 (b) Transverse distortional bending stress at mid-span (N/m^2)

Table 2.1 Effect of radius of curvature of box-girder bridge on responses

Radius of box-girder (R)m					
Response parameter	**38.10**	**76.2**	**152.4**	**304.8**	**∝**
v(m)	-1.46e-04	-1.40e-04	-1.38e-04	-1.37e-04	-1.36e-04
θ_z (radian)	1.36e-05	1.33e-05	1.33e-05	1.33e-05	1.33e-05
θ_x (radian)	6.03e-06	4.81e-06	4.26e-06	4.01e-06	3.75e-06
$\theta_x^{'}$ (radian/m)	6.00e-07	4.43e-07	3.54e-07	3.09e-07	2.63e-07
γ_d (radian)	2.08e-06	5.59e-06	7.40e-06	8.28e-06	8.63e-06
$\gamma_d^{'}$ (radian/m)	7.68e-07	9.21e-07	1.01e-06	1.05e-06	1.07e-06

Table 2.2 Effect of radius of box-girder bridge on stress resultants

Radius of box-girder (R)m					
Response parameter	**38.10**	**76.2**	**152.4**	**304.8**	**∝**
Q_Y (N)	2.22e3	2.22e3	2.22e3	2.22e3	2.22e3
M_z (N-m)	-3.39e4	-3.39e4	-3.39e4	-3.39e4	-3.39e4
M_x (N-m)	-1.18e4	-8.18e3	-6.44e3	-5.50e3	-4.75e3
B_I (N-m^2)	1.090e3	1.085e3	1.083e3	1.080e3	1.078e3
M_D (N-m)	2.28e3	2.33e3	2.35e3	2.36e3	2.37e3
B_{II} (N-m^2)	5.21e3	5.69e3	5.95e3	6.07e3	6.12e3

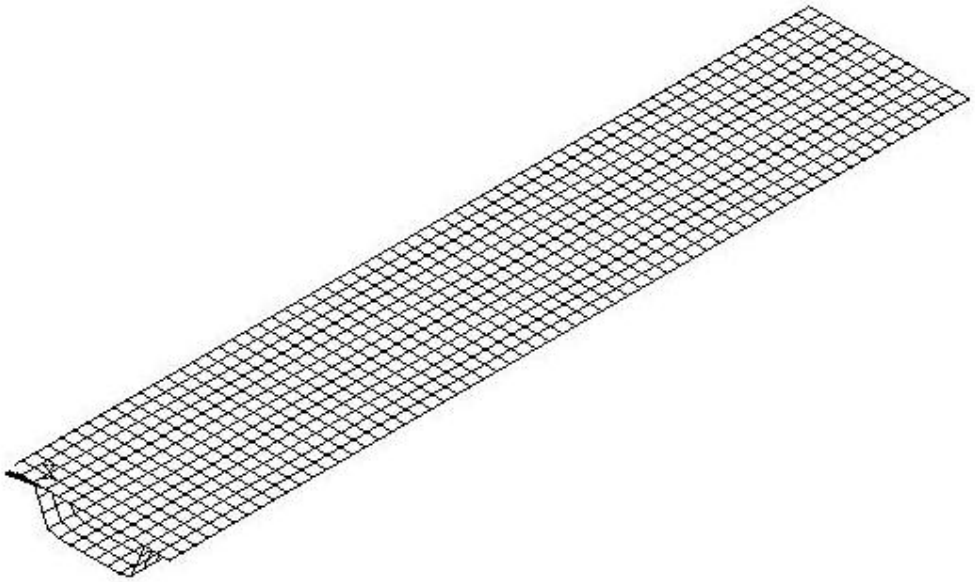

Fig. 2.32 Finite element model of box-girder bridge using shell element

Table 2.3 Different response parameters corresponding to a straight box-girder bridge modeled using shell elements

Response parameter	v(m)	θ_z (radian)	θ_x (radian)	Q_Y (N)	M_z (N-m)	M_x (N-m)
	-1.37e-4	1.33e-5	3.87e-6	2.22e3	-3.39e4	-4.72e3

Table 2.4 Displacement response due to IRC Loadings in two lane box-girder bridge

IRC Loadings						
IRC Loading Case	**IRC 70R Tracked Vehicle**		**IRC 70R Wheeled Vehicle**		**IRC A Train of Vehicle**	
Response parameter	**Symmetrical Loading**	**Non-Symmetrical Loading**	**Symmetrical Loading**	**Non-Symmetrical Loading**	**Symmetrical Loading**	**Non-Symmetrical Loading**
v (m)	-2.14e-02	-2.14e-02	-2.77e-02	-2.77e-02	-2.79e-02	-2.79e-02
θ_z (radian)	2.09e-03	2.09e-03	2.75e-03	2.75e-03	2.81e-03	2.81e-03
θ_x (radian)	**	1.86e-04	**	3.21e-04	**	2.72e-04
$\theta_x^{'}$ (radian/m)	**	3.10e-05	**	4.86e-05	**	4.88e-05
γ_d (radian)	**	-4.59e-04	**	-3.37e-04	**	-5.10e-04
$\gamma_d^{'}$ (radian/m)	**	4.70e-05	**	5.10e-05	**	5.27e-05
** Not applicable due to symmetric nature of the load						

Table 2.5 Stress resultant due to IRC Loadings in two lane box-girder bridge

IRC Loadings						
IRC Loading Case	**IRC 70R Tracked Vehicle**		**IRC 70R Wheeled Vehicle**		**IRC A Train of Vehicle**	
Response parameter	**Symmetrical Loading**	**Non-Symmetrical Loading**	**Symmetrical Loading**	**Non-Symmetrical Loading**	**Symmetrical Loading**	**Non-Symmetrical Loading**
Q_Y (N)	-3.43e05	-3.43e05	-4.91e05	-4.91e05	-5.389e05	-5.389e05
M_z (N-m)	-5.17e06	-5.17e06	-5.90e06	-5.90e06	-5.93e06	-5.93e06
M_x (N-m)	**	5.72e05	**	8.97e05	**	9.02e05
B_I (N-m^2)	**	5.56e03	**	1.05e04	**	8.81e03
M_D (N-m)	**	-2.73e04	**	-3.33e04	**	-3.91e03
B_{II} (N-m^2)	**	-5.33e04	**	-6.48e04	**	-6.33e04
** Not applicable due to symmetric nature of the load						

2.5.3 **A Two-Span Double-Cell Box- Girder Subjected to Eccentric Load**

A two span continuous double-celled straight box-girder model subjected to two-eccentric point loads has been analyzed. The span of each box-girder is 3.5 m. The longitudinal elevation and cross-section are shown in Fig. 2.33 (a) and (b). Diaphragms are located at the supports preventing in-plane distortion of the cross-section. Sixteen thin-walled box-girder elements were used for the present analysis. Fig.2.34 (a), (b), (c) and (d) show the distribution of bending moment, torsional bi moment distortional moment and distortional bi-moment along the span. Fig.2.35 (a) and (b) show the distribution of longitudinal stresses and transverse bending moments across the cross-section at mid-span. The results have been observed to match with Zhang and Lyons (1984).

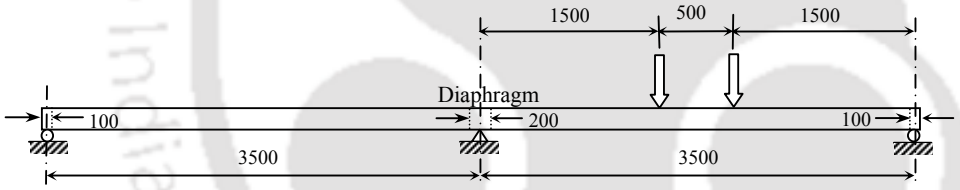

Fig. 2.33 (a) Longitudinal elevation (mm)

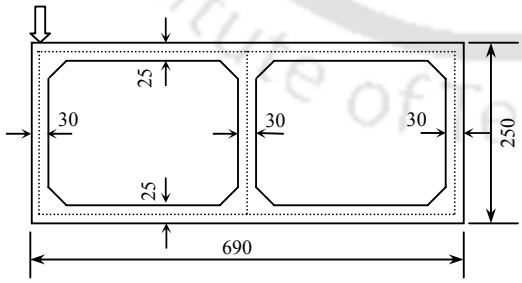

$E = 2.90 \times 10^{10}$ N/m^2
$\nu = 0.18$
$G = 1.229 \times 10^{10}$ N/m^2
$I_z = 5.0309 \times 10^{-4}$ m^4
$J = 1.314 \times 10^{-3}$ m^4
$J_I = 6.6403 \times 10^{-6}$ m^6
$J_{II} = 5.3408 \times 10^{-6}$ m^6
$J_d = 0.116 \times 10^{-3}$ m^2
$\mu_t = 0.311$
A = 0.05025 m^2

Fig. 2.33 (b) Cross-section (mm) and member properties

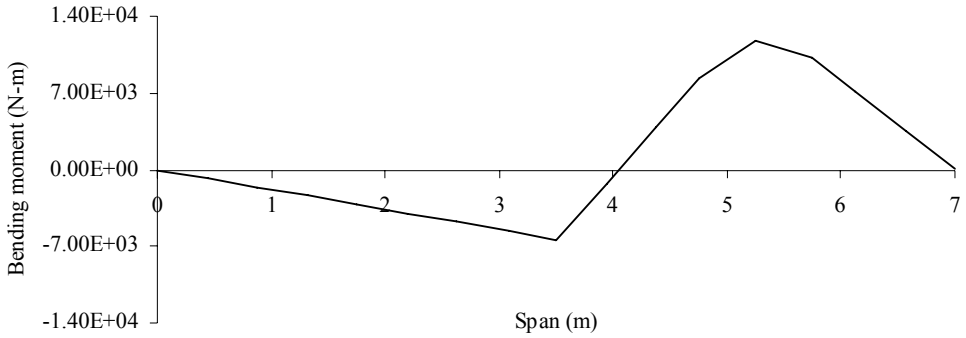

Fig 2.34 (a) Bending moment (M_z)

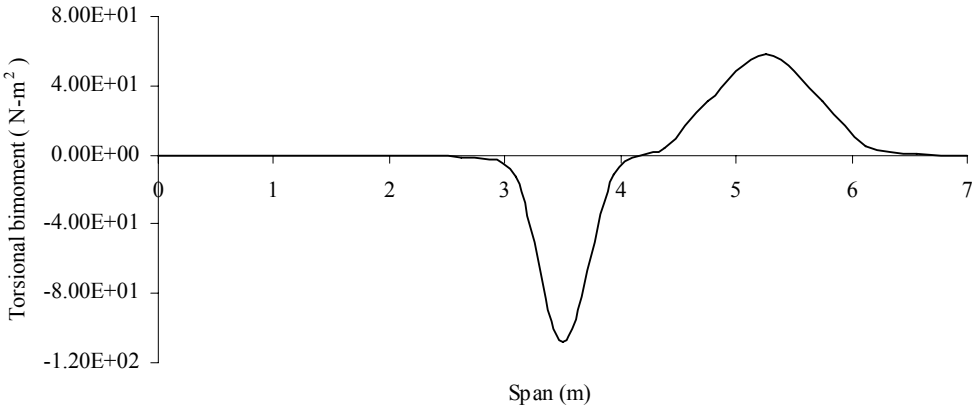

Fig 2.34 (b) Torsional bi-moment (B_I)

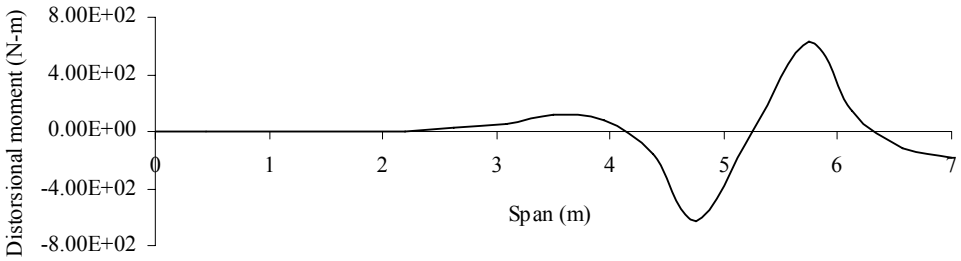

Fig 2.34 (c) Distortional moment (M_D)

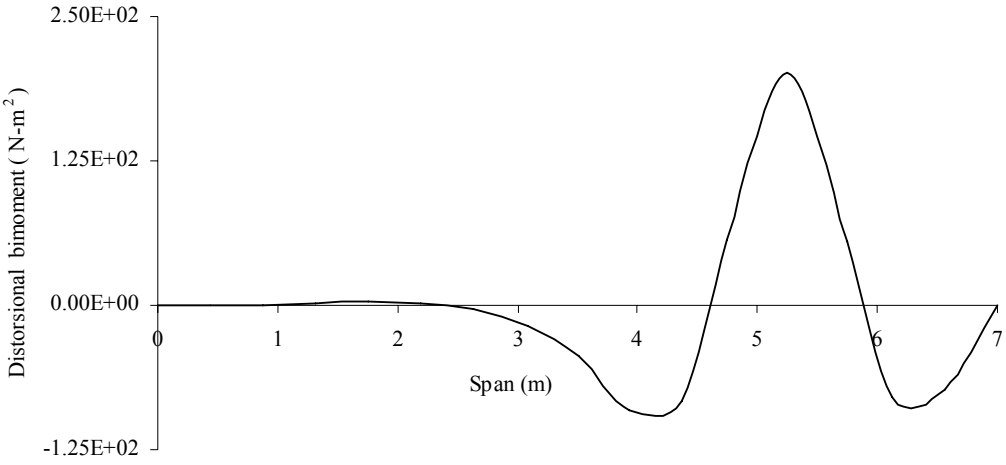

Fig.2.34 (d) Distortional bi-moment (B_{II})

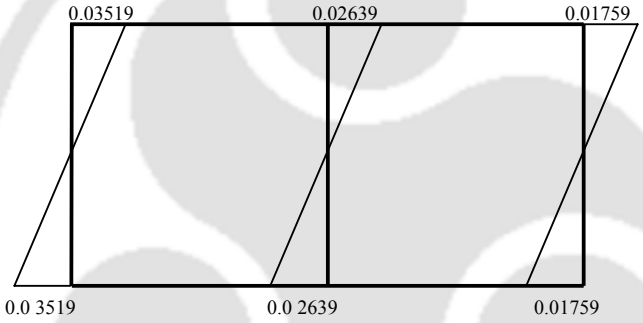

Fig. 2.35 (a) longitudinal normal stresses at mid-span section (N/m^2)

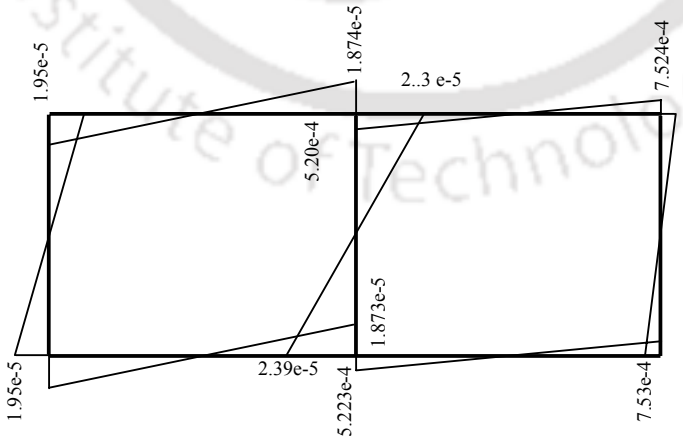

Fig.2.35 (b) Transverse distortional bending stress at mid-span section (N/m^2)

2.6 CLOSURE

The finite element formulation of thin-walled box-spine bridges as proposed by Zhang and Lyons (1984) has been adopted in this study. The three-noded one-dimensional beam model developed, takes into account torsional warping and distortion characteristics of thin-walled box-spine bridges, apart from the usual extensional, flexural and torsional behavior. The effect of shear lag has been taken into account using the effective breadth concept. A computer program, based on the above three-noded one-dimensional element, has been developed. A supplementary program that evaluates the sectional properties of a box-girder cross-section has also been developed. The main advantage of the proposed method of analysis is that it may be used for bridge analysis in situations where a full three-dimensional analysis is unnecessary, such as during preliminary design stages. Further, the dynamic analysis due to seismic excitation will be also very efficient as a substantial reduction in overall degrees of freedom is achievable by using three noded one dimensional beam model.

CHAPTER 3

FREE VIBRATION CHARACTERISTICS

3.1 INTRODUCTION

The studies on free vibrational characteristics of thin walled box girder bridges have been carried out since the modal parameters like natural frequencies and mode shapes are important for understanding the dynamic behavior of the structure. The bridge deck systems with continuously distributed mass have infinite number of natural frequencies, however, only few lower of those frequencies have practical significance. The thin-walled box beam finite element which has been introduced in chapter 2 has been considered for the free vibration analysis of thin walled box girder bridges. As per the records available, this element has not been used for the dynamic analysis. The experiment on free vibration has been conducted in the laboratory with a perspex sheet model of a curved bridge. The natural frequencies and mode shape obtained from the theoretical analysis have been validated by experimental data. The tensile test on the specimen made of perspex sheet has also been conducted in UTM (Make: INSTRON) to evaluate material properties that was used in FEM analysis to obtain modal parameters. The subsequent studies on complex bridge vehicle interaction problems have been carried out based on the satisfactory performance of the evaluated modal parameters.

3.2 EIGEN VALUE PROBLEM FOR UN-DAMPED SYSTEM

The general equation of motion for an un-damped free vibration system can be written as

$$[M]\left[\ddot{\delta}\right]+[K][\delta]=0 \tag{3.1}$$

where $[\delta]$, $\left[\ddot{\delta}\right]$ are the values of the global displacements and accelerations,

$[K]$and $[M]$ are the global stiffness and mass matrix after applying boundary conditions.

Assuming harmonic motion in natural mode of vibration, the response can be written as

$$\{\delta\} = \{X\} \sin(\omega t+\phi) \tag{3.2}$$

where $\{X\}$ is the vector of nodal amplitude of vibration, ω is the circular natural frequency of vibration [rad/sec] and ϕ is the phase angle.

Substitution of (3.2) in (3.1) leads to the generalized eigen value problem.

$$\left\{\ [K]-\omega^2[M]\ \right\}\{X\}=0 \tag{3.3}$$

Eq. (3.3) is solved using a standard eigen solver to obtain the values of natural frequencies and mode shapes of the box girder bridge.

3.3 VIBRATION TESTING

Free vibration testing has been carried out with the model of a curved thin walled box girder bridge. The modal parameters have been found experimentally for a simply supported thin-walled curved box girder model and compared with the finite element results.

3.3.1 Model Description and Evaluation of Material Properties

The model of the bridge has been fabricated from perspex sheets. The dimensions of the bridge were selected based on the model mentioned by Zhang (1983). The span of the model considered is 60 in (1.52 m) with the radius of curvature of 1200 in (30.48 m). The cross-

sectional dimension is shown in Fig.3.1. It was necessary to determine the material properties of which the model has been made so as to give realistic input to the finite element analysis. The tensile strength test has been carried out on a specimen from the same perspex sheet, which has been used for making the bridge model. Fig 3.2 shows the details of specimen used in tensile testing. The tensile testing has been carried out in a universal testing machine (Make: INSTRON, Model: 8801, Capacity: 100 KN) with extensometer that measures the strain which the sample undergoes during the tensile test. The tensile loading was applied with a crosshead speed of 2mm/min till failure. The extensometer is attached to the sample by small spring clamps. The stress-strain curve obtained in the experiment has been shown in Fig. 3.3. The slope of the initial linear portion of the stress-strain curve is taken as the modulus of elasticity (E) (Geore 1988). The linear relationship between stress-strain in the elastic region of stress-strain curve is described by Hooke's law as

$$\text{Modulus of Elasticity } (E) = \frac{\text{Tensile stress}}{\text{Tensile strain}} = \frac{11.62}{0.00398} = 2922.35\text{Mpa}$$

$$= 2.92235\times 10^{9}\ \text{Pa}\ (4.2385\times 10^{5}\ \text{psi})$$

The density of the material is obtained as 1108 kg/m^3 (0.04002 psi^3).

3.3.2 Fabrication of Support

The simulations of appropriate support conditions are very important as this influence the extraction of the desired modes of vibration. The fabrication of the pinned support end for the perspex sheet model of the curved box girder bridge has been done with the help of one half of a 150 mm long and 28 mm diameter steel pipe. 8mm mild steel bars (as inserts) have been welded at the bottom of the half pipe, which are embedded to a concrete block (250mm × 250mm ×150mm). 26 mm diameter solid plastic rods have been fixed at the bottom surface of

each end of the perspex sheet model. One end of the bridge model with the plastic solid pipe is placed inside the half steel pipe, thus allowing only rotations to occur. The other end (roller end) of the bridge with plastic solid pipe rests on a smooth concrete block (Fig.3.4).

3.3.3 Sensor Locations and Fittings

The locations of sensors for picking up responses play important role in extracting the mode shapes of the vibrating specimen under study. M5 thread holes have been drilled in appropriate locations of the thin-walled curved box girder model to provide mounting for the accelerometer on the specimen. The M5 thread holes have been made along two rows (one along the deck and the other along the vertical wall of the box girder) for nine different locations. The holes are placed uniformly at an interval of 100 mm as shown in Fig.3.4.

3.3.4 Instrument Setup

The responses have been picked up with the data acquisition front end of FFT analyzer in the form of frequency response function. Vibration testing in FFT analyzer also indicates the resonant frequencies with the help of its compatible PULSE software. The instrument, Bruel & Kjaer 3560 D Pulse Analyzer (Frequency range 0-112.5 kHZ) with data acquisition system has been used for picking up the responses from the specimens subjected to vibration. The system consists of a PC with LAN interface, PULSE software and IDA^{e} based data acquisition front-end hardware. Other accessories in the experimentation consist of transducers and condition amplifiers. The piezoelectric accelerometer is the optimum choice of vibration transducer. These piezoelectric accelerometers are used to measure all type of vibrations regardless of the nature of the vibration in the time domain and the frequency domain, as long as the accelerometer has the correct frequency and dynamic range. The types of accelerometers used in the present work are shown in Table 3.1. The Table contains details of frequency range,

sensitivity and weight of various accelerometers. The heart of the accelerometer is its piezoelectric elements, which are usually made from an artificially polarized ferroelectric ceramic. These piezoelectric elements have the property of producing an electric charge, which is directly proportional to strain and thus the applied force, when loaded either in tension, compression or shear.

NEXUS™ Conditioning Amplifier Type 2692 provides the interface between the transducers and PULSE for charge accelerometer. BNC input connectors are used to link up with amplifier. The channels have comprehensive high and low-pass filtering facilities. The filters can be set up for specific tasks. NEXUS™ conditioning amplifiers are contained with an optional rechargeable battery and hence as well suited for laboratory as well as field use.

3.3.5 Test Procedure

The bridge model has been subjected to impact load on the top surface at a particular location. This is carried out by giving impact with the help of 150 gm impact hammer on the top of the bridge deck. The complete experimental set up is shown in Fig.3.5. The accelerometers are fed to input channels in the front end of FFT analyzer. The FFT analyzer consists of acquisition front end with AC/DC power supply, 100 kHz input modules, generator modules, signal analyzer input modules and output modules. The signal analyzer interface module handles all digital data communication between the Digital Signal Processing unit (s) and modules in acquisition front end. All the input modules have a dynamic range greater than 80 dB. The output channels from FFT are connected to a PC loaded with PULSE software, which enables the processing of the response signals.

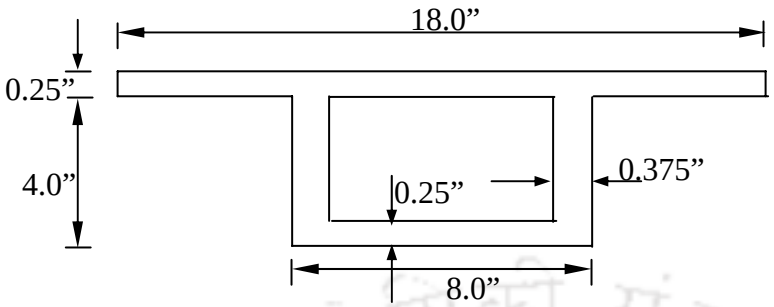

E = 4.2385× 10^5 psi
ν = 0.40
G = 1.5137 × 10^5 psi
ρ =0.04002 psi^3
I_z = 26.766 in^4
J = 45.470 in^4
J_I = 53.5049 in^6
J_{II} = 72.7878 in^6
J_d = 0.00355 in^2
μ_t = 0.322
A = 9.3125 in^2

Fig. 3.1 Geometry (inch) and properties of the box girder model

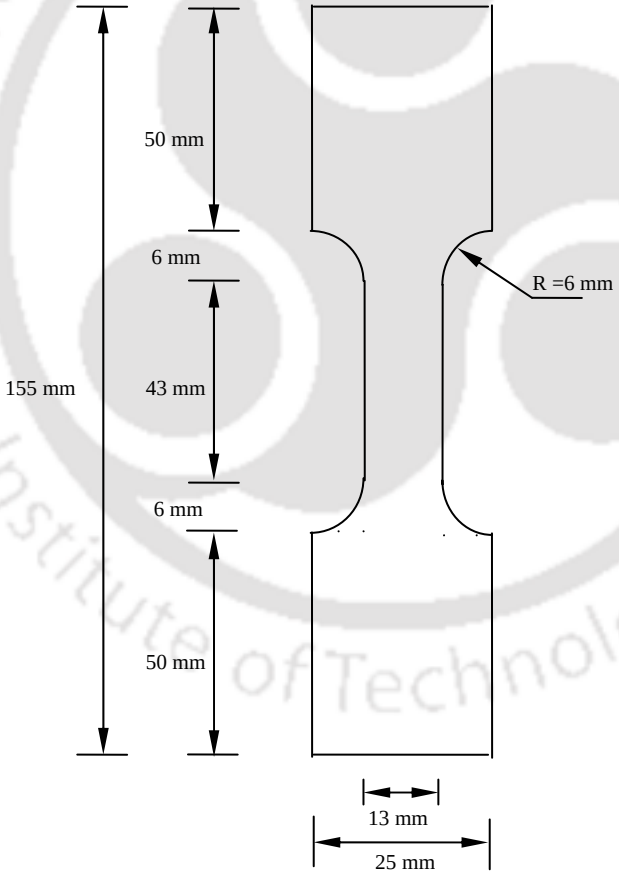

Fig 3.2 Perspex sheet specimen for tensile strength test

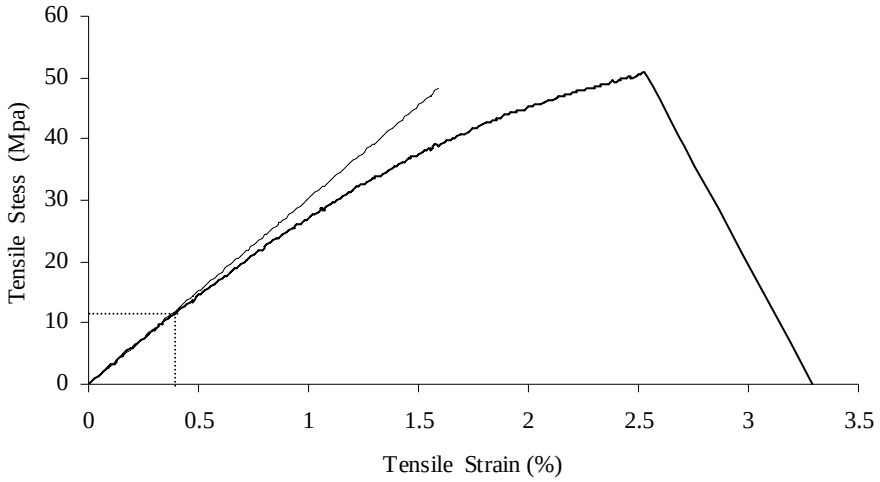

Fig. 3.3 The tensile stress-strain curve of the perspex sheet specimen

Table 3.1 Details of accelerometers used for the experiment

Property	Type 4371	Type 4381	Type 4396
Type	Charge	Charge	Deltatrone
Frequency range (Hz)	0.2-9100	0.2-3500	1-25000
Sensitivity (pC/ms^{-2})	1 ± 2%	10 ± 2%	10 ± 2% (mV/ms^{-2})
Weight (grams)	11	43	18.2

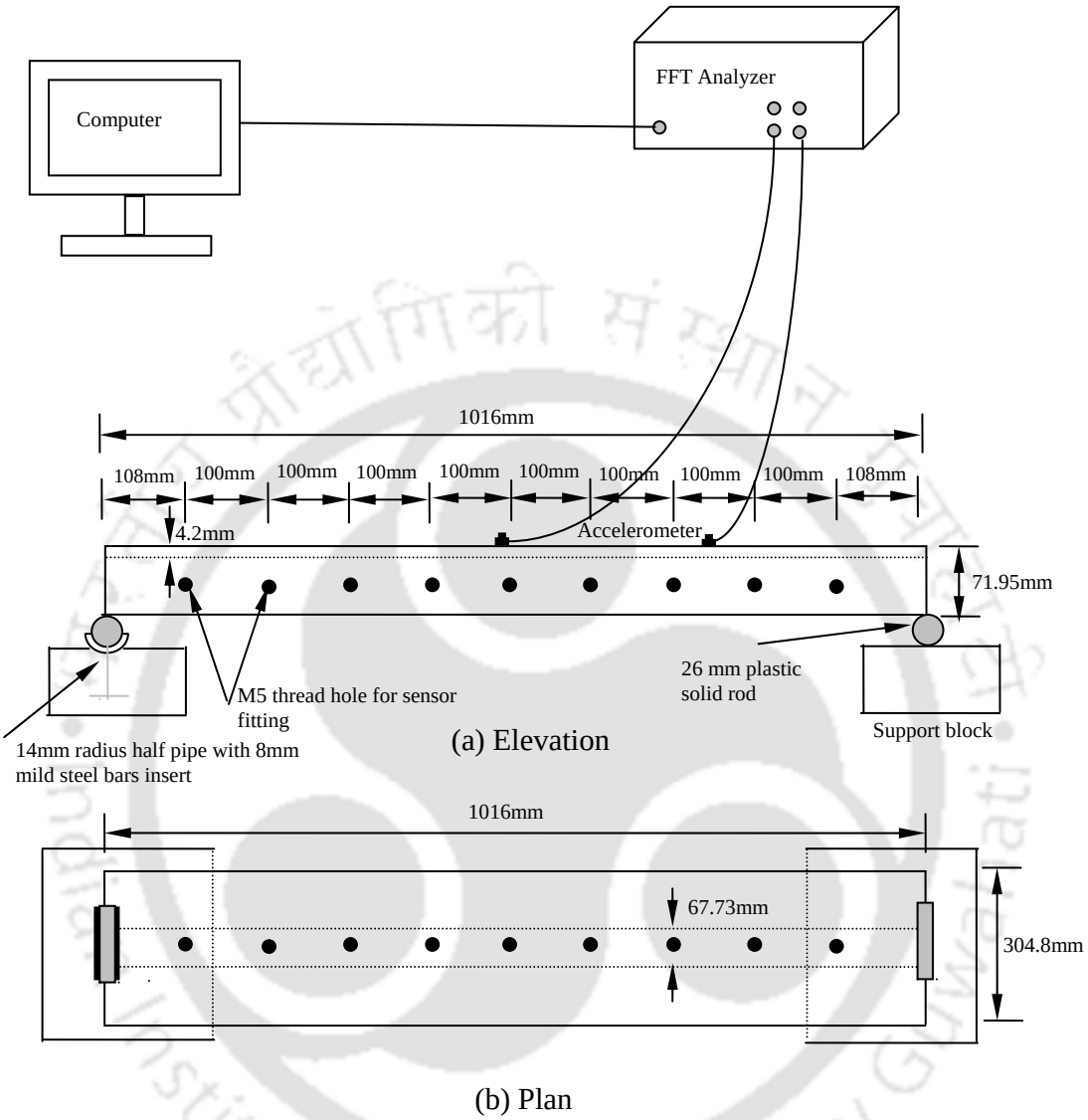

Fig. 3.4 Schematic diagram of experimental set-up for thin-walled curved box girder model fabricated from perspex sheets

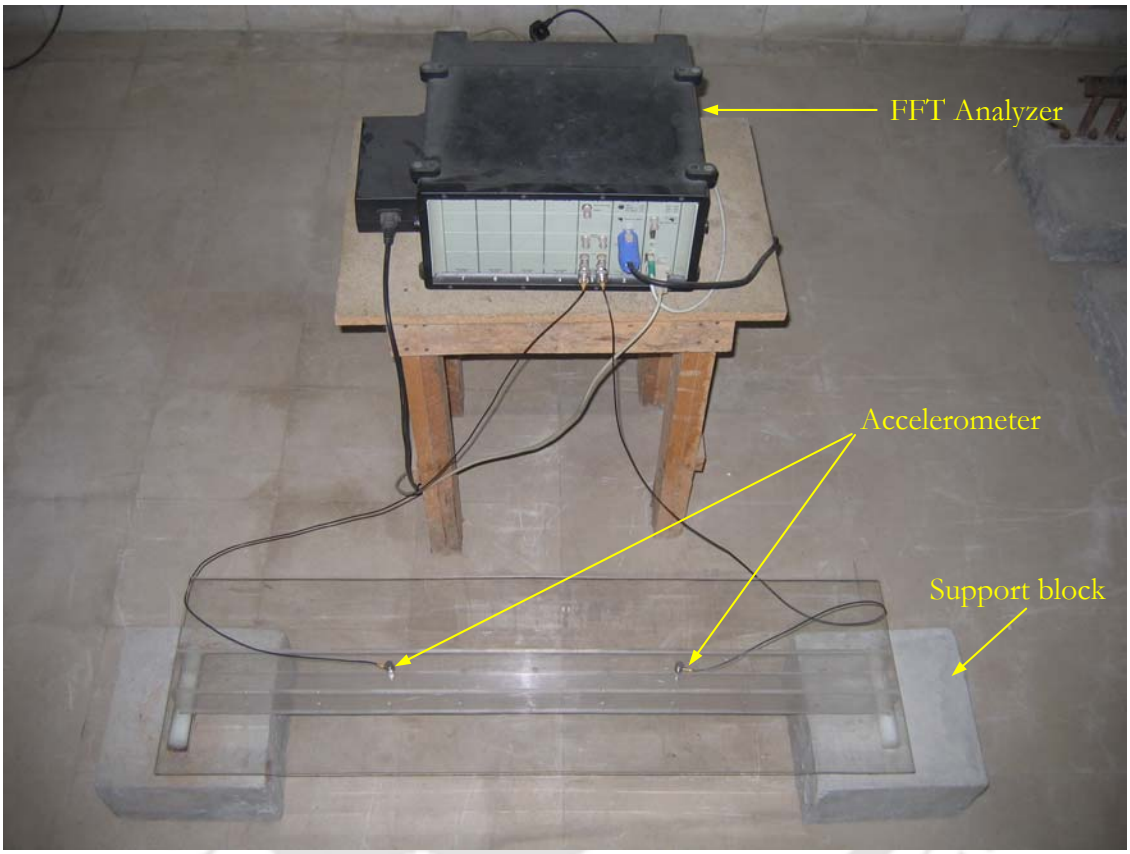

Fig. 3.5 Experimental setup for free vibration study of a curved box girder bridge model

3.3.6 Modal Data Extraction

Once the frequency response of a test structure is obtained, the post processing is done to evaluate damping ratios and modal amplitudes associated with each resonant peak of the measured frequency response function. The frequencies, damping ratios and mode shape of the test specimen are shown in the subsequent sections.

3.3.6.1 Natural Frequencies and Damping Ratio

The natural frequencies have been obtained by observing the frequencies at which peaks are prominent in the frequency response function. The damping ratio associated with each peak of the frequency response function is assumed to be the modal damping ratio ζ_i. Half Power Band Width Method (Inman 2001) has been utilized for the evaluation of the damping ratio (ζ) of the model bridge. To obtain the modal damping ratios, the frequency response functions (compliance) magnitude plot is considered as shown in Fig 3.6.

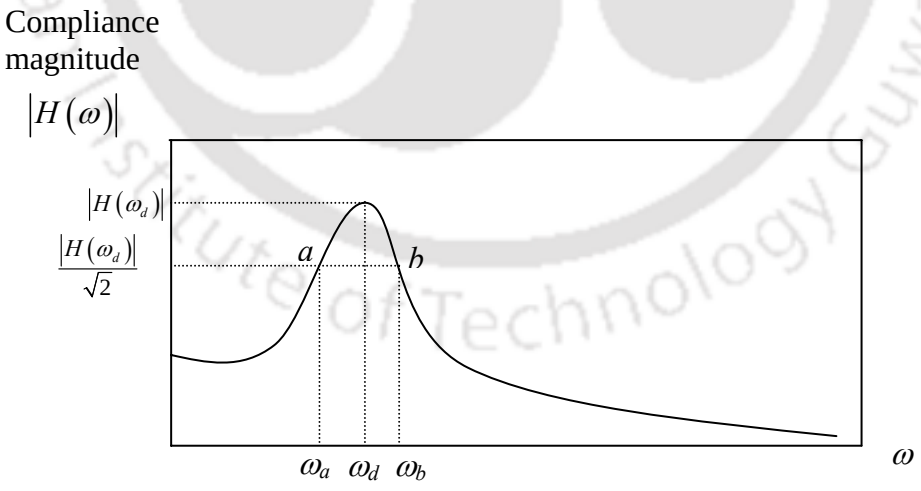

Fig.3.6 Magnitude of FRF for calculating modal damping ratio by using Half Power Band Width Method

For systems with small damping, the peak $|H(\omega)|$ at resonance is well defined. The modal damping ratio ζ is related to the frequencies corresponding to the two points (*a, b*) on the magnitude plot, where

$$|H(\omega_a)| = |H(\omega_b)| = \frac{|H(\omega_d)|}{\sqrt{2}} \tag{3.4}$$

The bandwidth $\omega_b - \omega_a$ is equal to $2\zeta\omega_d$, so that

$$\zeta = \frac{\omega_b - \omega_a}{2\omega_d} \tag{3.5}$$

Here ω_d is the damped natural frequency at resonance and ω_a and ω_b satisfy condition of Eq. (3.4).

3.3.6.2 Mode Shape Measurement

Determining the mode shapes from experimentally measured transfer function is slightly more complicated and involves the measurement of several transfer functions. Mode shapes have been experimentally determined from the Frequency Response Functions (FRF) and corresponding phase angle plot at different sensor locations. In the present study, data from nine sensor locations have been used. A Quadratic Peak Picking Method suggested by Inman (2001) has been adopted to extract the mode shape from observed data and compared with theoretical results. The basic idea was to establish a relation between the receptance matrix and the system's mode shapes, which can be utilized in testing to provide a measurement of the test specimen mode shapes.

The procedure for obtaining mode shape from experimentally observed frequency response function at different sensor locations are explained below:

Let us consider the response of the multiple degree of freedom system, subjected to harmonic force input, which is represented in a complex form by $\{f\}e^{j\omega t}$.

where f = amplitude of force

ω = circular natural frequency [rad/sec],

j is imaginary unit.

The equation of motion becomes

$$[M][\ddot{x}]+[C][\dot{x}]+[K][x]=\{f\}e^{j\omega t} \tag{3.6}$$

The forced response can be constructed by assuming that the solution *x(t)* is harmonic, of the form $\{x(t)\}=\{u\}e^{j\omega t}$. where {u} = amplitude of the displacement vector. Substitution of this form in Eq. (3.6) yields

$$\left([K]-\omega^2[M]+j\omega[C]\right)\{u\}=\{f\} \tag{3.7}$$

Thus $$\{u\}=\left([K]-\omega^2[M]+j\omega[C]\right)^{-1}\{f\} \tag{3.8}$$

The receptance matrix, denoted as $[\alpha(\omega)]$ is defined by

$$[\alpha(\omega)]=\left([K]-\omega^2[M]+j\omega[C]\right)^{-1} \tag{3.9}$$

The Eq.(3.8) can be written in simplified form as $\{u\}=[\alpha(\omega)]\{f\}$

The modal stiffness matrix can be represented in diagonal form as (Inman 2001).

$$[\Lambda_k]=diag[\omega_i^2]=[P]^T[M]^{-1/2}[K][M]^{-1/2}[P] \tag{3.10}$$

where [P]is the matrix of normalized eigenvectors of the matrix $[M]^{-1/2}[K][M]^{-1/2}$.

Similarly, if the modal damping is assumed to be proportional to mass, the modal damping matrix can be written as

$$[\Lambda_c] = diag[2\zeta_i\omega_i] = [P]^T[M]^{-1/2}[C][M]^{-1/2}[P] \tag{3.11}$$

Premultiplying Eq. (3.10) by $[M]^{1/2}[P]$ and post multiplying the same by $[P]^T[M]^{1/2}$ one gets

$$[K] = [M]^{1/2}[P][\Lambda_k][P]^T[M]^{1/2} \tag{3.12}$$

since $[P]^T[P] = [I]$. [I] is unitary matrix. Similarly, the damping matrix can be written from Eq. (3.11) as

$$[C] = [M]^{1/2}[P][\Lambda_c][P]^T[M]^{1/2} \tag{3.13}$$

Substitution of Eq. (3.12) and (3.13) for [K] and [C] into Eq. (3.9) for the receptance matrix yields

$$\begin{aligned}[\alpha(\omega)] &= \left[[M]^{1/2}[P]\left([\Lambda_k] - \omega^2[I] + j\omega[\Lambda_c]\right)[P]^T[M]^{1/2}\right]^{-1} \\ &= \left[[S]\left([\Lambda_k] - \omega^2[I] + j\omega[\Lambda_c]\right)[S]^T\right]^{-1} \\ &= \left[[S]\ diag\left(\omega_i^2 - \omega^2 + 2\zeta_i\omega_i\omega j\right)[S]^T\right]^{-1}\end{aligned} \tag{3.14}$$

where $[S] = [M]^{1/2}[P]$, called the matrix of mode shapes, each column of which is a mode shape vector.

The Eq. (3.14) can be written as

$$\left[\alpha(\omega)\right] = \left[S\right]^{-T} \; diag\left[\frac{1}{\omega_i^2 - \omega^2 + 2\zeta_i\omega_i\omega j}\right]\left[S\right]^{-1} \tag{3.15}$$

since the inverse of a diagonal matrix is obtained simply by inverting its nonzero diagonal elements.

Eq. (3.15) for receptance matrix can be expressed as a summation of *n* terms by realizing that the columns of S^{-T} are the mode shape vectors of the system, denoted by u_i. So Eq. (3.15) can be written as

$$\left[\alpha(\omega)\right] = \sum_{i=1}^{n}\left[\frac{u_i u_i^T}{\left(\omega_i^2 - \omega^2\right) + \left(2\zeta_i\omega_i\omega\right) j}\right] \tag{3.16}$$

where n is the number of modes.

This representation provides a connection between the receptance matrix and the system's mode shapes, which can be exploited in testing to provide a measurement of the test specimen mode shapes.

The element of the receptance matrix located at the intersection of the s^{th} row and r^{th} column $\left[\alpha(\omega)\right]$ is essentially the transfer function between the response (u_s) at point *s,* and the input (f_r) at point *r,* when all other inputs are held at zero.

The srth element of $\alpha(\omega)$ is given by

$$\left[\alpha_{sr}(\omega)\right] = \sum_{i=1}^{n}\frac{\left[u_i u_i^T\right]_{sr}}{\left(\omega_i^2 - \omega^2\right) + j\left(2\zeta_i\omega_i\omega\right)} \tag{3.17}$$

which relates the transfer function between a given input and output, $\left[\alpha_{sr}(\omega)\right]$, to elements of the mode shapes u_i.

Since $\left[\alpha(\omega)\right]$ is a matrix, it cannot be written as the ratio of an output to an input. However, each element of $\alpha(\omega)$ is a transfer function:

$$\frac{u_s}{f_r} = \left[\alpha(\omega)\right]_{sr} = H_{sr}(\omega) \tag{3.18}$$

where $H_{sr}(\omega)$ is the transfer function between an input at point *r* and an output at point *s.* If it is assumed that the modes, or peaks, of the system are well spaced, the summation in Eq. (3.17) evaluated at a natural frequency will be dominated by one term, the term corresponding to that frequency.

Substituting $\omega = \omega_i$ in Eq. (3.17) and taking the magnitude, one has

$$\left|\alpha_{sr}(\omega_i)\right| = \frac{\left|u_i u_i^T\right|_{sr}}{2\zeta_i \omega_r^2} \tag{3.19}$$

where it is assumed that the contributions from the other terms in the summation are much smaller because of the nonzero term $\omega_i^2 - \omega^2$ in their denominators.

Eq. (3.19) can be written as

$$\left|u_i u_i^T\right|_{sr} = \left|2\zeta_i \omega_i^2\right| \left|H_{sr}(\omega_i)\right| \tag{3.20}$$

where $\left|H_{sr}(\omega_i)\right| = \left|\alpha_{sr}(\omega_i)\right|$ is the magnitude of the frequency response function measured between points *s* and *r* and evaluated at the i^{th} natural frequency.

This equation relates the measured damping ratio, ζ_i, measured natural frequency, ω_i, and the measured magnitude of the transfer function, $\left|H_{sr}(\omega_i)\right|$, to the i^{th} mode shape, ω_i, and hence provides a measure of the mode shape of the test structure. The phase plot of $H(\omega_i)$ can be used to determine the sign of the element $\left|u_i u_i^T\right|_{sr}$.

Eq.(3.20) gives only the measurement of magnitude of one element of $\left[u_i\ u_i\right]_{sr}^T$.The phase plot of $H(\omega_i)$ is used to determine the sign of element. To construct the $\left[u_i\ u_i\right]_{sr}^T$ matrix, one has to obtain FRF at points i=1,2,.....s corresponding to each position of input i=1,2,……..r. In the experiment, FRF at nine sensor location have been obtained in pulse analyzer corresponding to each input locations. The peak of FRF is multiplied by $\left|2\zeta\omega_1^2\right|$ as given in Eq. (3.20) to obtain the mode shape vector $\{u_i\}$.

3.3.7 Experimental Results and Discussion

First two frequencies for the simply supported curved box girder model have been determined experimentally by picking up responses through the accelerometers mounted on the curved box girder model along the center line of deck. Accelerometers are also mounted on the web of the box girder to capture lateral mode if any. Experimental data were processed by the Bruel & Kjaer FFT analyzer with in-built PULSE software.

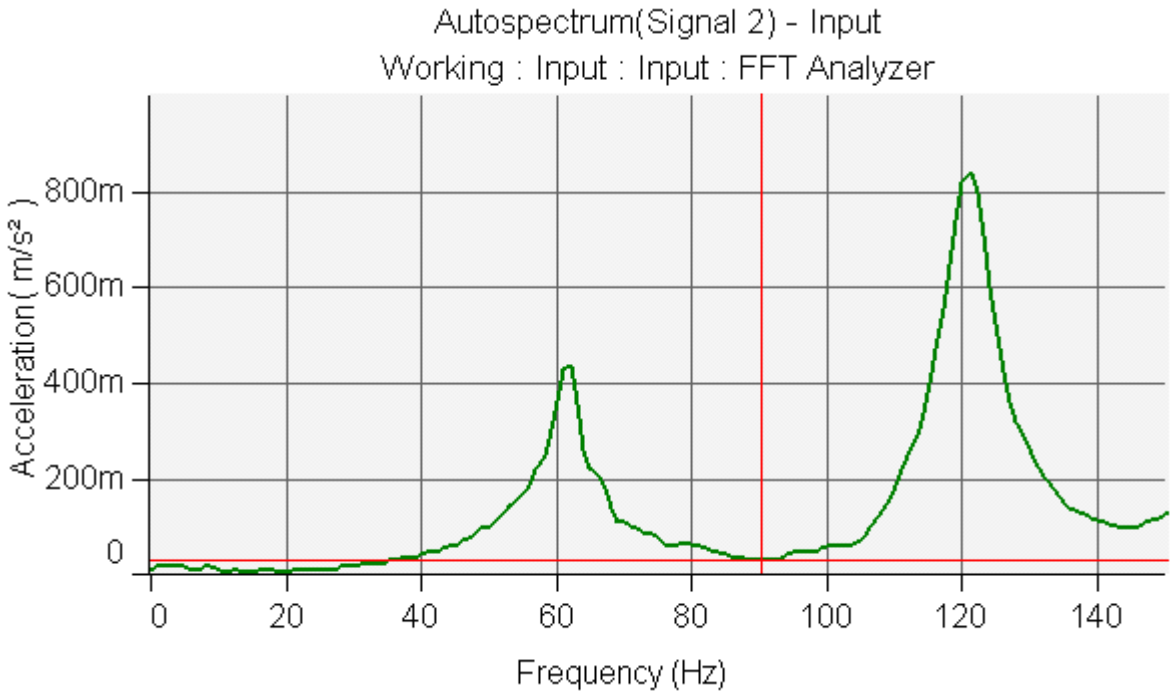

Fig. 3.7 Frequency response function plot for the simply supported curved box girder bridge model

The natural frequencies for the simply supported curved box girder model during an impact excitation could be observed accurately for the first two modes and hence results are presented for the first two modes. These two modes correspond to vertical and lateral bending of the bridge specimen.

Fig.3.7 shows a Frequency Response Function (FRF) obtained experimentally. The peaks of the FRF correspond to the natural frequencies of the bridge being tested. The variations between theoretical and experimental results of the first two frequencies have been presented in Table 3.2. The modes shapes as obtained theoretically as well as from experimental observation have been presented in Fig.3.8 and 3.9. The agreement obtained has been observed to be quite satisfactory. The experimentally evaluated damping ratios as obtained by Quadratic

Peak Picking method from the FRF plot have also been presented in Table 3.2. The FRF corresponding to different sensor locations have given identical values of both the natural frequencies observed experimentally.

Table 3.2 Structural natural frequencies and damping ratios of box girder bridge

Mode sequence	Frequency (Hz)		% Difference	Damping Ratio (ζ)
	Theoretical (FEM)	Experimental (FFT)		
First mode (flexural)	59.1726	61.50	3.93	0.04509
Second mode (lateral)	116.2049	121.00	3.96	0.03361

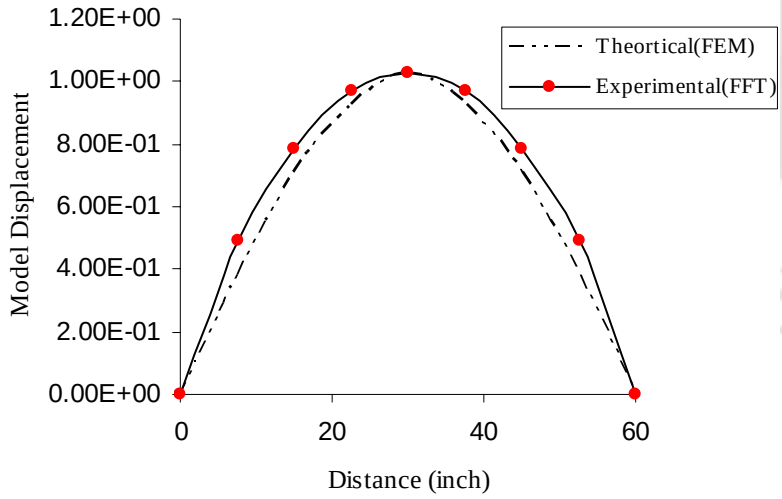

Fig. 3.8 1st mode (flexural) shape of curved box girder

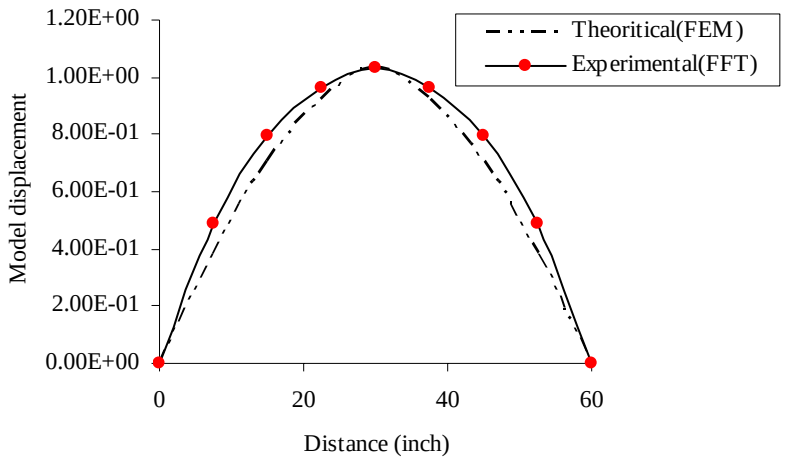

Fig. 3.9 2nd mode (lateral) shape of curved box girder

Further, in order to compare the natural frequencies of the curved box-girder model with standard results, analysis has been carried out using ANSYS (version 6.0) general purpose finite element software. Eight noded shell elements have been used for modeling the curved box-girder bridge model for the estimation of modal parameters. The frequencies as obtained from ANSYS are shown in Table 3.3 and have been observed to be very close to the finite element solution obtained using Zhang and Lyons (1984) element. The first mode shape of the bridge model, as observed from ANSYS is shown in Fig. 3.10.

Table 3.3 Verification of the performance of Zhang and Lyons (1984) element

Mode sequence	Frequency (Hz)	
	Zhang and Lyons (1984) element	Shell element (ANSYS)
First mode (Transverse Bending)	59.1726	60.13
Second mode (lateral bending)	116.2049	116.54

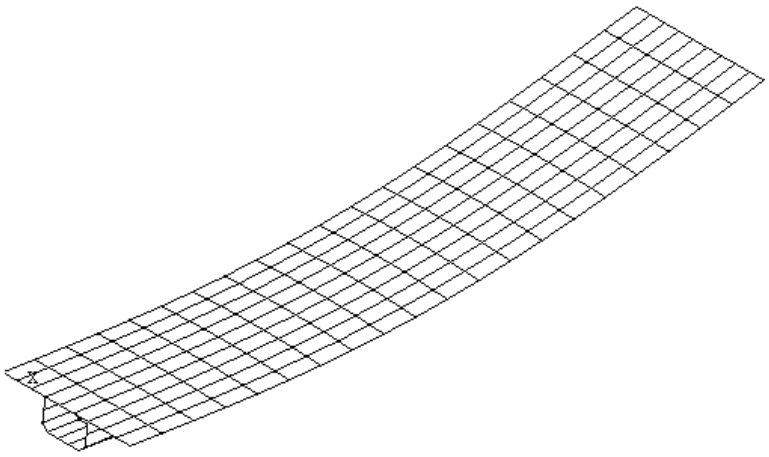

Fig. 3.10 First mode shape of curved box-girder bridge (using ANSYS)

3.4 PARAMETRIC STUDY

Having obtained the modal parameters of curved box girder bridge model by experiment, the natural frequencies and mode shapes have been evaluated again using the adopted finite element model for a simply supported concrete bridge with a span of 30 m for parametric study. Mainly, the effect of curvature on the free vibration characteristics of box-girder bridges has been studied. The cross-sectional dimension and geometry properties are shown in Fig.3.11 The bridge has got end diaphragms. The mass density of the bridge materials is 2403 kg/m^3, while modulus of elasticity and Poisson's ratios has been taken as 3.45 e+10 N/m^2 and 0.15. First ten frequencies and mode shapes have been presented in Table 3.4 for the bridge with the radius of curvature of 40 m. The modes shapes show the presence of coupled modes even in the early modes of the curved box-girder bridge. However the initial few modes show a significant contribution of either the conventional modes corresponding to the translational degrees of freedom or the eigen modes corresponding to the distortion and torsion. The evaluation of natural frequencies and mode shapes have also been carried out corresponding to a finite element representation using the conventional beam element having six degrees of freedom only and have been presented in Table 3.5. The exercises have been carried out in order to examine the differences of results with the present finite element adopted for the discretization of the thin walled box girder curved bridge. It has been observed that though the initial translational frequencies are quite identical corresponding to both the types of finite elements, the torsional frequency shows a significant difference. Further, in order to demonstrate the effect of curvature on the free-vibration, analyses have been carried out with varying radii of curvatures (40 m – 200 m) of the box girder bridge. Table 3.6 shows the variation of frequencies of the bridge with the change in the radius of curvature of the bridge.

The Table shows that the frequencies change slightly with the increase in the radius of curvature of simply supported box-girder bridge. In general, the effect of curvature of practical curved-box girder bridges on frequency is not significant. An identical observation has also been mentioned in Huang *et al* (1998) by carrying out similar parametric studies on a simply supported curved box-girder bridge.

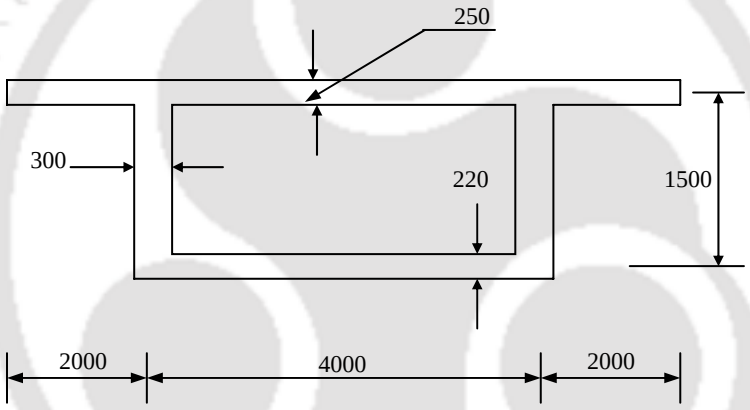

E = 3.45 e+10 N/m^2
ν = 0.15
G = 1.5 e+10 N/m^2
I_z = 1.6061 m^4
J = 3.2593 m^4
J_I = 0.79304 m^6
J_{II} = 1.01304 m^6
J_d = 0.00563 m^2
μ_t = 0.365
A = 3.7050 m^2

Fig. 3.11 Cross-section of the box-girder bridge

Table 3.4 Mode shape for curved box-girder bridge considering 9 d.o.f elements

Mode	Natural Frequencies (Hz)	Mode Shape
1.	4.1898	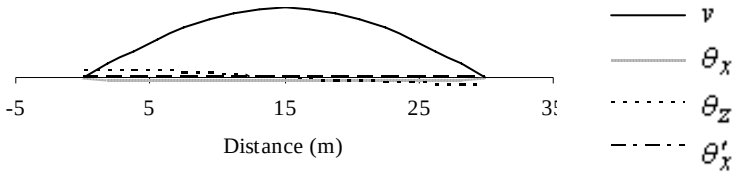
2.	11.7081	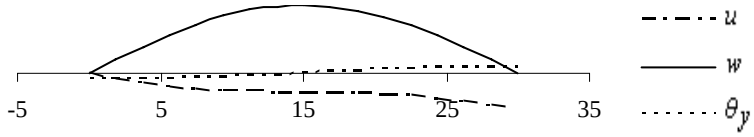
3.	16.3744	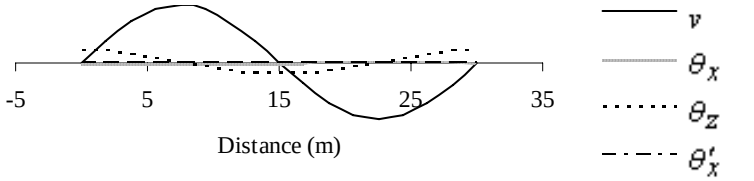
4.	23.8249	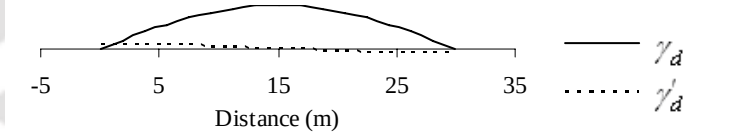
5.	26.6891	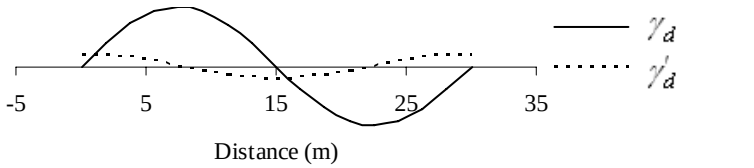
6.	31.1207	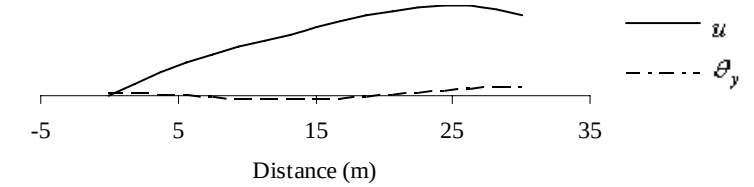

Table 3.4 (Contd.)

7.	33.8420	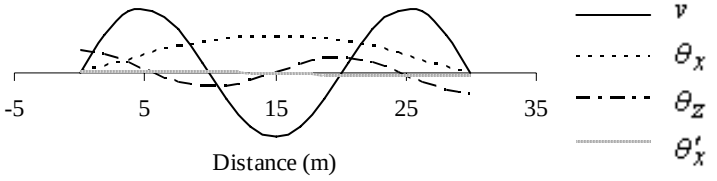
8.	36.5429	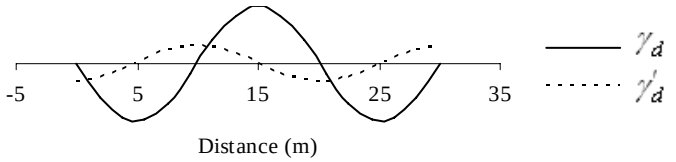
9.	40.2627	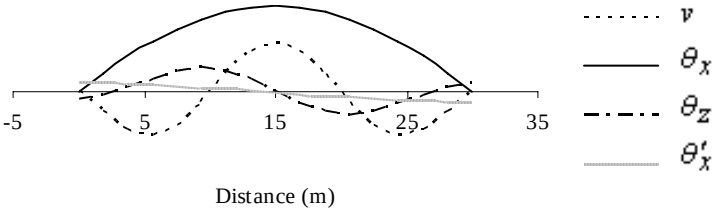
10.	44.8571	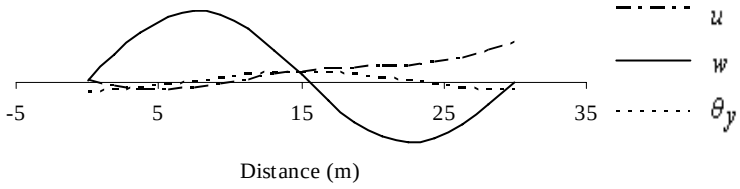

Table 3.5 Mode shape for curved box-girder bridge considering 6 d.o.f element

Mode	Natural Frequencies (Hz)	Mode Shape
1.	4.2209	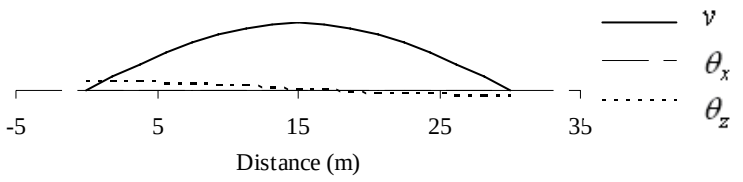
2.	11.7081	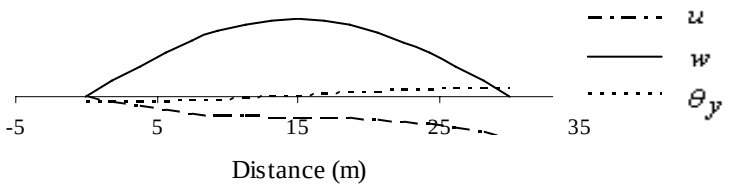
3.	16.4561	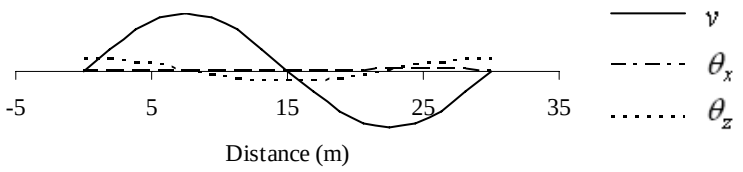
4.	31.1207	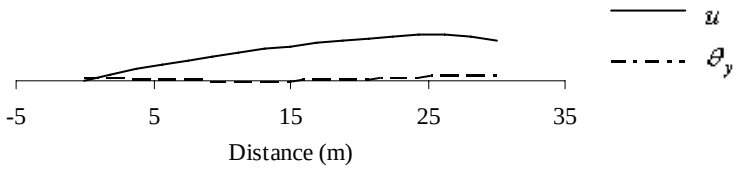
5.	34.2464	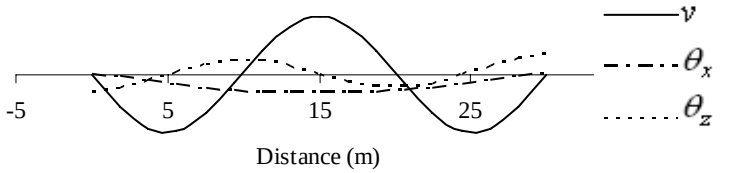

Table 3.5 (Contd.)

6.	44.8571	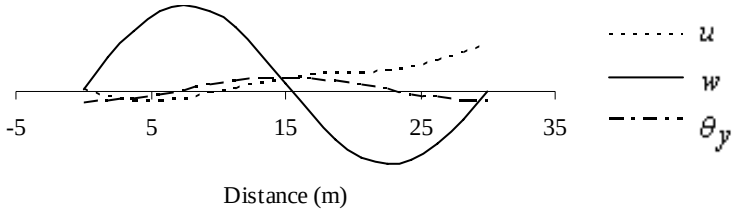
7.	46.5872	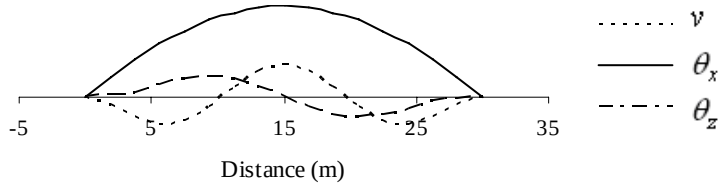
8.	59.2860	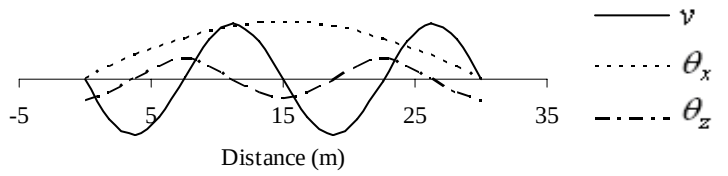
9.	80.0740	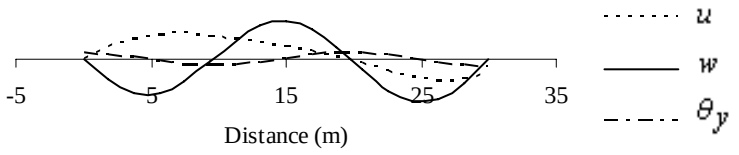
10.	89.2602	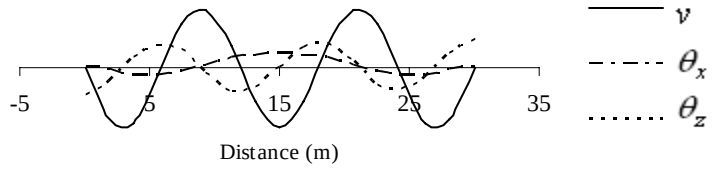

Table 3.6 Influence of radius of curvature on frequencies

Radius (m)	**Frequencies(Hz)**									
	1st Mode	***2nd*** Mode	***3rd*** Mode	***4th*** Mode	***5th*** Mode	***6th*** Mode	***7th*** Mode	***8th*** Mode	***9th*** Mode	***10th*** Mode
40	4.189	11.708	16.374	23.824	26.689	31.120	33.842	36.542	40.262	44.857
90	4.245	12.487	16.719	23.864	26.914	31.50	35.757	37.405	39.594	44.641
120	4.398	12.573	16.786	23.869	26.940	31.523	36.029	37.507	39.400	44.614
150	4.341	12.607	16.793	23.920	26.999	31.528	36.155	37.589	39.365	44.600
200	4.323	12.643	16.788	23.936	26.993	31.535	36.252	37.614	39.233	44.589

3. 5. CLOSURE

A computationally less expensive and realistic three noded thin-walled box beam element has been utilized for the modeling of the bridge curved in plan. The applicability of such an element for the dynamic analysis has been verified by evaluating the modal parameters of a curved box girder model theoretically as well as experimentally. The credibility of the adopted finite element for dynamic analysis has been further enhanced by carrying out analysis in ANSYS (version 6.0) general purpose finite element software for the estimation of modal parameters. The frequencies as obtained from ANSYS have been observed to be very close to the finite element solution obtained using Zhang and Lyons (1984) element. Further the

performances of the three noded thin-walled box-beam element have been compared with those of conventional (6-d.o.f) box-beam element and the necessity of the adopted finite element for handling of curved box-girder bridge have been very clearly realized. However, it has been observed that the effects of curvature of most of the practical bridges are insignificant.

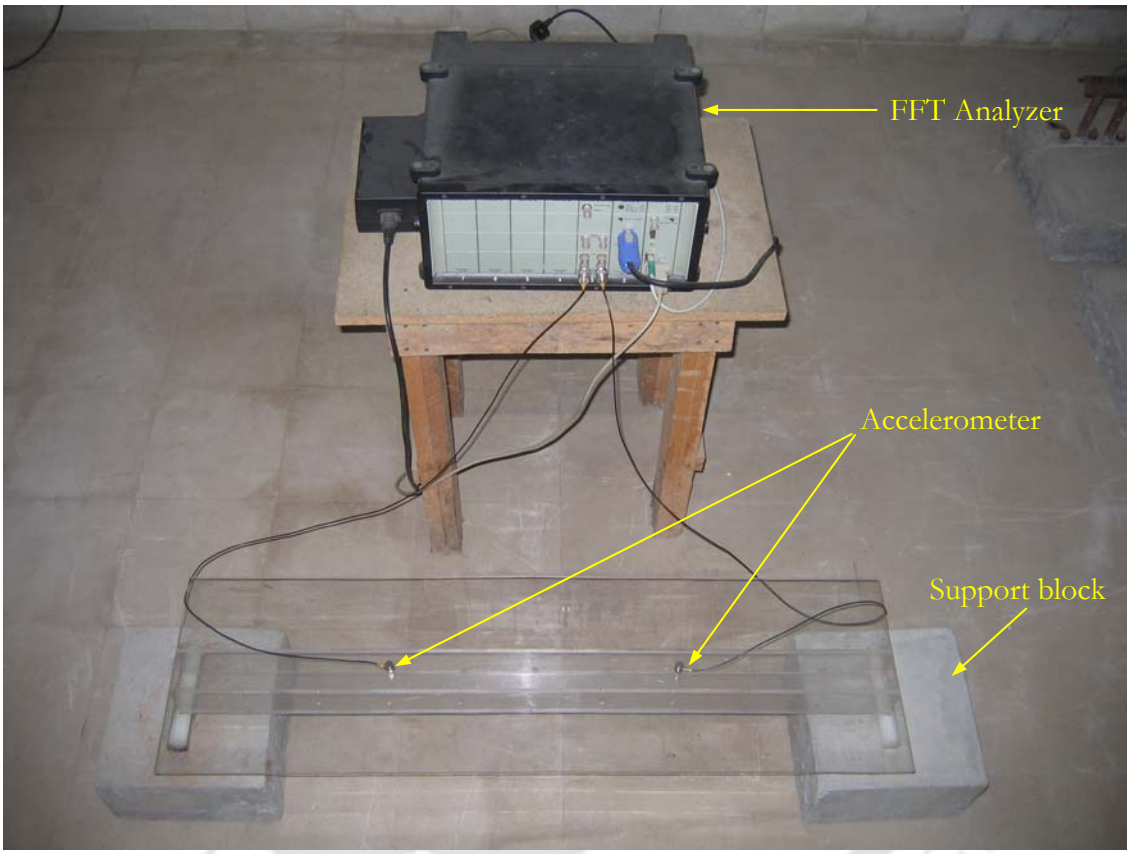

Fig. 3.5 Experimental setup for free vibration study of a curved box girder bridge model

CHAPTER 4

BRIDGE-VEHICLE INTERACTION

4.1 INTRODUCTION

The problem of vehicle-bridge dynamic interaction has been an important topic in the field of civil engineering. In particular, attention is paid to vibrations that might affect the durability of the structure as well as safety and comfort of passengers. Mathematical models have been developed to be able to describe the dynamic behavior of the supporting structure and the vehicles in terms of two uncoupled and coupled systems. Bridge vehicle vibration is a complex phenomenon governed by a large number of different parameters such as characteristics of vehicle, characteristics of bridge structure and their mutual influence on each other. In design practice, the dynamic effect caused by the fluctuating force component induced by the moving vehicle is taken into consideration by magnifying the live load effect by a multiplying factor termed as impact factor. In the present work, the impacts on curved box-girder bridges due to vehicle moving across rough bridge deck has been analyzed using bridge-vehicle coupled dynamics.

4.2 SYSTEM MODELS

The dynamic analysis of a bridge due to vehicle-induced vibration is considered as a coupled bridge-vehicle interaction problem with bridge deck surface irregularity significantly contributing to the overall response of the bridge structure. Thus, appropriate modeling of vehicle, deck surface and the bridge are very much essential for reliable evaluation of dynamic response.

4.2.1 Vehicle Model

A bridge is subjected to a variety of vehicular loading. The model of vehicle chosen for the present investigation of the dynamic interaction is seven degrees of freedom, heave-pitch-roll model (Yadav and Upadhyay 1993) as shown in Fig.4.1. The model is well representative of the prevailing design truck as available in India and surrounding South Asian countries and is fully capable of idealizing all the important motion components of the vehicle and their interaction. The model consists of one rigid beam representing vehicle body, whose mass is lumped at the centroid of the rigid beam and is known as "sprung mass" the vehicle. There are four unsprung masses which represent mass of the wheel, tires and part of suspension systems. The sprung mass has been assigned three degree of freedom, which corresponds to the vertical displacement z (heave motion along vertical axis), rotation about the longitudinal axis θ (pitch) and rotation about the transverse axis ψ (roll). The unsprung masses are assumed to have only heave motion, a vertical displacement z_{ip}. The first suffix i denotes wheel position. The suffix i can be taken 1 for the right wheel and 2 for the left wheel. The second suffix p gives the axle sequence, starting with the front axle. The vertical displacement of sprung, unsprung mass and that of box-girder bridge are considered positive upward. The pitch and roll motion of sprung mass are considered positive in clockwise direction.

The total seven independent degrees of freedom of the vehicle model can be written as

$$[D] = \left[z\ , \psi, \theta, z_{ip} \right] \quad i = 1,2;\ p = 1,2; \tag{4.1}$$

The centrifugal force (F_c) of each mass has been assumed to act horizontally at its centroid.

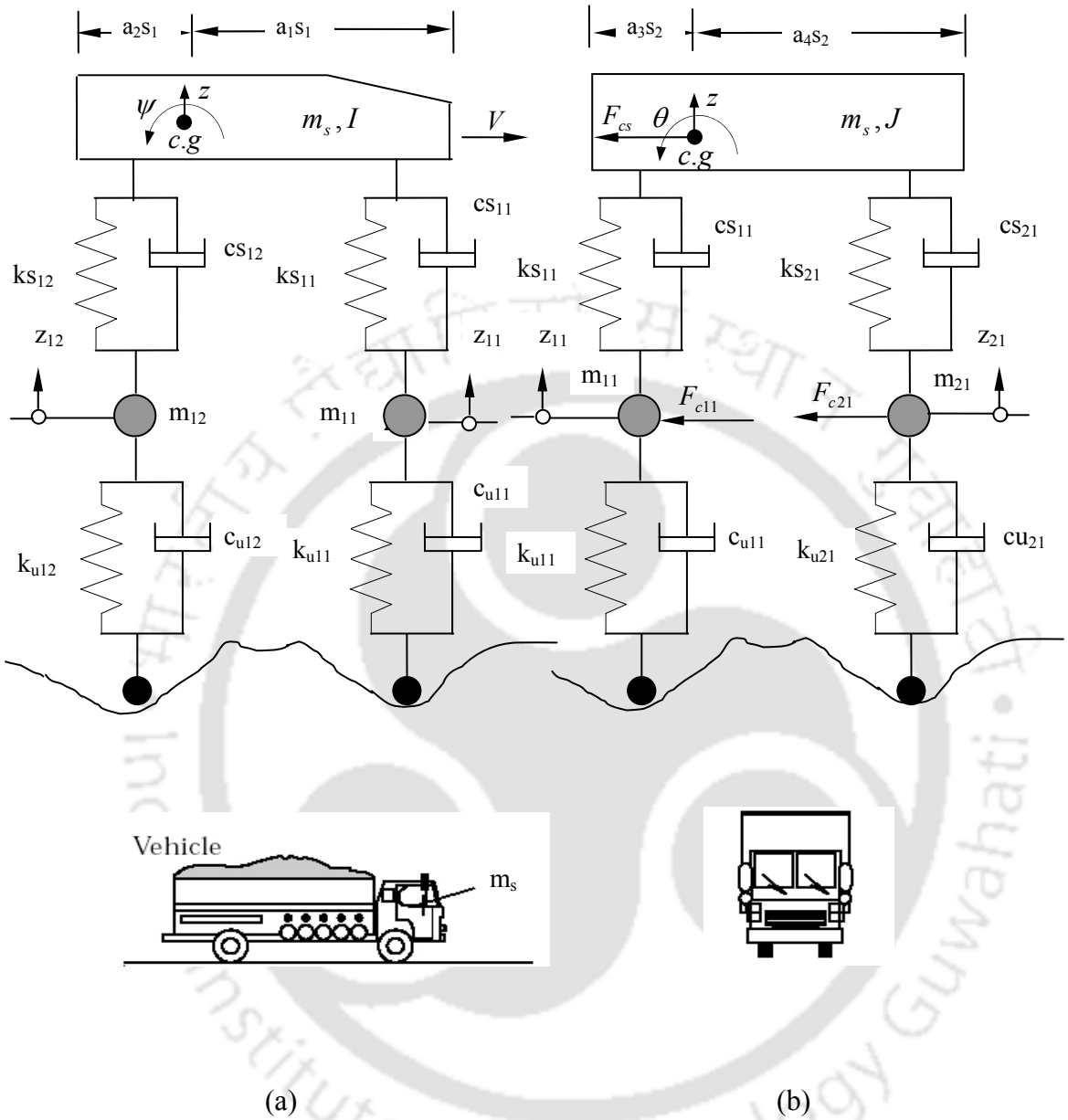

Fig.4.1 3-D Vehicle model with seven degrees of freedom (a) Side view (b) End view

4.2.2 Bridge Deck Roughness

The bridge deck unevenness causes moving vehicles to pick up dynamic excitation, which in turn imposes oscillatory loads on the deck. The degree of unevenness, however, varies depending upon the quality of construction and maintenance works. Simplified analysis can be performed assuming road surface in the form of sinusoidal wave, triangular wave or step function. But they do not reflect the actual behavior, since surface profiles are rarely of simple forms. The analyst needs to choose an appropriate model for the deck roughness. Investigations on road surface unevenness confirmed that it could be represented as the realization of random process, which may be assumed as homogeneous and ergodic in space (Dodds and Robson 1973). The vertical height of the bridge deck profile along the longitudinal axis measured with respect to flat datum are taken positive upward at a distance x from the reference station. This can be represented (Honda *et al.* 1982) as

$$h(x) = h_m(x) + h_r(x) \qquad \text{(4.2 (a))}$$

where $h_m(x)$ is the deterministic function describing the deck mean surface and $h_r(x)$ is a zero mean random process.

The location x can be taken as

$$x(t) = a_0 + a_1\, t + a_2\, t^2 \qquad \text{(4.2 (b))}$$

where a_0, a_1 and a_2 are constants. For constant velocity case $a_2 = 0$

4.2.2.1 Simulation of Road Roughness

To find the dynamic tyre force on the bridge deck, resulting from the vibration of moving vehicle it is necessary to specify input to the wheels. The random road surface irregularity has been taken as the source of dynamic excitation. In the present study, random road unevenness is

specified in terms of power spectral density (PSD) function. Vehicle response and hence dynamic tyre force can be obtained by using standard numerical integration scheme, with deck profile digitally simulated from the selected PSD function. The random road surface roughness $h_r(x)$ of the bridge can be described by zero mean, stationary Gaussian ergodic process in space. Shinozuka (1971) proposed that random road profile can be expressed as

$$h_r(x) = \sum_{k=1}^{N} \alpha_k \cos(2\pi\Omega_k x + \phi_k) \tag{4.3}$$

where α_k is the amplitude of the cosine wave, Ω_k, is the spatial frequency (rad/m) within the interval [Ω_l, Ω_u] in which power spectral density function is defined, φ_k, the random phase angle with uniform probability distribution in the interval [0, 2π]. x is the global coordinate measured from left end of the bridge and N is the total number of terms used to built up the road surface roughness in Eq.(4.3). The value of N depends on the velocity of the vehicle (hence the total time taken to cross the bridge) and size of the time increment chosen for the analysis of the dynamic response (N=Total time/Δt). The parameters α_k and Ω_k are computed as

$$\alpha^2{}_k = 4S_r(\Omega_k)\Delta\Omega \tag{4.4}$$

$$\Omega_k = \Omega_l + (k - 1/2)\Delta\Omega \tag{4.5}$$

$$\Delta\Omega = (\Omega_u - \Omega_l)/N \tag{4.6}$$

where $S_r(\Omega_k)$ is the PSD function (m^3/rad), Ω_l and Ω_u are the lower and upper cut-off spatial frequencies (rad/m), respectively.

The PSD function $S_r(\Omega_k)$ is expressed in terms of the spatial frequency of the road surface roughness Ω_k (in rad/m). The following form of PSD of deck roughness suggested by Hwang and Nowak (1991) has been used as the dynamic input to the moving vehicles.

$$S_r(\Omega_k) = \begin{cases} \alpha_s \Omega_k^{-\beta_r}, & for \quad \Omega_l < \Omega_k < \Omega_u \\ 0 & else\ where \end{cases} \tag{4.7}$$

where the parameter α_s is a spectral roughness coefficient in m^2/ (m/cycle), and β_r is the spectral exponent which is taken as 1.94. The spatial frequency can be transformed to temporal frequency ω (rad/sec) if the vehicle forward velocity is known. The relationship between spatial frequency Ω (rad/m) and temporal frequency ω (rad/sec) for the surface profile is given by

$$\omega = \Omega V \tag{4.8}$$

in which V is the vehicle forward velocity. The road surface condition may be classified in to five classes according to ISO specification in terms of coefficient α_s as shown in the Table 4.1**.**

Table 4.1 Road surface classification

Road surface condition	α_s (m^2/(m/cycle))
Very good	$\alpha_s \leq 0.24 \times 10^{-6}$
Good	$0.24 \times 10^{-6} \leq \alpha_s \leq 1.0 \times 10^{-6}$
Average	$1.0 \times 10^{-6} \leq \alpha_s \leq 4.0 \times 10^{-6}$
Poor	$4.0 \times 10^{-6} \leq \alpha_s \leq 16.0 \times 10^{-6}$
Very Poor	$\alpha_s > 16.0 \times 10^{-6}$

4.2.3 Bridge Model

The curved box-girder bridge has been numerically modeled using a thin-walled box-beam finite element which has been already introduced in section 2.4.

4.3 COUPLED BRIDGE-VEHICLE SYSTEM EQUATIONS

The equation of heave motion of the sprung mass can be written as

$$m_s\ddot{z} + \sum_{i=1}^{2}\sum_{p=1}^{2}\left\{cs_{ip}\left(\dot{z} - b_i\dot{\theta} - l_p\dot{\psi} - \dot{z}_{ip}\right) + ks_{ip}\left(z - b_i\theta - l_p\psi - z_{ip}\right)\right\} = 0 \tag{4.9}$$

As the random input of deck profile is not same for the front and rear wheels, the vehicle is subjected to pitching. The pitching motion of sprung mass is given by

$$J\ddot{\psi} + \sum_{i=1}^{2}\sum_{p=1}^{2}\left\{-cs_{ip}\left(\dot{z} - b_i\dot{\theta} - l_p\dot{\psi} - \dot{z}_{ip}\right)l_p - ks_{ip}\left(z - b_i\theta - l_p\psi - z_{ip}\right)l_p\right\} = 0 \tag{4.10}$$

The rolling motion of sprung mass is given by

$$I\ddot{\theta} + \sum_{i=1}^{2}\sum_{p=1}^{2}\left\{-cs_{ip}\left(\dot{z} - b_i\dot{\theta} - l_p\dot{\psi} - \dot{z}_{ip}\right)b_i - ks_{ip}\left(z - b_i\theta - l_p\psi - z_{ip}\right)b_i\right\} = 0 \tag{4.11}$$

The front and rear wheel bounce can be represented as

$$\begin{aligned} &m_{ip}\ddot{z}_{ip} - cs_{ip}\left(\dot{z} - b_i\dot{\theta} - l_p\dot{\psi} - \dot{z}_{ip}\right) - ks_{ip}\left(z - b_i\theta - l_p\psi - z_{ip}\right) \\ &+ cu_{ip}\left(\dot{z}_{ip} - \dot{h}_{ip} - \dot{v}_{ip}\right) + ku_{ip}\left(z_{ip} - h_{ip} - v_{ip}\right) = 0 \\ &i = 1,2; \quad p = 1,2; \end{aligned} \tag{4.12}$$

The governing differential equation of motion of the box-girder bridge can be expressed as

$$\begin{aligned} &[m_b]\left\{\ddot{\delta}\right\} + [c_b]\left\{\dot{\delta}\right\} + [k_b]\left\{\delta\right\} - \sum_{i=1}^{2}\sum_{i=1}^{2}\left\{cu_{ip}\left(\dot{z}_{ip} - \dot{h}_{ip} - \dot{v}_{ip}\right) + ku_{ip}\left(z_{ip} - h_{ip} - v_{ip}\right)\right\} \\ &+ \left(m_s g + \sum_{i=1}^{2}\sum_{p=1}^{2} m_{ip} g\right) + \left(\frac{m_s v^2}{R} + \sum_{i=1}^{2}\sum_{p=1}^{2}\frac{m_{ip} v^2}{R_i^{'}}\right) = 0 \end{aligned} \tag{4.13}$$

The weight of the vehicle and centrifugal forces will also act at appropriate location in addition to the damping and spring forces from vehicle as shown in Eq. (4.13).

Here, $b_1 = a_3 s_2, b_2 = a_4 s_2, l_1 = a_1 s_1, l_2 = a_2 s_1$, b_2 and l_2 are negative quantities. v_{ip} are the bridge displacements under front / rear wheels at any arbitrary time *t*. h_{ip} represents the random input of

deck profile under the front / rear wheels and $\dot{h}_{ip}$ are the time derivatives of the random input of deck profile.

The suspension stiffness and damping of the vehicle are denoted by ks_{ip} and cs_{ip}. Similarly, the tyre stiffness and damping are denoted by ku_{ip} and cu_{ip}. The sprung mass and unsprung masses are denoted by m_s and m_{ip} respectively. The pitch and roll moment of inertia of the vehicle are designated as *J* and *I*, while $[m_b]$, $[c_b]$, $[k_b]$ represents the bridge mass, damping and stiffness matrices respectively, g is the acceleration due to gravity. *R* is the radius of curvature with respect to the center of gravity of vehicle and R'_i is the corresponding radius of curvature with respect to the right and left wheel. The tyres of the vehicle always remain in contact with the bridge deck and the coupled bridge-vehicle system is solved for the range of velocities such that the interaction force is never less than zero.

The set of equations (4.9) to (4.13) can be expressed in matrix form amenable to its solution by a suitable numerical scheme as

$$[M]\{\ddot{\chi}\}+[C]\{\dot{\chi}\}+[K]\{\chi\}=\{P\} \qquad (4.14)$$

where [*M*], [*C*] and [*K*] are the global mass, damping and stiffness matrix respectively obtained after assembly and applying boundary conditions. The damping matrix has been taken as Rayleigh's damping matrix from the section 4.4. The response vector $\{\chi\}$ includes the vehicles sprung mass heave, pitch and roll degrees of freedom, unsprung mass vertical bounce and also displacement coordinates defined at the nodal points of the curved bridge. The vector {*P*} represents the generalized force vector which is dependent on pavement roughness, its derivative, moving vehicle mass and centrifugal force due to curvature effect.

4.4 CONSTRUCTION OF DAMPING MATRIX

The damping of the bridge is assumed to be Rayleigh damping (Chopra 2005). In this case, the damping matrix is assumed to be proportional to either the mass or the stiffness matrix or combination of both because the undamped mode shapes are orthogonal with respect to each of these. Thus the damping matrix can be expressed as

$$[c_b] = a_0[m_b] \quad \text{or} \quad [c_b] = a_1[k_b] \tag{4.15}$$

in which the proportionality constants a_0 and a_1 have units of sec^{-1} and sec, respectively. These are called mass proportional and stiffness proportional damping. The damping behavior associated with them may be recognized by evaluating the generalized modal damping value for each mode. These may be expressed as

$$c_n = \phi_n^T c_b \phi_n = a_0 \phi_n^T m_b \phi_n \quad \text{or} \quad a_1 \phi_n^T k_b \phi_n \tag{4.16}$$

$$\text{or} \quad 2\omega_n m_n \xi_n = a_0 m_n \quad \text{or} \quad a_1 k_n \qquad (\text{where } k_n = \omega_n^2 m_n) \tag{4.17}$$

where ϕ_n is the n^{th} mode shape, m_n, c_n and k_n are the normal-coordinate generalized mass, damping and stiffness corresponding n^{th} mode respectively.

From Eq.(4.17).

$$\xi_n = \frac{a_0}{2\omega_n} \quad \text{or} \quad \xi_n = \frac{a_1 \omega_n}{2} \tag{4.18}$$

An improvement of the results may be obtained, if the damping is assumed to be proportional to a combination of the mass and the stiffness matrices as given by the expressions shown in Eq (4.15).

$$[c_b] = a_0[m_b] + a_1[k_b] \tag{4.19}$$

which is called Rayleigh damping. Rayleigh damping leads to the following relation between damping ratio and frequency.

$$\xi_n = \frac{a_0}{2\omega_n} + \frac{a_1\omega_n}{2} \tag{4.20}$$

The relationships between damping ratio and frequency expressed in Eq. (4.18) and Eq. (4.20) are shown graphically in Fig 4.2. The combined form of damping as represented by Eq. (4.19) has been also shown in Fig.4.2.

It is apparent that the two damping factors, a_0 and a_1 can be evaluated by the solution of a pair of simultaneous equations if the damping ratio ξ_m and ξ_n associated with two frequencies ω_m and ω_n in m^{th} and n^{th} mode are known. Writing Eq.(4.20) for each of these two cases and expressing the two equations in matrix form leads to

$$\begin{Bmatrix} \xi_m \\ \xi_n \end{Bmatrix} = \frac{1}{2}\begin{bmatrix} 1/\omega_m & \omega_m \\ 1/\omega_n & \omega_n \end{bmatrix}\begin{Bmatrix} a_0 \\ a_1 \end{Bmatrix} \tag{4.21}$$

and the factors resulting from the simultaneous solution are

$$\begin{Bmatrix} a_0 \\ a_1 \end{Bmatrix} = 2\frac{\omega_m\omega_n}{\omega_n^2 - \omega_m^2}\begin{bmatrix} \omega_n & -\omega_m \\ -1/\omega_n & 1/\omega_m \end{bmatrix}\begin{Bmatrix} \xi_m \\ \xi_n \end{Bmatrix} \tag{4.22}$$

When these factors have been evaluated, the proportional damping matrix that will give required values of damping ratio at the specified frequencies. The variation of damping coefficient with frequency as can be obtained from Eq. (4.18) and Eq. (4.20) is shown in Fig 4.2.

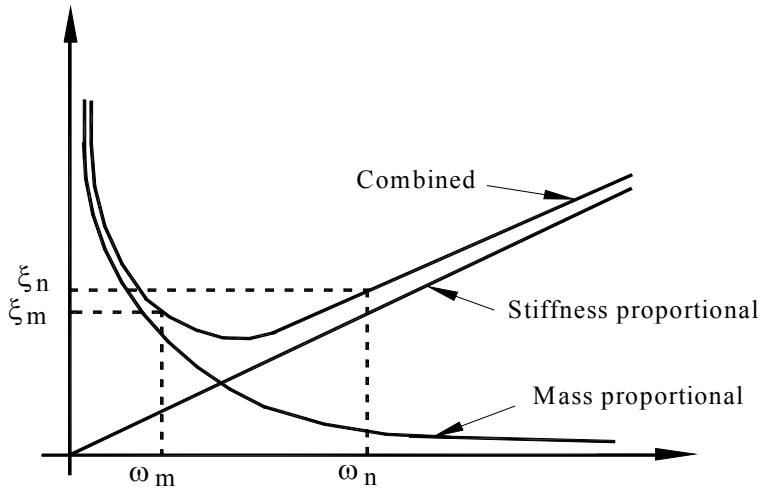

Fig 4.2 Relationship between damping ratio and frequency for Rayleigh damping

4.5 SOLUTION TECHNIQUE

Newmark-β scheme (average acceleration) with predictor-corrector algorithm (Owen and Hinton 1960) has been used for the evaluation of dynamic response of the bridge due to vehicle-induced vibration.

4.5.1 Explicit Predictor-Corrector Algorithm

The algorithm has been explained in the following steps.

1. Begin predictor phase by setting

$$d_{n+1}^{[0]} = \tilde{d}_{n+1} = d_n + \Delta t v_n + \Delta t^2 (1-2\beta) a_n / 2 \qquad (4.23(a))$$

$$v_{n+1}^{[0]} = \tilde{v}_{n+1} = v_n + \Delta t (1-\gamma) a_n \qquad (4.23(b))$$

$$a_{n+1}^{[0]} = 0 \tag{4.23(c)}$$

2. Evaluate the residual forces using the equation

$$\Psi^{[0]} = f_{n+1} - p\left(d_{n+1,}^{[0]} v_{n+1}^{[0]}, a_{n+1}^{[0]}\right) \tag{4.24}$$

3. If required, form the 'effective' stiffness matrix using the expression

$$K^* = M \Big/ \left(\Delta t^2 \beta\right) + C \Big/ \left(\Delta t \beta\right) + K\left(d_{n+1}^{[i]}\right) \tag{4.25}$$

Note that as the mass matrix M does not change K^* will be formed once only.

4. Performing factorization, forward reduction and back substitution as required to solve

$$K^* \Delta d^{[0]} = \Psi^{[0]} \tag{4.26}$$

5. Enter the corrector phase in which we set

$$d_{n+1}^{[1]} = d_{n+1}^{[0]} + \Delta d^{[0]} \tag{4.27(a)}$$

$$a_{n+1}^{[1]} = \left[d_{n+1}^{[1]} - \tilde{d}_{n+1}\right] \Big/ \left(\Delta t^2 \beta\right) \tag{4.27(b)}$$

$$v_{n+1}^{[1]} = \tilde{v}_{n+1} + \Delta t \gamma a_{n+1}^{[1]} \tag{4.27(c)}$$

6. $$d_{n+1} = d_{n+1}^{[1]} \tag{4.28(a)}$$

$$v_{n+1} = v_{n+1}^{[1]} \tag{4.28(b)}$$

$$a_{n+1} = a_{n+1}^{[1]} \tag{4.28(c)}$$

for use in the next time step. Also set n=n+1, form p and begin next time step where M, a_{n+1}, p_{n+1} and f_{n+1} are the mass matrix, acceleration vector, internal force vector (which may depend on the displacements d_{n+1} and velocity $\dot{d}_{n+1}$ and their histories) and applied force vector respectively. d_n, v_n and a_n are the approximation to $d(t_n), \dot{d}(t_n)$ and $\ddot{d}(t_n)$. The parameters β

and γ control the accuracy and stability of the method and these values are taken as 0.25 and 0.5 respectively. The values $\tilde{d}_{n+1}$ and $\tilde{v}_{n+1}$ are predictor values and d_{n+1} and v_{n+1} are corrector values. Δt is the time interval.

4.6 NUMERICAL SIMULATION

Free vibration studies have been conducted prior to the evaluation of dynamic response of curved thin-walled box girder bridge due to vehicle-induced vibration. The natural frequencies and mode shapes for first two modes have been obtained experimentally and compared with the theoretically evaluated values as documented in chapter 3. The validation of modal parameters demonstrated the applicability of the thin-walled box-beam finite element for the evaluation of dynamic response of the box girder bridge.

4.6.1 Vehicle Induced Vibration

The vibrations of the bridge induced by moving vehicles at different velocities have been studied for a set of bridge and vehicle parameters presented in the subsequent sections. One percent of critical damping is taken for the first and second modes. It is assumed that the bridge surfaces have the same roughness in the transverse direction. The initial conditions viz displacements and velocities of all degrees of freedom are taken zero. It is also assumed that the roadway approaches also have the same class of road surface as the bridge. Appendix-D illustrates the sequence of operation for the dynamic analysis of bridge vehicle coupled system.

4.6.2 Vehicle Parameters

The vehicle model as mentioned in section 4.2.1 is a heave-pitch-roll 3D model. All the parameters relevant to the vehicle are taken from ref. (Henchi et al. 1998) and have been presented in Table 4.2.

4.6.3 Road Roughness Profile

The details of the procedure for generation of random road surface roughness from PSD function have been given in the section 4.2.2.1. In this study, the values of spectral roughness coefficient, α_s have been taken as 0.24 $x10^{-6}$, $0.5x10^{-6}$, $3.0x10^{-6}$, $10.0x10^{-6}$ and $25.0x10^{-6}$ m^3/(m/cycle) according to International Organization for Standardization (ISO) specifications for the classes of very good, good, average, poor and very poor roads respectively. Twenty profiles of road roughness are generated for each type of road using the following parameters:

The lower and upper limits of the spatial frequencies of the road profile are taken as ω_l=0.01cycle/m and ω_u=3.0 cycle/m. The cut-off spatial frequencies are chosen in view of the practical size of a tyre. In generating the random road surface roughness, random numbers φ_k have been generated in MATLAB. Thus, for the bridge deck span of 30m, deck profile heights are generated along the span of the bridge at discrete points, which corresponds to the velocity of the vehicle and time step size chosen. A typical vertical highway surface profile of good road surface is as shown in Fig.4.3.(a). Dynamic responses are evaluated for each of the simulations corresponding to a particular vehicle velocity.

Table 4.2 Data of vehicle with seven degrees of freedom (Fig.4.1)

Parameter	Unit	Value
Sprung mass (m_s)	kg	15000
Unsprung mass in front axle (m_{11}, m_{21})	kg	800
Unsprung mass in rear axle (m_{12}, m_{22})	kg	710
Vehicle suspension stiffness (ks_{ip})	N/m	0.399×10^6
Vehicle tyre stiffness (ku_{ip})	N/m	0.351×10^6
vehicle suspension damping in front axle $(cs_{11},\ cs_{21})$	Ns/m	23210
vehicle suspension damping in rear axle $(cs_{12},\ cs_{22})$	Ns/m	5180
Vehicle tyre damping (cu_{ip})	Ns/m	800
Pitch moment of inertia (J)	kgm^2	154.536
Roll moment of inertia (I)	kgm^2	449
Position parameter (length wise) a_1	-	0.35
Position parameter (length wise) a_2	-	0.65
Position parameter (breath wise) a_3	-	0.5
Position parameter (breath wise) a_4	-	0.5
Vehicle axle spacing (length wise) s_1	m	2.66
Vehicle axle spacing (breath wise) s_2	m	1.5
Height of C.G. of vehicle from deck surface (h_v)	m	1.2

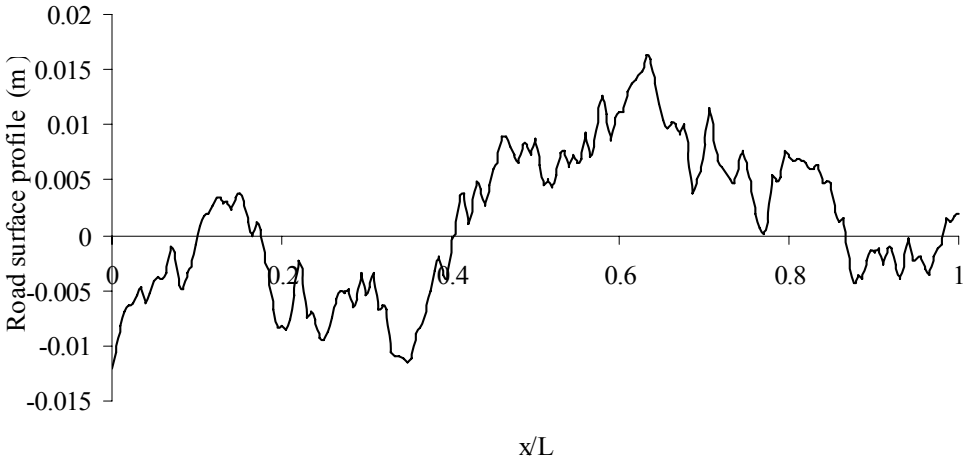

Fig .4.3(a) A typical good road surface profile for a box girder bridge

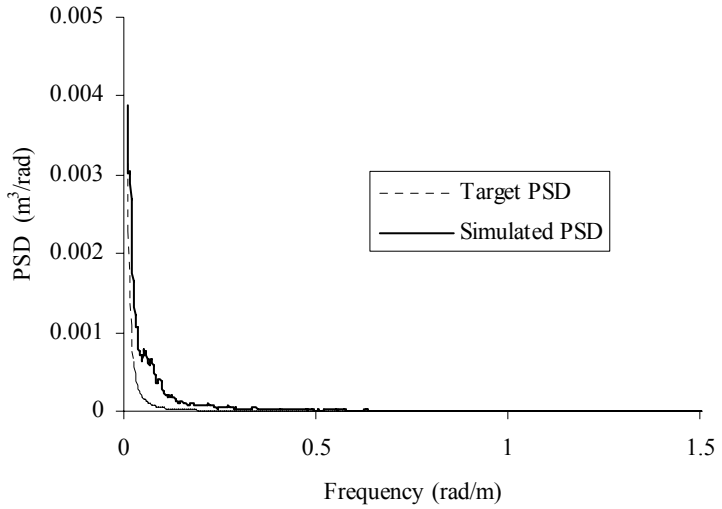

Fig. 4.3(b) Comparison of target PSD and simulated PSD for good road surface

The comparison of simulated PSD with the target PSD for good road surface condition has been shown in Fig.4.3 (b). The agreement is good towards higher cut-off frequencies where as in the middle of the frequency range, discrepancy appears mainly because of numerical noise in the simulation process.

4.6.4 Box-Girder Bridge Parameters

A simply supported curved box girder bridge (Fig.4.4) as considered by Kermani and Waldron (1993) has been chosen in the present study to obtain the dynamic response due to moving vehicles. The span of the simply supported bridge is 30 m with a radius of curvature of 150 m and the bridge has diaphragms at supports. The mass density, modulus of elasticity and Poisson's ratio of the material are 2403 kg/m^3, 3.45 x 10^{10} N/m^2 and 0.15 respectively. Though the chosen Newmark-β scheme is unconditionally stable, all the analyses have been carried out by choosing a time increment equal to 1/50th of first fundamental time period from the accuracy point of view. Further, more refined time increments values have also been considered, which did not show any significant changes in the dynamic response of the bridge under study. Thus, considering numerical error due to inappropriate space and time discretizations, the bridge has been discretized using thirty numbers of thin-walled box beam elements and a time step of 3.6 x 10^{-3} sec is chosen for the analysis.

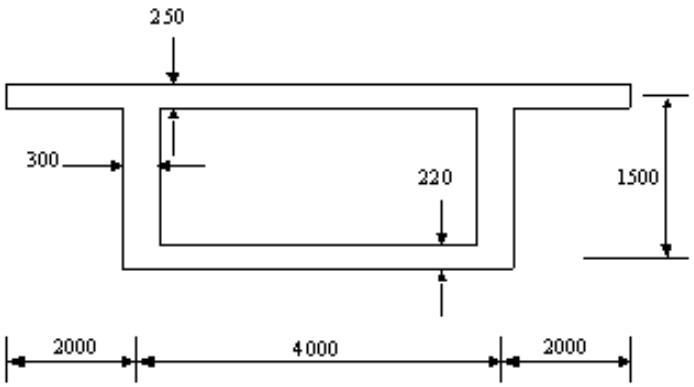

E = 3.45 e+10 N/m^2
ν = 0.15
G = 1.5 e+10 N/m^2
I_z = 1.6061 m^4
J = 3.2593 m^4
J_I = 0.79304 m^6
J_{II} = 1.01304 m^6
J_d = 0.00563 m^2
μ_t = 0.365
A = 3.7050 m^2

Fig .4.4 Geometry (mm) and properties of box girder bridge

4.6.5 Box-Girder Bridge Response

Some typical time histories for the bridge (Fig.4.4) are shown in Fig 4.5-4.11. The histories are obtained at the mid span of the curved thin-walled box-girder bridge corresponding to a good road surface roughness (ref. Table 4.1) with a vehicle speed of 20m/sec and asymmetric car loading (Fig. 4.12, loading case 2) as the vehicle crosses the bridge. The abscissa in those time histories is the distance measured from the left of the bridge to the front axle of the vehicle. Fig.4.5 and Fig.4.6 show the time history at the mid span of the bridge for the bending moment about the transverse axis and the vertical deflection at the center of the bridge as the vehicle moves along the span. From this figures, it can be observed that the vibration modes with higher frequencies significantly contributes to the dynamic response. Fig. 4.7 and 4.8 show the history of shear force and torsional moment at the center of the bridge. These figures indicate that the centrifugal force has greatly influenced the dynamic response of torque, while the shear force is almost unaffected by centrifugal force. Fig. 4.9-4.11 show the time history of torsional bimoment, distortional moment and distortional bimoment. A significant effect of higher frequency modes as well as centrifugal forces on those dynamic responses have been observed. Thus, similar to the established findings in the existing literature, it has been clearly observed

from Fig.4.5-4.11 that a substantial difference exist in all the response parameters between static and dynamic loading conditions. The impact factor have been suitably evaluated corresponding to each of these parameters.

4.6.6 Dynamic Amplification Factor (DAF)

Dynamic amplification factor can be defined as the ratio of absolute maximum dynamic response to static responses corresponding to the j^{th} simulation of random road surface. DAF can be represented as

$$DAF = \frac{\text{Absolute maximum dynamic response}}{\text{Absolute maximum static response}} \tag{4.29}$$

Since, a large majority of bridges are designed considering static vehicular load, such amplification due to dynamic effect has been considered using either IF (Impact factor based on span length relationship) or DLA (Dynamic Load Allowance based on the relationship of natural frequencies of bridge and vehicle) in many design codes. The impact factor usually adopted in design practices does not depend on time. Hence the largest absolute value of the impact factor calculated for a particular section has been presented in the report. Effects of various parameters such as damping of box-girder structure, load positions, vehicle speed, span, radius of curvature of the box girder bridge, surface roughness, suspension stiffness, sprung mass and acceleration of vehicle on the impact factor have been discussed in the present section. The impact factor as presented in Tables 4.3-4.11 represents the mean values corresponding to twenty simulation of road surface corresponding to a particular type of road condition.

The example problem as shown in Fig.4.4 with a span length of 30 m and a radius of curvature of 150 m with a good road surface roughness has been considered again. A vehicle speed of 20m/sec and an asymmetric car loading (Fig. 4.12, loading case 2) has been chosen. The

damping ratio for the bridge is taken as 1%. However, some of these physical parameters will be varied in order to evaluate the influence of them on impact factors based on the dynamic response.

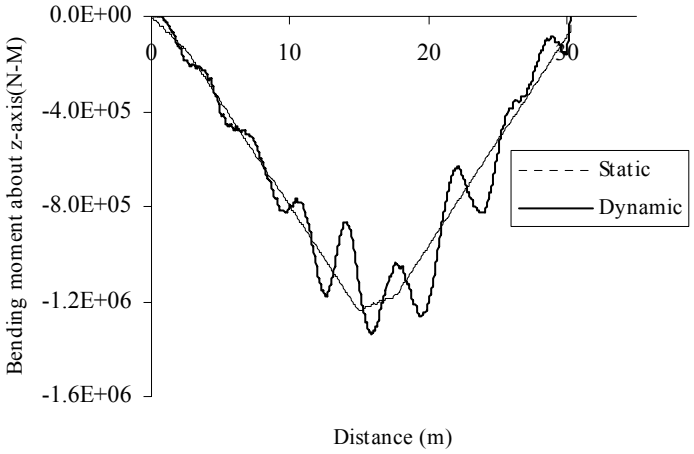

Fig .4.5 Time history for bending moment about transverse axis

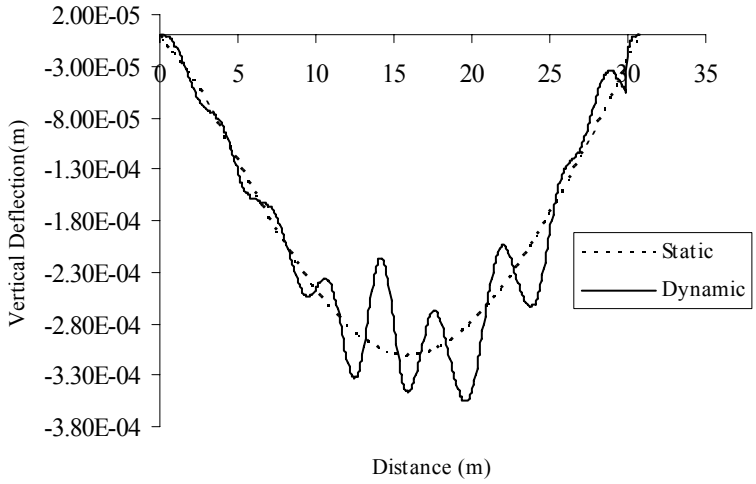

Fig.4.6 Time history for vertical deflection

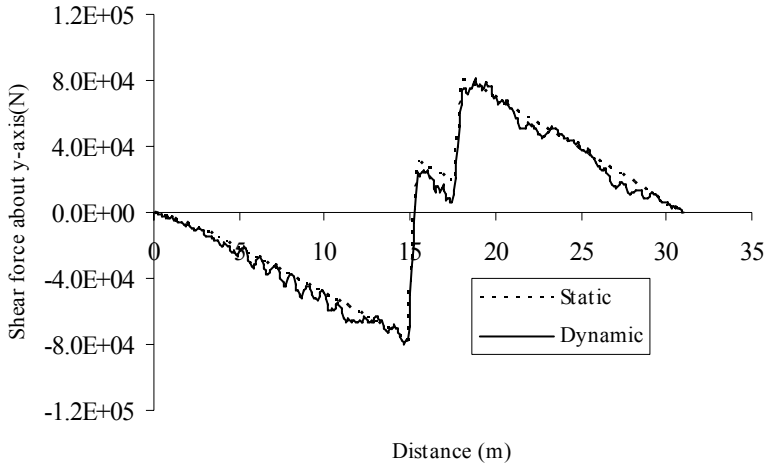

Fig .4.7 Time history for shear force

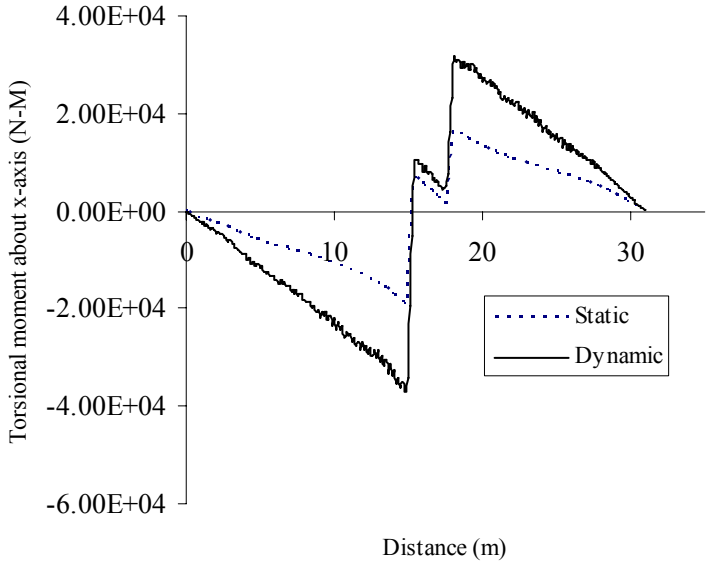

Fig .4.8 Time history for torsional moment

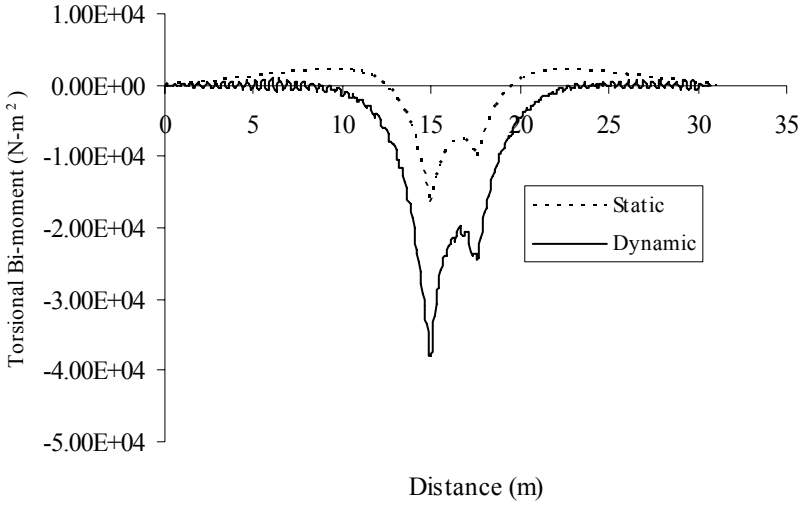

Fig .4.9 Time history for torsional bimoment

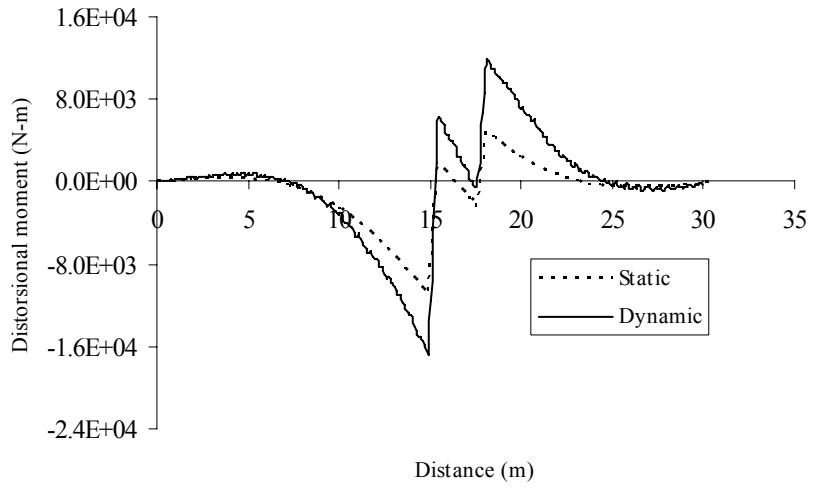

Fig.4.10 Time history for distortional moment

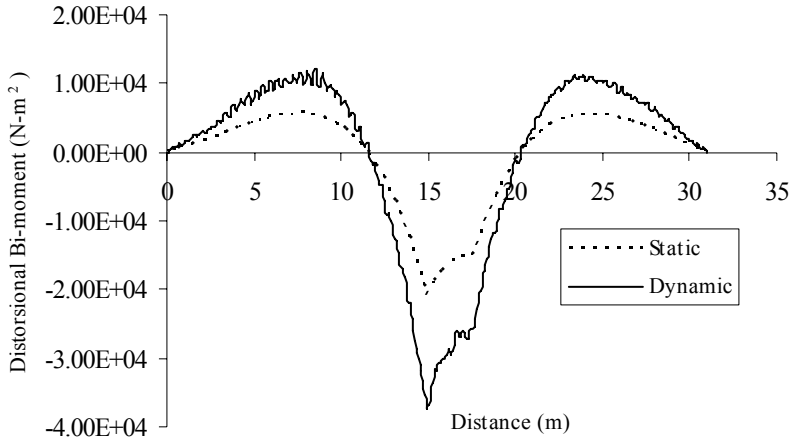

Fig.4.11 Time history for distortional bimoment

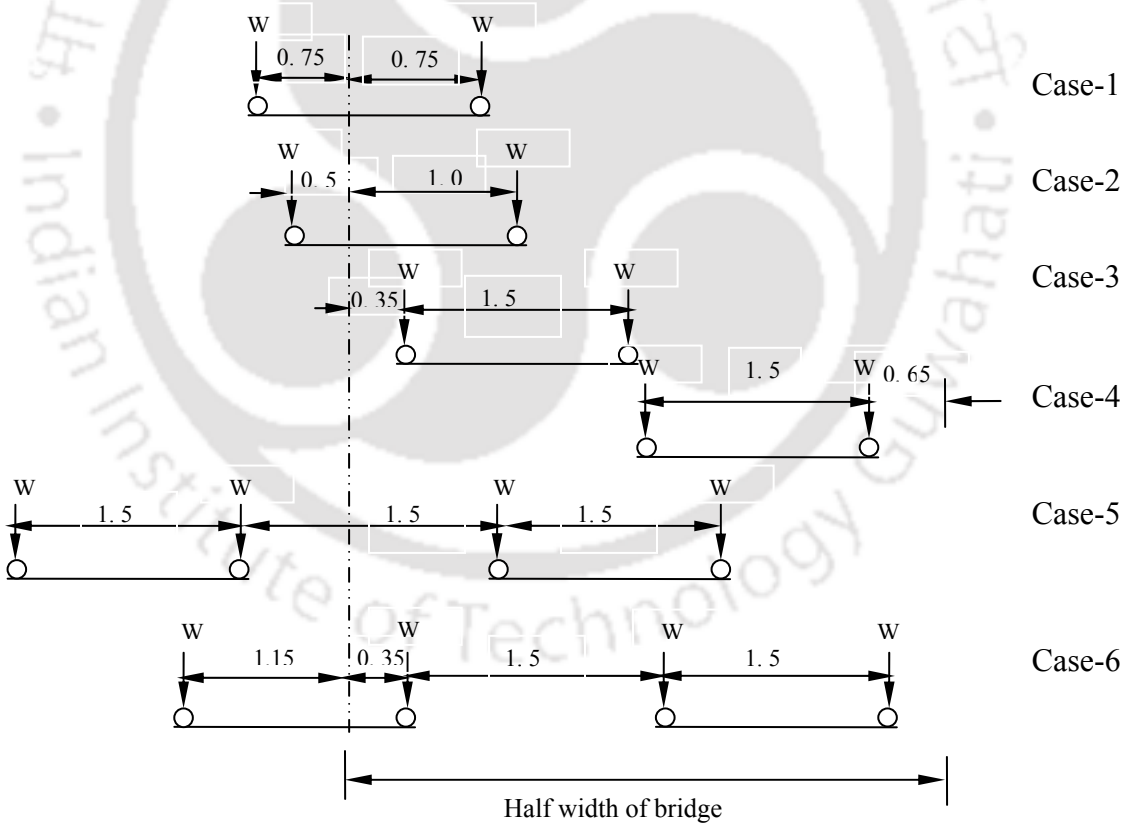

Fig .4.12 Traverse loading cases on curved box girder bridge

4.6.7 Parameter Study

The influence of certain physical parameters on the Bending moment about the transverse axis (M_z), Shear force (Q_y), Torsional moment (M_x), Torsional Bimoment (B_I), Distortional moment (M_d), Distortional Bimoment (B_{II}), Vertical deflection (v) have been studied in details here. It is fully appreciated that all these response parameters are highly significant for a thin-walled box girder bridge. Thus, the impact factor based on these response parameters will also accordingly reflect the significance of all the physical parameters considered for the present study.

4.6.7.1 Effect of Damping

Table 4.3 shows the variation of impact factor corresponding to various response parameters with varying damping ratio of bridge structure. It has been observed that neglecting the effect of damping will reasonably overestimates the impact factors of vertical deflection, bending moment and shear force for a curved box-girder bridge. However, with increasing damping ratio from 1% to 4%, only small decrease of impact factors have been observed for most of the response parameters. Hence, damped forced vibration analysis of the structure with any reasonable estimation of damping ratio will lead to the acceptable evaluation of impact factors.

Table 4.3 Effect of damping on impact factor

Damping ratio (ξ)					
Response parameter	**0%**	**1%**	**2%**	**3%**	**4%**
(M_z)	1.13	1.08	1.07	1.05	1.03
(Q_y)	1.15	1.08	1.07	1.06	1.05
(M_x)	2.05	1.93	1.92	1.92	1.92
(B_I)	2.25	2.24	2.24	2.24	2.24
(M_d)	1.53	1.52	1.52	1.51	1.51
(B_{II})	1.80	1.79	1.79	1.79	1.78
(v)	1.21	1.14	1.13	1.11	1.09

4.6.7.2 Effect of Load Positions

In order to find the most unfavorable loading position for the assessment of impact factor, six different positions of traverse load on a box-girder bridge have been considered as shown in Fig.4.12. The load positions have been selected from Huang *et al.* 2001. Appendix F shows the detailed calculation for the evaluation of equivalent load vector for an eccentrically placed vehicle. Table 4.4 shows the variation of impact factor corresponding to different response parameters with different loading cases. The impact factors of curved box-girder bridge for a double- truck loading have been observed to be higher than that for a single truck loading. The loading positions have lesser influence on vertical shear and bending moment, while impact factors of torque, distortional moments and bimoments are relatively more effected by the

loading positions. From the design point of view, it is observed that the loading case-6, which can produce maximum design internal forces, should be used.

Table 4.4 Effect of Loading Position on Impact Factor

Loading case						
Type of truck	**Single truck**				**Double truck**	
Response parameter	**Case-1**	**Case-2**	**Case-3**	**Case-4**	**Case-5**	**Case-6**
(M_z)	1.08	1.08	1.0960	1.10	1.56	1.56
(Q_y)	1.08	1.08	1.0552	1.05	1.45	1.45
(M_x)	**	1.92	1.1625	1.05	**	2.33
(B_I)	**	2.25	1.2208	1.08	**	2.56
(M_d)	**	1.52	1.02	1.01	**	2.05
(B_{II})	**	1.79	1.15	1.0397	**	2.21
(v)	1.14	1.14	1.17	1.18	1.78	1.78
** Not applicable due to symmetric nature of the load						

4.6.7.3 Effect of Vehicle Speed

Table 4.5 gives the variation of impact factor with vehicle speed. The Table shows that while the impact factors of torque, distortion and their corresponding bi-moments rapidly increase with vehicle speed, those of vertical deflection, bending moment and shear force do not show such tendency. A large range of velocities have been covered and significant influence of torsion, distortion and their corresponding bi-moments have been observed. Thus,

unless the torsion, distortion and their bi-moments are appropriately accounted for in the design, the safety and reliability can not be ensured in the conventional design predominantly based on bending moment and shear force.

Table 4.5 Effect of vehicle speed on impact factor

Vehicle speed $(v)\,{}^{m}/_{\text{sec}}$						
Response parameter	**5**	**10**	**15**	**20**	**25**	**30**
(M_z)	1.05	1.06	1.07	1.08	1.12	1.142
(Q_y)	1.04	1.06	1.0712	1.08	1.12	1.142
(M_x)	1.16	1.24	1.52	1.92	2.47	3.15
(B_I)	1.27	1.47	1.80	2.25	2.88	3.58
(M_d)	1.012	1.16	1.21	1.52	1.95	2.39
(B_{II})	1.04	1.17	1.43	1.79	2.26	2.86
(v)	1.11	1.12	1.13	1.14	1.161	1.184

4.6.7.4 Effect of Span of Box Girder Bridge

Table 4.6 shows the influence of span of curved box girder bridge on the impact factors based on different response parameters. It can be observed that the impact factors of all the responses decrease with the increase of span length. However, the variation of the impact factor of torsion, distortion and their corresponding bimoments are comparatively significant, while those of the vertical deflection, bending moment and shear force are almost unaffected for the range of span considered in the present study. Hence, for short span bridges, torsion,

distortion and their bi-moments are more significant and should be adequately considered in the design of curved box-girder bridge.

Table 4.6 Effect of span of box-girder bridge on impact factor

Span of box-girder (L)m			
Response parameter	**30**	**60**	**90**
(M_z)	1.08	1.041	1.025
(Q_y)	1.08	1.06	1.03
(M_x)	1.92	1.781	1.529
(B_I)	2.25	2.01	1.891
(M_d)	1.52	1.218	1.010
(B_{II})	1.79	1.44	1.29
(v)	1.14	1.125	1.103

4.6.7.5 Effect of Radius of Curvature of Box Girder Bridge

Table 4.7 shows the variation of impact factor with the varying radius of curvature of box-girder bridge. The Table shows that the impact factors corresponding to different response parameters of box-girder bridges decrease with the increase of radius of curvature. The parametric study shows very clearly that any attempt on using the existing codal provision on straight bridges to curved box-girder bridge may lead to serious under estimation of dynamic magnification effect on the bridge.

Table 4.7 Effect of radius of box-girder bridge on impact factor

Radius of box-girder (R) m				
Response parameter	**100**	**150**	**250**	∞
(M_z)	1.0907	1.08	1.0785	1.07
(Q_y)	1.092	1.081	1.0712	1.06
(M_x)	2.5061	1.92	1.5176	1.02
(B_I)	3.1636	2.25	1.6766	1.21
(M_d)	2.4597	1.52	1.3734	1.0051
(B_{II})	2.3198	1.79	1.50	1.14
(v)	1.1647	1.14	1.13	1.12

4.6.7.6 Effect of Bridge Deck Surface Condition

The surface characteristics play an important role on the dynamic excitation transmitted on the bridge by the moving vehicle. Five categories of surface characteristics have been considered to examine their effect on the response based on the spectral roughness coefficient and classified as very good, good, average, poor and very poor. The effect of any discrete form of roughness such as bump at the approach, construction joints etc are not taken into account. The impact factor corresponding to different response parameters for different categories of road surface has been presented in Table 4.8. It can be observed that surface roughness has more significant effect on impact factor for the vertical deflection, bending moment and shear force than any other parameters considered in the study. However, the effect of surface

roughness on torsion, distortion and their corresponding bi-moments are comparatively less significant. Thus, surface roughness is one of the predominant factors, which may cause large increase in the response magnitude. Increased deck roughness due to poor maintenance may cause appreciable increase in the impact factor in all span range.

Table 4.8 Effect of random road surface condition on impact factor

Random road surface condition					
Response parameter	**Very good**	**Good**	**Average**	**Poor**	**Very poor**
(M_z)	1.06	1.08	1.33	1.72	2.00
(Q_y)	1.07	1.08	1.26	1.60	1.83
(M_x)	1.91	1.92	1.93	2.00	2.05
(B_I)	2.24	2.25	2.26	2.28	2.29
(M_d)	1.51	1.52	1.53	1.55	1.56
(B_{II})	1.78	1.79	1.80	1.81	1.83
(v)	1.08	1.14	1.48	1.91	2.21

4.6.7.7 Effect of Sprung Mass and Suspension Stiffness of Vehicle

It can be observed from the Table 4.9 that the impact factors of most responses decrease with the increase of sprung mass**.** This is due to increase of static response of the bridge. It also indicates that with the reduction in vehicle mass, as fundamental natural frequency of the vehicle increases, the impact factor also increases. However, the impact factors of most

responses are unaffected with the increase of suspension stiffness of vehicle as can be observed from Table 4.10.

Table 4.9 Effect of sprung mass (m_s) on impact factor

Sprung mass (m_s)					
Response parameter	**0.7** (m_s)	**0.9** (m_s)	**1** (m_s)	**1.1** (m_s)	**1.3** (m_s)
(M_z)	1.1586	1.10	1.08	1.0782	1.06
(Q_y)	1.12	1.09	1.08	1.07	1.05
(M_x)	1.9189	1.92	1.9196	1.92	1.917
(B_I)	2.2453	2.24	2.2469	2.24	2.2411
(M_d)	1.5154	1.52	1.5165	1.52	1.5188
(B_{II})	1.7771	1.78	1.79	1.7858	1.7882
(v)	1.2880	1.19	1.14	1.13	1.1223

Table 4.10 Effect of vehicle suspension stiffness (k_s) on impact factor

Vehicle suspension stiffness (k_s)					
Response parameter	**0.7** (k_s)	**0.9** (k_s)	**1** (k_s)	**1.1** (k_s)	**1.3** (k_s)
(M_z)	1.12	1.11	1.08	1.07	1.06
(Q_y)	1.10	1.09	1.08	1.07	1.06
(M_x)	1.92	1.92	1.92	1.92	1.92
(B_I)	2.24	2.24	2.24	2.24	2.24
(M_d)	1.52	1.52	1.52	1.52	1.52
(B_{II})	1.78	1.78	1.78	1.78	1.78
(v)	1.18	1.17	1.14	1.13	1.12

4.6.7.8 Effect of Acceleration of Vehicle

Table 4.11 shows the effect of vehicular acceleration (constant) on the impact factors. Dynamic responses have been evaluated with the initial velocity of 5m/sec at the entry to the bridge and with different constant values of vehicle forward acceleration. It has been observed that while the impact factors corresponding to bending moment, shear force and vertical deflection have increased, the impact factors corresponding to torsional and distortional moments, their respective bi-moments have reduced significantly with the increase of acceleration of vehicular motion.

Table 4.11 Effect of acceleration of vehicle on impact factor

Acceleration $(a)^{m}/_{\sec^2}$				
Response parameter	**10**	**5**	**2.5**	**0**
(M_z)	1.31	1.25	1.20	1.08
(Q_y)	1.24	1.22	1.19	1.08
(M_x)	1.16	1.22	1.31	1.92
(B_I)	1.27	1.35	1.47	2.25
(M_d)	1.02	1.14	1.20	1.52
(B_{II})	1.13	1.19	1.28	1.79
(v)	1.38	1.31	1.27	1.14

4.6.7.9 Effect of Frequency Ratio

The largest bridge vibrations are known to occur when the natural frequency of the vehicle approaches close to that of the bridge.

The frequency ratio may be define as $f_r = \frac{f_b}{f_v}$ (4.30)

where f_v is the natural frequency of the vehicle corresponding to the heave degree of freedom of the sprung mass and f_b is first natural frequency of bridge corresponding to the transverse flexural mode of vibration.

The parametric studies have been carried out by varying the vehicle mass (both sprung and unsprung) and suspension stiffness, while the bridge parameters have not been altered. Table 4.12 shows that the DAF values corresponding to all the response parameters and it has

been observed that DAF has attained the maximum value when f_r is chosen as unity. The value of f_r for the actual vehicle parameter considered in the study has been calculated as 4.15 and significant values of DAF have been observed even for the frequency ratio of 4.5.

Table 4.12 Effect of frequency ratio (f_r) on impact factor

Frequency ratio $(f_r) = \frac{f_b}{f_v}$									
$f_r = \frac{f_b}{f_v}$	0.5	1.00	1.5	2.0	2.5	3.0	3.5	4.0	4.5
(M_z)	1.345	2.722	2.40	1.341	1.26	1.20	1.1586	1.08	1.06
(Q_y)	1.357	2.523	2.23	1.36	1.25	1.19	1.12	1.08	1.05
(M_x)	1.955	3.12	2.28	1.956	1.942	1.917	1.9189	1.9196	1.917
(B_I)	2.243	3.47	2.52	2.2422	2.241	2.2419	2.2453	2.2469	2.2411
(M_d)	1.541	1.75	1.62	1.555	1.53	1.522	1.5154	1.5165	1.5188
(B_{II})	1.85	2.051	1.95	1.86	1.81	1.79	1.7771	1.79	1.7882
(v)	1.95	2.88	2.53	1.96	1.425	1.323	1.2880	1.14	1.1223

4.7 GENERAL DESIGN GUIDELINE USING IMPACT FACTOR

4.7.1 Existing Codal Provisions

The bridge structures are greatly affected by heavy traffic-induced vibrations. Many bridge engineers treated such problems by considering only impact factors based on length specified in current design codes, even though the vibrations may depend on many other

factors such as vehicle and bridge dynamic characteristics, vehicle speed and deck conditions etc. The bridge codes usually provide for the dynamic effects in straight bridges, though some attention has been paid recently to curved bridge analysis. Mainly, there are two distinct codal provisions debated by many researchers. One is the impact factor-span length relationship and other one is DLA-natural frequency relationship.

In 1927, a joint committee of American Railway Engineering Association (AREA) and the American Association of State and Highway Transportation Officials (AASHTO) recommended for the dynamic effect through an impact factor as the standard specification for Highway bridges. The impact factor was computed based on the span-length only and given as

$$I = \frac{50}{(L + 125)} \tag{4.31}$$

where I is the impact factor and L, the span length in feet.

AASHTO (1993) specification has provided a separate provision for curved composite box-girder bridges and accounts for dynamic effects including centrifugal force produced by the vehicle on curved bridges. But these code provisions not applicable to all curved bridges as the validity of the expressions were restricted by speed, number of spans, ratio of vehicle mass to bridge mass, etc.

In 1979, the first edition of the Ontario Highway Bridge Design code (OHBDC) was published. In this code, the term IF was dropped in favour of DLA as the term 'Impact' indicates a loading due to impact action of wheels. The DLA was given as a function of first flexural frequency of the bridge. The Australian bridge design code (AUSTROADS 1992) also adopted the OHDBC provisions. Bridge designer using these code provisions have to calculate the first flexural frequency of the bridge to determine the DLA.

The current Indian code specifies impact factor in terms of span length only. The Indian Road Congress Code (IRC-6 2000) specified impact factor for concrete and steel bridges for different categories of live load specified as Class AA tracked and wheeled vehicles, Class A and B train of vehicles etc. However, the formulae are valid only for straight bridges. Hence, there are some necessities to evaluate appropriate impact factor for curved bridges.

4.7.2 Suggested Guidelines for Curved Box Girder Bridge

The present study attempts to establish general guidelines for the designer to account for the dynamic effect of live load by using simplified formula which incorporated the effect of predominant parameters influencing dynamic response of bridges. The key parameters that influence curved box girder bridge design are length, radius of curvature and speed of the vehicle. A multiple regression analysis has been carried out to fit a linear relationship for the impact factor.

The multiple linear regressional analyses are conducted using the large volume of data obtained from the parametric studies in the earlier section to derive empirical formulae for impact factors.

A multivariate modal of the data is given by

$$y = a_0 + a_1 x_1 + a_2 x_2 + a_3 x_3 \tag{4.32}$$

Multiple regressions solve for unknown co-efficient a_0, a_1, a_2, a_3 by performing a least squares fit. The set of simultaneous equations are constructed and have been solved by forming the regression matrix (X). The co-efficient have been evaluated using MAT LAB.

The regressional equation for the bending moment about the transverse axis (M_z), shear force (Q_y), torsional moment (M_x), torsional bimoment (B_I), distortional moment (M_d),

distortional bimoment (B_{II}) and vertical deflection (v) are as shown in Table 4.13. The empirical formulae for impact factors have been represented in terms of span length (L), vehicle speed (v) and radius of curvature(R) of a curved box-girder bridge. However, the formulae can be used for the following data range:

$30m \le L \le 90\ m$, $50m \le R \le 300m$ and $10m/\sec \le v \le 30\ m/\sec$

Table 4.13 General design guideline for impact factor

Response parameter	Impact factor
Bending moment about the transverse axis (M_z)	*1.0707 - 0.0012* L + *0.0035 v - 0.0001*R
Shear force (Q_y)	*1.0669 - 0.0010*L + *0.0038 v - 0.0002*R
Torsional moment (M_x)	*1.6061 - 0.0094* L + *0.0793 v - 0.0055*R
Torsional Bi-moment (B_I)	*1.9146 - 0.0102*L + *0.0927 v - 0.0068*R
Distortional moment (M_d)	*1.5975 - 0.00128* L + *0.0561 v - 0.0041*R
Distortional Bi-moment (B_{II})	*1.4529 - 0.0116* L + *0.0722 v - 0.0042*R
Vertical deflection (v)	*1.1356 - 0.0007* L + *0.0029 v - 0.0002*R

A population correlation coefficient (R^2) (Wesolowsky 1976) has been found to test how well the regression curve obtained fits the data obtained from the detailed dynamic analysis. The coefficient R^2 has been found for each of the regression formula of the impact factor. For vertical deflection, the regression equation gives an excellent fit whose R^2 value is close to 1. For bending moment, torsion, torsional bi-moment, distortion and distortion bi-moment and shear force, coefficient R^2 have been observed to lie between 0.82 to 0.94. These shows the regression equations for estimating Impact factor for various stress resultants are reasonably accurate to predict the dynamic effect of the vehicles on the bridge response.

4.8 CLOSURE

The dynamic response of thin-curved box girder bridge due to moving vehicle has been studied considering surface unevenness of the deck as the random input to the vehicle wheels. The effect of centrifugal force has been considered in the formulation of dynamic problem. The impact factors for several response parameters have been presented for the variations of several bridge and vehicle parameters. A computationally less expensive and realistic three noded thin-walled box beam element has been utilized for the modeling of the bridge. The applicability of such an element for the dynamic analysis has been verified by evaluating the modal parameters of a curved box girder model theoretically as well as experimentally. A generalized design guideline for curved thin walled box girder single span bridges has been suggested in terms of impact factor, which includes the effect of bridge span, radius of curvature and speed of vehicle.

CHAPTER 5

FATIGUE LIFE PREDICTION

5.1 INTRODUCTION

Structural fatigue is the process of accumulation of damage due to application of time varying stress. It can be expected to occur whenever a structure is subjected to time varying loads and in many situations may govern the design. Structures when subjected to cyclic, repeated or fluctuating load may fail in fatigue at a stress level much lower than that required to cause failure under static condition. Fatigue failure is viewed as the accumulation of localized permanent damage occurring in a structure subjected to repeated actions of time dependent stresses and strains. Each time a load cycle is applied, an incremental amount of damage occurs. This damage is cumulative in nature and accumulation continues till the failure occurs. If fatigue cracks are detected early, then repair may be possible. If not detected and properly repaired, the results may be disastrous failures. The bridges are one of the examples where similar situation may arise. In the present chapter, the procedure for the evaluation of fatigue life of bridges from vehicle induced stress history has been described. The linear damage accumulation theory has been adopted. Both time domain and frequency domain analysis have been presented. Time domain analysis employed cycle counting method where frequency domain method required spectral moments to be determined from the power spectral density of stress. The derivations of the analytical expressions for fatigue life using more than one spectral moment and only one spectral moment have been given in detail in this chapter. The underlying assumptions of spectral methods have been stated. The

numerical results have been obtained using both time domain and frequency domain approaches discussed in this chapter and the influence of some of key parameters affecting fatigue life of the curved box girder bridges have been studied.

5.2 FATIGUE STRENGTH TEST

Both the material properties and the dynamic load process are important for fatigue evaluation. The simplest of all fatigue load processes is periodic load, which is defined as constant amplitude load cycle. Empirical data from such constant amplitude tests form the basis for the prediction of fatigue life under complicated time history. Constant fatigue behavior is determined experimentally from tests in which a load or deflection is controlled and varied in simple periodic manner until failure. In this situation, fatigue failure is usually found to depend significantly on the stress range, which is defined as the difference between maximum and minimum stress. An alternative formulation uses the mean stress value, defined as the average of the minimum and maximum stress. The stress range effect is usually found to be considerably more important than mean stress. A typical stress history for the constant amplitude loading is shown in Fig.5.1

The result of a constant amplitude fatigue test is often described by stress range S_r, and number of cycles to failure denoted by N_f. A typical experimental investigation of constant amplitude fatigue for a specimen of given configuration and material involves a large number of tests. The test results are usually presented in the form of S-N curve with the stress range on the ordinate and the number of cycles on the abscissa as shown in Fig.5.2.

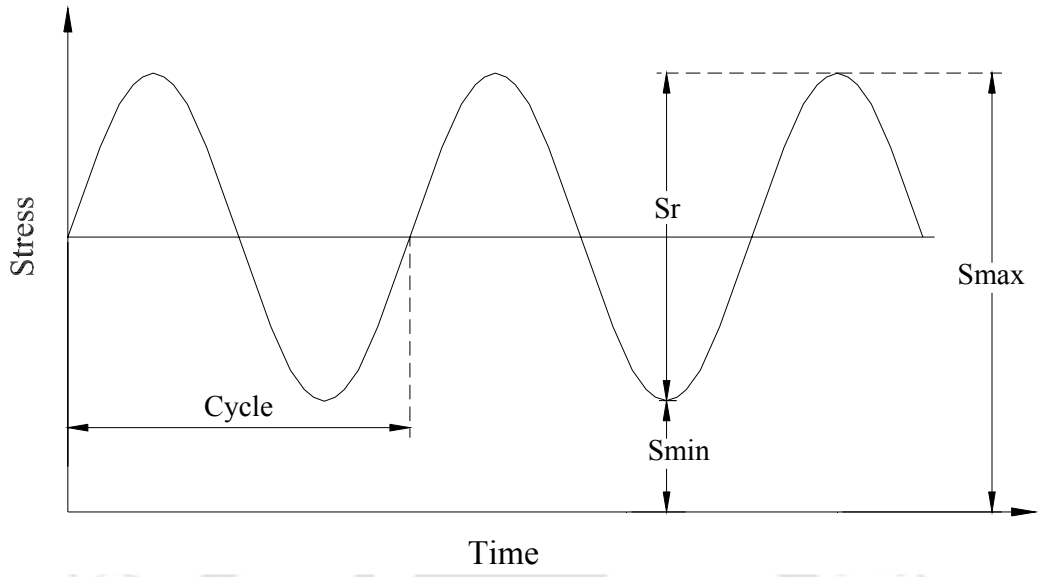

Fig.5.1 A typical stress history for the constant amplitude loading

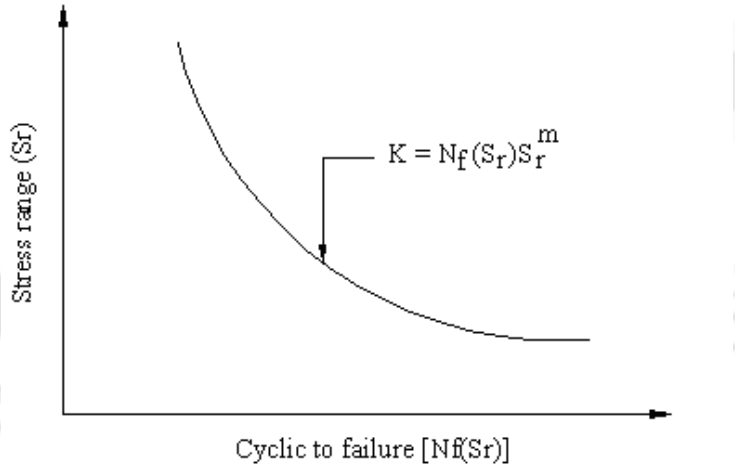

Fig. 5.2 A typical *S-N* Curve for constant amplitude test results

The experimental data usually show that a large portion of S-N curve can be fitted to an equation of the form (Lutes and Sarkani 1997)

$$N_f(S_r) = KS_r^{-m} \tag{5.1}$$

in which K and m are the positive material constants whose values depend on both materials and geometry of the specimen. The constants K and m for different metals and their alloys have been compiled by American Society of Metals **(**1986**)** which are readily applicable for the fatigue analysis of metallic specimen. A linear equation can be used to predict the value of S_r for any particular value of N_f and vice versa when S-N curve is plotted in a log-log scales. The following equation represents S-N curve on the log-log plot

$$y = c + \alpha x \tag{5.2}$$

where $y = \log(N_f);\ c = \log(K);\ \alpha = -m;\ x = \log(S_r)$

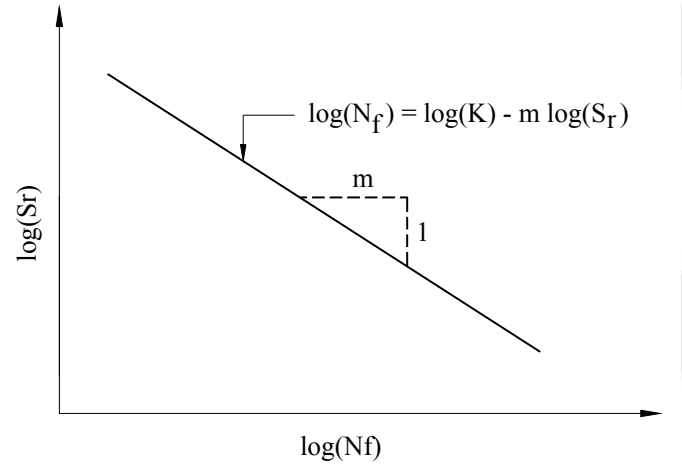

Fig.5.3 S-N Curve on log-log plot.

Sometimes, it becomes necessary to use mean stress instead of stress range as stated earlier. Simple empirical formulae are available in literature (Lutes and Sarkani 1997). The basis of such formulae were the equivalent stress range (S_e) with zero mean stress which experimentally correlates with stress range S_r having mean stress x_m in constant amplitude

fatigue loading. Two such formulae known as "Goodman correction" and "Gerber correction" are in use (Lutes and Sarkani 1997).

The Goodman correction is given below

$$\frac{S_r}{S_e}+\frac{x_m}{x_u}=1 \tag{5.3}$$

in which x_u denotes the ultimate stress capacity of the material, S_r denotes stress range having mean stress x_m, S_e is the equivalent stress range for zero mean process.

The Gerber correction is expressed in the following form.

$$\frac{S_r}{S_e}+\left(\frac{x_m}{x_u}\right)^2=1 \tag{5.4}$$

5.3 ACCUMULATED DAMAGE

The term fatigue is used to describe accumulation of damage, which is measured by damage function $D(t)$. This has been used to describe the progress towards failure whether the progress is observable or not observable. The damage function $D(t)$ is presumed to start at zero value for new structure and is normalized to be unity when failure occurs. Furthermore it is a non decreasing function of time. If some function f(t) goes monotonically from zero (at $t=0$) to 1 (at $t=T$, T is the failure time), then f(t) is one possible choice of damage function *D(t)*.

Having known the $S-N$ curve relationship, a linear damage assumption can be used to evaluate *D(t)* . Let ΔD_j be the incremental damage during the cycle j and $N(t)$ denote the number of applied cycles of load up to time t, such that it can be written as,

$$D(t) = \sum_{j=1}^{N(t)} \Delta D_j \tag{5.5}$$

Further, let T is the failure time, so that $N_f = N(T)$ is the number of cycles to failure. This gives $D(t) = 1$, so that

$$1 = \sum_{j=1}^{N(T)} \Delta D_j = \sum_{j=1}^{N_f} \Delta D_j \tag{5.6}$$

For periodic constant amplitude loading with the stress range S_r, the upper limit of the summation is $N_f(S_r)$. If we can assume that the ΔD_j values are all the same throughout the test, the damage per cycle is given by

$$\Delta D_j = \frac{1}{N_f(S_r)} = K^{-1}\ \mathrm{S_r^m} \tag{5.7}$$

5.4 DAMAGE ACCUMULATION HYPOTHESIS

In real situation, however, a vehicle passing over a bridge induces dynamic load as a result of the vehicle oscillation caused by pavement roughness. These load time histories are much more complicated compared to periodic loadings used in laboratory fatigue testing because of the random nature of the pavement roughness. The load-time history is generally dominated by one large cycle equal to the peak live load produced by the vehicle. Dynamic effects generate additional small cycles superimposed on the large cycle. In order to assess the fatigue damage caused by the passage of vehicle, it is necessary to account for both the large dominant cycle and the small-superimposed cycles. The basic problem of fatigue analysis is to use appropriately the S-N curve data from the periodic tests to predict fatigue life of an element or assembly, which is subjected to a service load having a complicated time history. In case of random load history, the Eq. (5.1) cannot be used without additional

information. The effect of variable-amplitude loading (i.e., random load or irregular) on fatigue performance is normally accounted for with cumulative damage rules. Typically, these rules attempt to relate fatigue behavior under a complex loading history to the known behavior under constant amplitude loading. The linear damage accumulation hypothesis, called "Palmgren-Miner" hypothesis (Lutes and Sarkani 1997) has been used in the present study. The cumulative damage accumulation under variable-amplitude loading is given by

$$D(t) = \sum_{j=1}^{n_b} \Delta D_j = \sum_{j=1}^{n_b} \frac{n_j}{N_j} \qquad \left(n_j \le N_j\right) \tag{5.8}$$

in which ΔD_j is the incremental damage, n_j is the number of stress cycles at stress range level Sr_j and N_j is the number of cycles at constant stress range level Sr_j from (*S-N* curve) to cause failure, n_b is the number of stress range blocks in the histogram. The fatigue life T is then calculated as $T=1/D(t)$. Using S-N curve relation in Eq.(5.8), the damage function at t=T can be written as

$$D(t) = \sum_{j=1}^{N(T)} \frac{n_t}{KS_r^{-m}} = K^{-1} \sum n_t S_r^m \tag{5.9}$$

5. 5 APPROACH FOR FATIGUE LIFE PREDICATION

Fatigue predictions can follow several approaches, differing in the level of stress and strain analysis used. Moving vehicle induces vibrations in curved box-girder bridge. The resulting fluctuating stresses lead to damage accumulation in the components of the bridge with the progress of time. In the present work, fatigue damage calculations for the thin walled curved box girder bridge has been performed based on vehicle induced stress history and fatigue strength parameters obtained from the standards. Two approaches have been employed, one in the time domain analysis using simulated response time history and other

in the frequency domain analysis using power spectral density of stress. In the first approach, cycle counting procedures has been used to identify cycle range and thereafter to develop the stress range frequency histogram taking into consideration of the annual traffic volume. The linear damage accumulation theory is applied to calculate fatigue life by finding number of cycles/year corresponding to specific stress range and number of cycles sustainable at that stress range to cause fatigue failure.

The second approach is based on spectral moment characteristics which assume Rayleigh's probability density function for the peak stresses. Improved version of spectral method using only single spectral moment has also been used. The spectral method is based on narrow band assumption of Gaussian process where as time Domain method using cycle counting does not rely on such assumption. The spectral method requires less computational time but its applicability will depend on the nature of the power spectral density function.

In the present investigation, the frequency domain approach for determining fatigue life of curved thin walled box girder bridge, analytical expressions have been used involving more than one or only one spectral moment which are to be obtained from the power spectral density function of the stresses. The step by step procedure for obtaining the expected damage rate in spectral methods has been given. The improvement of this method using single moment suggested by Lutes and Sarkani (1997) has also been incorporated and implemented for the curved thin walled section box girder bridge.

5.5.1 Cycle Counting Method

The cycle counting has been regarded as a procedure to transform a loading time history into a set of cycles. Various statistical counting methods for the classification of random time histories are available in the literature. Fryba (1996) discussed different counting methods for

the classification of random time history. In the present study, Rain-flow Counting method (RFCM) has been used in the time domain cycle counting method to identify cycle range. This method establishes one to one correspondence between local maximum and minima of the stress time history. It is observed that in RFCM, small cycles are interruptions of the larger cycles. In this way, the method identifies both slowly varying large amplitude cycles and more rapid small reversals on the top or bottom of these cycles. The sequence of operations followed in RFCM method has been illustrated in Appendix E.

5.5.1.1 Rain-flow Counting Method

The most frequently used method is the Rain-flow cycle counting method which characterizes the irreversible stress components of the stress-strain diagram that are decisive for the fatigue of structure. The rain-flow method of cycle counting is widely used in practice. The method was developed by Dowling (1972).Rain-flow Method is generally regarded as the method leading to better prediction to fatigue life. It can identify events in a complex stress sequence, which is compatible with constant-amplitude fatigue data. Furthermore, it identifies stress range cycles associated with low frequency components and the mean stress associated with each cycle. The basic idea behind any stress cycle identification scheme is to consider the segment of a stress time history $\sigma_r(x,t)$ between any two subsequent local extreme (from peak to a valley or from valley to a peak) to be a half cycle. The evaluation of random processes with reference to the fatigue of structures is based on the stress-time history. The fundamental assumption of the rain-flow counting method is that fatigue damage due to small induced stress cycles may be added to the fatigue damage due to large stress cycles. Referring Fig.5.4, it can be seen that if the cycle $1-4$ is

interrupted by a small cycle $2-3-2'$, the coordinate of the point $2'$ is very near to the point 2 and the material acts as if no interruption by an inserted cycle has taken place. Moreover, one complete cycle $2-3-2'$ has remained at disposal.

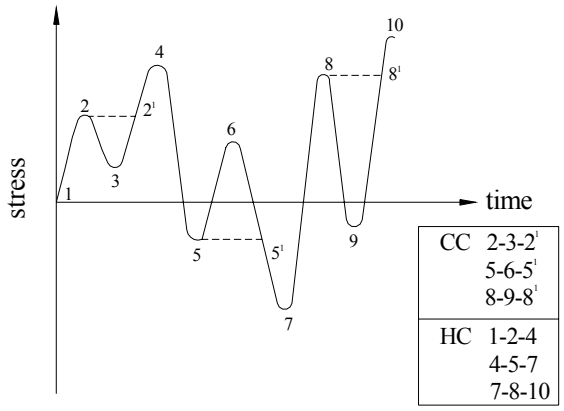

Fig.5.4 Stress-time history (CC-Complete Cycles, HC-Half Cycles)

5.5.1.2 Stress Counting Rule

The name "Rain-flow" method has derived it name from an analogy of water flowing along a pagoda-shaped roof. In order to obtain such a pagoda shaped roof, the stress time history is rotated by 90^0 (time axis downward) as shown in Fig.5.5. The following rules for the stress range counting are applied (one complete cycle = two stress ranges);

(1) One stress range is counted, when water flows from the initial stress to the maximum, from which it flows downwards along next roof slope to the next maximum.

The flowing water is stopped, when

(a) The stress minimum is lower than the initial stress.

(b) It meets some former rain-flow, or when,

(c) It reaches the end of the strain record.

(2) The stress range is counted, when the water flows (from the highest maximum attained during the preceding range) downwards along the roof to the nearest minimum, from where it flows down to the nearest roof slope and to the next minimum. It stops only when

(a) The stress maximum is higher than the initial maximum.

(b) It meets some former rain-flow.

(c) It reaches the end of the record.

(3) In this way, stress ranges are counted by successive application of rules (1) and (2).

(4) The roof parts, which have not been covered by the rain-flow so far, are counted as,

(a) The flow beginning in the maximum and flowing down across the following minima as described in rule (2) or

(b) The flow beginning in the minimum and flowing down across the following maxima as described in rule (1). In either case the flow stops, when

(c) It meets an earlier stress which is more extreme than the initial point of the flow, or when

(d) It meets an earlier flow.

The rain-flow counting method evaluates the stress-time history in the same way as the material reacts to a random loading process. It counts both the large amplitudes (half-cycles) and, separately, small inserted stress cycles (complete cycles).

The “Rain flow Counting” method faithfully reflects the behavior of the material and characterizes its hysteresis. For this reason it is recommended for the evaluation of random stress-time histories with reference to fatigue of materials. Every time interval of stress is counted only once and the same result is obtained, if the evaluation proceeded in the opposite direction

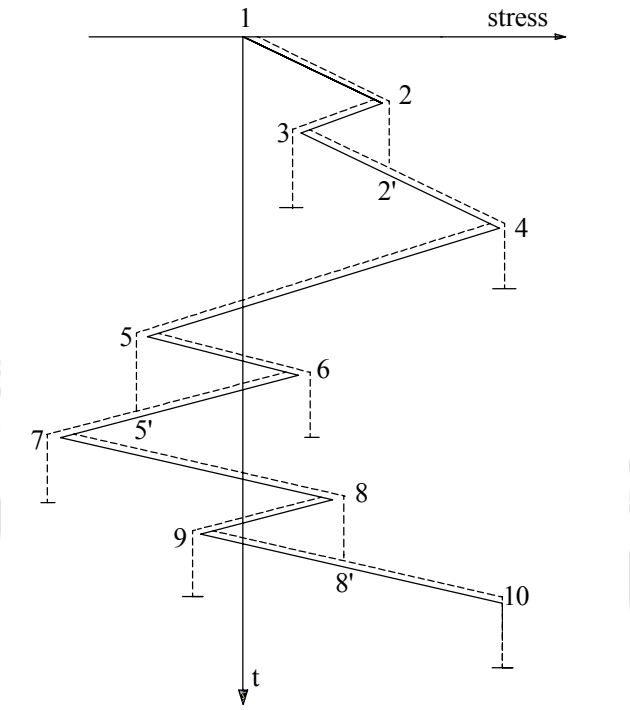

Fig.5.5 Rotated Stress Time history

5.5.1.3 Counting Algorithm

The algorithm for "Rain-flow Counting" is described below with help of schematic diagram of stress cycle in Fig.5.6.

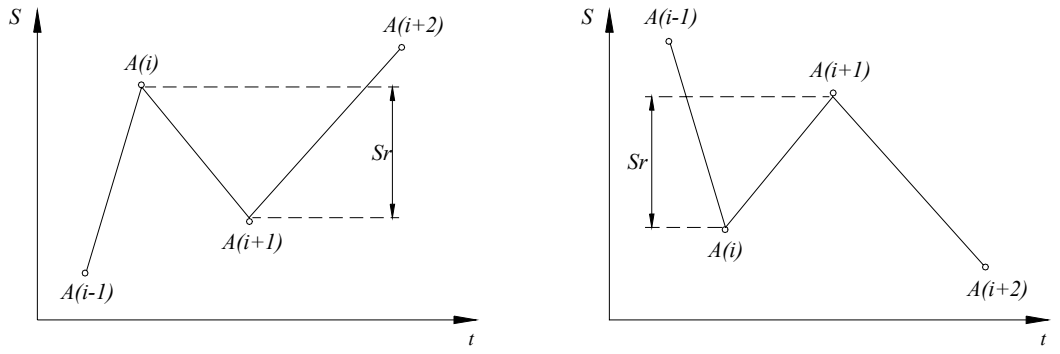

(a) Rising part of the time history. (b) Decaying part of the time history

Fig. 5.6 Two basic cases of complete cycle counting in the Rain-flow method

(1) The local peaks $A(0)$, $A(1)$, …, $A(k)$ are read from the stress time history and digitized.

(2) The set of local peaks obtained is decomposed into half-cycles and cycles.

(3) The condition for a cycle counting is defined by the relations

$$A(i-1) \le A(i+1) < A(i) \le A(i+2) \tag{5.10}$$

or

$$A(i-1) \ge A(i+1) > A(i) \ge A(i+2) \tag{5.11}$$

(3a) The computation proceeds from the lowest i=1 to the highest i=k-2. If the conditions (4) or (5) have been satisfied then, one cycle= two half cycles with the stress range

$$S_r = |A(i) - A(i+1)| \tag{5.12}$$

(3b) The peaks $A(i)$ and $A(i+1)$ are eliminated from the sequence of extremes and sequence is renumbered.

(3c) The procedure according to (3a) and (3b) are repeated until at least one cycle has remained from the remaining sequence.

(4) If the decomposition into cycle has been completed, the stress ranges (i.e. absolute values of differences of adjoining extremes) in the remaining sequence are called half-cycles.

(5) The cycles and the remaining half-cycles of equal magnitude are added in the course of the calculations; the result is a Table of stress range frequencies, usually represented in the form of a frequency histogram and called stress range spectrum. The cycles counted for each time history is extrapolated by the ratio of the annual and measured traffic loads yielding the total number of stress cycles per year for a bridge element.

5.5.2 Spectral Method

Spectral method of estimating fatigue life requires the evaluation of power spectral density of stress. In this section, the method to obtain PSD of stress at particular location of bridge has been discussed. The PSD of stress has been used to find spectral moments. With the help of spectral moment of various order (integer/ non integer), the fatigue damage for the bridge have been obtained based on the assumption of Gaussian Narrow Band process. Out of different spectral method, two methods have been applied to the problem under investigation and compared with time domain cycle counting method.

Let for a linear time invariant system like the one being presented here, the finite Fourier transform of the force $\{F(\omega)\}$ and response $\{X(\omega)\}$ are related by

$$\{X(\omega)\} = [H(\omega)]\{F(\omega)\} \tag{5.13}$$

where $[H(\omega)]$ is the complex frequency response function of the system, which is given by

$$[H(\omega)] = \left[[K] - \omega^2[M] + i\omega[C]\right]^{-1} \tag{5.14}$$

Transposing the complex conjugate of the Eq. (5.13) and then post multiplying the Eq. (5.13) by the transposed equation, the following expression is obtained

$$\{X(\omega)\}\{X^*(\omega)\}^T = [H(\omega)]\{F(\omega)\}\{F^*(\omega)\}^T[H^*(\omega)]^T \tag{5.15}$$

where asterisk (*) denotes complex conjugate.

Taking expectation on both sides of Eq. (5.15)

$$E\left[\{X(\omega)\}\{X^*(\omega)\}^T\right]^T = [H(\omega)]E\left[\{F(\omega)\}\{F^*(\omega)\}^T\right]^T[H^*(\omega)]^T \tag{5.16}$$

Using the definition of PSD, the Eq. (5.16) can be written as

$$[S_{XX}(\omega)] = E\left[\{X(\omega)\}\{X^*(\omega)\}\right] = [H(\omega)]^T[S_{FF}(\omega)][H^*(\omega)] \tag{5.17}$$

in which $\left[S_{XX}(\omega)\right]$ is the cross spectral density matrix of the response and $\left[S_{FF}(\omega)\right]$ is the cross spectral density matrix of excitation.

In frequency domain, fatigue of structures is estimated based on the statistical properties. The stress PSD functions are usually obtained after solving the equations of motions in frequency domain. To analyze the structural behavior with respect to fatigue, the response must be expressed in terms of stresses as follows

$$S(x,t) = \bar{S}(x) + s(x,t) \tag{5.18}$$

where $\bar{S}$ is the mean stress, s is the zero mean fluctuating stress at location x. Both S and s are Gaussian random stationary processes. The mean static stress $\bar{S}$ can be easily derived from the application of the mean static force. Furthermore, assuming that the ratio between the fluctuating and the mean value of stress is equal to the ratio between the fluctuating and

the mean value of displacement (Repetto and Solari 2001), the power spectral density of the stress at location x_1 can be derived as

$$S_\sigma(x_1,\omega)=\left[\frac{\bar{S}^2(z)}{\bar{X}^2(z)}\right]S_{XX}(x_1,\omega) \tag{5.19}$$

where

$$\{\bar{X}\}=[K]^{-1}\{\bar{F}\} \tag{5.20}$$

$\{\bar{F}\}$ is nodal load vector for mean force and $S_\sigma(x_1,\omega)$ is power spectral density of stress at location x_1 as function of circular frequency.

5.5.2.1 Rayleighs Approximation

In Rayleigh approximation method, the stress ranges are assumed to have Rayleigh distribution. In particular, each stress range is taken to be twice the random amplitude of the process, and for a Gaussian process, this amplitude has a Rayleigh's probability distribution. As an example, Let the random stress X(t) be a narrow-band Gaussian stationary random process with a zero mean. The probability density function of peak stress X(t) is Rayleigh distributed (Lutes and Sarkani 1997) which can be written as

$$p_X(\xi)=\frac{\xi}{\sigma_x^2}\exp\left(-\frac{\xi^2}{2\sigma_x^2}\right)\quad 0\le\xi<\infty \tag{5.21}$$

where σ_x is the standard deviation of process.

Calculation of the m^{th} moment of S_r in this situation is particularly simple if X (t) is also Gaussian, since the stress range (twice the stress amplitude) then follows the Rayleigh distribution. It is assumed that number of cycles of stress in actual structure produced by

moving vehicles over a time is independent of the magnitude of stress range in constant amplitude test.

The expected damage can be written using Eq. (5.7)

$$E[\Delta D] = K^{-1} \; E\left[S_r^m\right] = K^{-1} \; E\left[(2u)^m\right] \tag{5.22}$$

in which u is the peak stress assumed as $\frac{1}{2} S_r$

The Eq. (5.22) can be further expressed using Eq. (5.21)

$$E[\Delta D] = K^{-1} 2^m \int_0^\infty u^m \frac{u}{\sigma_u^2} e^{-\frac{u^2}{2\sigma_u^2}} du \tag{5.23}$$

$$= K^{-1} 2^m \left(\sigma_u\right)^{-2} \int_0^\infty u^{m+1} e^{-\frac{u^2}{2\sigma_u^2}} du = K^{-1} 2^m \left(\sigma_u\right)^{-2} I_R \tag{5.24}$$

where $$I_R = \int_0^\infty u^{m+1} e^{-\frac{u^2}{2\sigma_u^2}} du \tag{5.25}$$

To evaluate the integral in Eq.(5.25) let us substitute

$$t = \frac{u^2}{2\sigma_u^2} \quad \text{so that} \quad udu = \sigma_u^2 dt$$

Then $$I_R = \int_0^\infty \frac{u^m}{\sigma_u^2} e^{-\frac{u^2}{2\sigma_u^2}} udu = \int_0^\infty \frac{\left(u^2\right)^{\frac{m}{2}}}{\sigma_u^2} e^{-\frac{u^2}{2\sigma_u^2}} udu \tag{5.26}$$

$$= \int_0^\infty \frac{\left(2\sigma_u^2 t\right)^{\frac{m}{2}}}{\sigma_u^2} e^{-t} \sigma_u^2 dt = (2)^{\frac{m}{2}} \sigma_u^m \int_0^\infty t^{\frac{m}{2}} e^{-t} dt \tag{5.27}$$

Using Gamma function the integral can written as

$$I_R = (2)^{\frac{m}{2}} \sigma_u^m \Gamma\left(1+\frac{m}{2}\right) \tag{5.28}$$

The Gamma function $\Gamma(\lambda+1)$ is defined as $\int_0^\infty e^{-t} t^\lambda dt \ \ (\lambda > -1)$ (Potter and Goldberg 1991).

Thus $E(\Delta D) = K^{-1} (2)^{\frac{3m}{2}} \sigma_u^m \Gamma\left(1+\frac{m}{2}\right)$ (5.29)

Let the k[th] moment of the spectral density is defined as (Lutes and Sarkani 1997)

$$\lambda_k = \int_0^\infty \omega^k S_\sigma(x_1, \omega)\, d\omega \tag{5.30}$$

where $S_\sigma(x_1, \omega)$ is the spectral density of stress at location x_1 as function of circular frequency ω.

For k=0, $\lambda_0 = \int_0^\infty \omega^0 S_\sigma(x_1, \omega) d\omega = \int_0^\infty S_\sigma(x_1, \omega) d\omega = \sigma_x^2$ (5.31)

For k=2, $\lambda_2 = \int_0^\infty \omega^2 S_\sigma(x_1, \omega) d\omega = \dot{\sigma}_x^2$ (5.32)

For k=4, $\lambda_4 = \int_0^\infty \omega^4 S_\sigma(x_1, \omega) d\omega = \ddot{\sigma}_x^2$ (5.33)

Using Eq. (5.31) in Eq. (5.29), one obtains

$$E(\Delta D) = K^{-1} (2)^{\frac{3m}{2}} \lambda_0^{\frac{m}{2}} \Gamma\left(1+\frac{m}{2}\right) \tag{5.34}$$

The simplest form for the appropriate rate of cycle occurrence for this zero mean narrow band process is given by the rate of up crossing of the mean value.

Probability density of crossing the level "α" is given by (Nigam 1983)

$$N^{+}(\alpha) = N^{-}(\alpha) = \frac{1}{2\pi}\frac{\dot{\sigma}_x}{\sigma_x}\exp\left[\frac{1}{2}\left(\frac{\alpha^2}{\sigma_x^2}\right)\right] \tag{5.35}$$

where α-crossing level. Putting $\alpha = 0$, we get expected rate of zero crossings with positive and negative slope respectively

$$N^{+}(0) = N^{-}(0) = \frac{1}{2\pi}\frac{\dot{\sigma}_x}{\sigma_x} = \frac{1}{2\pi}\sqrt{\frac{\lambda_2}{\lambda_0}} \tag{5.36}$$

$$E\left[D(t)\right] = \frac{1}{2\pi}\frac{\dot{\sigma}_x}{\sigma_x}.E\left[\frac{1}{N_f}\right] = \frac{1}{2\pi}\left(\frac{\dot{\sigma}_x}{\sigma_x}\right).E\left[\Delta D\right] \tag{5.37}$$

Using Eq. (5.34) and Eq. (5.36) in Eq. (5.37) and assuming that S-N curve for the materials are defined, the expected fatigue damage accumulation rate can be expressed as

$$E\left[D(t)\right]_{RAY} = \frac{1}{2\pi}\sqrt{\frac{\lambda_2}{\lambda_0}}.E\left[\Delta D\right] = \frac{1}{2\pi}\sqrt{\frac{\lambda_2}{\lambda_0}}\;K^{-1}(2)^{\frac{3m}{2}}\lambda_0^{\frac{m}{2}}\;\Gamma\left(1+\frac{m}{2}\right) \tag{5.38}$$

Simplifying the above expression, one can write

$$E\left[D(t)_{t=T}\right]_{RAY} = \frac{K^{-1}2^{3m/2}\lambda_0^{(m-1)/2}\lambda_2^{1/2}\Gamma\left(1+\frac{m}{2}\right)}{2\pi} \tag{5.39}$$

where subscript "RAY" is used to indicate the expression based on Rayleigh's probability density function.

5.5.2.2 Single Moment Approximation

The spectral method based on Rayleigh's assumption developed in the proceeding section involves two spectral moments to be obtained from PSD function. To reduce computational effort in Rayleigh's method, Lutes and Sarkani (1997) established that only a single moment

is sufficient to yield reasonably accurate results. The method was, however, applied to different PSD of unimodal are bimodal characters taken without reference to the particular structural model and actual loading. Thus, this method has been tested in the present investigation on a curved box-girder bridge using stress spectra obtained after solving a complete bridge-vehicle interaction problem with random loading. As mentioned, the single moment method predicts the fatigue life based on only one moment of the power spectral density curve. The single moment method is found to be simpler than most spectral methods, and all spectral methods are much simpler than any method involving simulation of stress time histories. Two corrections have been suggested to Rayleigh's approximate method (Lutes and Sarkani 1997).

1. Lutes *et al*. (1984) proposed the correction as function of a band width parameter given by:

$$\alpha_b = \frac{\lambda_b}{\sqrt{\lambda_0 \lambda_{2b}}} \tag{5.40}$$

where $\lambda_b = \int_0^\infty \omega^b S(\omega)\, d\omega$ (5.41)

where α_b is the bandwidth parameters. The parameter "b" can be related empirically to m.

2. Ortiz and Chen (1987) suggested correction to a Rayleigh expression, using the five spectral moment $\lambda_0, \lambda_2, \lambda_4, \lambda_b$ and λ_{b+2} .

The damage function given by them is $\left(\frac{\beta_b}{\alpha_2}\right)^m$ times Rayleighs damage function. Thus one can write

$$E\left[D(t)\right]_{OC} = \frac{\beta_b^m}{\alpha_2} E\left[D(t)\right]_{RAY} \tag{5.42}$$

The subscript "OC" in the above expression indicate the corrected expression proposed by Ortiz and Chen. The factor β_b is given by

$$\beta_b = \left(\frac{\lambda_2 \lambda_b}{\lambda_0 \lambda_{2+b}} \right)^{\frac{1}{2}} \tag{5.43}$$

It was found that parameter b is related to S-N curve parameter as

$$b = \frac{2}{m} \tag{5.44}$$

Eq. (5.42) can also be written in expanded form.

$$E\left[D(t)\right]_{OC} = \frac{K^{-1} 2^{3m/2}}{2\pi} \Gamma\left(1+\frac{m}{2}\right) \lambda_2^{\frac{m-1}{2}} \lambda_4^{1/2} \left(\frac{\lambda_{2/m}}{\lambda_{2+2/m}} \right)^{\frac{m}{2}} \tag{5.45}$$

Since λ_0 term in the correction factor cancels out with the λ_0 term in the Rayleigh approximate expression, the damage rate in fact depends on the four spectral moments $\lambda_2, \lambda_4, \lambda_{2/m}$ and $\lambda_{2+2/m}$.

Accuracy in fatigue life prediction is expected to improve since the method involves four spectral moments instead of two in Rayleigh's method. However, computations are lengthy as the process requires four times integration of PSD curves to obtain integer/ non integer spectral moments.

A new approximate method introduced by Lutes and Sarkani (1997) involves only a single spectral moment, which considerably reduces the computational time. The method, found to yield results closer to rain-flow counting method as reported by Lutes and Sarkani (1997). In the present work, single moment method has been applied to estimate fatigue life of the

curved box girder bridge. The expression given by Lutes and Sarkani (1997) was based on the assumption of very narrow band random process. The single moment method has been explained in detail as follows.

Let the autospectral density of very narrow band random process concentrated at frequencies $\pm\ \omega_0$ be represented by

$$S_{XX}(\omega) = \frac{\sigma_X^2}{2}\{\delta(\omega+\omega_0)+\delta(\omega-\omega_0)\} \tag{5.46}$$

where σ_X is the standard deviation, "δ" is the Direct delta function, having the following properties.

$$\delta(x) = 0 \text{ for } x \neq 0 \text{ and } \delta(0) \to \infty \tag{5.47}$$

and $\int_{-\infty}^{+\infty} \delta(x-x_0)\, f(x)\ \mathrm{dx} = f(x_0)$

Let us assume $E[D(t)] = \mathrm{C}^{-1}\ (\lambda_a)^{-b}$ (5.48)

where a, b and c are constants which depends on the specimen characteristics but not on the power spectral density curve.

The spectral moment of order “a” is defined for the narrow band process (Lutes and Sarkani 1997).

$$\lambda_a = \int_{-\infty}^{\infty} |\omega|^a\, S_{XX}(x_1,\omega)\, \mathrm{d}\omega \tag{5.49}$$

where $S_{XX}(x_1,\omega)$ is the PSD of stress at location x_1 in the structure.

On the substitution of Eq. (5.46) in Eq. (5.49) and using the property of Direct delta function, a^{th} moment of PSD of stress at location x_1 may be obtained as

$$\lambda_a = \sigma_x^2\ \omega_0^a \tag{5.50}$$

Since $\lambda_0 = \sigma_x^2$, one can write $\omega_0 = \left(\frac{\lambda_a}{\lambda_0} \right)^{\frac{1}{a}}$ (5.51)

Hence expected damage function is Eq. (5.48) can be expressed as

$$E\left[D(t)\right] = \mathrm{C}^{-1} \left(\sigma_X^2 \ \omega_0^{\mathrm{a}}\right)^{-b} = \mathrm{C}^{-1} \ \sigma_X^{-2b} \ \omega_0^{-\mathrm{ab}} \tag{5.52}$$

From, Rayleigh's approximation expression one has

$$E\left[D(t)\right] = \frac{1}{2\pi} \sqrt{\frac{\lambda_2}{\lambda_0}} \ E\left[\Delta D\right] \tag{5.53}$$

Since $\lambda_2 = \sigma_x^2 \ \omega_0^2$ one can write $\sqrt{\frac{\lambda_2}{\lambda_0}} = \omega_0 = \left(\frac{\lambda_a}{\lambda_0} \right)^{-b}$ (5.54)

The Eq. (5.53) becomes

$$E\left[D(t)\right] = \frac{\omega_0}{2\pi} \ E\left[\Delta D\right] = \frac{\omega_0}{2\pi} \ K^{-1} (2)^{\frac{3\mathrm{m}}{2}} \ \lambda_0^{\frac{m}{2}} \ \Gamma\left(1 + \frac{m}{2}\right) \tag{5.55}$$

$$= \frac{\omega_0}{2\pi} \ K^{-1} (2)^{\frac{3\mathrm{m}}{2}} \ \sigma_x^{\mathrm{m}} \ \Gamma\left(1 + \frac{m}{2}\right) \tag{5.56}$$

To make an agreement of single moment method with Rayleigh's method, Eq. (5.52) and Eq. (5.56) may be compared to conclude that single moment method agrees fully when

$$a = \frac{2}{m}, \quad b = -\frac{m}{2} \quad \text{and} \quad \frac{1}{c} = \frac{(2)^{3m/2} \ \Gamma\left(1 + \frac{m}{2}\right)}{2\pi K} \tag{5.57}$$

Thus substituting a, b and c from Eq. (5.57) in Eq. (5.52) and utilizating Eq. (5.54), one yields expression for the expected damage rate as

$$E\left[D(t)_{t=T}\right]_{SM} = \frac{K^{-1} 2^{3m/2} \lambda_{2/m}^{m/2} \ \Gamma\left(1 + \frac{m}{2}\right)}{2\pi} \tag{5.58}$$

The subscript "SM" refers to single moment method. The above expression, therefore contains only one spectral moment of order 2/m. It is known that single moment method yields better results with less computational effort. The accuracy of this method has been termed in the present work in order to obtain fatigue life of curved box girder bridge.

5.6 RESULTS AND DISCUSSION

A simply supported single cell thin walled section box girder bridge (Fig.5.7) as considered by Heins and Oleinik (1976) has been chosen in the present study to obtain the dynamic response due to moving vehicles from which the fatigue life has been estimated. The bridge considered is a steel bridge. The span of the simply supported bridge is 30 m with a radius of curvature of 150 m and the bridge has diaphragms at supports. The vehicle model is a heave-pitch-roll 3D model. All the parameters relevant to the vehicle are taken from the work of Henchi *et al.* (1998) and have been presented in Fig 5.7. The mass density, modulus of elasticity and Poisson's ratio of the material are taken as 7840 kg/m^3, 2×10 ^{11} N/m^2 and 0.3 respectively. The numerical simulation has been carried out to find the dynamic response of the bridge. The details of the simulation procedure has been described in Chapter 4.

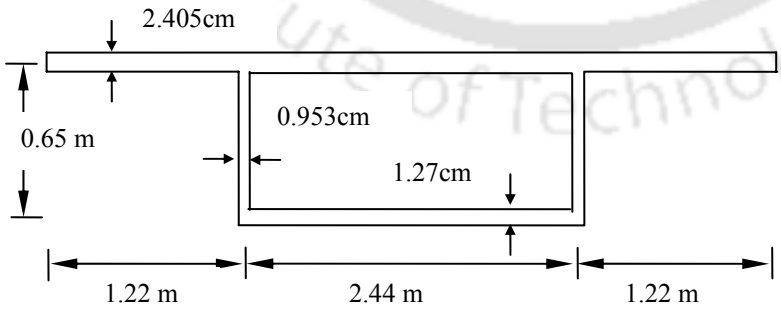

E = 2 e+11 N/m^2
ν = 0.3
G = 7.6923 e+10 N/m^2
ρ = 7840 kg/m^3
I_z = 0.011203 m^4
J = 2.342e-2 m^4
J_I = 9.791e-4 m^6
J_{II} = 2.033e-3 m^6
J_d = 1.485e-6 m^2
μ_t = 0.205
A = 0.160391 m^2

Fig .5.7 Geometry and properties of steel box girder bridge

5.6.1 Time History of Stress

The moving vehicle induces flexural, torsional warping and distortional warping stresses in thin-walled curved box girder bridge. In the present analysis, for the chosen parameters of the bridge, the magnitudes of flexural stresses dominate over other stresses. Hence for evaluating fatigue life, flexural stresses at mid span have been considered only. Some typical time histories of stress for the bridge are shown in Fig 5.8-5.10. The abscissa in those stress histories is the distance measured from the left end of the bridge to the front axle of the vehicle. The time histories have been obtained for various road surface conditions, varying vehicle speeds and vehicle weight to examine their influence on the fatigue life of the curved bridge.

Slow and fast moving vehicles are covered in the study adopting operating speed range 5 m/sec (17.8 km/h) to 20 m/sec (71.4 km/h). Fig. 5.8 shows the flexural stress at mid span in good road surface condition for different vehicle forward velocities. Fig. 5.9 and Fig.5.10 show the flexural stress at the same location for different road conditions and for different vehicle mass corresponding to constant vehicular velocity of 20 m/sec. The results indicate the presence of fluctuating stress component due to dynamic excitation of the bridge. The high frequency components are found all along the response time history. The peak magnitude is seen to occur when vehicle c.g is close to the center of the span, the magnitude of peak being greater for higher velocity, deteriorated road surface condition and increased vehicle weight.

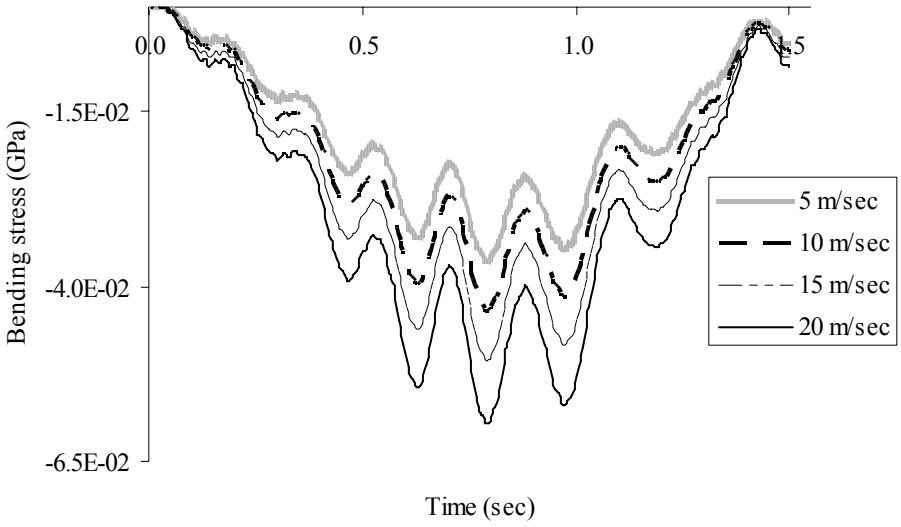

Fig .5.8 Flexural stress histories at mid span for different vehicle forward velocities

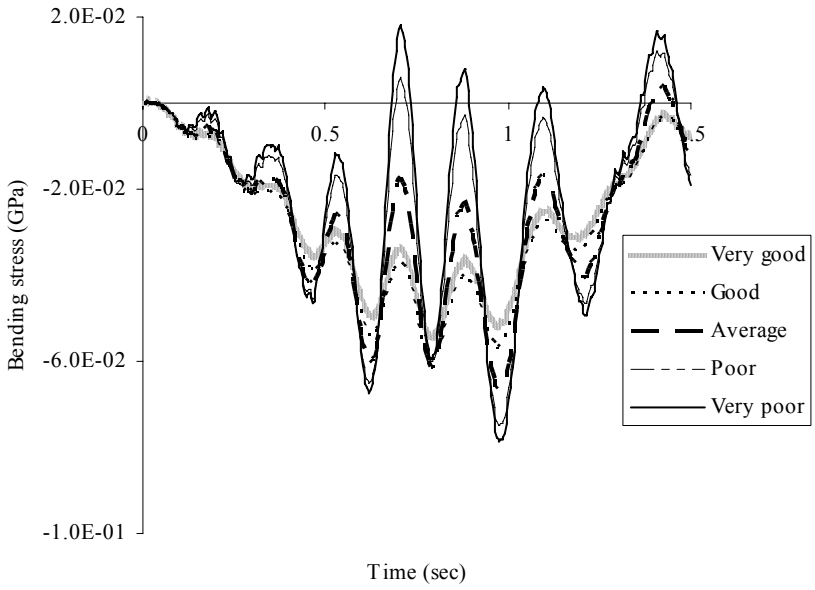

Fig .5.9 Flexural stress histories at mid span for different surface category

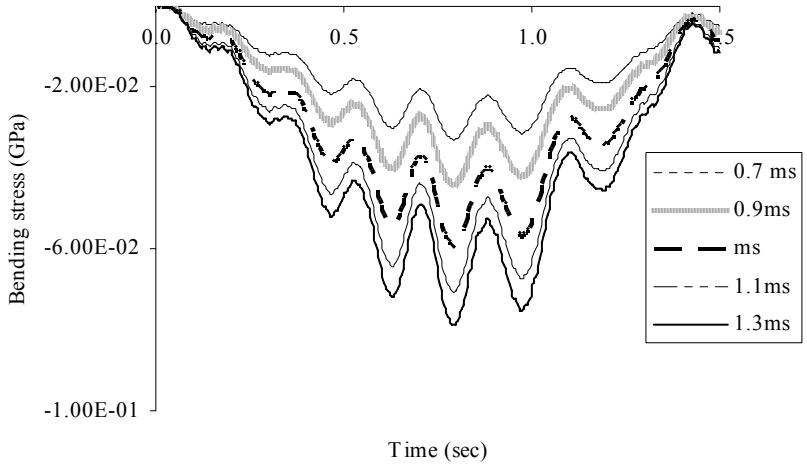

Fig .5.10 Flexural stress histories at mid span for different vehicle mass

5.6.2 Stress Range Histogram

The stress range histogram is needed for the calculation of fatigue life of the bridge. Corresponding to the flexural stress samples at mid span of the bridge obtained by numerical simulation, the stress histogram is prepared after synthesizing the time history by Rain flow counting method. It may be noted that the flexural stresses have been calculated considering the passage of single vehicle over the bridge. Assuming uniform traffic for all the days in a year, number of cycles obtained by Rainflow analysis is simply converted into the annual cycles by using a constant multiplier (Average daily traffic x 365). The flow rates of vehicles over the bridge have been taken 5×10^5 vehicles annually. Fig.5.11 shows a typical stress range vs. frequency (number of cycles/year) histogram with different vehicle forward velocity ranging from 5 m/sec to 20 m/sec in good pavement condition. It is found that the bridge is subjected to maximum 5.2 $\times10^7$ cycles/year in the stress range of 0.01 GPa –

0.02GPa (mean stress 0.015 GPa) in the operating vehicle speed 5 m/sec to 20 m/sec. In the higher stress range, the numbers of stress cycles experienced by the bridge seem to decline. Fig.5.12 presents the stress range vs. frequency histogram obtained for the stress histories corresponding to five different categories of the pavement such as very good, good, average and poor, very poor. The vehicle speed considered is 20 m/sec. It reveals from the histogram analysis, maximum number of stress cycle generated annually corresponds to approximately 4.55×10^7 cycles/year in the stress range 0.01 GPa – 0.02GPa for the good condition of the bridge deck. The histogram reveals that the number of stress cycles in higher stress range, although very small, is associated with the poor surface condition of the pavement. The number of stress cycles in significant stress range does not reflect much variation due to change of vehicle weight within ±30% limit. This is evident in Fig.5.13.

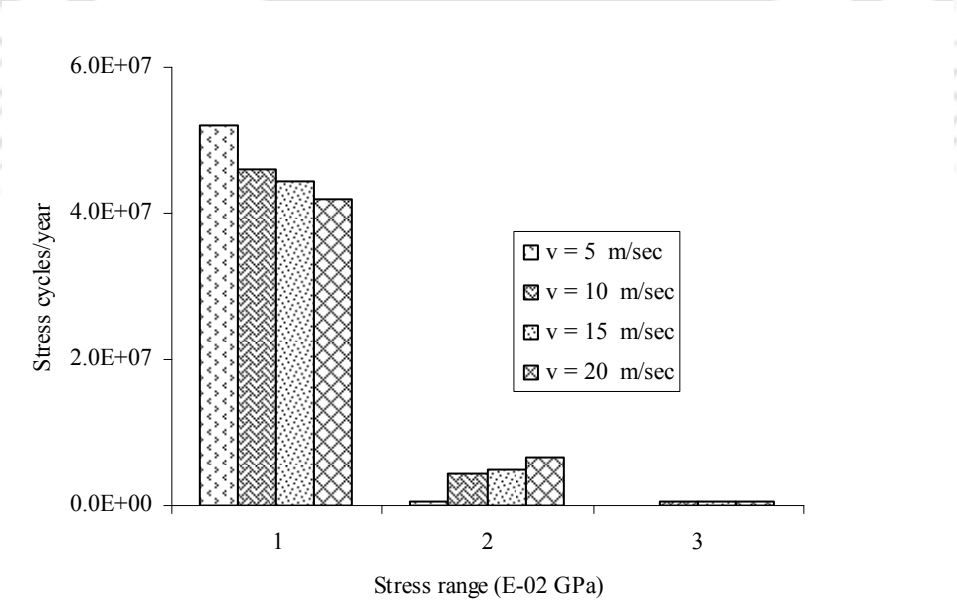

Fig.5.11 Stress ranges versus Frequency (cycles/year) Histogram for different vehicle velocity

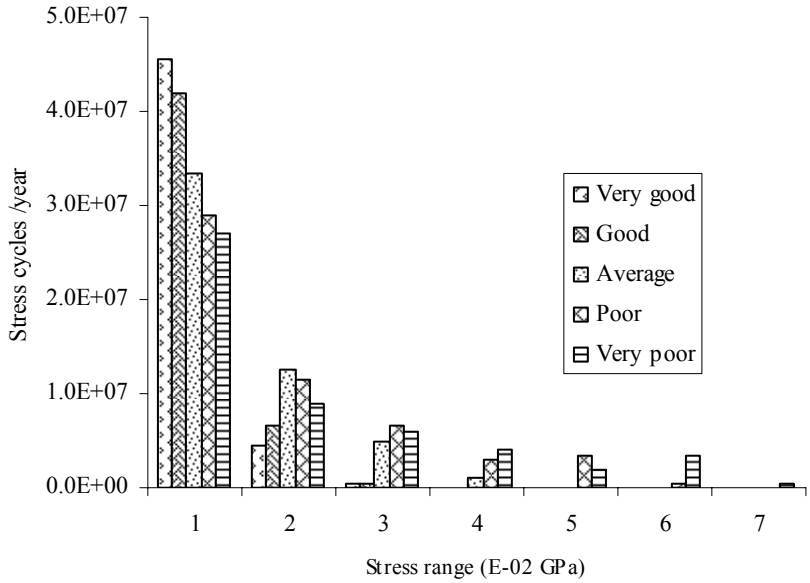

Fig.5.12 Stress ranges versus Frequency (cycles/year) Histogram for various surface condition of the deck

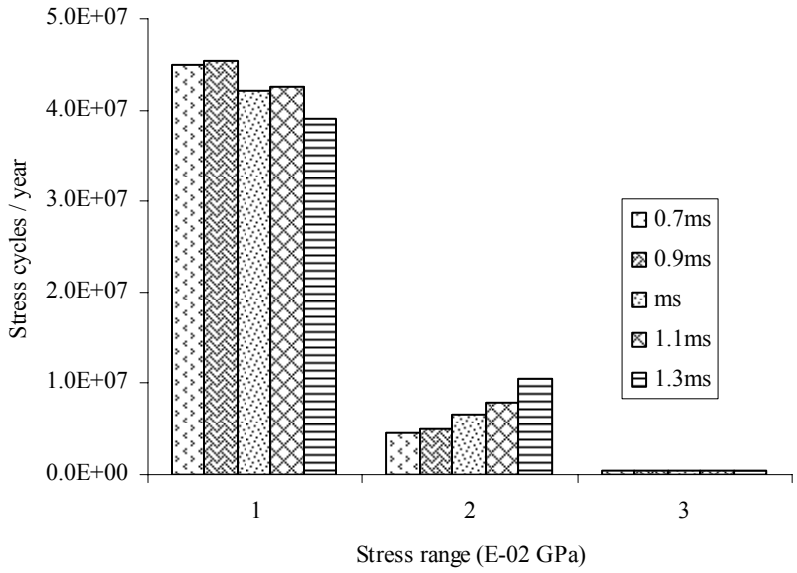

Fig.5.13 Stress ranges versus Frequency (cycles/year) Histogram for different vehicle mass

5.6.3 Power Spectral Density of Stress

The power spectral density (PSD) of stress process is necessary for the calculation of spectral moments required to be used to determine fatigue life using spectral moment method. To illustrate the nature of the power spectral density of stress, the spectral curve of stresses for the box-girder bridge have been plotted. Fig.5.14, 5.15 and 5.16 show the effect of vehicle forward velocity, road roughness and vehicle mass on PSD of stress at the mid-span of box-girder bridge. Results show that all the peaks occur at the fundamental natural frequency of the bridge and has narrow band width centered about the fundamental frequency.

Thus the nature of PSD curves shows that stresses induced by moving vehicle is the realization of narrow band random process, which justifies the applicability of the Rayleigh's expression for the evaluation of fatigue life. The magnitude of peak for spectral density of stresses increases with the increase of vehicle velocity, road roughness and vehicle mass, which indicates the increase of variance of the flexural stresses.

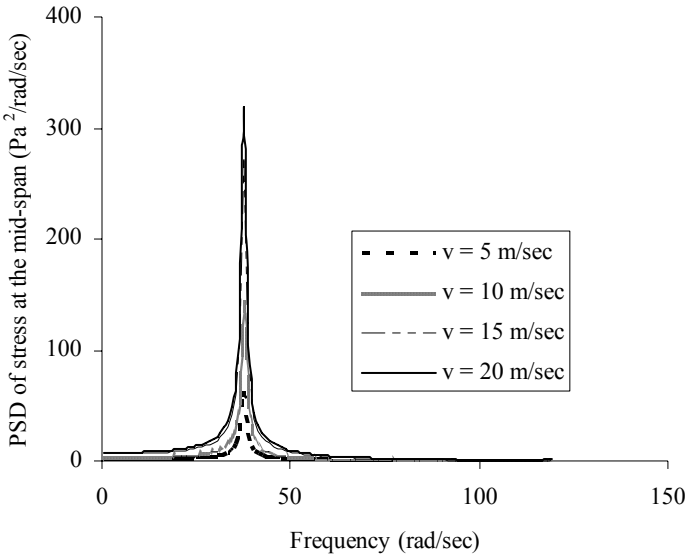

Fig. 5.14 PSD of flexural stress at mid span for different vehicle velocity

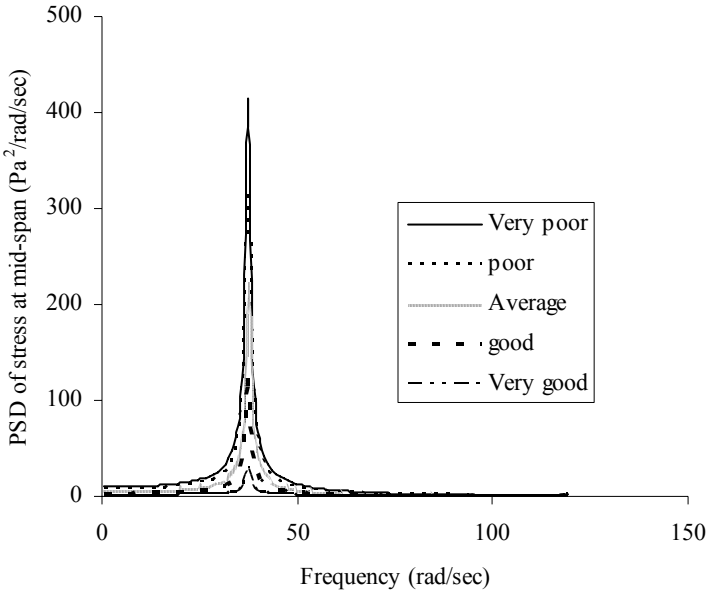

Fig. 5.15 PSD of flexural stress at mid span for different road surface

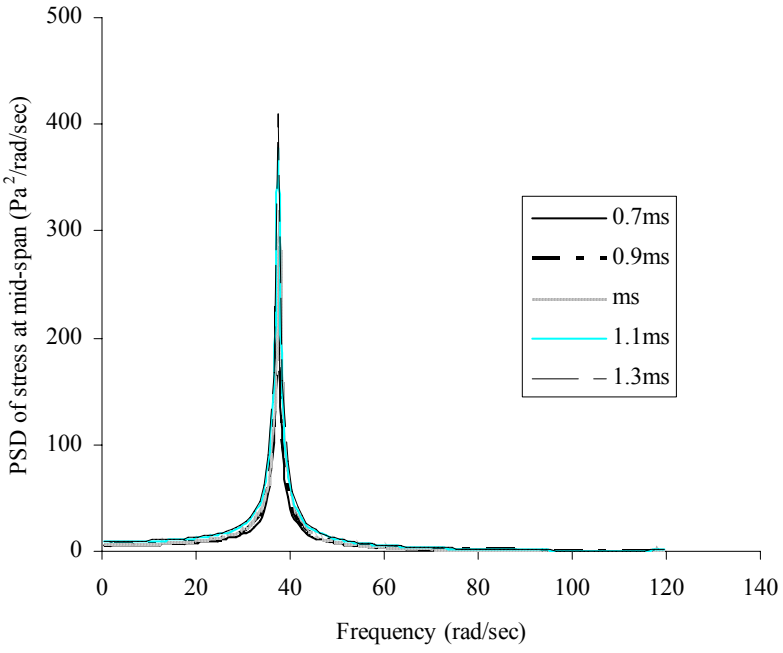

Fig. 5.16 PSD of flexural stress at mid span for different vehicle mass

5.6.4 Effect of Different Parameters on Fatigue life

This section examines the effect of some of the important factors, which are believed to influence the fatigue life of the bridge. Fatigue life of the curved thin walled box girder bridge section has been evaluated both by time domain cycle counting analysis and spectral analysis using Rayleigh's approximation and Single moment method.

5.6.4.1 Effect of S-N curve Constants on Fatigue Life

The constants *m* and *K* that are used in the computation of fatigue life of the structure play a very significant role. In procedure for calculating fatigue life mentioned in the present work, the evaluation of material constants from S-N curve test data is a perquisite. It is difficult to choose the constants *m* and *K* without obtaining data of the fatigue test conducted on the specimen. Because of non-availability of parameters of S-N curve after performing fatigue test, it is desired to examine the sensitivity of the predicted life of the bridge due to variation of those material constants. The S-N curves for steel have been presented for eight categories of weld details in AASHTO specifications (1998). These fatigue constants *K* of S-N curve for the steel specimens have also been used by Chung (2004) for fatigue reliability analysis of steel bridges. The same constants have been used in the present study to examine the change of fatigue life of the horizontally curved box girder steel bridges. The constant '*m*' has been taken as 3 for steel structures. The results are presented in Table 5.1. The damage accumulation rates have been computed using Rain flow counting method, Rayleigh approximation and Single moment method. The vehicle velocity has been assumed as of 20m/sec and road surface condition has been considered good. Since the constants are varied

(through A to E') in order of decreasing fatigue strength, the predicted life systematically decreases with weaker details. Although, the results are expected, the study ensures correct behaviour of the model adopted in two approaches for finding fatigue life of the horizontally curved box girder bridges. The results obtained by two approaches are sufficiently closer. The fatigue constant directly influences number of cycles to failure of the specimen. For some category of bridge detail, higher value of fatigue constant decreases cumulative damage index which ultimately lead to increase of fatigue life.

Table 5.1 Influence of S-N curve constant '*K'* (AASHTO-LRFD Fatigue Categories) on fatigue life

Detailed Category (AASHTO specifications 1998)	Fatigue constant(*K)* (10^8)	Fatigue life(*T*) Years		
		Spectral Method		Cycle Counting Method
		Rayleigh Approximation Method	Single Moment Method	
A	250.0	234.943	238.593	228.315
B	120.0	112.772	114.215	109.5890
B'	61.0	57.326	60.022	55.7078
C	44.0	41.350	47.746	40.1826
C'	44.0	41.350	47.746	40.1826
D	22.0	20.675	28.214	20.0913
E	11.0	10.337	14.186	10.0457
E'	3.9	3.665	5.0298	3.5616

5.6.4.2 Effect of Vehicle Forward Velocity on Fatigue Life

Table 5.2 shows the variation of fatigue life due to the variation of vehicle velocity. The fatigue life of the bridge has been computed for good road surface condition with velocity of the vehicle varying from 5 m/sec to 20 m/sec. The effect of increase of speed of the vehicle over the bridge increases the dynamic deflection as well as the peak flexural stress. This leads to the increases of the stress range as well. Higher magnitude of the stress range is expected to reduce the number of cycles to failure. The result would be the increase of cumulative damage index and reduction of fatigue life. A decrease in fatigue life of the girder has been observed at high-speed vehicle movements along the bridge in the Table 5.2. It is observed that two methods adopted in the estimation of fatigue life closely agree with each other, having slight conservative estimate in Rayleigh's approach. As the vehicle velocity increases, the frequency of dynamic excitation in temporal domain increases directly for given surface condition as the spatial frequency or wave number of surface roughness is related to the temporal frequency of excitation imposed on the vehicle through vehicle velocity. It may be noted that high frequency of oscillation of vehicle, in turn imposes high stress cycle on the bridge superstructure. The cumulative effect leads to increase of damage index. However, initially after construction of bridge, the surface condition generally remains good, in the later stage the damage rate increases rapidly. The study reveals some restriction should be imposed on vehicles regarding speed limit in order to avoid fatigue stresses not to become critical for the bridge. This was also depicted in the earlier study for dynamic load allowance.

Table 5.2 Influence of vehicle speed on fatigue life

Vehicle forward velocity m/sec	Fatigue life(T) Years		
	Spectral Method		Cycle Counting Method
	Rayleigh Approximation Method	Single Moment Method	
5	323.891	331.040	316.478
10	288.205	296.822	276.257
15	262.117	268.250	255.102
20	234.943	238.593	228.310

5.6.4.3 Effect of Pavement Roughness on Fatigue Life

The surface characteristics play an important role on the dynamic excitation transmitted to the bridge by the moving vehicle. Five categories of surface characteristics have been considered to examine their effect on the response. Based on the spectral roughness coefficient, the road is classified as very good, good, average, poor and very poor. The effect of any discrete form of roughness such as bump at the approach, construction joints etc are not taken into account. The fatigue life corresponding to different response parameters for different categories of road surface has been presented in Table 5.3. The vehicle velocity has been assumed as 20m/sec. The fatigue life decreases with the increase in surface roughness. Higher amplitude of tire force imposed on the pavement due to increased pavement roughness coefficient causes a high value of stress ranges in the bridge girder at the critical sections. The fatigue life reduces irrespective of the vehicle speed for degraded pavement

condition. When computed by two methods, Rayleigh's method is again found to yield higher estimate of fatigue life. The spectral roughness is characterized by two constants related to surface condition. The parameter spectral exponent is selected to represent a narrow band process with central frequency very near to lower cut off frequency. The result showed direct dependence on roughness coefficient rather than spectral exponent, reflecting reduction of fatigue life of bridge with deterioration of the pavement.

Table 5.3 Influence of pavement surface condition on fatigue life

Surface condition	Fatigue life(T) Years		
	Spectral Method		Cycle Counting Method
	Rayleigh Approximation Method	Single Moment Method	
Very Good	277.884	286.193	263.157
Good	234.943	238.593	228.315
Average	83.847	92.236	75.188
Poor	31.225	37.990	24.177
Very Poor	21.792	28.456	14.7536

5.6.4.4 Effect of Sprung Mass on Fatigue Life

In case of emergency and from strategic point of view, special permits are issued to allow extra heavy loads to pass over the bridge. Therefore, it is necessary to examine the fatigue life of the bridge at increased vehicle weight. The numerical experiment is performed by decreasing and increasing the weight of the vehicle (up to maximum 30%). Table 5.4 shows the effect of increased (or decreased) vehicle mass on the fatigue life of the bridge. The

surface condition of the pavement is assumed as 'good'. Uniform vehicle velocity of 20 m/sec is considered for the evaluation of effect of sprung mass variation. It is expected that the deflection and flexural stress in the bridge would increase for the increase of vehicle load. This may result in the increase of higher magnitude stress range causing reduction in the number of cycles to failure. It is observed from the result shown in Table 5.4 that the fatigue life decreases with the increase of sprung mass. However, it is seen that with maximum 30% increase of vehicle weight in the present case, the decrease of fatigue life is about 15%-20%. Such type of quantitative study is also useful to take decision on the restriction of payload of the vehicle plying over the bridge. The importance of studying the effect of sprung mass on fatigue life is to focus the attention of designers is to take into account the annual rate of traffic growth in estimating remaining life of the bridge.

Table 5.4 Influence of vehicle mass on fatigue life

Vehicle mass	Fatigue life(T) Years		
	Spectral Method		Cycle Counting Method
	Rayleigh Approximation Method	Single Moment Method	
$0.7m_s$	278.000	286.3574	264.550
$0.9\ m_s$	258.3532	264.418	252.525
$1.0\ m_s$	234.943	238.593	228.315
$1.1\ m_s$	222.615	231.365	208.333
$1.3\ m_s$	191.935	200.653	183.150

5.6.4.5 Effect of Bridge Span on Fatigue Life

The single span curved box girder bridge in the span range 10m to 30m has been considered to examine the effect of the bridge span on fatigue life. The vehicle velocity is taken as 20 m/sec. The results are tabulated in Table.5.5 for the class of bridge pavement taken as good. It has been observed that with the increase of the bridge span, natural frequencies of the bridge decrease in all the modes. The decrease in natural frequencies results in large amplitude stress cycles. The number of stress cycles in higher stress range decreases which yield lower value of damage index. This effect may be attributed to the increase of fatigue life of the bridge which is reflected in Table 5.5. It may be observed that fatigue life estimated by spectral methods yield higher value compared to rain-flow counting method. The increase of fatigue or in other words decrease in damage index in a longer span bridge may also be thought of as a minor effect of fluctuating live load on the bridge compared to dead load of the superstructure. The dead load generally varies directly with the span for a given cross section. The study shows that effect of high cycle fatigue caused by traffic is not of serious concern for the design of superstructure in long span bridge.

Table 5.5 Influence of bridge span on fatigue life

Span m	Fatigue life (T) Years		
	Spectral Method		Cycle Counting Method
	Rayleigh Approximation Method	Single Moment Method	
10	183.053	189.843	171.1351
20	196.178	204.04	189.393
30	234.943	238.593	228.310

5.7 CLOSURE

A systematic theoretical approach has been outlined for the calculation of the fatigue life of a horizontally curved thin walled box girder bridge considering its dynamic interaction with the vehicle. The key feature of the study is the estimate of fatigue life through the solution of bridge vehicle coupled dynamics with the application of linear damage accumulation rule. Both time domain cycle counting and frequency domain spectral method using Rayleigh's approximate and single moment theory have been employed. The spectral method uses an analytical expression for the calculation of fatigue life which is simpler in application and requires less computational time compared to cycle counting method in time domain. The comparative study of the fatigue life of the bridge shows that results of the spectral method, although provides conservative estimate are reasonably closer to the estimates in time domain cycle counting method. However, the spectral methods can only be applied to narrow band Gaussian process where the time domain cycle counting method is not restricted by such assumption and can be expected to a wide class of problems. The detail parametric study conducted in this chapter is expected to become helpful to identify several

factors that may be responsible for the damage and degradation of the bridges. The parameters that influence fatigue life was found to be important but presently missing in the existing formula given in the bridge specification. Even, the bridge specification at present has not given any recommendation of fatigue life of box girder curved bridge. The usefulness of present study was discussed that by the histograms of stress cycle obtained from detail dynamic analysis including the effect of different parameters can be used to find remaining life of structure knowing the present age of the bridge. As such, the study is not only useful in the design stage but also finds application to know the remaining service life. This helps to take important decision to periodical maintenance and major repairing. The actual traffic history and annual growth rate may be obtained by field survey to use the technique of present study.

CHAPTER 6

CONCLUSION AND SCOPE OF FUTURE WORK

6.1 INTRODUCTION

In this chapter, a critical analysis of the results obtained through this investigation and a summary of conclusions are presented. Further, the proposals for future research are also given.

6.2 ANALYSIS OF RESULTS AND SUMMARY OF CONCLUSIONS

A computationally efficient thin-walled box-beam finite element has been used to model curved box-girder bridge which takes into account the torsional warping, distortion and distortional warping characteristics of thin-walled box-spine bridges, apart from the usual extensional, flexural and torsional behavior. The effect of shear lag has also been taken into account using the effective width concept. A supplementary program that evaluates the sectional properties of a box-girder cross-section has also been developed. The stress resultants for curved thin walled box girder bridge for static loading has been evaluated for single and double cell section for single and two span bridges. The static analysis reveals that with increasing curvature, the torsional and distortional stress resultants are significantly changed whereas other stress resultants corresponding to bending and shear remain almost unaffected. The applicability of such an element for the dynamic analysis has been verified by evaluating the modal parameters of a curved box girder model theoretically as well as experimentally. The dynamic response of thin-walled curved box girder bridge due to moving vehicle has been studied considering surface unevenness of the deck as the random input to the vehicle wheels. Impact factors for several response parameters have been evaluated for the variations of various bridge and vehicle

parameters, which would be very much useful for the design of curved thin walled box girder bridges.

Another important feature of the present study is the estimate of fatigue life through the solution of bridge vehicle coupled dynamics with the application of linear damage accumulation rule. The time domain cycle counting method yields the stress histogram from which fatigue life has been evaluated. Frequency domain approach using Rayleigh's assumption with two spectral moments of integer order and single spectral moment of non integer order have also been applied to evaluate expected fatigue life of steel curved thin walled box girder bridge. The comparison of time domain and frequency domain results shows close agreement between the two methods. It was observed that stress being a narrow band process, the spectral method provides quick estimate compared to cycle counting, which depends on the simulated time history. The parametric studies indicate that increase of pay load and vehicle velocity decreases the fatigue life. The major factor responsible for the reduction of fatigue life of the bridge has been found to be the deck surface condition. This indicates that proper maintenance and periodic inspection is necessary to reduce the tendency of fatigue failure in the bridge component.

The major observations from the present study may be summarized as follows:

1. The results obtained from the present study have been validated, thus supporting the appropriateness and accuracy of the code developed. The code developed can thus be used successfully for the elastic analysis of single-spine (single cell and multi cell) box girder bridges.
2. The results obtained from the present study have reaffirmed the significance of warping, distortion and shear lag in the analysis of thin walled box girder bridges. The static analysis reveals that with increasing radius of curvature, the

torsional and distortional stress resultants are significantly reduced, whereas other stress resultants (bending moment and shear force) are unaffected.

3. A computationally less expensive and realistic three noded thin-walled box beam element has been utilized for the modeling of the bridge. The main advantage of the proposed method of analysis is that it may be used for bridge analysis in situations where a full three-dimensional analysis is unnecessary, such as during preliminary design stages. Further, the dynamic analysis due to vehicle induced excitation will be also very efficient as a substantial reduction in overall degrees of freedom is achievable by using three noded one dimensional beam models. The applicability of such an element for the dynamic analysis has been verified by evaluating the modal parameters of a curved box girder model theoretically as well as experimentally.
4. Free vibration studies of thin-walled box-girder bridges show that the natural frequencies of curved box-girders increase with the increase of radius of curvature. However, the effect of curvature on the frequency of practical box girder bridges is insignificant.
5. Due to the effect of centrifugal force in a curved bridge, the impact factors due to torque, distortion and their corresponding bi-moments are generally higher than those of vertical deflection, bending moment and shear force. Further, it has been observed that the impact factors of torque, distortion and their corresponding bi-moments rapidly increase with vehicle speed, while those of vertical deflection, bending moment and shear force do not show such tendency.

6. Surface roughness is one of the predominant factors, which may cause large increase in the magnitude of dynamic response particularly of vertical deflection, bending moment and shear force.
7. The transverse load position on the bridge deck as well as number of vehicles at a section influence the values of impact factor. The impact factors in a curved box-girder bridge corresponding to a two- truck loading have been observed to be higher than that for a single truck loading. The loading positions have lesser influence on vertical shear and bending moment, while impact factors of torque, distortional moments and bi-moments are relatively more affected by the loading positions.
8. Vehicle suspension stiffness has lesser influence on impact factors corresponding to different response parameters in comparison to the sprung mass variation.
9. It has been observed that by completely neglecting the effect of damping will overestimate the impact factors corresponding to vertical deflection, bending moment and shear force for a curved box-girder bridge.
10. With the increase in acceleration of vehicle, impact factors corresponding to bending moment, shear force and vertical deflection increases, while those of torsional moments, distortional moments and their respective bi-moments reduces.
11. The moving vehicle induces flexural, torsional warping and distortional warping stresses in thin-walled curved box girder bridge. The magnitudes of flexural stresses dominate over other stresses. Hence for evaluating fatigue life, flexural stresses at mid span have been found important. The magnitude of

peak stresses becomes larger with higher vehicle forward velocity, deteriorated road surface condition and increased vehicle weight.

12. The first largest peak of the power spectral density of stresses (PSD) is found to occur at fundamental natural frequency. The PSD curve also exhibits a significant value over narrow band width.
13. Out of two methods used in fatigue life estimation, time domain method is computationally more expensive compared to spectral method. The spectral method used in the present study has to restrict its application only to narrow band Gaussian process. The time domain method based on cycle counting, however, is general in applications.
14. The fatigue life according to Rayleigh and Single moment approximation are very close to each other. However, rain flow method predicts lower values of fatigue life compared to spectral methods.
15. The fatigue life of the bridge is dependent on the vehicle weight and the speed of the vehicle. The damage accumulation progresses rapidly due to increase of the vehicle weight, decreasing the fatigue life. The increase of the vehicle speed also decreases the fatigue life. Thus it is important to regulate the vehicle load and speed over the bridge to increase the safety limit of the bridge.
16. The condition of the bridge pavement is found to be an important parameter affecting the fatigue life of the bridge. The deteriorated bridge pavement decreases the fatigue life of the bridge.
17. The S-N curve constant to be used in fatigue life prediction plays an important role. These constants can drastically change the value of fatigue life.
18. The fatigue life of the bridge increases with the increase of bridge span.

The integrated module has been developed involving analysis of thin-walled box-girder bridge using a computationally efficient finite element, computing impact factor incorporating all the complexities of bridge-vehicle parameters and assessing the safety limit of the bridge by evaluating fatigue life. This module could be used for many important observations critical to efficient design of the box-girder bridges.

6.3 SCOPE OF FUTURE WORK

1. An empirical procedure for the prediction of shear lag (Moffat and Dowling 1975) has been used in this study. The generalized coordinate method of Vlasov (1961) could perhaps be used to include the structural action of shear lag directly in the element formulation.
2. The initial conditions of the vehicle and entry velocity may be considered random.
3. Nonlinearity in suspension of the vehicle can be included in the future study.
4. Fatigue prediction method in the present study depends on linear damage rule, which may be modified taking into account of the non-linearity of damage accumulation with time.
5. The initiation of the crack and its growth in fatigue model of the bridge may be included.
6. The super elevation consideration may be included in the modeling of bridge and equivalent load vectors may be accordingly incorporated.
7. The present formulation has been carried out based on only one type of vehicle model. However, the realistic simulation will require the modeling of mixed vehicular type and also considering congestion effect in the evaluation of impact factor.

REFERENCES

1. AASHTO Guide specifications for fatigue of steel bridges, “American Association of State Highway and Transportation Officials”, Washington, D.C, 1989.
2. AASHTO Guide specifications for horizontally curved steel girder highway bridges, “American Association of State Highway and Transportation Officials”, Washington, D.C, 1993.
3. AASHTO-LRFD Bridge Design Specifications, “American Association of State Highway and Transportation Officials”, Washington, D.C, 1998.
4. AASHTO standard specifications for highway bridges, “American Association of State Highway and Transportation Officials”, Washington, D.C, 2002.
5. AASHTO Guide specifications for horizontally curved highway bridges, “American Association of State Highway and Transportation Officials”, Washington, D.C, 2003.
6. Abdullah, M.A., and Abul-Razzak, A.A., “Finite strip analysis of prestressed box -girder”, Computers and Structures, 36(5), pp. 817-822, 1990.
7. Agerskov, H., and Nielsen, J.A., “Fatigue in steel highway bridges under random loading”, Journal of the Structural Division ASCE, 125 (2), pp. 152-162, 1999.
8. American Society for Metals, “Atlas of fatigue curves”, Ed. H. E. Boyer, 1986.
9. Au, F.T.K., Cheng, Y.S., and Cheung, Y.K., “Effects of random road surface roughness and long-term deflection of prestressed concrete girder and cable-stayed bridges on impact due to moving vehicles”, Computers and Structures, 79, pp.853-872, 2000.

10. AUSTROADS Bridge Design Code, Sydney, NSW, Australia, 1992.
11. Bennantine, J. A., Commer, J. J., and Handrock, J. L., “Fundamentals of Metal Fatigue Analysis”, Prentice Hall, Englewood Cliffs, New Jersey, 1990.
12. Bennantine, J. A., and Tovo, J.A., “Comparison of spectral method for fatigue analysis of broad-band Gaussian random processes”, Probabilistic Engineering Mechanics, 21(4), 287-299, 2006.
13. Boswell, L. F., and Zhang, S. H., “The effect of distortion in thin-walled box-spine beams”, Computers and Structures, 20(9), pp. 845-862, 1984.
14. Boswell, L. F., and Li, Q., “Consideration of the relationships between torsion, distortion and warping of thin-walled beams”, Thin-walled Structures, 21, pp. 147-161, 1995.
15. Boswell, L. F., and Zhang, S. H., “An Experimental investigation of the behavior of thin-walled box beams”, Thin-walled Structures, 3, pp. 35-65, 1985.
16. Boswell, L. F., and Zhang, S. H., “A box beam finite element for the elastic analysis of thin-walled structures”, Thin-walled Structures, 1, pp. 353-383, 1983.
17. Bridge Rules (in SI units), Ministry of Railways, Govt. of India., Revised, 1964.
18. BS: 5400: Part 10, Steel, concrete and composite Bridges-Part10: Code of practice for fatigue, British Standards Institution, 1980.
19. Burgan, B. A., and Dowling, P. J., “The treatment of shear lag in design”, Thin-walled Structures, 9, pp. 121-134, 1990.
20. Chang, D., “Impact factors for simple span highway girder bridges”, Journal of Structural Engineering ASCE, 120(3), pp. 704-715, 1994.
21. Chatterjee, P.K., Datta, T.K., and Surana, C.S., “Vibration of continuous bridge under moving vehicles”, Journal of Sound and Vibration, 169, pp. 619-632, 1994.

22. Chatterjee, P.K., Dattta, T.K., and Surana C.S., “Vibration of Suspension Bridges under Vehicular Movement” Journal of Structural Engineering, ASCE, 120(3), pp.681-703,1994.
23. Cheung, Y.K., “Orthotropic right bridges by the finite strip method”, concrete bridge design, ACI publications SP26, pp.182-205, 1971.
24. Cheung, Y.K., “Analysis of box girder bridge by finite strip method”, American Concrete Institute, pp. 357-378, 1971.
25. Cheung, Y.K., “Analysis of curvilinear orthotropic curved bridge decks”, Int Assoc of Bridge and Structural Engineering, 29-II, 1969.
26. Chopra, A. K., “Dynamics of Structures: Theory and Applications to Earthquake Engineering”, Prentice Hall of India, 2005.
27. Chotickai, P., and Bowman, M.D., “Truck models for fatigue life predictions of steel bridges”, Journal of Bridge Engineering, 11(1), pp. 71-80, 2006.
28. Chung, H.Y., “Fatigue Reliability and Optimal Inspection Strategies for Steel Bridges”, Ph.D Thesis, The University of Texas, Austin, 2004.
29. Coussy, O., Said, M., and Van Hoove, J.P., “The influence of random surface irregularities on the dynamic response of bridges under suspended moving loads”, Journal of Sound and Vibration, 130, pp .313-320, 1988.
30. Culver, C.G., “Natural frequencies of horizontally curved beams”, Journal of Structural Engineering ASCE, 93, pp.189-203, 1967.
31. Desantiago, E., and Mohammadi, J., “Analysis of horizontally curved bridges using simple finite element models”, Practice Periodical on Structural Design and Construction ASCE, 10, pp.18-21, 2005.

32. Dicleli, M., and Bruneau, M., “Fatigue-Based Methodology for managing impact of heavy-permit trucks on steel highway bridges”, Journal of the Structural Division ASCE, 121(11), pp .1651-1659, 1995.
33. Dodds, C.J., and Robson, J.D., “The description of road surface roughness”, Journal of Sound and Vibration, 31, pp .175-183, 1973.
34. Dougall, C.M., Green, M.F., and Shillinglaw, S., “Bridge Fatigue life estimation from field data”, Journal of Bridge Engineering, 11(3), pp.320-328, 2006.
35. Dowling, N.E., “Fatigue failure predictions for complicated stress-strain time histories”, Journal of Materials, 7(1), pp.71-87, 1972.
36. Erzurumlu, H., and Toprac A.A., “Fatigue of orthotropic steel decks”, Journal of the Structural Division ASCE, 98, pp. 813-830,1972.
37. Fam, A., and Turkstra, C.J., “A finite element scheme for box bridges analysis”, Computers and Structures, 5, pp. 179-186, 1975.
38. Fan, S,C., “Spline finite strip in structural analysis”, PhD thesis, Department of Civil and Structural Engineering, University of Hongkong.1982.
39. Fleming, J, F., Romualdi, J.F., “Dynamic response highway bridge”, Journal of the Structural Division ASCE, 87(7), pp. 31-61, 1961.
40. Fisher, J.W., and Yuceoglu, U., “A Survey of localized cracking in steel bridges”, Interim Report (DOT-FT-11-9506), Washington, Federal Highway Administration, 1981.
41. Fryba, L., “Dynamics of railway bridges”, Thomas Telford, 1996.
42. Fybra, L., “Vibration of solids and structures under moving loads”, Groningen, The Netherlands, Noordh of International Publishing Co. 1972.
43. Fu, T.T., and Cebon, D., “Predicting fatigue lives for bi-model stress spectral densities”, International Journal of fatigue, 22, pp. 11-21, 2000.

44. Galdos, N.H., Schelling, D.R., and Sahin, M.A., “Methodology for Impact factor of horizontally curved box-bridges”, Journal of Structural Engineering ASCE, 119(6), pp .1917-1934, 1993.
45. Geore, E.D, “Mechanical metallurgy”, McGraw-Hill, Inc, 1988.
46. Green M.F and Cebon D., “Dynamic Response of Highway Bridges to Heavy Vehicle Loads: Theory and Experimental Validation”, Journal of Sound and Vibration, 170(1), pp.51-78, 1994.
47. Green, M. F., Cebon, D., and Cole, D. J, “Effects of Vehicle Suspension Design on Dynamics of Highway Bridges”, Journal of Structural Engineering, ASCE, 121(2), pp. 272-282, 1995.
48. Green, M.F., and Cebon, D., “Dynamic interaction between heave vehicles and highway bridges”, Journal of Computers and Structures, 62, pp.253-264, 1997.
49. Gu, M., Xu, Y.L., Chen, L.Z., and Xiang, H.F., “Fatigue life estimation of steel girder of Yangpu cable-stayed Bridge due to buffeting”, Journal of Wind Engineering and Industrial Aerodynamics, 80, pp. 383-400,1999.
50. Gunnlaugsson, G. A., and Pedersen, P. T., “A finite element formulation for beams with thin walled cross-sections”, Computers and Structures, 15(6), pp. 691-699, 1982.
51. Gupta, R., and Rupert, T.N., “Vehicle Braking on Highway Bridges”, Journal of the Engineering Mechanics Division, ASCE, 106(EM4), pp.641-658, 1980.
52. Hahin, C., South, J.M., Mohammadi, J., and Polepeddi, R.K., “Accurate and rapid determination of fatigue damage in steel bridges”, Journal of Structural Engineering ASCE, 119, pp. 150-166, 1993.

53. Hasebe, K., Usuki, S., and Horie, Y., “Shear lag analysis and effective width of curved box girder bridge”, Journal of Engineering Mechanics ASCE, 111(1), pp. 87-92, 1985.
54. Heins, C.P., and Oleinik, J.C., “Curved box beam bridge analysis”, Computers and Structures, 6, pp. 65-73, 1976.
55. Henchi, K., Fafard, M., Dhatta, G., and Talbot, M., “An efficient Algorithm for Dynamic analysis of bridge under moving vehicle using a coupled model and physical components approach”, Journal of Sound and Vibration, 212(4), pp .663-683, 1998.
56. Henchi, K., Fafard, M., Dhatta, G., and Talbot, M., “Dynamic behavior of multi-span beams under moving loads”, Journal of Sound and Vibration, 199, pp. 33-50, 1997.
57. Hino, J., Yoshimura, T., and Konishi, K., “A Finite Element Method Prediction of the Vibration of a Bridge Subjected to a Moving Vehicle Load”, Journal of Sound and Vibration, 96(1), pp. 45-53, 1984.
58. Holmes, J.D., “Fatigue life under along-wind loading- closed-form solutions”, Engineering Structures, 24, pp. 109-114, 2002.
59. Honda, H., Kajkawa, Y., and Kobori, T., “Spectra of road surfaces on bridges”, Journal of Structural Engineering ASCE, 108, pp.1956-1966, 1982.
60. Hsu, Y.T., Fu, C.C., and Schelling, R.R., “An improved horizontally Curved box beam element”, Computers and Structures, 34(2), pp. 313-318, 1990.
61. Huang, D.Z., Wang TL., and Shahaway, M., “Impact analysis of continues multi-girder bridges due to moving vehicles”, Journal of Structural Engineering ASCE, 118(12), pp. 3427-3443, 1992.

62. Huang, D.Z., and Wang, T.L., “Impact Analysis of Cable-Stayed Bridges”, Computers and Structures, 43(5), pp.897-908, 1992.
63. Huang, D.Z., Wang, T.L, Shahaway, M., “Probabilistic fatigue life analysis of highway steel bridges”, Journal of Computers and Structures, 48(2), pp. 241-248, 1993.
64. Huang, D.Z., Wang, T.L., and Shahaway, M., “Dynamic behavior of horizontally curved I- girder bridges”, Journal of Computers and Structures, 57, pp. 703-714, 1995.
65. Huang, D.Z., Wang, T.L., and Shahaway, M., “Vibration of thin-walled box-girder bridges excited by vehicles”, Journal of Structural Engineering, 121(9), pp. 1330-1337, 1995.
66. Huang, D.Z., Wang, T.L., and Shahaway, M., “Vibration of horizontally curved box-girder bridges due to vehicles”, Journal of Computers and Structures, 68, pp. 513-528, 1998.
67. Huang, D.Z., Wang, T.L., and Shahaway, M., “Dynamic analysis of steel curved box girder bridges”, Journal of Bridge Engineering ASCE, 6, pp.506-513, 2001.
68. Hwang, E.S., and Nowak, A.S., “Simulation of dynamic load for bridges”, Journal of Structural Engineering ASCE, 117, pp.1413-1434.1991.
69. Illinois Department of Transport, Bureau of Materials and Physical research, “Accurate and rapid determination of fatigue damage in bridge superstructures”, Physical research report no. 106, 1992.
70. Inbanathan, M.J., and Wieland, M., “Bridge vibration due to vehicle moving over rough surface”, Journal of Structural Engineering ASCE, 113(9), pp. 1994-2008, 1987.
71. Inman, D. J., “Engineering Vibration”, Prentice Hall, Inc., second edition.2001.

72. IRC-22: Standard specifications and code of road bridges, Section-VI, composite construction, 1986.
73. IRC-6: Standard specifications and code of road bridges, Section-II, Load and Stresses, 2000.
74. Jag Mohan Humar, L., and Ahmed, H.K., "Dynamic response analysis of slab type bridges", Journal of Structural Engineering ASCE 121, pp. 48-62, 1995.
75. Jonsson, J., "Distortional warping functions and shear distributions in thin-walled beams", Thin-Walled Structures, 33, pp. 245-268, 1999.
76. Kermani, B., and Waldron, P., "Analysis of continuous box girder bridges including the effects of distortion", Computers and Structures, 47(3), pp. 427-440, 1993.
77. Kim, Y.Y., and Kim, J. H., "Thin-walled closed box beam element for static and dynamic analysis", International Journal for Numerical Methods in Engineering, 45, pp. 473-490, 1999.
78. Kim, Y.Y., and Kim, Y.,"A one-dimensional theory of thin-walled curved rectangular box beams under torsion and out-of-plane bending", International Journal for Numerical Methods in Engineering,53, pp. 1675-1693, 2002.
79. Kou, C.H., Benzley, S.E., and Huang, J.Y., "Free Vibration analysis of curved Thin-walled Box-girder bridges", Journal of Structural Engineering ASCE, 118, pp.2890-2910, 1992.
80. Kwasniewski, L., Li, H., Wekezer, J., and Malachowski, J., "Review Finite element analysis of vehicle-bridge interaction", Finite Element Analysis and Design, 42, pp. 950-959. 2006.

81. Lee, S.Y., and Yhim, S.S., “Dynamic behavior of long-span box girder bridges subjected to moving loads: Numerical analysis and experimental verification”, Journal of Solids and Structures, 42, pp .5021-5035, 2005.
82. Lee, S. C., Yoo, C. H., and Yoon, D. Y., “Analysis of shear lag anomaly in box girders”, Journal of Structural Engineering, 128(11), pp .1379-1386,2002.
83. Lees, A.W., Thomas, D.L., and Wilson, R.R., “Analysis of the vibration of box beams”, Journal of Sound and Vibration, 45(4), pp .559-568, 1976.
84. Li, Z.X., Chan, T.H.T., and Ko, J.M., “Fatigue damage model for bridge under traffic loading: application made to Tsing Ma”, Theoretical and Applied Fracture Mechanics, 35, pp. 81-91, 2001.
85. Li, Z.X., Chan, T.H.T., and Ko, J.M., “Evaluation of typhoon induced fatigue damage for Tsing Ma bridge”, Engineering Structures, 24(8), pp.1035-1047.2002.
86. Li, W.Y., Tham, L.G., and Cheung, Y.K., “Curved box-girder bridge”, Journal of Structural Engineering, ASCE, 114(6), pp.1324-1338, 1988.
87. Lu Sun., “Computer simulation and field measurement”, Mathematics and Computer in Simulation, 56, pp. 297-313, 2001.
88. Luo, Q.Z., and Li, Q.S., “Shear lag of thin-walled curved box girder bridges”, Journal of Engineering Mechanics, 126(10), pp. 1111-1114, 2000.
89. Luo, Q.Z., Wu, Y.M., Tang, J., and Li, Q.S., “Experimental studies on Shear lag of box girder”, Engineering Structures, 24, pp. 467-477, 2002.
90. Lutes, L.D., Corazao, M., Hu, S. J., and Zimmerman, J., “Stochastic fatigue damage accumulation”, Journal of Structural Engineering, ASCE, 110(11), 2585-2601, 1984.

91. Lutes, L.D., and Larsen, C.E., “Improved spectral method for variable amplitude fatigue prediction”, Journal of Structural Engineering, 116(4), pp.1149-1164, 1990.
92. Lutes, L.D., and Sarkani, S., “Stochastic analysis of structural and mechanical vibrations”, Prentice Hall, Upper Saddle River, New Jersey, 1997.
93. Maisel, B. I., “Analysis of concrete box beams using small computer capacity”, Canadian Journal of Civil Engineering, 12, pp. 265-278, 1985.
94. Marcondes, J., Burgess, G.J., Harichandran, R., and Snyder, M. B., “Spectral analysis of highway pavement roughness”, Journal of Transportation Engineering, 117, pp. 540-549, 1991.
95. Marchesiello, S., Fasana, A., Gaibaldi, L., and Piombo, B.A.D., “Dynamics of Multi-span Continuous Straight bridges subject to Multi-degrees of freedom moving vehicle excitation”, Journal of Sound and Vibration, 224(3), pp. 541-561, 1999.
96. Mermertas, V., “Dynamic interaction between the vehicle and simply supported curved bridges deck”, Computer Methods in Applied Mechanics and Engineering, 162, pp. 125-131, 1998.
97. Michaltsos, G., Sophianopoulos, D., and Kounaids, A.N., “The effect of moving mass and other parameters on the dynamic response of highway bridges”, Journal of Sound and Vibration, 191, pp. 357-362, 1996.
98. Mikkola, M.J., and Paavola, J., “Finite element analysis of box girders”, Journal of Structural Engineering ASCE, 108, pp. 1956-1966, 1980.
99. Miner, M. A., “Cumulative damage in fatigue”, Journal of Applied Mechanics, ASME, 67, pp.159-164, 1945.

100. Minguillon, C.C., and Cases, J.R., “Fatigue Reliability analysis of prestressed concrete bridge”, Journal of Structural Engineering ASCE, 124(12), pp.1458-1466, 1998.

101. Moffat, K. R., and Dowling, P. J., “Shear lag in steel box-girder bridges”, The Structural Engineer, 53(10), pp. 439-448, 1975.

102. Mohammadi, J., Guralnick, S.A., and Polepeddi, R., “Bridge fatigue life estimation from field data” Practice Periodical on Structural Design and Construction ASCE, 3, pp. 128-133, 1998.

103. Mukhopadhyay, M., and Sheikh, A.H., “Large amplitude vibration of horizontally curved beams: A Finite element approach”, Journal of Sound and Vibration, 180(2), pp. 239-251, 1995.

104. Munirudrappa, N., and Dhruvaraja Iyengar, H.N., “Dynamic analysis of continuous span highway bridge”, ISET Journal of Earthquake Technology, 36(392), pp .73-84, 1999.

105. Nigam, N. C., “Introduction to Random Vibration”, MIT Press, Cambridge, 1983.

106. Noor, A.K., Peters, J.M., and Min, B.J., “Mixed finite element models for free vibration of thin-walled beams”, Finite Element Analysis and Design, 5, pp. 291-305. 1989.

107. Oh, B. H., “Fatigue analysis of plain concrete in flexure”, Journal of Structural Engineering, ASCE, 112 (2), pp. 273-286, 1986.

108. Ontario Highway Bridge Design code (OHBDC), “Ministry of Transportation and Communication”, Downs views, Ontario, Canada, 1983.

109. Oritz, K., and Chen, N. K., "Fatigue damage prediction for stationary wideband processes", Proc. Fifth Int. Conf on Application of Statistics and Probability in Soil and Struct. Engrg, 1987.

110. Owen, D.R.J., and Hinton, E., "Finite Elements in Plasticity: Theory and Practice", Pine ridge Press Limited, Swansea, U.K, 1960.

111. Paavola, J., "A Finite element Technique for thin-walled girders", Computers and Structures, 44(1), pp. 159-175, 1992.

112. Paris, P. and Erdogen, F., "A critical analysis of crack growth propagation laws", Journal of Basic Engineering, ASME, 85 (3), pp.528-534, 1963.

113. Park, N.H., Choi, S., and Kang, Y.J., "Exact distortional behavior and practical distortional analysis of multi-cell box girders using an expanded method", Computers and Structures, 83, pp. 1607-1626, 2005.

114. Perdikaris, P.C., Beim, S.R., and Bousias, S.N., "Slab continuity on ultimate and fatigue strength of reinforced concrete bridge deck models", Journal of Structural Engineering ASCE, 86, pp. 483-491, 1989.

115. Petyt, M., and Fleischer, C.C., "Free vibration of a curved beam", Journal of Sound and Vibration, 18(1), pp. 17-30, 1971.

116. Piombo, B.A.D., Fasana, A., Marchesiello, S., and Ruzzene, M., "Modelling and identification of the dynamic response of a supported bridge", Mechanical Systems and Signal Processing, 14(1), pp. 75-89, 2004.

117. Potter, M.G., and Gold berg, J., "Mathematical methods" Prentice Hall of India, 1991.

118. Ravi, G. and Ranganathan, R., "Fatigue crack reliability of riveted bridge", International Journal of Structures, 14(2), pp.103-108, 1994.

119. Razaqpur, A. G., and Li, H. G., “Refined analysis of curved thin-walled Multi-cell Box Girders”, Computers and Structures, 53(1), pp.133-142, 1994.

120. Repetto, M.P., and Solari, G., “Dynamic along wind fatigue of slender vertical structures”, Engineering Structures, 23, pp. 1622-1633.2001.

121. Repetto, M.P., “Cycle counting methods for bi-model stationary Gaussian processes”, Probabilistic Engineering Mechanics, 20, pp. 229-238, 2005.

122. Schlaffi, M., and Bruhwiler, E., “Fatigue of existing reinforced concrete bridge deck slabs”, Engineering Structures, 20(11), pp. 991-998, 1998.

123. Seible, F., Priestley, M.J.N., and Sun, Z., “Fatigue strength of coupling joints of prestressing tendons in continuous post-tensioned concrete bridge” Proc., III Int. Workshop on bridge Rehabilitation, Ernst and Sohn, Berlin, Germany, pp. 613-626,1992.

124. Sennah, K.M., Zhang, X., and Kennedy, J.B., “Impact factors for horizontally curved composite box-girder bridges”, Journal of Bridge Engineering ASCE, 9(6), pp .512-520, 2004.

125. Senthilvasan., Thambiratnam, D.P., and Brameld, G.H., “Dynamic response of a curved bridge under moving track loads”, Engineering Structures,24, pp .1283-1293, 2002.

126. Shanmugam, N.E., and Balendra, T., “An experimental and theoretical study of multi-cell structures curved in plan”, Thin-walled Structures, 12, pp. 373-387, 1991.

127. Shanmugam, N.E., and Balendra, T., “Free vibration of thin-walled multi-cell structures”, Thin-walled Structures, 4, pp. 467-485, 1986.

128. Shinozuka, M., “Simulation of multivariate and multidimensional random process”, Journal of Acoustical Society of America, 49, pp .357-367, 1971.

129. Snyder J.M., and Wilson, J.F., “Free vibration of continuous horizontally curved beams”, Journal of Sound and Vibration, 157(2), pp.345-355, 1992.

130. Stavridis, L.T., and Michaltsos, G.T., “Eigen frequency analysis of thin-walled girders curved in plan”, Journal of Sound and Vibration, 227(2), pp.383-396, 1999.

131. Tabba, T.M., and Turkstra, C.J., “Free vibration of curved box girders”, Journal of Sound and Vibration, 54(4), pp.501-514, 1997.

132. Tan, C.P., and Shore S.M., “Response of horizontally curved bridge to moving load”, Journal of Structural Engineering ASCE, 94(9), pp .2135-2151, 1968.

133. Tan, G.H., Brameld, G.H., and Thambiratnam, D.P., “Development of an analytical model for treating bridge-vehicle interaction”, Engineering structures, 20, pp.54-61, 1998.

134. Sasidhar, M.N.V., and Talukdar, S., “Vehicle induced non-stationary response of bridge”, High way Research Bulletin, 68, pp .106-122, 2003.

135. Tesar, A., “Shear lag in the behavior of thin-walled box beam bridges”, Computers and Structures, 59(4), pp. 607-612, 1996.

136. Turkstra, C.J., and Fam,A., “Behavior study of curved box girders”, Journal of Structural Engineering ASCE, 104, pp. 453-462, 1978.

137. Vlasov, V. Z., “Thin-Walled Elastic Beams”, Israel Program for Scientific Translation Ltd, Jerusalem, 1961.

138. Waldron, P., “Elastic analysis of curved thin-walled girders including the effects of warping restraint”, Engineering Structures, 7, pp. 93-104, 1985.

139. Waldron, P., “Equivalent beam analysis of thin-walled beam structures”, Computers and Structures, 26(4), pp. 609-620, 1987.

140. Wang, T.L., Liu, M., and Huang, D., “Truck loading and fatigue damage analysis for girder bridges based on the weight-in-motion data Bridge”, Journal of Bridge Engineering, 10(1), pp. 12-20,2000.

141. Wesolowsky, G. O., “Multiple Regression and Analysis of Variance”, John Wiley & Sons Inc, 1976.

142. Wirsching, P.H., and Light, M.C., “Fatigue under wide band random stresses”, Journal of the Structural Division, 106(7), pp. 1593-1607, 1980.

143. Wirsching, P. H., Albrecht, P., Artley-Dean, M., Ellingwood, B., Schilling, C. G., and Zettlemoyer, N., “Fatigue Reliability: Variable Amplitude Loading”, Journal of Structural Division, 108, pp. 47-69, 1982.

144. Wollmann, G.P., Yates, D.L., Breen, J.E., and Kreger, M.E., “Fretting Fatigue in post-tensioned concrete”. Res Rep. 465-2F, Ctr. for Transp. Res., Univ. of Texas at Austin, Austin, Tex, 1988.

145. Wu, Y., Liu, S., Zhu, Y., and Lai, Y., “Matrix analysis of shear lag and shear deformation in thin-walled box beams”, Engineering Structures, 129(8), pp. 944-950, 2003.

146. Yadav, D., and Upadhyay, H.C., “Heave-Pitch-Roll Dynamics of vehicle with a variable velocity over a non-homogeneously profile flexible track”, Journal of Sound and Vibration, 164(2), pp. 337-348, 1993.

147. Yang, Y.B., “Impact Formulas for Vehicles Moving over Simple and Continuous Beams”, Journal of Structural Engineering ASCE, 121, pp. 1644-1650, 1995.

148. Yang, Y.B., and Wu, Y.S., “A versatile element for analyzing vehicle-bridge interaction response”, Engineering Structures, 23, pp. 452-469, 2001.

149. Yaping, W., Yuanming, L., Yuanlin, Z., and Weidong, P., "A curved beam element considering shear lag effect and its static and dynamic applications", Journal of Sound and vibration, 253(5), pp. 1131-1139, 2002.

150. Yoo, C.H., and Fehrebach, J.P., "Natural frequencies of Curved Girder", Journal of Engineering Mechanics Division, 107(2), pp .339-354, 1981.

151. Yoon, K.Y., Kang, Y.J., Choi, Y.J., and Park, N.H., "Free vibration analysis of horizontally curved steel I- girder bridges", Thin-Walled Structures, 43, pp.679-699, 2005.

152. Yoon, K.Y., Kang, Y.J., Choi, Y.J., and Park, N.H., "Natural frequencies of thin-walled curved beams", Thin-Walled Structures, 42(13), pp.1176-1186, 2006.

153. Zhang, S. H., and Lyons, L. P. R., "A Thin-Walled Box Beam Finite Element for Curved Bridge Analysis", Computers and Structures, 18(6), pp. 1035-1046, 1984.

154. Zhang, S. H., "The finite element analysis of thin-walled box spine-beam bridges", Ph.D. Thesis, The City University, London, 1983.

155. Zhao, Z., Halder, A., and Breen, F. L. Jr., "Fatigue reliability evaluation of steel bridges", Journal of Structural Engineering, ASCE, 120 (5), pp.1608-1622, 1994.

156. Zhu, X.Q., and Law, S.S., "Bridge dynamic response due to road surface roughness and braking of vehicle", Journal of Sound and Vibration, 282, pp.805-830, 2005.

157. Zhu, X.Q., and Law, S.S., "Identification of moving interaction forces with incomplete velocity information", Mechanical Systems and Signal Processing, 17(6), pp.1349-1366, 2003.

LIST OF PUBLICATIONS

1. K.Nallasivam, Anjan Dutta, S.Talukdar, "Dynamic Analysis of Horizontally Curved Thin-Walled Box-Girder Bridge due to Moving Vehicle", Shock and Vibration,14(3),pp.229-248,2007.
2. K.Nallasivam, S.Talukdar and Anjan Dutta, "Fatigue life Prediction of Horizontally Curved Thin Walled Box Girder Steel Bridges", Structural Engineering and Mechanics, (Under Review).
3. K.Nallasivam, S.Hopeful, Anjan Dutta and S.Talukdar, "Static Analysis of Horizontally Curved Thin-Walled Box-Girder Bridge", Highway Research Bulletin, Indian Road Congress,76,pp.117-127,2007.
4. K.Nallasivam, Vineet Jain, S.Talukdar and Anjan Dutta, "Free Vibration Characteristics of Horizontally Curved Thin-Walled Box-Girder Bridge", Journal of Advances in Vibration Engineering, (In Press).
5. K.Nallasivam, S.Talukdar and Anjan Dutta, "An Approximate Solution for the Natural Frequencies of Curved Bridge Girder considering Gravitational and Centrifugal Effect of Moving Load", National Conference, SEC-2003 held in IIT Kharagpur, pp.272-279, 2003.

APPENDIX - A

A.1 DETERMINATION OF CROSS–SECTIONAL PROPERTIES OF THIN-WALLED BOX-GIRDERS

A.1.1 Introduction

For the calculation of stresses due to bending, warping torsion and distortional warping, cross-sectional properties of the box-girder are required to be evaluated. The evaluation of cross sectional properties is tedious, time consuming and numerical errors are easily introduced. A computer program has been developed for the determination of cross-sectional properties of thin-walled box-girder with at least one vertical axis of symmetry.

A.1.2 Scheme of integration

In the course of determining cross-sectional properties, a certain number of definite integrals must be found. Consider a straight element *j-k* of the mid-line of the section with thickness t_i (Fig.A.1). For this segment, let the ordinates η and $\overline{\eta}$ of two different diagrams be given, whose form is linear.

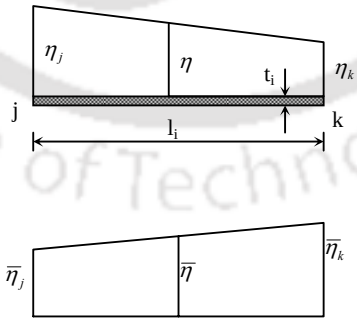

Fig. A.1 Integral along a straight element

The integral

$$I_{jk} = \int_j^k \eta\, \bar{\eta}\, dA \quad = t_i \int_j^k \eta\, \bar{\eta}\, ds \tag{A.1}$$

is given by $$I_{jk} = \frac{l_i t_i}{6}\left[\bar{\eta}_j(2\eta_j + \eta_k) + \bar{\eta}_k(2\eta_k + \eta_j)\right] \tag{A.2}$$

or

$$I_{jk} = \frac{l_i t_i}{6}\left[\eta_j(2\bar{\eta}_j + \bar{\eta}_k) + \bar{\eta}_k(2\bar{\eta}_k + \bar{\eta}_j)\right] \tag{A.3}$$

when $\eta = \bar{\eta}$, Eq. A.2 and A.3 may be simplified as

$$I_{jk} = \frac{l_i t_i}{3}\left[\eta_j^2 + \eta_k^2 + \eta_j \eta_k)\right] \tag{A.4}$$

A.1.3 Calculation of Sectional Properties in Bending and Torsion

Applying the numerical integration as described in Eq.A.2 and A.3, we obtain for the moment of inertia about the *z* axis as

$$I_z = \tfrac{1}{3}\sum_{i=1}^{m} l_i t_i\left[y_j^2 + y_k^2 + y_j y_k\right] \tag{A.5}$$

where m is the total number of plate elements in the section,

l_i is the length of the i^{th} element and t_i is its thickness,

j and k indicate the number of the end nodes of the individual elements.

Similarly, the moment of inertia about the *y* axis is given by

$$I_y = \tfrac{1}{3}\sum_{i=1}^{m} l_i t_i\left[z_j^2 + z_k^2 + z_j z_k\right] \tag{A.6}$$

To determine the position of the shear center and to obtain the diagram of the reduced sectorial co-ordinates $\hat{\omega}_I$, the intersection of the *y* axis and the mid-line of the top flange B is chosen as the principal integral origin (Fig.A.2). The sectorial coordinates $\hat{\omega}_{IB}$ of individual characteristic points can be calculated by the following expressions

$$\left(\hat{\omega}_{IB}\right)_0 = -\sum_{i}^{k}\left(\bar{\tau}_B\right)_{m,i}\left(z_{i-1}-z_i\right)-\left(\tau_B\right)_{m,k+1}z_k = -\left(\hat{\omega}_{IB}\right)_{n+2} \tag{A.7}$$

where, $k=\frac{n}{2}$, when *n* is an even number and $k=\frac{n+1}{2}$, when *n* is an odd number

$$\left(\hat{\omega}_{IB}\right)_i = \left(\hat{\omega}_{IB}\right)_{i-1}+\left(\bar{\tau}_B\right)_{m,i}\left(z_{i-1}-z_i\right) \qquad i=1,2,\ldots..,\ n+2 \tag{A.8}$$

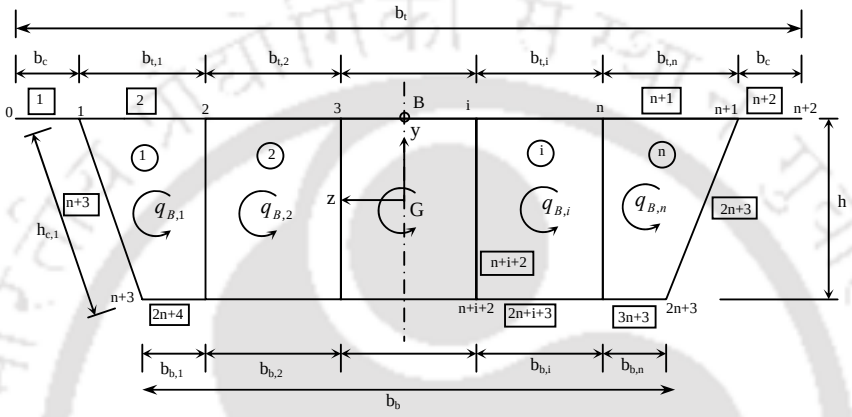

Fig. A.2 Multi-cell cross-section

$$\left(\hat{\omega}_{IB}\right)_{n+i+2} = \left(\hat{\omega}_{IB}\right)_i + z_i h - \left(\bar{\tau}_B\right)_{m,n+i+2} h_{c,i} \qquad i=1,2,\ldots..,\ n+1 \tag{A.9}$$

where,

$$\left(\bar{\tau}_B\right)_{m,1} = \left(\bar{\tau}_B\right)_{m,n+2} = 0 \tag{A.10}$$

$$\left(\bar{\tau}_B\right)_{m,i+1} = \frac{\bar{q}_{B,i}}{t_{t,i}} \qquad i=1,2,\ldots..,\ n \tag{A.11}$$

$$\left(\bar{\tau}_B\right)_{m,n+i+2} = \frac{\bar{q}_{B,i}-\bar{q}_{B,i-1}}{t_{h,i}} \qquad i=1,2,\ldots..,\ n+1 \tag{A.12}$$

$$\left(\bar{\tau}_B\right)_{m,2n+i+3} = \frac{\bar{q}_{B,i}}{t_{b,i}} \qquad i=1,2,\ldots..,\ n \tag{A.13}$$

in which shear flow $\bar{q}_{B,0} = \bar{q}_{B,n+1} = 0$, and *n* is the total number of cells in the cross-section.

Applying the numerical integration as described in Eq A.2, we obtain from the diagram of $\hat{\omega}_{IB}$, the sectortial product of inertia about the y axis $I_{y\hat{\omega}_B}$ as

$$I_{y\hat{\omega}_B} = \tfrac{1}{6}\sum_{i=1}^{m} l_i t_i \left[\left(\hat{\omega}_{IB}\right)_j \left(2z_j + z_k\right) + \left(\hat{\omega}_{IB}\right)_k \left(2z_k + z_j\right) \right] \tag{A.14}$$

The shear center y_s can thus be obtained from Eq.2.36 as

$$e_y = -\frac{I_{y\hat{\omega}_B}}{I_y} \tag{A.15}$$

$\overline{q}_{B,i}$ can be evaluated using the flexibility equations (Zhang 1983).

$$[f]\{\overline{q}\} = \{\Omega\} \tag{A.16}$$

where, flexibility coefficients $\boldsymbol{f}$ is given by

$$f_{ii} = \oint_i \frac{ds}{t} \qquad \text{or} \qquad f_{ik} = -\oint_{i,k} \frac{ds}{t}, \tag{A.17}$$

Ω is twice the enclosed area of each cell.

The normalized reduced sectorial coordinates $\bar{\omega}_I$ at individual nodes can then be evaluated by the following expressions

$$\hat{\omega}_{I,0} = z_0 y_S - \sum_{i=1}^{k} \left(\overline{\tau}_B\right)_{m,i} \left(z_{i-1} - z_i\right) - \left(\overline{\tau}_B\right)_{m,k+1} z_k = -\hat{\omega}_{I,n+2} \tag{A.18}$$

where, $k = \frac{n}{2}$ when n is an even number, and $k = \frac{n+1}{2}$ when n is and odd number,

$$\hat{\omega}_{I,i} = \hat{\omega}_{I,i-1} - \left[y_S - \left(\overline{\tau}_B\right)_{m,i} \right] \left(z_{i-1} - z_i\right) \qquad \left(i = 1, 2, ..., n+2\right) \tag{A.19}$$

$$\hat{\omega}_{I,n+i+2} = \hat{\omega}_{I,i} + h z_i + y_S \left(z_{n+i+2} - z_i\right) - \left(\overline{\tau}_B\right)_{m,n+i+2} h_{c,i} \qquad \left(i = 1, 2, ..., n+1\right) \tag{A.20}$$

Using the diagram of normalized sectorial coordinates $\hat{\omega}_I$ we obtain from Eq.A.2, the value of torsional warping moment of inertia J_I as

$$J_I = \tfrac{1}{3}\sum_{i=1}^{m} l_i t_i \left(\hat{\omega}_{I,j}^2 + \hat{\omega}_{I,k}^2 + \hat{\omega}_{I,j} \hat{\omega}_{I,k} \right) \tag{A.21}$$

The central moment of area J_C can be expressed as

$$J_C = \sum_{i=1}^{m} \frac{t_i \left(z_j y_k - z_k y_E - z_k y_j + z_j y_E \right)^2}{l_i} \tag{A.22}$$

where, $z_E = 0$

$$y_E = y_S - y_G \tag{A.23}$$

A.1.4 Calculation of Sectional Properties in Distortion

For a section with a vertical axis of symmetry as shown in Fig. A.2, the warping stress pattern has a linear variation across each element plate as shown in Fig.A.3.

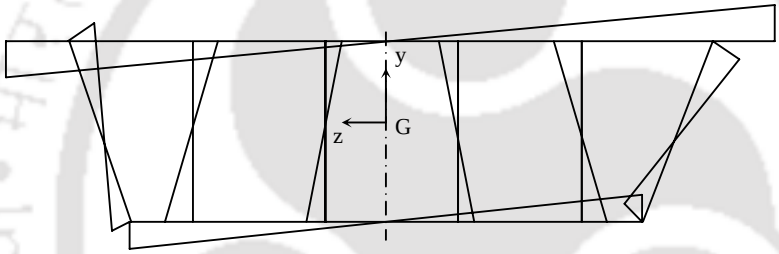

Fig.A.3. Distribution of unit distortional warping function

From the linear variation of unit distortional warping function ω_{II} we may define

$$\alpha_i = \frac{\omega_{II,i}}{\omega_{II,1}} = \frac{z_i}{z_1} \qquad \left(i = 0,1,2,...,n+2\right) \tag{A.24a}$$

$$\lambda_i = \frac{\omega_{II,n+i+2}}{\omega_{II,n+3}} = \frac{z_{n+i+2}}{z_{n+3}} \qquad \left(i = 1,2,...,n+1\right) \tag{A.24b}$$

$$\beta = -\frac{\omega_{II,n+3}}{\omega_{II,1}} \qquad \left(i = 1,2,...,n+1\right) \tag{A.24c}$$

$$\alpha_{b,i} = \frac{\omega_{II,n+i+2}}{\omega_{II,1}} = -\lambda_i \beta \qquad \left(i = 1,2,...,n+1\right) \tag{A.24d}$$

where $z_0, z_1 ..... z_{2n+3}$ are the coordinates related to the local coordinate system.

Thus, the ratio of ω_{II} at the two ends of individual webs can be obtained as

$$\frac{\omega_{II,n+i+2}}{\omega_{II,i}} = \beta\psi_i \tag{A.25}$$

where,

$$\psi_i = -\frac{\lambda_i}{\alpha_i} \qquad (i = 1, 2, ..., n+1) \tag{A.26}$$

The ratio β is obtained from the equilibrium $\int_A \sigma_{II} z \, dA = 0$

i) The moment with respect to the *y* axis of symmetry due to the normal stresses at the upper flange is

$$M_t = \frac{b_c t_c}{3}\left[\alpha_0\left(2z_0 + z_1\right) + \alpha_1\left(2z_1 + z_0\right)\right] + \sum_{i=1}^{n}\frac{b_{t,i}t_{t,i}}{6}\left[\alpha_i\left(2z_i + z_{i+1}\right) + \alpha_{i+1}\left(2z_{i+1} + z_i\right)\right] \tag{A.27}$$

ii) The moment with respect to the *y* axis of symmetry due to the normal stresses at the lower flange is

$$\begin{aligned} M_b &= -\beta\sum_{i=1}^{n}\frac{b_{b,i}t_{b,i}}{6}\left[\lambda_i\left(2z_{n+i+2} + z_{n+i+3}\right) + \lambda_{i+1}\left(2z_{n+i+3} + z_{n+i+2}\right)\right] \\ &= -\beta\bar{M}_b \end{aligned} \tag{A.28}$$

where

$$\bar{M}_b = \sum_{i=1}^{n}\frac{b_{b,i}t_{b,i}}{6}\left[\lambda_i\left(2z_{n+i+2} + z_{n+i+3}\right) + \lambda_{i+1}\left(2z_{n+i+3} + z_{n+i+2}\right)\right] \tag{A.29}$$

iii) The moment with respect to the *y* axis of symmetry due to the normal stresses at the webs

$$\begin{aligned} M_h &= \sum_{i=1}^{n+1}\frac{h_{c,i}t_{h,i}}{6}\left[\alpha_i\left(2z_i + z_{n+i+2}\right) - \lambda_i\beta\left(2z_{n+i+2} + z_i\right)\right] \\ &= \bar{M}_{h,1} - \beta\bar{M}_{h,2} \end{aligned} \tag{A.30}$$

where

$$\bar{M}_{h,1} = \sum_{i=1}^{n+1}\frac{h_{c,i}t_{h,i}}{6}\alpha_i\left(2z_i + z_{n+i+2}\right) \tag{A.31}$$

$$\bar{M}_{h,2} = \sum_{i=1}^{n+1}\frac{h_{c,i}t_{h,i}}{6}\lambda_i\left(2z_{n+i+2} + z_i\right) \tag{A.32}$$

From the equilibrium condition $M_t + M_b + M_h = 0$, we obtain

$$\beta = \frac{M_t + \bar{M}_{h,1}}{\bar{M}_b + \bar{M}_{h,2}} \tag{A.33}$$

The unit distortional warping function for *node 1* of the cross-section as shown in Fig.A.2 is given by (Zhang 1983).

$$\omega_{II,1} = -\frac{hb_t^2 b_b}{2\left(b_t + b_b\right)\left(\beta b_t + b_b\right)} \tag{A.34}$$

Again, using the diagram of normalized sectorial coordinates $\omega_{II,1}$, we obtain from Eq.A.2, the distortional moment of inertia J_{II} as

$$J_{II} = \tfrac{1}{3}\sum_{i=1}^{m} l_i t_i \left(\omega_{II,j}^2 + \omega_{II,k}^2 + \omega_{II,j}\omega_{II,k}\right) \tag{A.35}$$

APPENDIX – B

B.1 FLOW CHART FOR FINITE ELEMENT ANALYSIS (STATIC) OF CURVED BOX-GIRDER BRIDGE

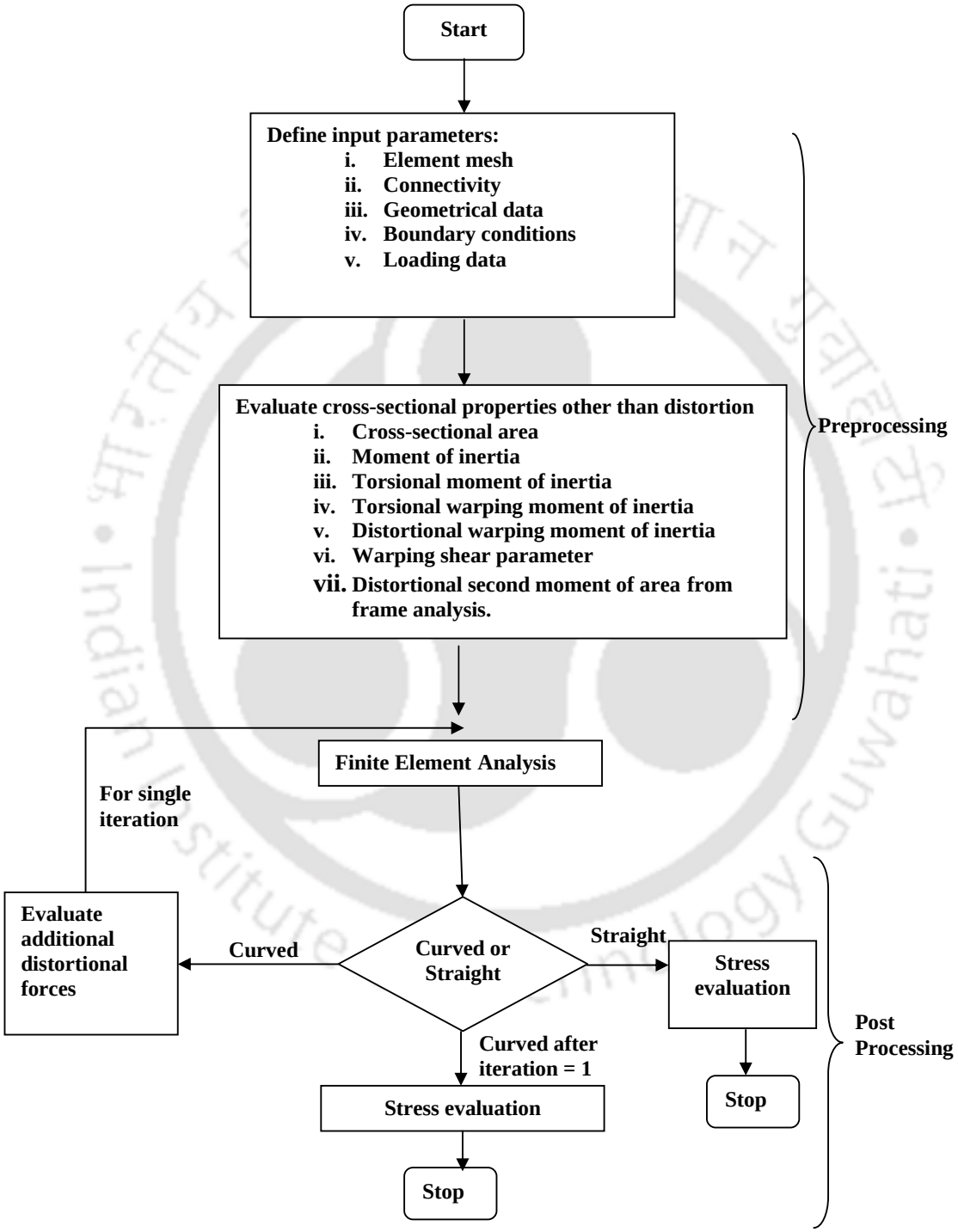

APPENDIX – C

C.1 DETAILS OF IRC LOADINGS

C.1.1 IRC 70R TRACKED VEHICLE

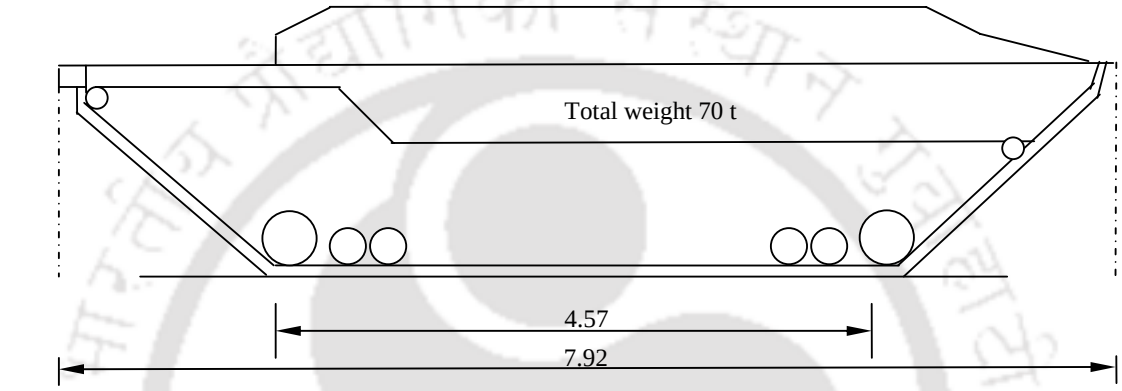

(a) Elevation

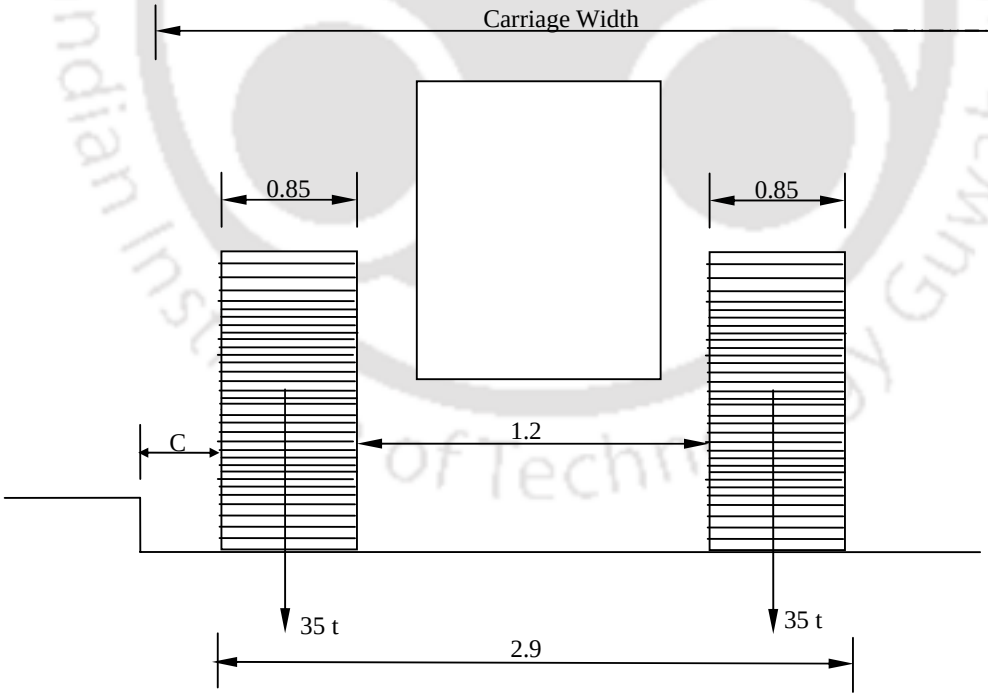

(b) Cross-section

C.1.2 IRC 70R WHEELED VEHICLES

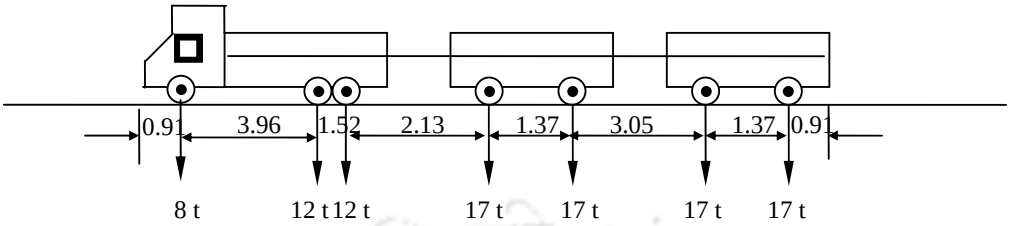

(a) Elevation

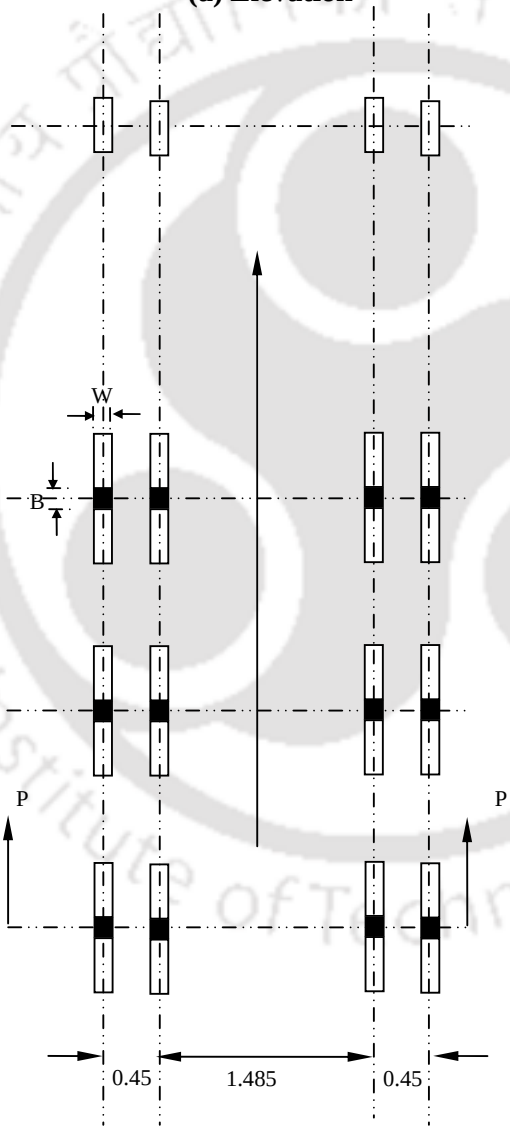

(b) Plan

C.1.3 IRC CLASS A TRAIN OF VEHICLES

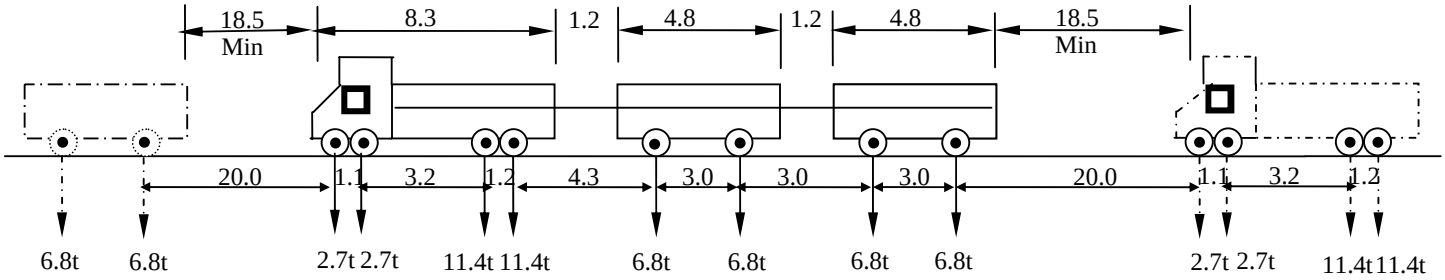

(a) Elevation

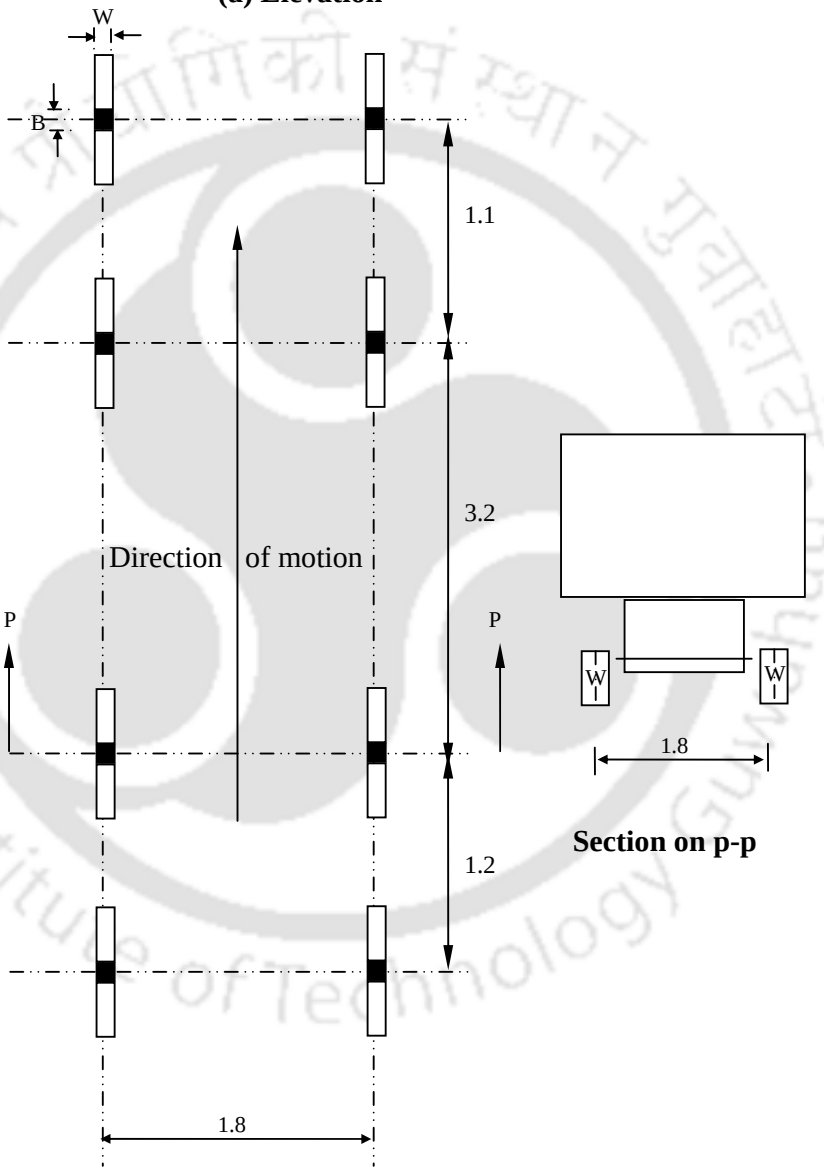

Section on p-p

(b) Plan

Note: All axle loads are in tonne and linear dimensions are in metre.

Table C.1.1 The Minimum clearance distance between outer edge of the wheel and the roadway face of the kerb, (C) for IRC 70R Vehicles

Carriageway width	**Minimum value of C**
Single Lane Bridges 3.8m and above	0.3m
Multi-Lane Bridges	
Less than 5.5m	0.6m
5.5m or above	1.2 m

Table C.1.2 Minimum clearance on multi-lane bridge for IRC Class A Train of Vehicles

Clear carriageway width	**Minimum clearance distance between outer edge of the wheel and the roadway face of the kerb (g)**	**Minimum clearance distance between outer edge of the passing or crossing vehicles (f)**
5.5 m to 7.5 m	Uniformly increasing from 0.4m to 1.2m	150 mm for all carriageway width
Above 7.5m	1.2m	

APPENDIX – D

D.1 DYNAMIC ANALYSIS PROCEDURE FOR VEHICLE-BRIDGE INTERACTION

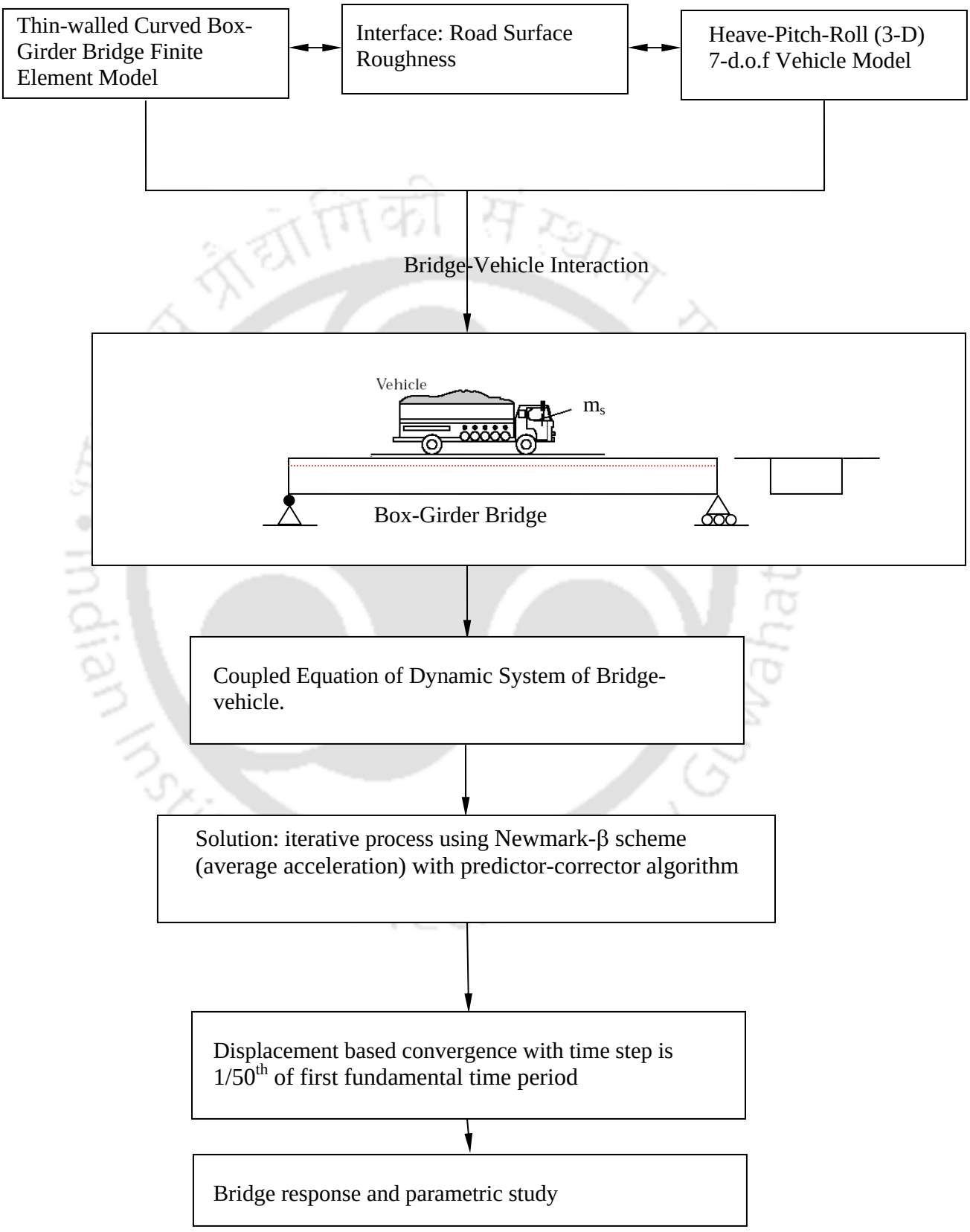

APPENDIX – E

E.1 FLOW DIAGRAM FOR THE RAIN FLOW COUNTING METHOD

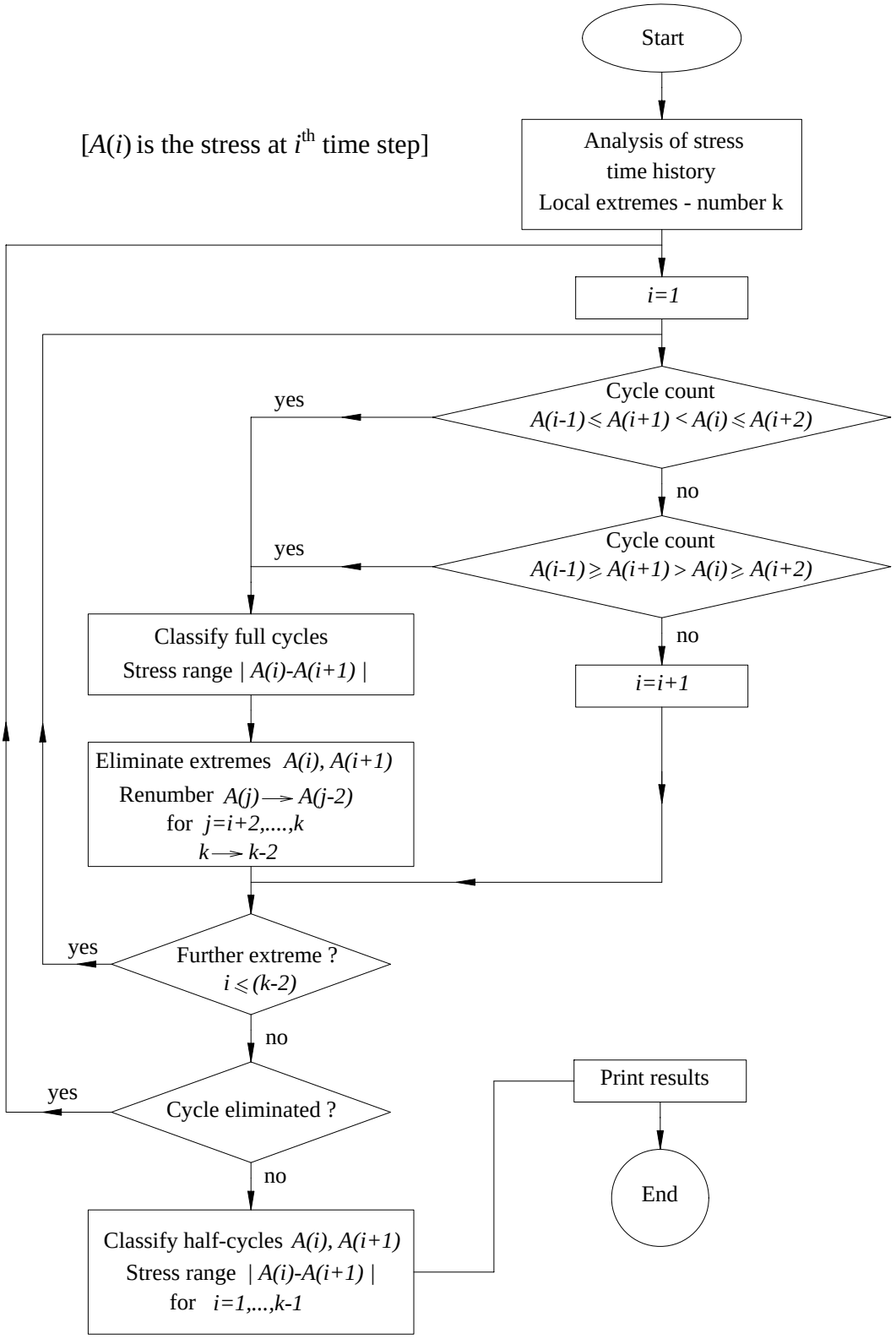

APPENDIX – F

F.1 DETERMINATION OF EQUIVALENT LOAD VECTOR FOR A ECCENTRICALLY PLACED VEHICLE ON THIN-WALLED BOX-GIRDER BRIDGE

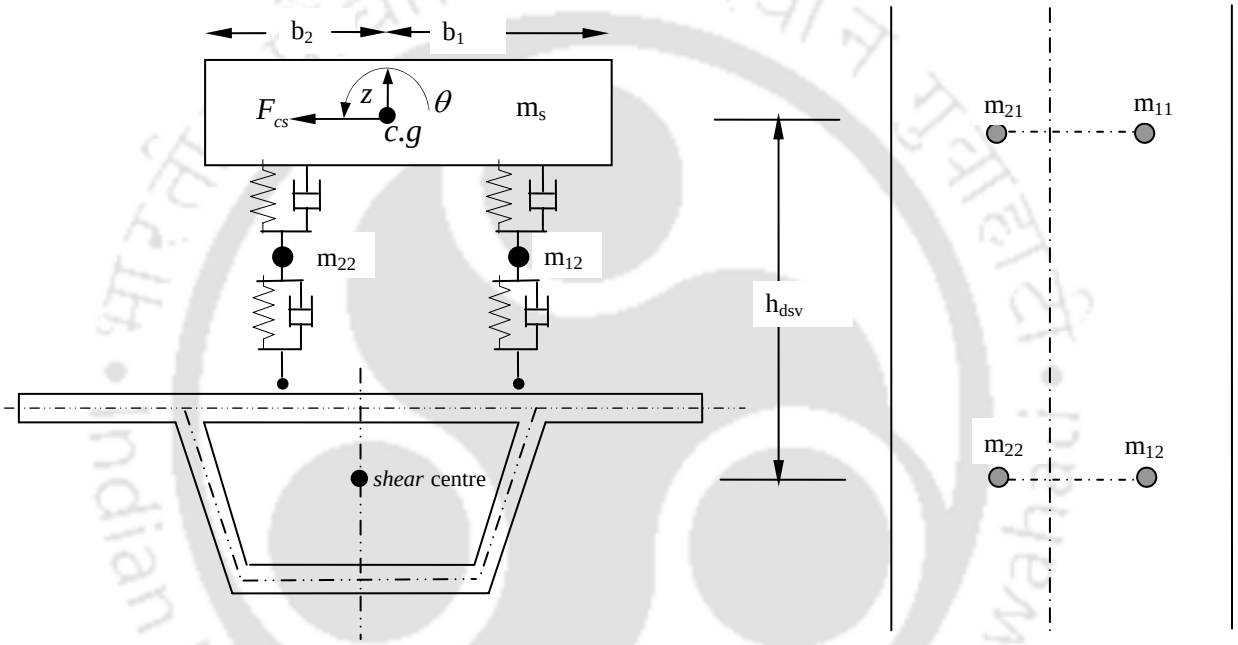

Fig .F.1 box girder bridge with vehicle model

Load from sprung and unsprung mass in front axle

$$W_f = \left[\frac{m_s}{2} + m_{11} + m_{21} \right] \times g$$

Load from sprung and unsprung mass in rear axle

$$W_r = \left[\frac{m_s}{2} + m_{12} + m_{22} \right] \times g$$

Torsional moment in front axle $T_f = \left(m_{Vf} - m_{Hf} \right)$

Torsional moment in in rear axle $T_r = \left(m_{Vr} - m_{Hr} \right)$

Ref section 2.3.4.2 for distortional moment calculation

Distortional moment in front axle $M_{df} = \frac{1}{2}\left(\frac{b_t}{b_b} m_{Vf} - m_{Hf} \right)$

Distortional moment in rear axle $M_{dr} = \frac{1}{2}\left(\frac{b_t}{b_b} m_{Vr} - m_{Hr} \right)$

The torsional moment due to vehicle eccentricity in front axle is written as

$$m_{Vf} = \left[\left(\frac{m_s}{4} + m_{11} \right) \times b_1 - \left(\frac{m_s}{4} + m_{21} \right) \times b_2 \right] \times g$$

The torsional moment due to vehicle eccentricity in rear axle

$$m_{Vr} = \left[\left(\frac{m_s}{4} + m_{12} \right) \times b_1 - \left(\frac{m_s}{4} + m_{22} \right) \times b_2 \right] \times g$$

The resultant torsional moment due to resultant centrifugal force $T_c = F_c * h_{dsv}$

The torsional moment due to centrifugal force in rear axle

$$m_{Hr} = \frac{Tc * \bar{X}_{t2}}{(\text{Distance between two axles})}$$

The torsional moment due to centrifugal force in front axle $m_{Hf} = T_c - m_{Hr}$

where

b_1, b_2= distance between front wheel and rear wheel (breath wise)

b_t, b_b= breath of top and bottom flange

m_s=mass of vehicle(sprung mass)

m_{11}=m_{21}= front wheel mass (unsprung mass)

m_{21}=m_{22}= rear wheel mass (unsprung mass)

F_c =resultant centrifugal forces

h_{dsv} =distance between shear centre of box-girder bridge to the point of resultant centrifugal force acting on the vehicle.

$\bar{X}_{t1}, \bar{X}_{t2}$ =Position of the resultant torsional moment due to centrifugal force from rear and front axle respectively.

APPENDIX – G

G.1 FLOW CHART FOR EVALVATION OF STRESSES FOR CURVED BOX-GIRDER BRIDGE